

Fatigue Crack Propagation and Delamination Growth in Glare

René Alderliesten

**Fatigue Crack Propagation
and
Delamination Growth in Glare**

Fatigue Crack Propagation and Delamination Growth in Glare

Proefschrift

ter verkrijging van de graad van doctor
aan de Technische Universiteit Delft,
op gezag van de Rector Magnificus prof.dr.ir. J.T. Fokkema,
voorzitter van het College voor Promoties,
in het openbaar te verdedigen op dinsdag 31 mei 2005 om 10:30 uur

door

Reyndert Christiaan ALDERLIESTEN
ingenieur luchtvaart en ruimtevaart
geboren te Maassluis

Dit proefschrift is goedgekeurd door de promotoren:
Prof.dr.ir. S. van der Zwaag
Prof.dr.ir. M.J.L. van Tooren

Samenstelling promotiecommissie:

Rector Magnificus,	voorzitter
Prof.dr.ir. S. van der Zwaag,	Technische Universiteit Delft, promotor
Prof.dr.ir. M.J.L. van Tooren,	Technische Universiteit Delft, promotor
Prof.dr.ir. J. Schijve,	Technische Universiteit Delft
Prof.dr.ir. R. Marissen,	Technische Universiteit Delft
Prof.dr.ir. R. Benedictus,	Technische Universiteit Delft
Prof.dr.ir. J.G. Rots,	Technische Universiteit Delft
Dr. J.F. Imbert	Airbus S.A.S., Frankrijk

Published and distributed by: DUP Science

DUP Science is an imprint of
Delft University Press
P.O. Box 98
2600 MG Delft
The Netherlands
Telephone: +31 15 27 85 678
Telefax: +31 15 27 85 706
E-mail: info@library.tudelft.nl

ISBN 90-407-2588-8

Keywords: Glare, Crack propagation, Delamination growth

Copyright © 2005 by René Alderliesten

All rights reserved. No part of the material protected by this copyright notice may be reproduced or utilized in any form or by any means, electronic or mechanical, including photocopying, recording or by any information storage and retrieval system, without written permission from the publisher: Delft University Press

Printed in The Netherlands

In honour of Ad Vlot

Summary

“Fatigue crack propagation and delamination growth in Glare”

René Alderliesten

This thesis presents the investigation into the fatigue crack propagation behaviour and delamination growth behaviour of the Fibre Metal Laminate Glare. This phenomenon is studied for constant-amplitude loading, which is significant for fatigue loading of aircraft pressurized fuselages. As defined in the first chapter, the objective of the investigation is twofold: First, to obtain a clear understanding and a detailed characterisation of the failure mechanisms in Glare under fatigue loading, and second, to obtain an accurate prediction model for fatigue crack propagation in Glare accounting for fibre bridging and delamination.

The major concept in this thesis is that the stress intensity at a crack tip in the metal layers of a Fibre Metal Laminate is the factor determining the extension of that crack under cyclic loading. This means that the stress intensity factor can be described with Linear Elastic Fracture Mechanics, including the contribution of the fibre layers and the with the crack growth associated delamination behaviour.

This investigation covers the theoretical analysis of the crack growth phenomenon and a complementary experimental programme to support and validate the new prediction model. This investigation has been restricted to through cracks with the same crack length in all metal layers.

In the second chapter, the various Glare grades and lay-ups are defined, together with a description of the manufacturing process and quality assurance procedures. A qualitative description of the fatigue crack growth phenomenon in Glare is presented in chapter 3. The aspects introduced are the fatigue crack growth in the aluminium layers, controlled by the stress intensity factor at the crack tip, and delamination of the aluminium and prepreg layers, which occurs in the wake of the propagating crack. The crack opening is constrained by the bridging fibre layers, while the stress in these fibre layers determines the delamination growth. Empirical and analytical crack growth prediction models proposed in the literature and their limitations are discussed in chapter 4.

The experimental programme is presented in chapter 5. The programme covers the delamination behaviour at the aluminium/fibre interface, the fatigue crack curve of monolithic aluminium, the crack opening contour and the corresponding delamination shape measurements of fatigue cracks in Glare together with the fatigue crack growth curves. The measurement techniques used in the test programme are described in detail.

The most important chapter of this thesis is chapter 6, in which a new crack growth prediction model is derived in four subsequent steps. The model describes the crack propagation of the fatigue cracks in the aluminium layers and the corresponding delamination growth at the aluminium/fibre interfaces in the wake of the crack.

In the model the stress intensity factor at the crack tip is a function of the far field opening stress and the crack closing bridging stress in the aluminium layers. The bridging stress along the crack length is calculated on the basis of the crack opening relations for the individual mechanisms. It is then used to calculate the delamination extension, using a correlation between the delamination growth rate and the energy release rate.

The prediction model is implemented in a numerical programme and is validated with a wide range of test data. A good correlation between predicted and experimental crack growth rates, crack opening contours and delamination shapes has been obtained.

Chapter 7 summarises the conclusions of the investigation. It can be concluded that with the proposed prediction model, the mechanism of crack propagation and delamination growth in Glare is fully described and characterised. The prediction model obtained and validated is accurate and has the potential to be extended to other material-, geometrical- and test parameters.

Table of Contents

Nomenclature	xii
1. Introduction	1
2. Fibre Metal Laminates	5
2.1 Introduction	5
2.2 Material Definition	6
2.3 Fibre Bridging	6
2.4 Manufacturing Process	8
2.5 Post-stretching	9
2.6 Quality Control	11
3. Fatigue Crack Growth Phenomenon in Glare	13
3.1 Introduction	13
3.2 Fatigue initiation	14
3.3 Fatigue crack propagation	17
3.3.1 <i>Crack bridging and restraint on crack opening</i>	18
3.3.2 <i>Delamination of layers</i>	20
3.3.3 <i>Adhesive shear deformation</i>	22
3.3.4 <i>Effect on fatigue performance of Glare</i>	22
3.4 Fatigue crack geometries in Glare	23
3.4.1 <i>Surface cracks in Glare</i>	24
3.4.2 <i>Part through cracks in Glare</i>	24
3.4.3 <i>Through cracks in Glare</i>	25
4. Fatigue in FML Modelling approaches from Literature	29
4.1 Introduction	29
4.2 Phenomenological methods	30
4.2.1 <i>Method of Toi</i>	30
4.2.2 <i>Application of compliance method</i>	31
4.2.3 <i>Methods of Cox</i>	34
4.2.4 <i>Method of Guo and Wu</i>	35

4.3	Analytical Methods	36
4.3.1	<i>Method of Marissen</i>	36
4.3.2	<i>Method of Lin and Kao</i>	39
4.3.3	<i>Method of De Koning</i>	41
4.3.4	<i>Bridging stress modelled as elastic springs</i>	44
4.3.5	<i>Method of Guo and Wu</i>	45
4.3.6	<i>Method of Wu</i>	48
4.4	Finite Element and Boundary Element Methods	50
4.4.1	<i>Method Yeh</i>	50
4.4.2	<i>Method of Burianek</i>	51
4.5	Conclusions	52

5. Description of Experimental Programmes and Data Evaluation Introduction

57

5.1	Introduction	57
5.2	Delamination growth behaviour	57
5.2.1	<i>Programme objective</i>	57
5.2.2	<i>Specimen geometry</i>	58
5.2.3	<i>Test matrix and test set-up</i>	59
5.2.4	<i>Measurements and observations</i>	60
5.3	Crack Opening Shape	61
5.3.1	<i>Programme objective</i>	61
5.3.2	<i>Specimen geometry and test set-up</i>	61
5.3.3	<i>Measurement and analysis approach</i>	62
5.4	Delamination shape	63
5.4.1	<i>Programme Objective</i>	63
5.4.2	<i>Specimen geometry</i>	63
5.4.3	<i>Measurement and analysis approach</i>	64
5.5	Fatigue crack growth in aluminium	65
5.5.1	<i>Programme objective</i>	65
5.5.2	<i>Specimen geometry</i>	66
5.5.3	<i>Test matrix and test set-up</i>	66
5.6	Fatigue crack propagation tests on Glare	67
5.6.1	<i>Programme objective</i>	67
5.6.2	<i>Specimen geometry</i>	67
5.6.3	<i>Test matrix and test set-up</i>	68
5.6.4	<i>Measurement and analysis approach</i>	68
5.7	Measurement Techniques	71
5.7.1	<i>Digital Imaging System</i>	72
5.7.2	<i>Potential Drop Method</i>	72
5.7.3	<i>Application of Strain Gauges</i>	75
5.7.4	<i>Etching the outer aluminium layers</i>	76
5.8	Data Evaluation	77

6.	Crack Growth Prediction Model	79
6.1	Introduction	79
6.2	Step1: delamination growth behaviour	81
6.2.1	<i>Energy Release Rate and delamination growth</i>	82
6.2.2	<i>Delamination growth experiments</i>	83
6.2.3	<i>Delamination growth relation for Glare</i>	89
6.3	Step2: bridging stress for arbitrary crack	91
6.3.1	<i>Crack opening due to applied and bridging stresses</i>	92
6.3.2	<i>Crack opening due to elongation and deformation</i>	93
6.3.3	<i>Derivation of the bridging stress distribution</i>	95
6.4	Step3: determination of delamination shape	98
6.5	Step4: determination of the Stress Intensity Factor	99
6.6	Numerical Calculation Approach	100
6.7	Results and discussion	103
6.7.1	<i>Comparison between model and reference test</i>	103
6.7.2	<i>Model robustness</i>	107
6.7.3	<i>Delamination shape near the crack tip</i>	109
6.7.4	<i>Validity range of the model</i>	113
6.8	Summary	118
7.	Conclusions and future prospects	121
7.1	Conclusions	121
7.2	Future prospects	123
A.	Crack Opening Shape	125
A.1	Introduction	125
A.2	Crack Opening Shapes due to point loads	125
A.3	Crack Opening Shapes due to bridging stresses	130
B.	Prepreg Shear Deformation	133
B.1	Prepreg shear deformation of uni-directional fibre layers	133
B.2	Prepreg shear deformation of cross-ply fibre layers	137
B.3	Prepreg shear deformation of uni-directional fibre layers for small delamination lengths	143
B.4	Prepreg shear deformation of cross-ply fibre layers for small delamination lengths	146

C.	Delamination Growth Calculation	151
C.1	Introduction	151
C.2	Matrix size considerations	152
C.3	Delamination extension calculation	152
C.4	Delamination tip approximation	155
D.	Model Validation	157
D.1	Introduction	157
	Samenvatting	167
	Curriculum Vitae	169
	Publications	170
	Acknowledgements	172

Nomenclature

Symbol	Unit	Description
a	mm	Half crack length
a_0	mm	Half starter crack length
a_i	mm	Half crack length after i^{th} calculation
a_s	mm	Half saw-cut length
b	mm	Half delamination length
b_s	mm	Half delamination length at the saw-cut tip
$C_{ad,d}$	-	Correction for adhesive shear deformation
C_{cg}	-	Constant in Paris crack growth relation
C_d	-	Constant in Paris delamination growth relation
C_d	-	Correction for crack bridging and delamination
C_s	-	Correction for the saw-cut size
da/dN	mm/cycle	Crack growth rate
db/dN	mm/cycle	Delamination growth rate
E	MPa	Modulus of Elasticity
E_{lam}	MPa	Modulus of Elasticity of the total laminate
F	MPa mm	Stiffness parameter
F	-	Finite width correction factor
F_0	-	Finite width correction factor for the starter notch
F_{al}	MPa mm	Stiffness of the aluminium in a laminate
F_f	MPa mm	Stiffness of the fibres in a laminate
f	Hz	Test frequency
G	MPa	Shear modulus
$G_{d,max}$	MPa mm	Maximum Energy Release Rate for delamination
$G_{d,min}$	MPa mm	Minimum Energy Release Rate for delamination
j	-	Number of aluminium/fibre interfaces
K	MPa	Stress Intensity Factor
K_{ff}	MPa	Stress Intensity Factor as result of far field stress
K_{br}	MPa	Stress Intensity Factor as results of bridging stress
K_{tip}	MPa	Stress Intensity Factor at the crack tip
K_{ss}	MPa	Stress Intensity Factor in the steady state regime
k	-	Material constant
L	mm	Specimen length
L_{gauge}	mm	Gauge length to measure the compliance
n_{al}	-	Number of aluminium layers
n_{f0}	-	Number of fibre layers \parallel to the loading direction
n_{f90}	-	Number of fibre layers \perp to the loading direction
n_{cg}	-	Paris constant in crack growth relation
n_d	-	Paris constant in delamination growth relation

N	-	Number of bar elements
N	-	Number of cycles
P	MPa mm	Load per unit thickness
R	-	Stress ratio (S_{min}/S_{max})
r	mm	Radius
$S_{al,r}$	MPa	Residual curing stress in the aluminium layers
$S_{applied}$	MPa	Applied stress
S_{br}	MPa	Bridging stress
S_{max}	MPa	Maximum stress
S_{min}	MPa	Minimum stress
t	mm	Thickness
t_{al}	mm	Aluminium layer thickness
t_f	mm	Fibre layer thickness
t_{lam}	mm	Laminate thickness
u_{br}	mm	Crack opening due to fibre bridging
V_0	volt	Potential over the specimen length
V_a	volt	Potential over the crack
v_∞	mm	Crack opening due to far field opening stress
v_{br}	mm	Crack opening due to bridging stress
W	mm	Specimen width
x	mm	Coordinate parameter
x_p	mm	Location of point load P along the crack
α	-	Finite width factor ($2a/W$)
α_{CP}	-	Stiffness parameter for cross-ply prepreg
α_{UD}	-	Stiffness parameter for uni-directional prepreg
β	-	Factor characterising effect of delamination shape
β_{geom}	-	Geometry correction factor
β_{geom}	-	Correction factor for FML's
β_{notch}	-	Correction factor for the presence of a notch
δ_{ad}	mm	Displacement due to adhesive shear deformation
δ_f	mm	Displacement due to fibre elongation
δ_{pp}	mm	Displacement due to prepreg shear deformation
δ_τ	mm	Displacement due to shear stress singularity
ε	-	Strain
γ	-	Shear strain
λ_c	-	Compliance component
η	-	Correction for adhesive thickness in the prepreg
ν_f	-	Poisson's ratio of the fibre layer
ν_m	-	fibre volume content
θ	rad	Angle
σ_{max}	MPa	Maximum Stress
τ_{al}	MPa	Shear stress in the aluminium layers
τ_f	MPa	Shear stress in the fibre layers

Abbreviations

Arall	Aluminium
CARE	Carbon Reinforced aluminium
CP	Cross-ply
BEM	Boundary Element Method
CCT	Centre Crack Tension
COD	Crack Opening Displacement
ERR	Energy Release Rate
FEM	Finite Element Method
FML	Fibre Metal Laminate
Glare	Glass Reinforced aluminium
LEFM	Linear Elastic Fracture Mechanics
L-T	Longitudinal-Transverse
PDM	Potential Drop Method
SIF	Stress Intensity Factor
T-L	Transverse-Longitudinal
TiGr	Titanium carbon laminate
UD	Uni-directional

1

Introduction



Fibre Metal Laminates were developed at Delft University of Technology as a family of hybrid materials that consist of bonded thin metal sheets and fibres embedded in epoxy [1]. Two variants were successively developed for their excellent fatigue crack propagation behaviour: Arall, containing aramid fibres, and Glare, containing glass fibres. Besides the laminates with fibres oriented in one direction, denoted as uni-directional, the laminated concept provides the possibility to insert fibre layers in any direction. An illustration of a typical cross-ply lay-up is given in Figure 1.1, where two cross-ply prepreg layers ($0^\circ/90^\circ$) are laminated between three metal layers.

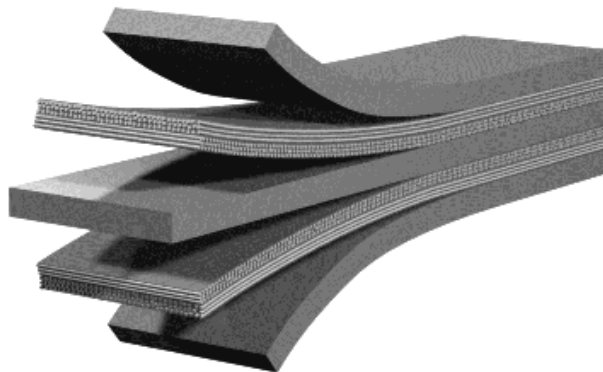


Figure 1.1 Typical lay-up for a cross-ply Fibre Metal Laminate

Extensive investigative work has been performed on the fatigue crack growth behaviour of the Fibre Metal Laminate Glare, which is close to achieve its technology readiness for application in primary aircraft structures [2]. Glare has become known for its excellent fatigue and damage tolerance behaviour, due to the

fatigue insensitive fibres present in the material [3]. The fatigue crack growth rates in Glare are not only considerably lower than for monolithic aluminium in equal loading cases, but they are also approximately constant for the major part of the fatigue life [4]. Acceleration of crack growth observed at larger crack lengths in Glare is mainly related to the finite width of panels and specimens.

In contrast to aluminium, where the fatigue life consists mainly of a long crack initiation phase and a small crack propagation phase, Glare has a shorter crack initiation life, but a remarkably longer crack propagation life. Therefore, the fatigue life of Glare consists mainly of the crack propagation phase. It is therefore worthwhile to investigate the crack propagation behaviour of Glare and cover it with validated analytical or finite element methods, to support the design of Glare structures.

Beside the excellent fatigue characteristics, the laminated layout creates also a material with good impact and damage tolerance characteristics [5]. The fibre/epoxy layers act as barriers against corrosion of the inner metallic sheets, whereas the metal layers protect the fibre/epoxy layers from picking up moisture. The laminate has an inherent high burn-through resistance as well as good thermal insulation properties.

Although several fatigue crack growth prediction methods were available in the literature, it was desirable to develop a new analytical method for the following reasons.

First, the analytic method of Marissen [6], which was developed at Delft University of Technology for Arall, could not be adapted to Glare due to differences in the crack propagation mechanisms. The characteristic crack propagation behaviour of Glare could not be captured within the method of Marissen [7].

Second, due to the development of aircrafts with the potential of Glare applications in the primary structure, the need for accurate crack growth prediction methods covering an increasing number of crack configurations became paramount.

The available empirical methods, developed for dedicated types of Glare and for small ranges of test- and geometrical conditions [8, 9], were too simplified to be extended to a broader range of FML configurations and test conditions, such as off-axis crack propagation and the effect of environmental temperature. On the other hand, several methods had been developed based on either FEM or BEM technology [10], which were convenient for material investigation purposes, but were impractical for usage during design studies [11].

Finally, attempts to adapt the available methods to describe the crack growth behaviour in part-through crack and surface crack configurations did not give satisfactory results, due to the empirical nature of the methods [12].

The major argument of this thesis is that the stress intensity at a crack tip in the metal layer of a Fibre Metal Laminate is the determining factor for the extension of that crack under cyclic loading. This means that the stress intensity at that crack tip should be determined as a function of all the fatigue crack propagation mechanisms occurring in Fibre Metal Laminates that directly affect the effective stress intensity

at that particular crack tip in the metal layer. Based on the similarity concept between the metal layers in the Fibre Metal Laminate and the monolithic metal the crack growth behaviour can be derived from the effective stress intensity factor.

The objective of the present investigation is twofold: First, to obtain a clear understanding and a detailed description and characterisation of the failure mechanisms in Glare under fatigue loading. Second, to obtain an accurate predictive method for fatigue crack propagation in Glare accounting for the described mechanisms and characteristics.

In order to gain substantial experimental evidence to support the method development for fatigue crack propagation in Glare, a large number of tests were performed. The tests consisted of constant amplitude fatigue loading of Glare specimens with through the thickness cracks loaded in-axis. The influence of starter notches, such as boreholes and saw-cuts up to lengths equivalent to accidental damage sizes was investigated.

Chapter 2 discusses the composition of and the manufacturing process for Glare. In chapter 3 a general description of the fatigue mechanisms and characteristics is given with respect to crack initiation and crack propagation, of which the through crack, part through crack and surface crack configuration will be highlighted. The mechanisms of crack bridging and delamination are discussed. Chapter 4 presents and discusses several crack growth prediction methods available from literature with respect to their assumptions, boundary conditions and validation. In this chapter the effect of applied load parameters, material- and configuration parameters are discussed. A complete overview of the experimental programmes that serve as basis for this thesis is presented in chapter 5. A new prediction method is presented in chapter 6. In this chapter, the method is also compared and validated with experimental results. The final chapter presents the conclusions and outlines the further research.

References

- [1] **Vlot, A.**, *Glare, history of the development of a new aircraft material*, Kluwer Academic Publishers, Dordrecht, The Netherlands, 2001.
- [2] **Vlot, A.**, *Towards Technology Readiness of Fibre Metal Laminates - GLARE Technology Development 1997-2000*, Proceedings of the 22nd International Congress of Aeronautical Sciences, Harrogate, United Kingdom, 1-15 (2000).
- [3] **Roebroeks, G.H.J.J.**, *Towards GLARE - The Development of a fatigue insensitive and damage tolerant aircraft material*, PhD Thesis, Delft University of Technology, Delft, 1991.
- [4] **Alderliesten, R.C., Vlot, A.**, *Fatigue Crack Growth Mechanism of Glare*, Proceedings of the 22nd International SAMPE Europe Conference, Paris, France, 41-52 (1991).

- [5] **Vlot, A., Gunnink, J.W.**, *Fibre Metal Laminates, an introduction*, Kluwer Academic Publishers, Dordrecht, The Netherlands, 2001.
- [6] **Marissen, R.**, *Fatigue Crack Growth in ARALL, A hybrid Aluminium-Aramid Composite Material, crack growth mechanisms and quantitative predictions of the crack growth rate*, PhD Thesis, Delft University of Technology, 1988.
- [7] **Alderliesten, R.C.**, *An empirical crack growth model for Fiber Metal Laminates*, Preliminary (Master) Thesis, Delft University of Technology, 1998.
- [8] **Toi, R.**, *An Empirical Crack Growth Model for Fiber/Metal Laminates*, Proceedings of the 18th Symposium of the International Committee on Aeronautical Fatigue, Melbourne, Australia, 899-909 (1995).
- [9] **Guo, Y.J. and Wu, X.R.**, *A phenomenological model for predicting crack growth in fiber-reinforced metal laminates under constant-amplitude loading*, Composites Science and Technology, **59**, 1825-1831 (1999).
- [10] **Burianek, D.A.**, *Mechanics of Fatigue Damage in Titanium-Graphite Hybrid Laminates*, PhD Thesis, Massachusetts Institute of Technology, 2001.
- [11] **Antonelli, V., Rijck, J.J.M. de**, *Initial study on crack growth modelling in FML with FE-Analysis*, TNO report, TUD-TNO, Delft, The Netherlands, 2002.
- [12] **Alderliesten, R.C., Homan, J.J.**, *Fatigue crack growth behaviour of surface cracks in Glare*, Proceedings of the first international conference on Fatigue Damage of Materials, WIT press, Southampton, UK, 213-222 (2003).

2

Fibre Metal Laminates

Abstract — This chapter gives the definition of the Fibre Metal Laminate parameters and describes the main characteristics of the Fibre Metal Laminates Arall and Glare. An overview of the manufacturing process is given and the post-stretching procedure for Arall is briefly discussed.



2.1 Introduction

Since the introduction of Arall (aluminium layers with aramid fibres), several other Fibre Metal Laminates (FML's) have been developed, such as Glare (aluminium with glass fibres) [1], CARE (aluminium with carbon fibres) [2,3] and TiGr (titanium with carbon fibres) [4,5]. Each development was driven by the need for specific or enhanced properties with respect to the predecessors. Examples are the enhanced fatigue behaviour in combination with compressive loading (Glare), higher strength and stiffness (CARE) and application of FML's at elevated temperatures (TiGr). Besides superimposing the advantages of both worlds (metals and composites), the developed FML's have their drawbacks. Examples are the poor fatigue properties of Arall in combination with compressive loading [1], the lower stiffness of Glare compared to monolithic aluminium [6] and the problem of galvanic corrosion in CARE [7]. For structural applications, these drawbacks have to be solved or require a different design philosophy.

In general, the advantage of FML's is the possibility to tailor the material to the application requirements. Depending on the application the designer has the ability to add extra layers or apply different fibre orientations. For the current FML Glare six typical grades are listed in Table 2.1.

The current investigation into fatigue crack growth behaviour focuses on Glare, which consists of aluminium 2024-T3, S2-glass fibres and the FM94 adhesive system [8]. The FML characteristics and manufacturing processes presented in this chapter are therefore mainly related to Glare, except for the post stretching process, which is applied on Arall laminates.

2.2 Material definition

Since several Glare grades with a large amount of lay-ups are possible, a clear coding system must be used to identify the Glare grade and lay-up. This coding system is important for design, production and material qualification. The cross-ply laminate illustrated in Figure 1.1 with three aluminium layers of 0.3 mm thickness is coded as: Glare 3-3/2-0.3, which refers to respectively the Glare grade, the lay-up and the aluminium layer thickness. The lay-up for this case is defined as

$$[2024-T3/0^\circ \text{ glass}/90^\circ \text{ glass}/2024-T3/90^\circ \text{ glass}/0^\circ \text{ glass}/2024-T3]$$

The Glare laminates have a symmetrical lay-up except for the Glare 3 and Glare 6 grades with an even amount of aluminium layers. In these cases, the lay-up is not symmetric due to the cross-ply prepreg layer in the middle of the laminate. However, the asymmetry for these cases and the potential unfavourable effect on the residual stress system remains very small, because the asymmetric prepreg layers are close to the neutral line of the laminate.

Table 2.1 Standard Glare grades [8]

Glare grade	Sub	Metal sheet thickness [mm] & alloy	Prepreg orientation* in each fibre layer**	Main beneficial characteristics
Glare 1	-	0.3-0.4 7475-T761	0/0	fatigue, strength, yields stress
Glare 2	Glare 2A	0.2-0.5 2024-T3	0/0	fatigue, strength
	Glare 2B	0.2-0.5 2024-T3	90/90	fatigue, strength
Glare 3	-	0.2-0.5 2024-T3	0/90	fatigue, impact
Glare 4	Glare 4A	0.2-0.5 2024-T3	0/90/0	fatigue, strength in 0° direction
	Glare 4B	0.2-0.5 2024-T3	90/0/90	fatigue, strength in 90° direction
Glare 5	-	0.2-0.5 2024-T3	0/90/90/0	impact
Glare 6	Glare 6A	0.2-0.5 2024-T3	+45/-45	shear, off-axis properties
	Glare 6B	0.2-0.5 2024-T3	-45/+45	shear, off-axis properties

* All aluminium rolling directions in standard laminates are in the same orientation; the rolling direction is defined as 0°, the transverse rolling direction is defined as 90°.

** The number of orientations in this column is equal to the number of prepreg layers (each nominally 0.133 mm thick) in each fibre layer.

2.3 Fibre Bridging

Experimental research on laminated metal sheets, showed a significant increase of the crack growth life in comparison to single metal sheets. The next step in research on the laminated metal sheets consisted of the application of fibres in the adhesive between the metal sheets, which formed the start of the development of Fibre Metal Laminates [9].

The main driver for the application of fibres between the metal layers was the objective to increase the fatigue life of materials and structures [10]. The fibres between the metal layers are insensitive to the fatigue loading, opposite to the metal layers, where cracks will initiate and propagate. The fibres transfer load over the fatigue crack in the metal layers and restrain the crack opening. This phenomenon is called fibre bridging and is illustrated in Figure 2.1.

Another phenomenon visible in Figure 2.1 is the occurrence of delamination at the interface between the metal and fibre layers in the wake of the crack. The cyclic shear stresses at the interface as result of the load transfer from the metal to the fibre layers induce delamination growth. Both the fatigue crack growth in the metal layers and the delamination growth at the interfaces form a balanced process.

For the development of structural Fibre Metal Laminates, the main keys are the crack growth behaviour of the metal layers and the delamination resistance of the fibre/adhesive layers. The choice of for instance the aluminium alloy in Glare determines for a greater part the fatigue behaviour. If the metal type is determined by other (static) requirements, the fatigue behaviour can only be influenced by controlling the delamination resistance of the fibre/adhesive layers.

Increasing the delamination resistance results in better fibre bridging and thus slower crack growth in the metal layers. However, too high delamination resistance will induce too high stresses in the fibre layers causing fibre failure. This means that control of the delamination resistance requires knowledge of the fibres and the adhesive.

The fatigue crack growth phenomenon in Glare is discussed in detail in Chapter 3.

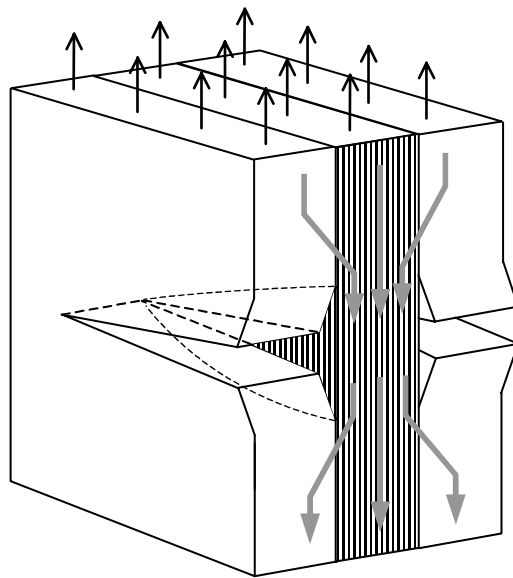


Figure 2.1 Crack bridging of the fibres and delamination of the layers [11]

2.4 Manufacturing Process

The aluminium layers in Glare have a thickness range of 0.3 – 0.5 mm and are pre-treated before being laminated into a Glare panel. This pre-treatment consists of chromic acid anodising or phosphoric acid anodising and subsequent priming with BR-127 corrosion inhibiting bond primer [12]. The fibres are delivered as a prepreg including the FM94 adhesive system [8].

The aluminium and prepreg layers are bonded together in an autoclave curing process at an elevated temperature of 120 °C at a maximum pressure of 6 bar [13]. This implies that the layers are bonded together at a high temperature and are cooled down in bonded condition. As result of the difference in coefficients of thermal expansion, given in Table 2.2 and Table 2.3, the aluminium layers want to shrink more than the prepreg layers.

Assuming rigid bond between the aluminium and prepreg layers during cooling, this results in tensile residual stresses in the aluminium layers and compressive residual stresses in the prepreg layers.

The tensile curing stresses must be incorporated in the calculation of the stresses in the aluminium layers. Following from the coefficients of thermal expansion, the tensile stresses in the aluminium layers are lower at elevated temperatures and higher at temperatures below room temperature.

Table 2.2 Mechanical properties of Aluminium 2024-T3

	Unit	2024-T3	
		L	LT
Young's Modulus	MPa	72400	
Strength at 4.7% strain	MPa	420	420
Tensile Yield Strength	MPa	347	299
Shear Modulus	MPa	27600	
Poisson's Ratio	-	0.33	
Thermal Expansion Coefficient	1/°C	22·10 ⁻⁶	

Table 2.3 Mechanical properties of the prepreg

	Unit	S2-glass, FM-73/BR127	
		L	LT
Thickness of single layer	mm	0.133	
Young's Modulus	MPa	48900	5500
Shear Modulus	MPa	5550	
Poisson's Ratio, ν_{xy}	-	0.33	
Poisson's Ratio, ν_{yx}	-	0.0371	
Thermal Expansion Coefficient	1/°C	6.1·10 ⁻⁶	26.2·10 ⁻⁶
Curing Temperature	°C	120	

2.5 Post-stretching

A method to change this unfavourable residual stress system in FML's is post-stretching (sometimes denoted as pre-straining) [14, 15]. During post-stretching of the material, the metal layers will be strained into the plastic region of the stress-strain curve, while the fibre layers remain elastic. After unloading, the residual stress system due to curing will be reduced or even reversed dependent on the amount of stretching. The mechanism of stress reversal due to stretching is illustrated with the stress strain curves in Figure 2.2.

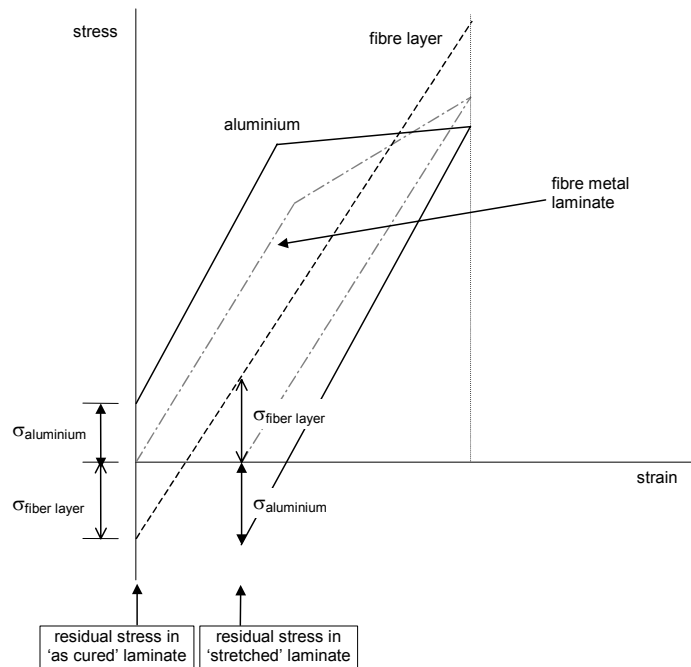


Figure 2.2 Illustration of the post-stretch process with the stress strain curves [1]

An illustration of the residual stresses in the aluminium and fibre layers of Arall is given in Figure 2.3 for room temperature and -55°C . As mentioned in the previous section, the residual stresses in the individual layers of the as cured laminate increase for decreasing temperatures, which is clearly visible in Figure 2.3. Post-stretching of 0.4% reverses the residual stresses, resulting in compressive stresses in the aluminium layers and tensile stresses in the fibre layers.

The effect of the post-stretch level on the crack growth behaviour in Glare 1 is illustrated in Figure 2.4. The effective stress cycle in the aluminium layers depends on both the stress cycle as result of the applied stress, and the residual stress level in the aluminium layer. The effective stress cycle in the aluminium layer will shift downward as result of increased stretching, resulting in lower crack growth rates.

Fatigue crack propagation and delamination growth in Glare

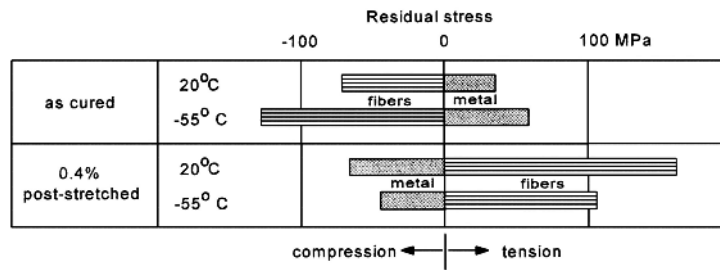


Figure 2.3 Residual stresses in the aluminium and fibre layers of Arall in the as cured conditions and after post-stretching for room temperature and -55 °C [9]

Although the post-stretching process gives enhanced fatigue characteristics, it is not used for the application of Glare skin structures. The reasons are not only related to the manufacturing costs, but also to the impossibility of post-stretching large panels. With the introduction of the splicing concept in 1995, it became possible to cure large Glare panels up to a width of 4.5 m [8]. The splice consists of aluminium sheets that end with an overlap on the next aluminium sheet, while the uni-directional fibre layers are positioned continuously over the overlap. This enables manufacturing panels larger than the limited aluminium sheet dimensions, with the same overall strength as the virgin Glare material.

However, due to the interrupted aluminium sheets in the panel, post-stretching the panel into the plastic region of the aluminium stress-strain curve is no longer possible. Stretching would load the splice without stressing in the individual aluminium layers into the plastic region.

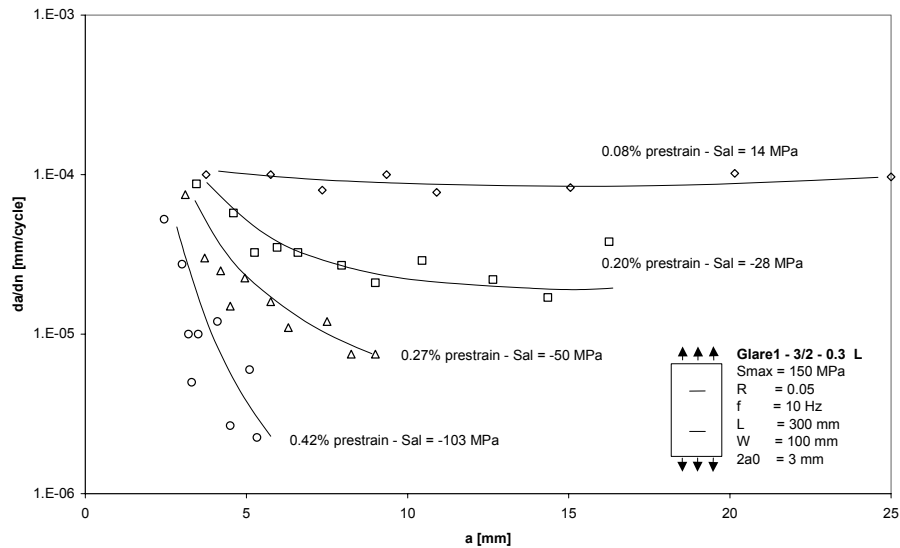


Figure 2.4 Effect of prestrain level on the crack growth behaviour [15]

On the other hand, Glare has such excellent fatigue characteristics in 'as-cured' condition that the current structural applications are designed with respect to static strength requirements, rather than the fatigue strength [16]. This means that increasing the fatigue characteristics without increasing the static strength properties, would not add any potential to the structure.

2.6 Quality Control

To verify the quality of manufactured Glare panels, the ultrasonic C-scan method is applied, because the ultrasonic is able to detect disbonds and porosities within the laminate [8,13,17]. The objective of this non-destructive testing method is to determine whether any indication of a defect can be found before application of the panel in an aircraft structure.

The defects in a Glare panel after manufacturing can be attributed to foreign material contamination, like wrapping foil, raw material contamination, such as glass splinters, or porosities or delaminations due to air inclusions. The method is also able to detect whether any positioning error has been made with splices or doublers or whether fibres are oriented in incorrect directions.

To inspect the quality of the manufactured Glare panels, rejection criteria for the ultrasonic C-scan method are necessary to determine whether the panel quality is acceptable. These rejection criteria must be obtained from an experimental programme correlating the detected defects with the static and fatigue properties of the panel.

References

- [1] **Roebroeks, G.H.J.J.**, *Towards GLARE - The Development of a fatigue insensitive and damage tolerant aircraft material*, PhD Thesis, Delft University of Technology, Delft, 1991.
- [2] **Vermeeren, C.A.J.R.**, *Ultra high modulus carbon fibres in Arall Laminates*, Memorandum M-641, Delft University of Technology, 1990.
- [3] **Vermeeren, C.A.J.R.**, *The application of carbon fibres in ARALL Laminates*, Report LR-658, Delft University of Technology, 1991.
- [4] **Medenblik, E.W.**, *Titanium fibre-metal laminates*, Master Thesis, Delft University of Technology, 1994.
- [5] **Koos, M.G. de**, *PEEK Carbon Fibre Reinforced Titanium Laminates*, Master Thesis, Delft University of Technology, 1990.
- [6] **Gunnink, J.W., Vlot, A.**, *Glare Technology Development 1997–2000*, Applied Composite Materials **9** 201–219, 2002.
- [7] **Kleinendorst, R.G.J.**, *Corrosion properties of Carbon ARALL*, Master Thesis, Delft University of Technology, 1990.

- [8] **Vlot, A., Gunnink, J.W.**, *Fibre Metal Laminates, an introduction*, Kluwer Academic Publishers, Dordrecht, The Netherlands, 2001.
- [9] **Schijve, J.**, *Fatigue of Structures and Materials*, Kluwer Academic Publishers, Dordrecht, The Netherlands, 2001.
- [10] **Vlot, A.**, *Glare, history of the development of a new aircraft material*, Kluwer Academic Publishers, Dordrecht, The Netherlands, 2001.
- [11] **Alderliesten, R.C.**, *Fatigue Crack Growth Modelling in Glare*, Proceedings of the USAF Aircraft Structural Integrity Program Conference, San Antonio, Texas, USA (2000).
- [12] *BR®127 Corrosion Inhibiting Primer*, Datasheet, Cytec Industries Inc., 2003.
- [13] **Kroon, E.**, *Influence of general quality on Glare material performance*, Report TD-R-02-007 issue 2, FMLC, The Netherlands, 2002.
- [14] **Marissen, R.**, *Fatigue Crack Growth in ARALL, A hybrid Aluminium-Aramid Composite Material, crack growth mechanisms and quantitative predictions of the crack growth rate*, PhD Thesis, June 1988, Report LR-574, Faculty of Aerospace Engineering, University of Technology Delft.
- [15] **Pegels, C.S.**, *A study on the Residual Stress of GLARE I*, Master Thesis, Delft University of Technology, 1995.
- [16] **Vries, T.J. de**, *Blunt and sharp notch behaviour of Glare laminates*, PhD Thesis, Delft University of Technology, 2001.
- [17] **Coenen, R.A.M.**, *Design of a Quality Assurance System for Structural Laminates*, PhD Thesis, Delft University of Technology, 1998.

3

Fatigue Crack Growth Phenomenon in Glare

Abstract – Fatigue initiation and crack propagation occur in the metal layers of Fibre Metal Laminates. The phenomenon of initiation and crack propagation are presented in this chapter with respect to Glare. The mechanisms are described with Linear Elastic Fracture Mechanics similar to monolithic metals, including additional effects due to the presence of the constraining fibre/adhesive layers.



3.1 Introduction

The fatigue damage that occurs in aircraft structures consists of crack initiation and crack propagation. In Fibre Metal Laminates (FML's) such as Glare initiation and propagation of fatigue cracks occur in the metal constituents, as the fibres are insensitive to the fatigue loading. Nevertheless, the fatigue initiation and crack propagation are not the only damage mode in Glare under cyclic loading, as other damage mechanisms also occur, such as delamination at the interface between metal and fibres.

The assumption is that the crack initiation and crack growth can be described with Linear Elastic Fracture Mechanics (LEFM) as has been developed for monolithic metals, but taking into account the contribution of the fibre layers and the occurrence of delamination of layers.

The difference between the crack growth behaviour of the aluminium layers in Glare and monolithic aluminium can be attributed to the presence of the fibre layers. However, the contribution of the fibre layers to the crack initiation behaviour and the crack propagation behaviour is different.

In case of fatigue initiation, there is no fibre bridging effect, but the stiffness of the fibre layers and the residual stress as result of curing determine the actual stress in the aluminium layers. These actual stresses are higher than the applied stresses in case of Glare, as a result of which the crack initiation life is shorter compared to monolithic aluminium.

These actual stresses in the metal layers change once an initiated fatigue crack starts propagating, because the fibres remain intact and bridge the cracks. The favourable effect of the bridging fibres results in a significant increase of the crack propagation life compared to monolithic aluminium. Despite the shorter crack initiation life, the overall fatigue life of Glare is significantly longer than monolithic aluminium under equal applied loads.

The difference in fatigue life for monolithic aluminium and Glare is illustrated in Figure 3.1. For monolithic aluminium, the main part of the fatigue life consists of the crack initiation phase, while the crack propagation phase covers a few percent of the fatigue life, depending on the maximum stress level [1]. Due to the better crack growth properties of Glare, the fatigue life of Glare consists mainly of the crack propagation phase [2, 3].

In this chapter the fatigue initiation and the crack propagation behaviour of Glare are discussed and the differences in characteristics for the two phases is explained.

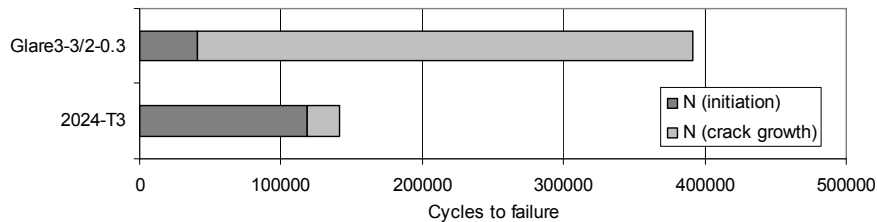


Figure 3.1 Illustration of the initiation life and the crack propagation life of monolithic aluminium and Glare 3-3/2-0.3[3,4]

3.2 Fatigue initiation

Fatigue crack initiation in monolithic metals can be divided in crack nucleation and micro crack growth. Because the mechanism of crack nucleation and micro crack growth are material surface phenomena, these mechanisms in the metal layers of Glare do not differ from the mechanisms in monolithic metals. Therefore, the basic mechanisms for crack initiation in aluminium are not discussed here in detail. For this topic, the reader is referred to the literature, e.g. [1]. This section focuses on the difference between the crack initiation behaviour of FML's and monolithic metals in general.

Although the statement that crack initiation occurs in the metal layers only is in general correct and for the methodology sufficient, it should be noted that a more correct statement would be, that crack initiation affects mainly the aluminium layers in Glare. For orthotropic laminates, the stresses around a notch are different compared to isotropic monolithic materials and depend on the orientation of the fibre layers. Due to the presence of orthotropic fibre layers in Glare, the stresses in the isotropic aluminium layers are also different, resulting in stress concentrations at different locations compared to monolithic aluminium. Fatigue crack initiation occurs at locations at the notch contour with stress concentrations.

3 Fatigue Crack Growth Phenomenon in Glare

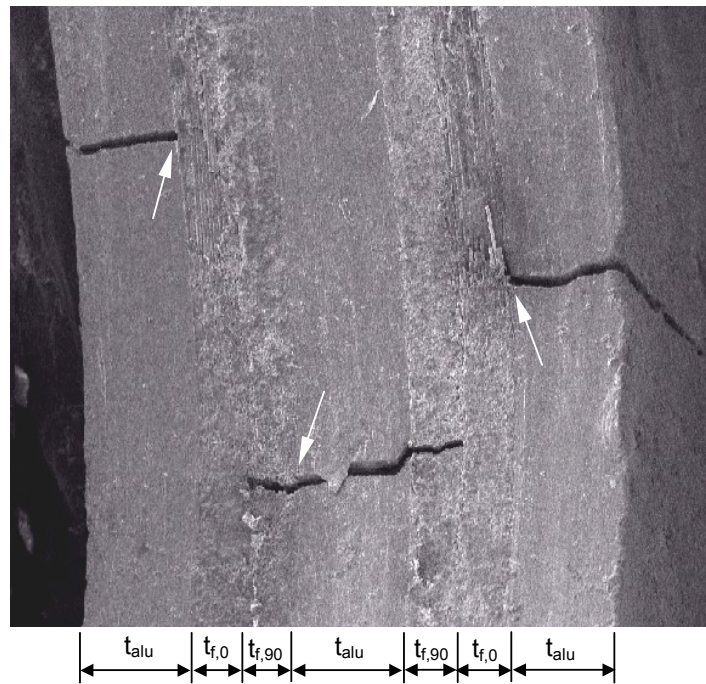


Figure 3.2 Crack initiation locations at the notch contour of a Glare 3-3/2-0.3 open hole specimen after cracks have reached the crack propagation phase [6]. Arrows indicate initiation location.

For monolithic materials crack initiation most often occurs at the notch root, since the stress concentration is at the maximum at the notch root. For Glare the stress concentration is not necessarily the maximum at the notch root, as was shown by Vašek et al [5]. In the aluminium layers of Glare, the crack initiation location at the blunt notch contour can be located a small distance away from the notch root and depends on the adjacent fibre/adhesive layers. Vašek stated that the crack in an aluminium layer adjacent to a prepreg layer with fibres in loading direction tends to initiate in the area close to the notch root where the fibres are cut during milling the notch. This finding was supported by the results obtained by Kieboom [6], who performed fatigue crack initiation tests on Glare specimens. An illustration of the crack initiation locations at the notch contour, obtained from his experiments, is given in Figure 3.2. In this figure, it can be seen that the maximum distance between the initiation locations is small (less than 1 mm). However, Vašek investigated the effect of the notch radius and the maximum applied stress on the location of initiation and observed that the distances between the initiation locations increase for increasing maximum stresses.

Furthermore, the presence of a matrix with fibres perpendicular to the loading direction will induce matrix cracking parallel to crack initiation in the metal layers, see Figure 3.2. Whether such matrix cracking occurs prior to the crack initiation in

the metal layers or as result of crack initiation, has not been reported in the literature. In the latter case, the effect of matrix cracking with respect to crack initiation can be ignored, but in case the matrix cracking occurs prior to crack initiation, it can have an influence on the crack initiation behaviour. However, since the fibre layers perpendicular to the loading direction carry only a small part of the load, it is believed that matrix cracking only affects the crack initiation location, but not the crack initiation life. Therefore, in the following description of the crack initiation mechanism in Glare this phenomenon is disregarded.

The fatigue initiation mechanism in Glare can be treated similar to that of monolithic metals if a similarity approach is used [7]: A similar stress state in the aluminium layers in Glare and in monolithic material gives the same result, i.e., the same crack initiation life. The crack initiation behaviour of the aluminium layers in Glare can therefore be compared to the behaviour in monolithic aluminium if the stress conditions are equivalent for both materials. With respect to the stress conditions in the metal layers of Glare, this means that the actual stresses in the particular layers should be known as function of the applied stresses, but also the stress concentration factor. Stress concentration factors for the aluminium layers in Glare can be a few percent higher or lower than monolithic aluminium depending on the laminate lay-up and the loading direction. The equations to calculate the stress concentration factor for the aluminium layers in Glare are given in [4].

The actual stresses in the aluminium layers in Glare consist of static residual stress due to the curing process and stresses due to the external loading [8], see Figure 3.3. The residual stress due to curing depends on the lay-up and laminate type of Glare.

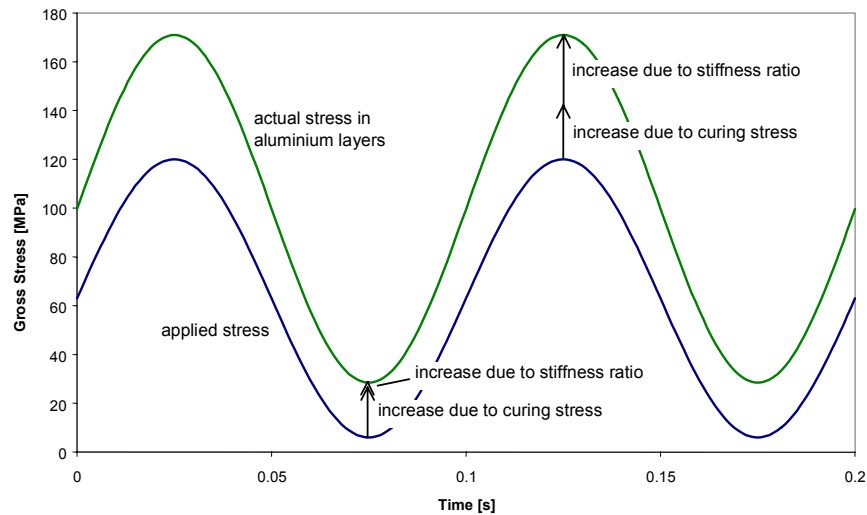


Figure 3.3 The stress cycle in the aluminium layers in Glare 3-3/2-0.3 L is a superposition of the stress cycle induced by the applied stress and the curing stress [6].

The actual stresses in the aluminium layers are determined by the different stiffnesses of the constituents of Glare. Because the material stiffness of aluminium is larger than the stiffness of the glass fibre/epoxy, the stresses in the aluminium layers are higher than the applied stresses.

By superposition of the curing stresses and the calculated stresses the actual stresses in the aluminium layers of Glare are obtained, see Figure 3.3. The approach to calculate the actual stresses in the aluminium layers of Glare is described in [4].

Once the actual stresses in the metal layers are known, the crack initiation life can be determined from monolithic aluminium [6,7]. However, in the literature only S-N data, consisting of the number of cycles to failure, are given for monolithic aluminium.

The engineering approach proposed in [4] is based on the assumption that if the crack initiation life is defined as the life until a crack reaches 1 mm, the initiation life will consist of at least 95% of the total fatigue life [1]. This means that the S-N data can be recalculated to S-N_i data for initiation.

The second assumption on which this proposed approach is based, is that the stress concentration factors are applicable as in monolithic metals disregarding the small difference due to the presence of orthotropic fibre layers. The fatigue initiation life in the aluminium layers of Glare (crack reaches 1 mm) can then be determined using the S-N_i data with the actual stress in the aluminium layers.

3.3 Fatigue crack propagation

With respect to the fatigue crack propagation mechanism, two major mechanisms can be distinguished: crack propagation in the aluminium layers and delamination growth at the interface between the aluminium and fibre layers. From the crack propagation and delamination growth observed in experiments, it is concluded that both mechanisms are in balance with each other [3].

As mentioned before, the crack growth behaviour is described with Linear Elastic Fracture Mechanics. This means that the crack growth rate in the aluminium layers is related to the stress intensity factor, in a similar way as for monolithic aluminium. To predict the crack propagation behaviour, the stress intensity factor at the crack tip in the aluminium layers must then be described by physically explainable parameters.

This principle is only valid when the stress intensity factor is described at the crack tip in the individual aluminium layers. This means that the stress intensity factor cannot be described based on the overall laminate properties and stresses, similar to monolithic aluminium, where one can write for an infinite sheet

$$K = S_{\text{applied}} \sqrt{\pi a} \quad (3.1)$$

The stress intensity factor must describe the actual stress state at the crack, which includes the contribution of the bridging fibres and the delamination at the interface.

A significant amount of stress is transferred from the aluminium layers to the fibre layers, which stay intact over the crack, restraining the crack opening displacement. As a consequence, less load needs to be transferred around the crack tip in the aluminium layers, resulting in a lower stress intensity factor.

During propagation of the fatigue cracks in the aluminium layers, a continuous redistribution of the stresses in each layer and shear stresses at the interfaces occurs. As a result of this redistribution, the stress intensity factor remains approximately constant during crack growth for the major part of the crack propagation life.

The fibre bridging mechanism depends on several laminate parameters, such as the stiffness and thickness of each individual layer, the number of metal/fibre interfaces, the direction of each fibre/adhesive layer with respect to the loading direction, and the applied loading [2, 3, 9, 10]. The behaviour is also dependent on the occurrence of (secondary) bending [11], on crack configurations, such as surface or part through cracks [12] and on the environmental temperature [13].

Delamination growth is a process where the layers adjacent to the cracked aluminium layers delaminate due to the cyclic shear stresses that occur, because of stress transfer between the aluminium and fibre layers [14]. Due to the separation of the individual layers in the delamination area no stress redistribution between the layers is possible. Only stress relaxation in the layer itself may occur.

The advantage of delamination growth is the fact that the length over which the bridging fibres are elongated increases. As a consequence, decreasing strains and stresses in the fibres, preventing fibre failure.

In the following sections, the major mechanisms will be discussed in more detail.

3.3.1 Crack bridging and restraint on crack opening

The fatigue insensitive glass fibres transfer a significant part of the load over the crack and restrain the crack opening, as is shown in Figure 2.1. As result of the restraining fibres, the crack opening in Glare is smaller as compared to monolithic aluminium. The amount of load that is transferred around the crack in the aluminium layers is smaller, due to the load transfer through the fibres over the crack.

This means that the stress intensity factor at the crack tip in the aluminium layers in Glare is substantially smaller compared to cracks in monolithic aluminium with equal length, where the entire load has to be transferred around the crack tip.

During the main part of the fatigue crack growth life the stress intensity factor at the crack tip in the aluminium layers of Glare remains practically constant. Increase of the crack length does not have the same effect on the behaviour of Glare, as is the case for monolithic aluminium.

Previous research revealed that the magnitude of the bridging stresses in the fibres is related to the crack opening displacement and the length over which the fibres are elongated [14]. For a given delamination length, increasing the crack opening displacement means increasing the fibre strain and thus increasing the fibre bridging stresses. On the other hand, increasing the delamination length over which the fibres are elongated lowers the strain, resulting in a reduction of the bridging stresses.

Crack bridging will become fully effective after a certain crack length is reached, which means, after the crack opening displacement reached a certain magnitude. Small crack opening means low strain in the fibres and as a consequence low bridging stress. Therefore the fibre bridging and the restraint on crack opening will be small for small crack lengths, but will become effective after the crack length reaches a certain size [1,3].

Marissen [14] derived from the relation between the crack opening contour and the elliptical delamination shape that the fibre bridging stress over the whole crack length is constant. The argumentation for a constant bridging stress was, that a local increase of bridging stress would imply a local increase of delamination growth reducing that bridging stress, which seemed to be convincing at that time. However, this argumentation only holds for the balance between the bridging stress and the delamination growth at a particular location and does not justify the assumption of a constant bridging stress along the crack length.

Furthermore, the fact that the delamination length and the crack opening are zero at the crack tip, means that the bridging stress according to the definition of Marissen is also zero at the crack tip. This indicates that whatever the bridging stress distribution is along the crack length, it has to decrease to zero at the crack tip.

Guo and Wu [15] presented a method to calculate the bridging stresses along the crack length based on the delamination shape. Their calculations and experiments show that the bridging stress for an elliptical delamination shape is approximately constant along the crack, while the bridging stress for a triangular delamination shape increases towards the crack tip, see Figure 3.4. However, both bridging stresses have in common that they drop to zero at the crack tip.

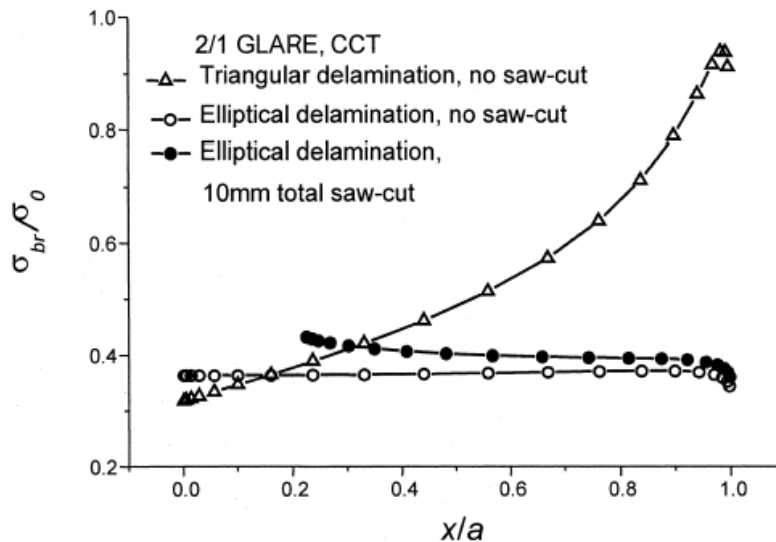


Figure 3.4 Bridging stress distributions in centre crack tension Glare specimens calculated by Guo and Wu [15]

For large crack lengths, it is often assumed that the crack opening remains constant along the crack, except for the locations near the crack tip, where the effect of the stress intensity, due to adhesive shear deformation and reduction of bridging stresses, is more dominant than at the crack centre [14,16]. However, as will be discussed in the following chapters, the crack opening remains not constant along the crack length, but gradually increases towards the crack centre.

3.3.2 Delamination of layers

According to Marissen [14] the crack opening during the crack propagation phase occurs due to two factors:

- Fibre elongation in the delamination area, see Figure 3.5 (a)
- Adhesive shear deformation, see Figure 3.5 (b)

Guo and Wu [15] also mentioned the deformation of the metal layer, see Figure 3.5 (c), but ignored its contribution as it is very small compared to the other two factors.

A consequence of the bridging stresses in the fibres transferring load over the crack is the presence of cyclic shear stresses at the interface between the aluminium and the fibre layers. Due to these cyclic shear stresses, delamination growth occurs at the interface between the metal and fibre layers.

The magnitude of the cyclic shear stresses is determined by the material and loading parameters, such as the thickness and stiffness of the individual layers, the lay-up, the fibre orientation in the prepreg, and the minimum and maximum applied stress. In addition to the level of these cyclic shear stresses, the delamination growth rate depends on the delamination resistance of the prepreg. Increasing the delamination resistance provides better fibre bridging [14].

When the crack in the aluminium layer opens, the fibres are elongated over the delamination length. This means for a given crack opening, that the delamination length determines the strain and thus the stress in the fibre layers, as visualised in Figure 3.5. Large delamination lengths result in small bridging stresses, with small cyclic shear stresses at the interface inducing small delamination growth rates. In other words, the delamination growth rate and the bridging stress are in balance, continuously influencing each other.

The bridging stress also contributes to the stress intensity factor at the crack tip in the aluminium layers, which determines the crack growth rate. High bridging stresses along the crack result in low stress intensities at the crack tip and thus small crack growth rates.

This means that the fatigue crack growth mechanism in Glare is characterised by the processes of crack growth in the aluminium layers and delamination growth at the interfaces, which continuously influence each other.

The ratio between crack length and delamination length depends on the laminate lay-up and on the crack growth characteristics of the aluminium and the delamination resistance of the prepreg.

3 Fatigue Crack Growth Phenomenon in Glare

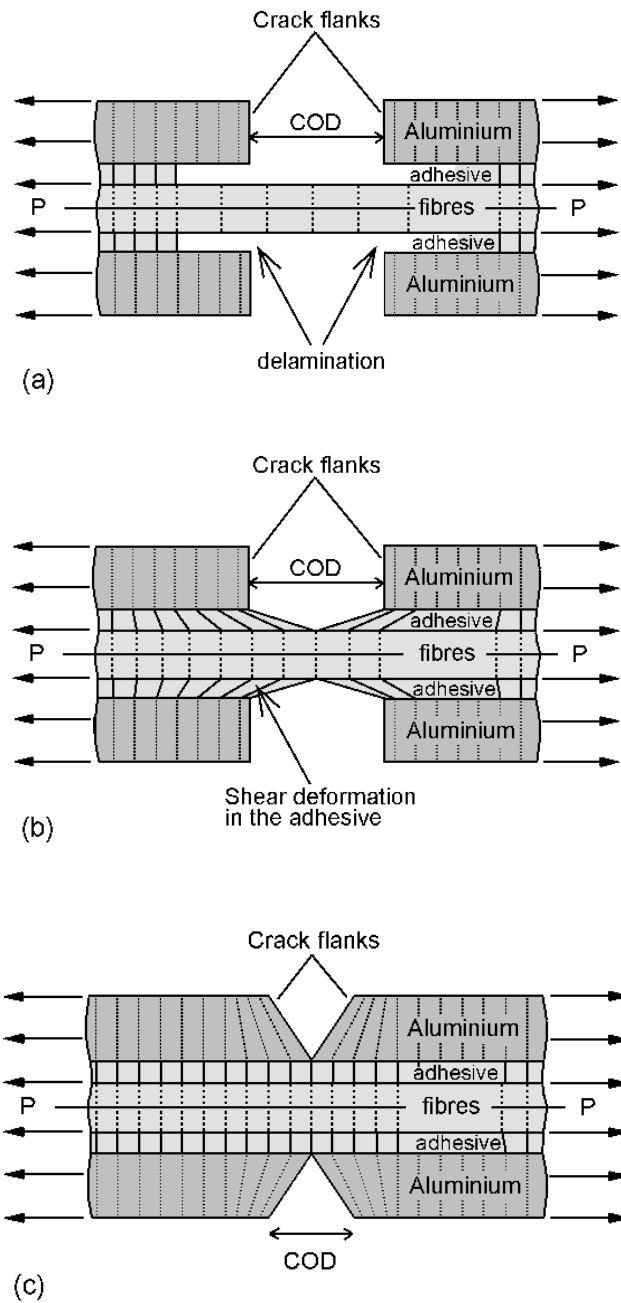


Figure 3.5 Crack opening displacement due to delamination (a), adhesive shear deformation (b) and metal layer deformation (c)

3.3.3 Adhesive shear deformation

Besides the elongation of the fibres, Marissen attributes a part of the crack opening to the deformation of the adhesive rich layers in the prepreg in Arall. Due to the fibre bridging, the load has to be transferred from the aluminium layers to the fibre layers, through the interface. This results in shear stresses at the interface, inducing shear deformation of the adhesive rich layer.

Marissen concluded that in the ideal situation of an infinitely stiff adhesive between the layers, the crack opening and the stress intensity factor would be zero for a laminate without a starter notch and without delamination. However, in the actual situation due to local shear deformation of the adhesive, some crack opening will occur. This is schematically represented in Figure 3.5 (b). As result of the slightly opened crack, the stress intensity factor in the aluminium layers is no longer zero. In the case that linear elastic material is assumed, the crack opening is proportional to the bridging stress. Along the crack away from the crack tip the crack opening is constrained by the deformation field as illustrated by Figure 3.5 (b). However, the situation near the crack tip is dominated by the stress intensity field [14], where the crack opening displacement and the bridging stresses decrease to zero at the crack tip, as mentioned in the previous section.

In the above discussion, the effect of delamination was neglected. If delamination of the layers occurs, the length over which the fibres will be elongated increases, resulting in lower fibre stresses. The situation however, will be qualitatively the same.

3.3.4 Effect on fatigue performance of Glare

The fatigue crack growth behaviour of Glare was described with the stress intensity factor approach in a qualitative way. The argument of this thesis is that the stress intensity factor at the crack tip determines the crack growth rate in the aluminium layers. Control of the stress intensity factor means control of the crack growth rates in the Glare material.

The stress intensity factor at the crack tip can be reduced by [14]

- Increasing the stiffness of the fibre layers. This can be obtained by applying fibres with a higher Young's modulus, or by increasing the fibre layer thickness or by increasing the fibre volume fraction within the prepreg. The bridging stresses in these cases will be higher at the same crack opening displacement.
- Decreasing the stiffness of the aluminium layers, by decreasing the thickness of the aluminium layers. This option is the opposite of the previous option.
- Increasing the delamination resistance. The delamination areas will be smaller, resulting in higher bridging stresses and thus lower stress intensities.
- Increasing the adhesive or prepreg shear stiffness, which restrains the crack opening more and lowers the stress intensity at the crack tip.

In general, the fatigue characteristics of Glare can be enhanced by optimisation of the laminate with respect to fibres and adhesives in combination with the laminate lay-up.

3.4 Fatigue crack geometries in Glare

In monolithic aluminium aircraft structures, it is known that fatigue cracks initiate as corner cracks at holes or as surface cracks from scratches. This also holds for Glare structures, but due to the laminated composition of the material, the crack propagation will be different, since the cracks will not grow through the thickness in the same way, as is the case for monolithic aluminium. The difference in crack growth between monolithic and laminated materials was shown by Schijve [1].

Therefore, with respect to fatigue crack propagation in Glare, several crack geometries can be observed. Crack initiation from a scratch in a Glare laminate propagates through the thickness of the outer surface layer, but due to the fibres/adhesive layer, which acts as a barrier, the crack will not initiate immediately in the next aluminium layer. This crack configuration is depicted in Figure 3.6 (a) and will be denoted from here on as surface crack configuration.

The part through crack configuration, see Figure 3.6 (b), occurs at open or pin loaded holes, under combined tensile and bending loading. Examples are the mechanically fastened joints where secondary bending will induce part through cracks. Part through cracks can also occur when a surface crack causes crack initiation in the subsurface layers.

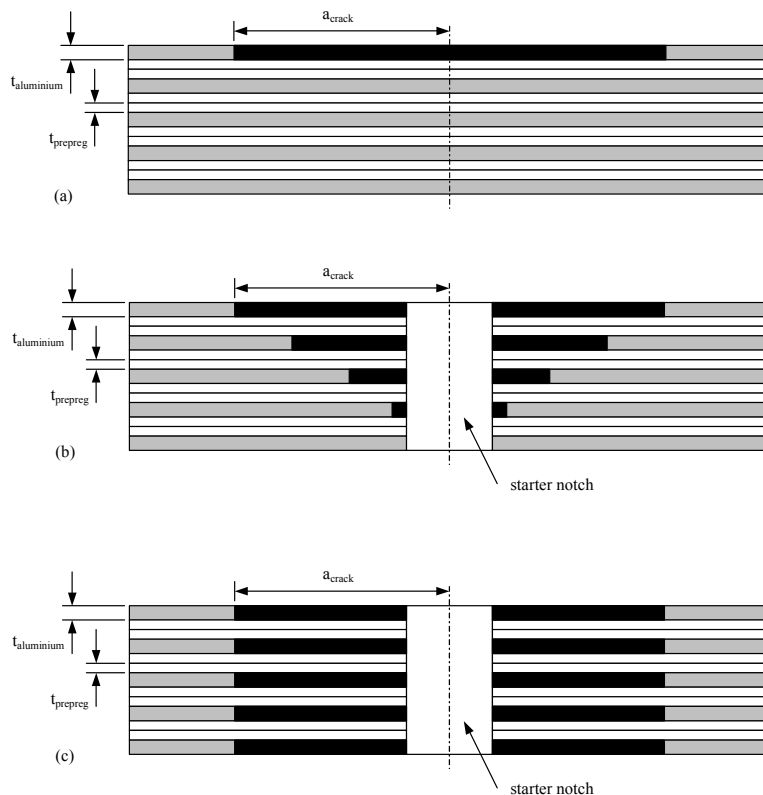


Figure 3.6 Most significant fatigue crack scenarios in fibre metal laminates

The worst crack geometry is the through crack configuration where the cracks have initiated and propagated in all aluminium layers, Figure 3.6 (c). The current investigation into crack propagation and delamination growth in Glare focuses on this crack geometry, which occurs when loading flat panels in cyclic tension. Because the outer aluminium layers are supported on one side by the fibre layers, while the inner aluminium layers are supported on both sides, the actual crack lengths vary through the thickness of the laminate. However, the main assumption for the current investigation is that the cracks in the through crack configuration in Glare have the same length in all layers. This assumption has been investigated for Glare 3-5/4-0.3 in [17] and appeared to be quite accurate.

3.4.1 Surface cracks in Glare

The definition of surface cracks in fibre metal laminates is that only one outer layer contains a crack, initiated either from a scratch, Figure 3.6 (a), or from a notch. The main characteristic of this crack configuration in Glare is that the effect of fibre bridging as discussed in the previous section, is extended in the form of 'laminar bridging'. The outer aluminium surface layer is supported by the rest of the intact laminate, reducing the stresses in the cracked layer significantly. Gonesh [12] suggested that this crack configuration could be treated with the Rose model [18] as a cracked aluminium sheet containing a bonded Glare reinforcement.

As can be seen in Figure 3.6 (a), the surface crack configuration is asymmetric. Theoretically, this will add stresses in the layers due to secondary bending. From the experimental investigation reported in [12], it was found that the effect depends on the laminate thickness and the crack length.

For thick laminates (minimum 4/3 lay-up) the shift in the neutral axis of the laminate induced by the cracked outer aluminium layer with a maximum thickness of 0.5 mm, is small and the corresponding secondary bending is of such a small magnitude that it can be neglected.

The crack length relative to the size of the structure has also an influence on the amount of secondary bending. The illustration in Figure 3.6 is a 2-dimensional representation of the crack configuration, which is representative for large crack lengths. Small surface crack lengths induce locally only a small shift of the neutral axis, which has a negligible bending effect on the stress intensity at the crack tip.

3.4.2 Part through cracks in Glare

The part through configuration is not unambiguous, since this type consists basically of all the crack configurations in Glare that do not belong to the through crack and the surface crack configuration. The nature of a part through crack depends on the cause of the crack in the structure.

Part through cracks can initiate at a hole under combined bending-tension loading, causing initiation in the subsequent layers in order of load level. This type of part through crack is given in Figure 3.6 (b). Such a part through crack will propagate

into a through crack configuration where the cracks do not have equal lengths in each individual layer, due to the difference in sheet stresses as result of the bending load [19]. The majority of the part through crack cases occurs in mechanically fastened joint structures, where secondary bending occurs induced by the eccentricity of the joint.

To describe the crack growth in Glare joints accurately, goes beyond the description of propagating part through cracks under combined bending tension. Additional issues as for instance the presence of high pin loads due to the load transfer by the fasteners from one mating surface to the other, the occurrence of joint curvature, the quality of fastener instalment must be incorporated as well [8]. Methods were developed for determining the load transfer [20], to model the joint bending [21-23] and extensive research is performed on the fatigue crack growth in riveted monolithic and Glare joints [22, 24]. On the other hand, the crack growth in joints cannot be fully understood without the knowledge of the part through crack growth under combined bending and tension loading.

Another possible part through crack configuration is a surface crack initiated from a scratch in the outer layer that causes crack initiation in the subsurface aluminium layers after reaching a certain length. In this case, applied bending loading is not necessarily present. However, secondary bending might play a role in such cases due to the neutral axis shifting in the thickness direction over the cracked layers.

3.4.3 Through cracks in Glare

The through crack configuration is the geometry of fatigue cracks in all aluminium layers of Glare. As mentioned before, the cracks in the aluminium layers have in practice not always the same length. The inner metal layers show a slight delay in crack growth with respect to the outer metal layers, because the outer layers are supported at one side only by bridging fibres, while the inner layers are supported at both sides. The difference between the crack lengths of the outer and centre aluminium layers in Glare 3-5/4-0.3 has been investigated by Takamatsu et al. [17]. They reported that for short cracks the crack lengths in the middle aluminium layer was about 8% shorter than the outer aluminium layer, and about 2% for large crack lengths. This seems to justify the assumption of equal crack lengths in all layers, especially when taking into account that this approach is conservative if the generalised crack length is taken equal to the crack in the outer aluminium layer.

It is also assumed that the fibre layers remain intact during crack propagation, which is proven to be valid if glass fibres are applied, but was not correct for aramid fibres at low stress ratios [14, 25].

From the qualitative discussion in this chapter, it becomes clear that material, geometrical and loading parameters play an important role in the crack propagation mechanism of Glare under fatigue loading conditions. Depending on the structural application and loading cases different crack geometries occur in Glare.

To understand the basic fatigue crack growth mechanism in Glare and to develop an analytical crack growth prediction method describing the occurring mechanisms,

one has to start with a simple generic fatigue crack geometry. For this reason, the current investigation focuses on the centre crack tension configuration and to avoid any effect of the presented asymmetric crack geometries, only the through crack configuration is concerned. It is assumed that the generalised crack length is equal to the crack length in the outer aluminium layers. Corresponding to this assumption it is furthermore assumed that the delamination areas at the interfaces between all aluminium and fibre layers are identical as well.

References

- [1] **Schijve, J.**, *Fatigue of Structures and Materials*, Kluwer Academic Publishers, Dordrecht, The Netherlands, 2001.
- [2] **Alderliesten, R.C.**, *An empirical crack growth model for Fibre Metal Laminates*, Preliminary (Master) Thesis, Delft University of Technology, 1998.
- [3] **Alderliesten, R.C.**, *Development of an empirical fatigue crack growth prediction method for the Fibre Metal Laminate Glare*, Masters Thesis, Delft University of Technology, 1999.
- [4] **Homan, J.J.**, *Fatigue Initiation in Fibre Metal Laminates*, International Journal of Fatigue, submitted 2004.
- [5] **Vašek, A., Polák, J., Kozák, V.**, *Fatigue crack initiation in fibre-metal laminate GLARE2*, Materials Science and Engineering, A234-236, 1997.
- [6] **Kieboom, O.T.**, *Fatigue Crack Initiation and Early Crack Growth in Glare at different temperatures*. Master Thesis, Delft University of Technology, 2000.
- [7] **Homan, J.J., Schra, L.**, *Application of aluminium alloy 2024-T3 fatigue life data to Glare laminates, GTP Methods Projects 2.4.3.2-B, 2.4.3.3-B and 2.4.3.4-B*, Report NLR-CR-2001, National Aerospace Laboratory NLR, 2001.
- [8] **Vlot, A., Gunnink, J.W.**, *Fibre Metal Laminates - An introduction*, Kluwer Academic Publishers, Dordrecht, The Netherlands, 2001.
- [9] **Gonesh, K.A.M.**, *Test results and evaluation of crack propagation in off-axis Glare*, Test Report, Report B2V-01-24, Delft University of Technology, 2001.
- [10] **Gonesh, K.A.M.**, *Off-axis fatigue crack propagation. Additional crack propagation tests*, Test Report, Report B2V-02-02, Delft University of Technology, 2002.
- [11] **Pellenkoff, F.J.**, *Secondary Bending in Glare, Investigation on the elastic behaviour and crack propagation in Glare loaded by combined tension and bending*, Master Thesis, Delft University of Technology, 2000.
- [12] **Gonesh, K.A.M.**, *Development of a fatigue crack growth model for surface cracks in GLARE*. Master Thesis, Delft University of Technology, 2000.

- [13] **Bär, H.**, *Verifikation und Ergänzung von Berechnungsmethoden für die statische und dynamische Auslegung von Glare-Strukturen*, Diplomarbeit, Institut für Flugzeugbau der Universität Stuttgart, 1992.
- [14] **Marissen, R.**, *Fatigue Crack Growth in ARALL, A hybrid Aluminium-Aramid Composite Material, crack growth mechanisms and quantitative predictions of the crack growth rate*, PhD Thesis, Delft University of Technology, 1988.
- [15] **Guo, Y.J., Wu, X.R.**, *Bridging stress distribution in center-cracked fiber reinforced metal laminates: modelling and experiment*, *Engineering Fracture Mechanics*, **63** 147-163, 1999.
- [16] **Cox, B.N.**, *Life prediction for bridged fatigue cracks, Life prediction methodology for Titanium Matrix Composites*, ASTM STP 1253, W.S. Johnson, J.M. Larsen and B.N. Cox, Eds. American Society for Testing and Materials, 552-572, 1996.
- [17] **Takamatsu, T., Matsumura, T., Ogura, N., Shimokawa, T., Kakuta, Y.**, *Fatigue crack growth properties of a GLARE 3-5/4 Fiber Metal Laminate*, *Engineering Fracture Mechanics* **63** 253-272, 1999.
- [18] **Rose, L.R.F.**, *An application of the inclusion analogy for bonded reinforcements*, *International Journal of Solid Structures*, **17** 827-838, 1981.
- [19] **Mortier, W., Homan, J.J.**, *Crack propagation in surface cracks and part-through cracks*, Report B2V-02-31, Delft University of Technology, 2002.
- [20] **Jarfall, L.**, *Shear loaded fastener installations*, SAAB-SCANIA, report KHR-3360, 1983.
- [21] **Schijve, J.**, *The influence of the dimensions of riveted lap joints and strap joints on the secondary bending*, NLR, Report NLR TR 68026 LI, 1968.
- [22] **Müller, R.P.G.**, *An Experimental and Analytical Investigation on the Fatigue Behaviour of Fuselage Riveted Lap Joints*, Ph.D. Thesis, Delft University of Technology, 1996.
- [23] **Rijck, J.J.M. and Fawaz, S.A.**, *A Simplified Approach for Stress Analysis of Mechanically Fastened Joints*, Proceedings of the Fourth Joint DoD/FAA/NASA Conference on Aging Aircraft, St Louis, 2000.
- [24] **Fawaz, S.A.**, *Fatigue crack growth in riveted joints*, Ph.D. Thesis, Delft University of Technology, 1997.
- [25] **Roebroeks, G.H.J.J.**, *Towards GLARE - The Development of and Fatigue Insensitive and Damage Tolerant Aircraft Material*, PhD thesis, Delft University of Technology, 1991.

Fatigue crack propagation and delamination growth in Glare

4

Fatigue in FML Modelling Approaches from Literature

Abstract – This chapter provides an overview of the relevant modelling approaches for fatigue crack propagation in Fibre Metal Laminates obtained from the literature. The approaches, consisting of empirical, phenomenological, analytical and Finite Element methods, are discussed in this chapter with respect to their applicability on fatigue crack growth in Glare.



4.1 Introduction

Since the development of Fibre Metal Laminates, several authors [1-31] have published their research on fatigue crack growth investigation of Arall and Glare and have presented methods to describe the fatigue crack growth behaviour. Within The Netherlands, a large research program has been performed to generate sufficient amount of fatigue crack growth data on Glare Centre Crack Tension specimen varying several material-, geometrical- and loading parameters to develop an accurate prediction model.

The prediction methods available from the literature have been evaluated using the test data generated within this research program, and are discussed in this chapter with respect to applicability, assumptions and findings. For the current discussion, the prediction methods are divided into three categories: phenomenological methods, analytical methods and Finite Element/Boundary Element methods.

These methods are summarised and compared in this chapter to provide a reference framework for the research described in chapters 5 and 6.

4.2 Phenomenological methods

4.2.1 Method of Toi

An empirical method has been developed by Toi [1] based on the assumption that one correction factor β_{FML} is sufficient to correct the monolithic aluminium stress intensity factor equation in the case it is applied on Glare. In formula form this gives

$$\Delta K_{Glare} = \beta_{FML} \Delta K_{alum} = \beta_{FML} \beta_{geom} \Delta S_{applied} \sqrt{\pi a} \quad (4.1)$$

where β_{geom} is the geometrical correction factor usually described by the Dixon, Feddersen, or similar relations. The applied stress in equation (4.1) is the applied stress calculated over the total laminate thickness. This means that Toi treats the Fibre Metal Laminate as a monolithic metal structure, which implies that all the characteristic fatigue characteristics of Glare, discussed in chapter 3, are incorporated in one correction factor β_{FML} . The method to determine this factor is illustrated in Figure 4.1, where ΔK_{lam} is equal to ΔK_{Glare} in equation (4.1).

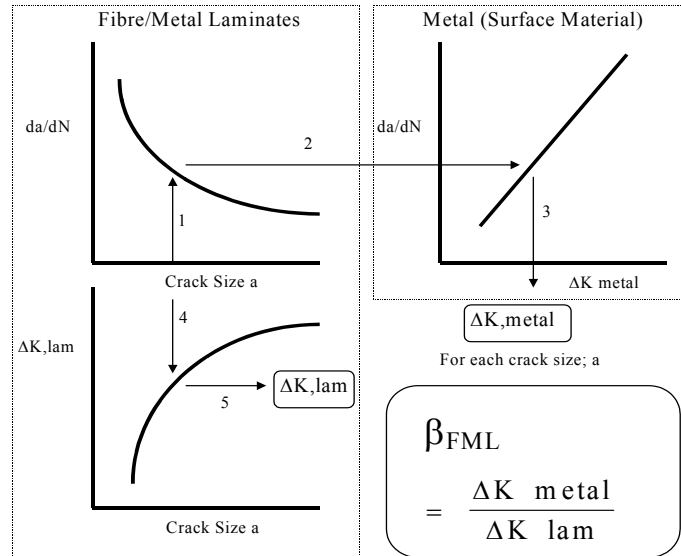


Figure 4.1 Approach to determine the bridging factor β_{FML} according to Toi [1]

According to his results the correction factor is a function of the crack length only and does not depend on any other loading or geometrical parameter. The dependency of the correction factor on the crack length was described by Toi using a polynomial fit function of the shape

$$\beta_{FML} = \frac{A}{a^3} + \frac{B}{a^2} + \frac{C}{a} + D \quad (4.2)$$

where the parameters A-D were determined for Glare 2, Glare 3 and Glare 4 centre crack specimens containing through the thickness fatigue cracks. The dependency of the correction factor on the lay-up, i.e. the number of aluminium and fibre layers, was not incorporated or the factor was assumed to be insensitive to the lay-up. As Toi only tested only one lay-up for Glare 2 and Glare 4 and only two lay-ups for Glare 3 he could not determine such dependency on the lay-up.

However, several authors [2,3] have shown that this approach is in general inapplicable, as the correction factor β_{FML} is dependent on many parameters related to the loading and crack configuration in Glare, which are not quantified. Although Toi states that crack growth results from several experiments tested at different maximum applied stress levels fall along one functional line, the experimental results from [2,3] show a significant dependency of β_{FML} on the applied stress level. Takamatsu [4] incorporated this dependency in the method of Toi using the following fit function

$$\beta_{FML} = C_0 + C_1 \ln a + C_2 \sigma_{max} \quad (4.3)$$

Takamatsu determined this relationship and the value of C_0 , C_1 and C_2 on the results from tests at three different maximum applied stress levels at one stress ratio R . However, if the maximum applied stress level affects the correction factor significantly, the stress ratio most likely will have its influence as well, limiting the validity of equation (4.3) to the stress ratio R used by Takamatsu.

The limitations to the applicability of the modified method were emphasized by the results from the research performed by Alderliesten [2]. This investigation revealed not only the dependency of the correction factor on the maximum applied stress level, but also on the laminate lay-up, on the residual stresses present in the individual layers due to curing and post-stretching, and on the starter notch size.

An attempt could be made to include these parameters in the expression for β_{FML} in order to increase the range of application. However, using this approach the effect of each parameter does not have any physical meaning, as the correction factor β_{FML} itself is based on the total ‘monolithic’ laminate. For this reason it was concluded that the method as proposed by Toi and modified by Takamatsu can not be applied on Fibre Metal Laminates such as Glare [2].

4.2.2 Application of Compliance method

In the attempt to model the fatigue crack growth for Glare, using the assumption of a monolithic material, Takamatsu et al. [5] presented another method based on the application of the compliance method. The stress intensity factor for a ‘monolithic Glare’ specimen with width W can be represented with

$$\Delta K_{lam} = \Delta S_{lam} \sqrt{\pi a} \sqrt{\frac{E_{lam} t_{lam}}{\pi \alpha} \left(\frac{d\lambda_c}{d\alpha} \right)} \quad (4.4)$$

where $\alpha = 2a/W$ and λ_c is the compliance component given by

$$\lambda_c = \frac{L_{gauge}}{W t_{lam}} \left(\frac{1}{E_{test}} - \frac{1}{E_{lam}} \right) \quad (4.5)$$

L_{gauge} is the gauge length over which the compliance is measured. From the experimental data the authors derived a third-order polynomial relation for $d\lambda_c/d\alpha$. They derive the same expression as equation (4.4) for the aluminium layer only

$$\Delta K_{exp} = \Delta S_{al} \sqrt{\pi a} \sqrt{\frac{E_{al} t_{al}}{\pi \alpha} \left(\frac{d\lambda_{c,al}}{d\alpha} \right)} \quad (4.6)$$

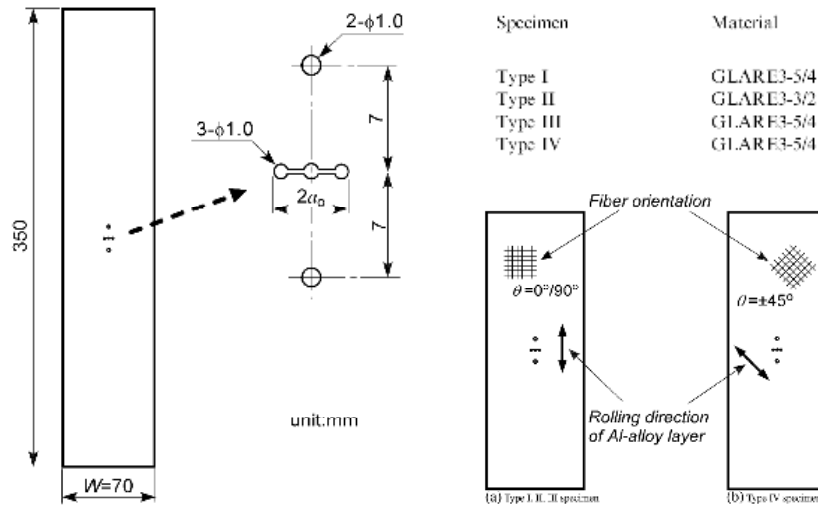


Figure 4.2 Material and specimen definition for fatigue tests in [5]

Assuming that the strain and displacement of the aluminium layer and the total laminate are identical, they derive for the stress relationship ignoring the residual stress due to curing

$$\Delta S_{al} = \frac{E_{al}}{E_{lam}} \Delta S_{lam} \quad (4.7)$$

and for the compliance components

$$\lambda_{c,al} = \frac{E_{lam} t_{lam}}{E_{al} t_{al}} \lambda_c \quad (4.8)$$

Substitution of equations yields the relation between the ‘monolithic Glare’ stress intensity factor ΔK_{lam} , calculated with equation (4.1), and the stress intensity factor based on the aluminium layer in the laminate ΔK_{exp} , which differ only a constant factor equal to E_{al}/E_{lam} .

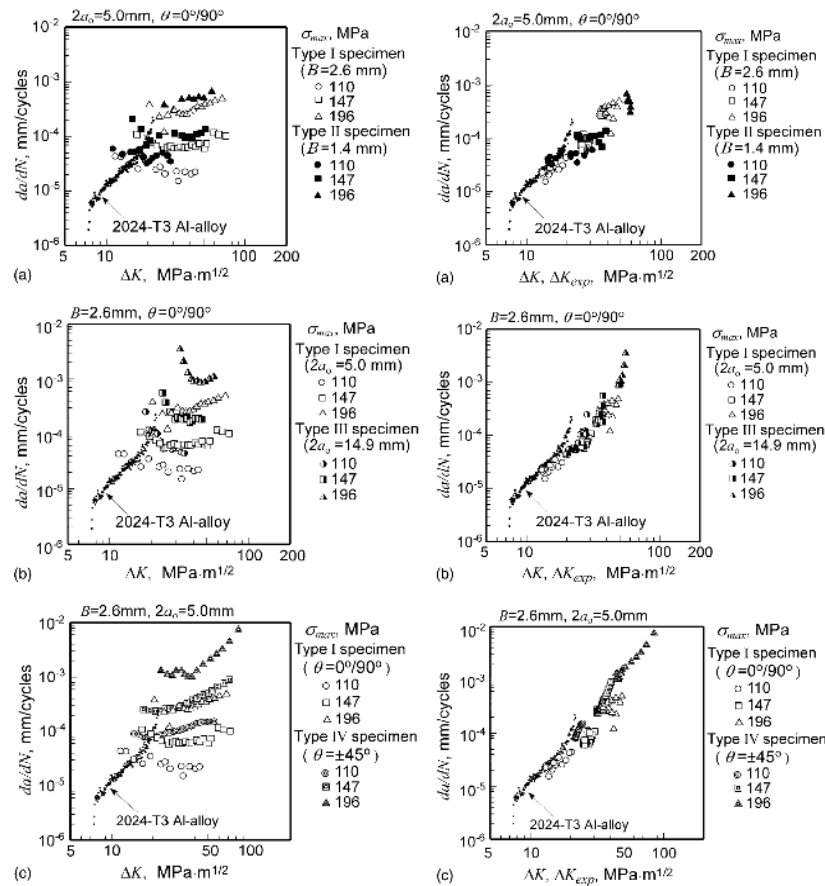


Figure 4.3 Comparison between relationships for $\Delta K_{lam}-da/dN$ and $\Delta K_{exp}-da/dN$ (B is the thickness) and correlation with the monolithic aluminium behaviour [5]

From the experimental data, it is known that the crack growth behaviour of monolithic aluminium is completely different from that of ‘monolithic Glare’. Where the stress intensity factor in monolithic aluminium increases with increasing crack lengths, the stress intensity factor in Glare remains approximately constant.

That leaves the authors with correcting the expression for the effective stress intensity factor range in the aluminium layer. They claim that application of the compliance method yields ΔK_{exp} in the aluminium layers corresponding to the values for monolithic aluminium, see Figure 4.3, but that is inconsistent with equation (4.4)-(4.8).

Takamatsu et al. did not perform a sensitivity study on the gauge lengths. As the non-physical polynomial expressions need to be corrected for maximum stress, specimen thickness (Glare grade and lay-up), notch length and fibre orientation, as the authors conclude, this approach is not suitable for description of fatigue crack growth behaviour in Glare over a wide range of conditions.

4.2.3 Methods of Cox

Two examples of empirical methods were presented by Cox [6] as an alternative for the so called micro-mechanical methods that were used to describe the fatigue crack growth behaviour of SiC fibre-reinforced titanium laminates. The main objective of the work reported was to develop engineering designer tools that need no knowledge of the micro-mechanics.

The first method Cox proposed in [6] is a phenomenological method based on the effective stress intensity factor at the crack tip in the metal layer. Cox states that for a propagating crack without a starter notch the stress intensity factor increases gradually to the steady state level. This behaviour is due to weak bridging, or as explained in the previous chapter, not yet fully effective fibre bridging. When a notch is present, the stress intensity factor gradually decreases to the steady state level over a crack length range indicated as ‘notch dominated transient’. For the bridging stress, Cox assumes a linear relation with the crack opening

$$p(u) = \beta u \tag{4.9}$$

which he further adapted to include the effect of the hysteresis. The crack opening shape according to Cox is illustrated in Figure 4.4.

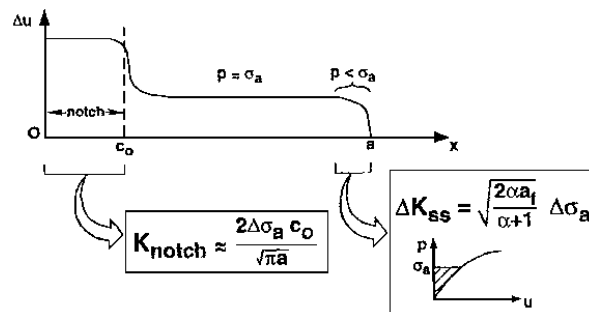


Figure 4.4 Constant crack opening shape in steady state regime with the effect of notch and crack tip in the stress intensity factor according to Cox [6]

The second method is highly empirical as it utilizes the relation between the applied stress correlated to the steady state and the crack growth rate only

$$\frac{da}{dN} = f_s \Delta\sigma_a \quad (4.10)$$

where f_s is the only function required and assumed to be a characteristic for each material and $\Delta\sigma_a$ is the applied stress range. From the discussion of the method of Toi [1], it follows that such a simplistic approach does not work for Fibre Metal Laminates, as too many parameters are affecting the crack growth behaviour that cannot be described by one function f_s .

4.2.4 Method of Guo and Wu

A phenomenological method has also been proposed by Guo and Wu [7] to address the constant crack growth rates observed during experiments. Analogue to the method of Toi, this approach assumes the Fibre Metal Laminate to be a monolithic material, which enables the application of the stress intensity factor

$$\Delta K = \beta_{geom} \Delta S_{applied} \sqrt{\pi a} \quad (4.11)$$

Guo and Wu concluded that the constant crack growth rate yields that the stress intensity factor is not dependent on the crack length a . This means that for the stress intensity factor in Glare the crack length a in equation (4.11) should be replaced by a constant. Guo and Wu called this constant the equivalent crack length, denoted as l_0 , and assumed it to be a material characteristic. Knowing this characteristic allows calculating the crack growth in Glare easily, according to Guo and Wu.

As explained in chapter 3, the fibre bridging becomes fully effective after the crack has reached a certain length. This length depends on the starter notch size over which length the fibres are cut. This effect is visible when looking at the crack growth rate as function of the crack length. To incorporate this effect at small crack lengths, Guo and Wu added a correction factor in the expression for the stress intensity factor

$$\Delta K = \beta_{notch} \Delta S_{applied} \sqrt{\pi l_0} \quad (4.12)$$

with

$$\beta_{notch} = \frac{\sqrt{a}}{\sqrt{(a - a_0) + l_0 / F_0^2}} \quad (4.13)$$

where F_0 is the Feddersen finite width correction for the case the crack length equals the starter notch length ($a = a_0$).

Investigation of this method and comparison with a large amount of experimental data [8,9] has revealed that the equivalent crack length l_0 as determined by Guo and Wu is not solely a material parameter, but that it also depends on geometrical parameters, such as the starter notch length, the crack length and the specimen width. Moreover, the effect of the starter notch was not described correctly by equation (4.13). Following from the investigation [9] a disadvantage of the method appeared to be, that the equivalent crack length l_0 had to be determined for every Glare type and lay-up.

Therefore, a modified method was presented. Using an empirical fit function based on the geometry parameters, the effect of configuration was included in the expression for the equivalent crack length. Furthermore, within the range of the experimental work reported in [8] fit functions were developed to estimate the value of the equivalent crack length as function of the Glare grade and lay-up.

The fit function parameters were determined at that time based on the available test data. However, even for that data range, the best parameter fit did not give good correlation between method and experiments for all tests. Therefore, in spite of the modifications, the approach itself is too empirical to apply the method to a wider range of conditions.

4.3 Analytical methods

4.3.1 Method of Marissen

Marissen [10] presented a two-dimensional analytical method to describe the crack growth behaviour in Arall. The two major phenomena investigated by Marissen are the delamination growth and the adhesive shear deformation, which both determine the crack opening in the aluminium layers.

The effective stress intensity factor experienced at the crack tip in the aluminium layer is directly related to the crack opening. If the adhesive between the fibres and the metal is infinitely stiff, the adhesive would not deform under the cyclic shear loading, restraining the crack from opening. An infinitely stiff bond would thus yield a stress intensity factor at the crack tip equal to zero.

Since the adhesive will allow shear deformation, the crack will open, resulting in a stress intensity factor larger than zero. Due to the cyclic shear loading and cyclic shear deformation, delamination at the interfaces will occur. As results of the delamination, the fibres elongate over an increased length, reducing the fibre stresses. These reduced fibre stresses in their turn induce reduction of the cyclic shear stresses, which means that the mechanism forms a balance between several parameters.

The delamination growth rate depends highly on the delamination resistance of the fibre adhesive layer. Marissen investigated this delamination resistance using two different adhesive systems; BSL-312-UL and AF163-2, of which the latter showed significantly better delamination resistance compared to BSL-312-UL.

With respect to the location of delamination, Ritchie et al. [12] concluded from their observations that the delamination primarily occurred at the individual fibre/adhesive interfaces, instead of delamination at the interface between the aluminium/fibre layers. However, the authors fail to report which adhesive system they used for their experiments.

Marissen did not report this observation for the AF163-2 adhesive system. Although the location of the delamination might influence the delamination resistance, it is believed to be irrelevant for the current research.

Arall showed a significant reduction of fatigue crack resistance at low stress ratios due to the poor compressive strength and poor adhesion between fibres and adhesive. At low stresses, the fibres pull out the matrix under pressure and fail after a number of cycles. This phenomenon was one of the drivers behind the investigation by Roebroeks on application of glass fibres in Arall, instead of the aramid fibres [11].

Following the approach of Marissen, the crack growth rate is determined using a Paris relation obtained from monolithic aluminium. The total stress intensity factor experienced at the crack tip in the aluminium layer is determined by

$$\Delta K_{tot} = K_{t,al} + K_{ad} \quad (4.14)$$

where $K_{t,al}$ is the stress intensity factor in the aluminium layer due to residual curing stresses and applied stresses

$$K_{t,al} = C_d (S_{al} - S_{al,0}) \sqrt{\pi a} \quad (4.15)$$

and K_{ad} is the stress intensity factor due to the adhesive shear deformation

$$K_{ad} = C_s C_{ad,d} (S_{al} - S_{al,0}) \sqrt{h \tanh\left(\frac{\pi a}{h}\right)} \quad (4.16)$$

where C_d , C_s and $C_{ad,d}$ are factors correcting for respectively crack bridging and delamination, the saw-cut size and the adhesive shear deformation. The parameter h represents the distance between two parallel cracks in Marissen's derivation and is considered a material property. The stress $S_{al,0}$ is the applied stress at which the stress intensity factor is zero and is determined using the residual stresses due to curing

$$S_{al,0} = -\frac{2}{\pi} \arccos \left[\frac{\sin\left(\frac{\pi a_0}{W}\right)}{\sin\left(\frac{\pi a}{W}\right)} \right] S_{al,r} \quad (4.17)$$

The effect of the bridging fibres is thus incorporated in the relations for $K_{t,al}$ and K_{ad} . Based on the energy release rate approach, Marissen described the delamination growth, assuming the delamination shape to remain perfectly elliptical. The relation between the delamination growth db/dN and the energy release rate G is described in a way similar to the Paris relation

$$\frac{db}{dN} = C_d \left(\sqrt{G_{d,max}} - k \sqrt{G_{d,min}} \right)^{n_d} \quad (4.18)$$

where C_d , n_d and k are material constants.

Some typical values for the two adhesive systems Marissen applied in Arall [10] are presented in Table 4.1.

Table 4.1 Material constants for equation (4.18)*

Adhesive system	C_d	n_d	k
BSL-132-UL	0.55	11	0.69
AF163-2	0.047	10	0.69

*related to db/dN in [mm/cycle] and G in [MPa mm]

The method Marissen proposed faces some limitations due to the assumptions made. For instance, the assumption of the elliptical delamination shape and crack opening shape simplifies the method, but appears to be incorrect when observing delaminations in Glare.

Furthermore, Marissen attributes the deformation due to cyclic shear stresses to the adhesive rich layer only. For Arall this can be physically explained, because analysis of the cross-sections of Arall revealed that the fibres were located in the centre of the fibre/adhesive layer; leaving resin rich layers between the fibres and aluminium, see Figure 4.5. This through the thickness distribution is attributed to the manufacturing process, where the fibre layer was obtained by laminating unidirectional aramid fabric between two adhesive films [10]. Marissen concluded that the adhesive would deform due to the shear stresses at the interfaces between the aluminium and the fibre layers.

This adhesive shear deformation allows the crack in the aluminium layer to open, inducing a stress intensity factor at the crack tip, which is no longer equal to zero.

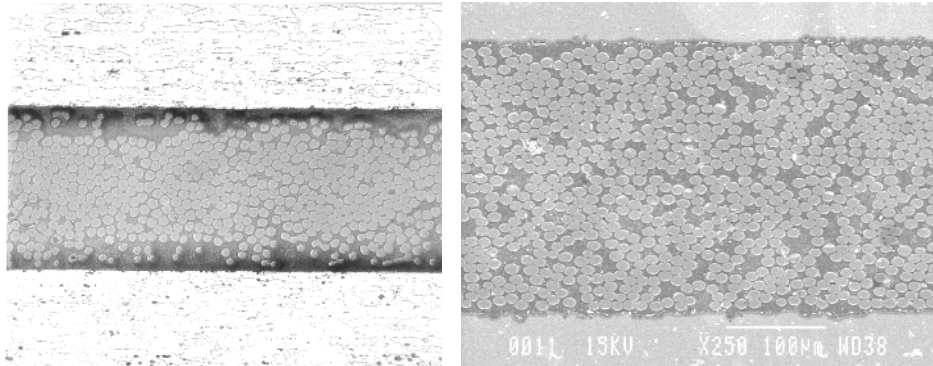


Figure 4.5 Example of a fibre distribution through the thickness in Arall [11] (left) and Glare (right)

However, cross-section analysis of Glare laminates does not show the adhesive rich layer which was observed in Arall, as can be seen in Figure 4.5. The reason is that Glare is manufactured with unidirectional prepreg layers, obtained by pre-impregnating the fibres with adhesive instead of stacking dry fabric between adhesive films. As a result, the fibres are evenly distributed through the thickness of the prepreg layer with a higher overall fibre content.

Taking into account the adhesive between the fibres, by means of the fibre volume content v_m , the thickness of the adhesive layer at the fibre/metal interface in Arall can be calculated with the equation from [10]

$$t_{ad} = \frac{\eta v_m t_f}{j} \quad (4.19)$$

where j is the number of aluminium/fibre interfaces and t_f the total fibre layer thickness in the laminate. Marissen obtained for the correction factor $\eta=0.8$, which means that the adhesive thickness is about 20% of the prepreg layer.

From the cross-section analysis of the Glare laminates, the thickness of the adhesive layers appears to be less than 5% of the prepreg layers. Substituting this percentage in the expression for the adhesive shear deformation according to Marissen, results in a significant smaller contribution to the crack opening contour and the stress intensity factor, than can be deduced from the experimental results [16].

Because the cross-sections of Arall and Glare are different, the validity of Marissen's assumption of adhesive shear deformation for Glare has to be investigated.

4.3.2 Method of Lin and Kao

Lin and Kao [13] investigated the crack growth behaviour of carbon fibre aluminium laminate (CARALL) and presented a simplified prediction method for a bridged edge crack configuration in CARALL. With respect to crack opening and delamination shape, they assume the same elliptical shape as Marissen, with as a

consequence a constant bridging stress in the wake of the fatigue crack. The effective stress intensity factor is defined as

$$\Delta K_{eff} = K_{tot,max} - K_{tot,min} \quad (4.20)$$

where K_{tot} is defined as

$$K_{tot} = K_{ex} - K_{r,a} \quad (4.21)$$

The first component in equation (4.21) describes the contribution of the far field opening stress in the aluminium layers minus the closure effect of fibre bridging and the second component describes the effect of the far field residual curing stress minus the closure effect of fibre bridging.

Lin and Kao do not incorporate any R-correction in the definition of the effective stress intensity factor range, correlated to crack closure. Although they tested at two different stress ratio levels, they do not report any observation or include any correction in their method with respect to the stress ratio. This suggests that they either did not investigate this effect and ignored it in their analysis, or they assumed it to be covered by their definition of K.

Furthermore their definition of the total stress intensity factor, given by equation (4.21) seems to be arbitrary as both the aluminium stress and the residual stress in the aluminium layer are far field stresses calculated with the two-dimensional laminate theory, as described in [10]. Defining the total stress intensity factor as

$$K_{tot} = K_{al} - K_{cl} \quad (4.22)$$

with

$$\begin{aligned} K_{al} &= f(S_a + S_{r,a}) \\ K_{cl} &= f(S_{cl}) \end{aligned} \quad (4.23)$$

would have made more sense, as the sum of applied aluminium stress and the residual stress due to curing form the far field opening stress, which can be described by the stress intensity factor expression for monolithic aluminium.

As the authors mention, the stress in the fibres is only described as a function of the strain due to crack opening over the delamination length. Only when the crack opening shape and the delamination shape are similar a constant closing stress in the wake of the crack is justified. However, the authors did not check the crack opening shape to prove the validity of their assumption.

Besides, Lin and Kao did not consider any adhesive or prepreg deformation in the definition of the crack closing stress in the fibres. Without any investigation, they expect that the contribution of the deformation in the carbon fibre metal laminate is less than in the aramid fibre metal laminate, investigated by Marissen [10]. Incorporating the effect of adhesive deformation analogue to the approach used by

Marissen, their expression for the strain in the fibre layer should be more accurate if it was defined as

$$\varepsilon_f = \frac{COD}{2b} + \delta_{ad} \quad (4.24)$$

This would have made their derivation more complex, as it follows directly from equation (4.24) that the closing fibre stress is no longer constant along the crack. Both the crack opening displacement and the delamination length decrease gradually to zero at the crack tip, while the adhesive shear deformation is approximately constant along the crack length except at the crack tip, where the shear deformation is zero.

Comparing calculated and measured crack growth rates, a clear trend is visible. With increasing number of fibre layers between the aluminium layers, the delamination length decreases (affecting ε_f), with consequently an increasing error in the predicted crack growth rates. This trend suggests that the assumption of the closing fibre stress based on the delamination and crack opening shape only is not accurate enough. Although the authors claim good agreement between predictions and measurements, there are quite some errors in the predictions up to 52% on the un-conservative side.

4.3.3 Method of De Koning

De Koning [14] proposed a method using a different approach. Based on the assumption that an infinitely large Glare panel will face the same elongation under a given applied stress for the case with and without a fatigue crack, De Koning compared both cases to derive an expression for the effective stress intensity factor including the fibre bridging.

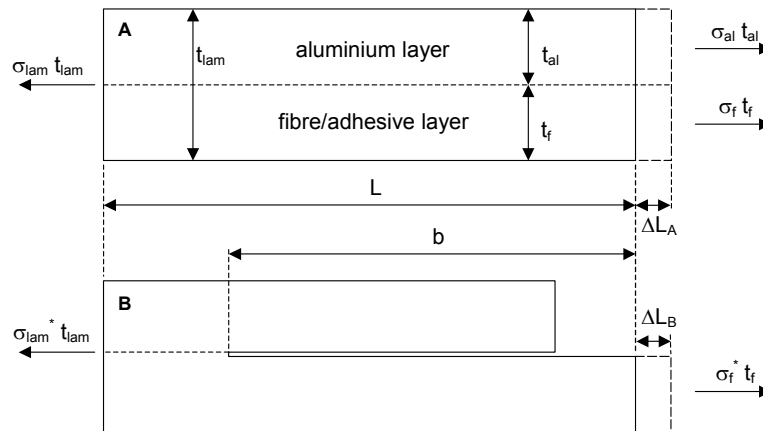


Figure 4.6 Delamination model used by De Koning

With the delamination model used by Marissen [10], see Figure 4.6, the same expression for the energy release rate is derived, which is then used to calculate the plane strain mode II stress intensity factor at the delamination tip

$$K_{II} = \sqrt{\frac{GE_f}{1-\nu_f^2}} \quad (4.25)$$

where G is the prepreg shear modulus. De Koning states that this mode II stress intensity factor has an associated displacement, which is given by Tada et al. [15]

$$u = \frac{K_{II}}{G} \sqrt{\frac{r}{2\pi}} \sin \frac{\theta}{2} \left(\beta + \cos^2 \frac{\theta}{2} \right) \quad (4.26)$$

where

$$\beta \begin{cases} = 2(1-\nu) & \text{plane strain} \\ = \frac{2}{1+\nu} & \text{plane stress} \end{cases} \quad (4.27)$$

Rewriting gives the extra displacement component associated with the singularity at the delamination tip as function of the delamination length b [16]

$$\delta_\tau = -4 \frac{K_{II}}{E_f} (1-\nu_f^2) \sqrt{\frac{b}{2\pi}} \quad (4.28)$$

which he adds to the two components describing the elongation of the delaminated and non-delaminated part

$$\Delta L_B = \delta_{delam} + \delta_{non-delam} + \delta_\tau \quad (4.29)$$

Using the assumption that the infinite Glare panel restricts the delaminated part to elongate further, he concludes that

$$\Delta L_A = \Delta L_B \quad (4.30)$$

From equation (4.30), De Koning then derives an expression for the load reduction coefficient γ , including a dimensionless stiffness parameter E^*

$$\gamma = \frac{\sigma_f - \sigma_f^*}{\sigma_f^*} = \sqrt{\frac{t_{al} E^*}{b}} \quad (4.31)$$

Looking at a centre crack tension specimen, De Koning correlates the infinite laminate without crack and delamination and the infinite laminate containing the fatigue crack with corresponding delamination. The bridging stress is described by multiplying the load reduction coefficient with the stress in the intact laminate.

De Koning assumes that a linear relationship exists between the crack growth rate and the delamination growth rate. This linear relationship is described with a constant α , which is according to De Koning a measure for the slope of the assumed triangular delamination shape.

Integrating the contribution of the bridging stress over the crack length, using the assumption of a triangular delamination shape then results in an expression for the maximum stress intensity factor at the crack tip in the aluminium layer.

$$K = f\left(\frac{a_0}{W}\right)f\left(\frac{a}{W}\right)S_{at}\sqrt{\pi a}\frac{\beta\sqrt{t_{at}E^*}}{\sqrt{b_0+(a-a_0)\alpha}} \quad (4.32)$$

where β is the parameter characterising the effect of the delamination shape. De Koning assumed the delamination growth rate at the starter notch tip to be proportional to the calculated crack growth rate.

Three comments can be made on the approach proposed by De Koning. First, the displacement given by equation (4.28) is derived from the relation in [15], which describes the displacement field in the vicinity of the crack tip or delamination tip. This means that the displacement is described with a very localised linear elastic stress field near the tip, excluding the effect of through the thickness deformations which are not incorporated in the calculated elongations in equation (4.29).

Therefore, the assumption that these relations describe the displacement field accurately at a distance equal to the delamination length b away from the delamination tip is very doubtful.

The second comment to the method concerns the assumption that the elongation experienced by the surrounding intact laminate restricts the elongation of the delaminated area, given by equation (4.30).

De Koning supported his assumption with two arguments. First, he argued that the elongation of an infinite large panel is not affected by the presence of a fatigue crack with corresponding delamination. Second, he argued that the stiffness of the delaminated area is determined by the prepreg layers only, while outside the delaminated area the stiffness is determined by the complete laminate. Since the laminate stiffness is higher than the prepreg stiffness, the surrounding laminate determines the elongation.

However, the fact that the overall elongation of an infinite large panel is not affected by the presence of a crack with corresponding delamination, does not justify the assumption that the elongation at the delamination contour is determined by the undisturbed material. The delaminated area with the lower stiffness influences the

elongation at the delamination contour, which makes the assumption too simple, as follow-up research has proven [17].

The third comment concerns the relation for the stress intensity factor given by equation (4.32). According to this equation, the stress intensity factor experienced at the crack tip decreases if the delamination length increases, while it was discussed in chapter 3 that increasing delamination lengths results in lower bridging efficiency and thus higher stress intensity factors. This means that although equation (4.32) after fitting the parameters on the test data gave sufficient predictions within the validation range [14,17], it is physically incorrect.

4.3.4 Bridging stress modelled as elastic springs

Another approach to model the bridged fatigue crack in Fibre Metal Laminates is to replace the bridging fibres by fully elastic or elastic/plastic springs, as presented by several authors [18-20]. In most cases, the model was developed for materials reinforced with a bonded patch.

The basic assumption of application of elastic springs in the wake of the crack is, that the stress in the spring is directly correlated to the crack opening, thus the spring elongation, by means of a parameter k characterizing the linear spring stiffness behaviour. This assumption was in fact also adopted by Lin and Kao [13] when determining the closing stress.

The approach Cox [20] uses to determine the stress intensity factor at the crack tip is equivalent to equation (4.22), where the first component describes the stress intensity factor in monolithic aluminium due to a far field opening stress and the second component is utilized to describe the closing effect due to the elastic springs.

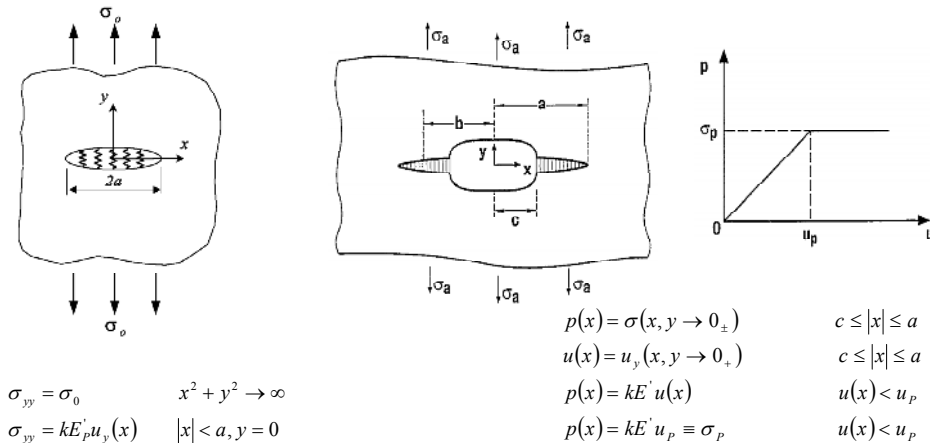


Figure 4.7 Distributed elastic springs model for a patched crack, with corresponding boundary conditions [18] and the distributed elastic/perfect plastic springs model including notch size with corresponding boundary conditions [20]

Cox determines the expression for the stress intensity factor for the case of elastic/perfect plastic spring behaviour, see right hand side in Figure 4.7, which is not relevant for fatigue crack growth configurations in FML's, where the cracks are being bridged by fibres that remain elastic until final failure [11]. However, he deduces the expressions for the case of elastic spring behaviour from his general solution and compares this simplified solution with the relations that were obtained by Rose [19]. Comparison reveals that both solutions match quite well.

As the effect of delamination shape and delamination growth - the springs are attached to the crack flanks instead of the delamination boundary and spring elongation is related to crack opening only - is not incorporated in these methods, application is quite limited for cases of fatigue cracks in FML's.

Relating the spring elongation to the crack opening and the delaminated length, attaching the springs to the delamination boundary, equivalent to Lin and Kao [13] would result in more accurate predictions. However, the complexity of the derivation would increase significantly as the locations where the springs are attached depend on the delamination shape. This can also be seen in the work of Marissen, where the effect of bridging stress acting on the delamination boundary is investigated [10].

4.3.5 Method of Guo and Wu

Similar to the methods discussed above, Guo and Wu presented a method [21,22] in which they determine the stress intensity factor at the crack tip in the metal layers based on the applied far field stress and the presence of the bridging stress. They derive the relation for the bridging stress, which contributes to the stress intensity solution at the crack tip in the aluminium layers, from the relations for the crack opening shapes.

The approach in its simplest form can be formulated as

$$COD(x)_{physical} = COD(x)_{aluminium} \quad (4.33)$$

The physical crack opening can be contributed to mainly three factors:

- Fibre elongation over the delamination length, Figure 3.5 (a)
- Adhesive shear deformation, Figure 3.5 (b)
- Aluminium deformation, Figure 3.5 (c)

The crack opening in the aluminium layers can be contributed to

- Applied load
- Bridging stress

Guo and Wu derive the expressions for the crack opening displacements due to fibre elongation, adhesive shear deformation and the remote applied stress analogue to Marissen [10] for arbitrary delamination shapes.

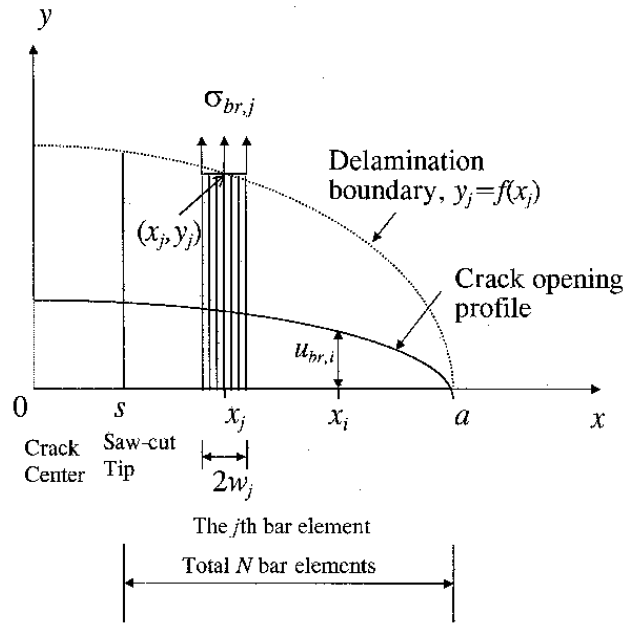


Figure 4.8 Crack opening displacement caused by bridging stress

The crack opening due to the bridging stress, Figure 4.8, is given by

$$u_{br}(x_i) = 2 \sum_{j=1}^N \sigma_{br,j} g(x_i, x_j) L(x_j, y_j) \quad (4.34)$$

with

$$g(x_i, x_j) = G(-x_i, x_j) + G(x_i, x_j) \quad (4.35)$$

where $G(x_i, x_j)$ is the Green's function considering the effect of the finite plate width. The term $L(x_j, y_j)$ takes into account that the bridging stress acts on the delamination boundary instead of the crack flanks.

Incorporating the expressions into equation (4.33) gives the possibility to calculate the bridging stress. The general form of the equation obtained is

$$H_{i,j} \sigma_{br,j} = Q_i \quad (4.36)$$

which can be numerically solved.

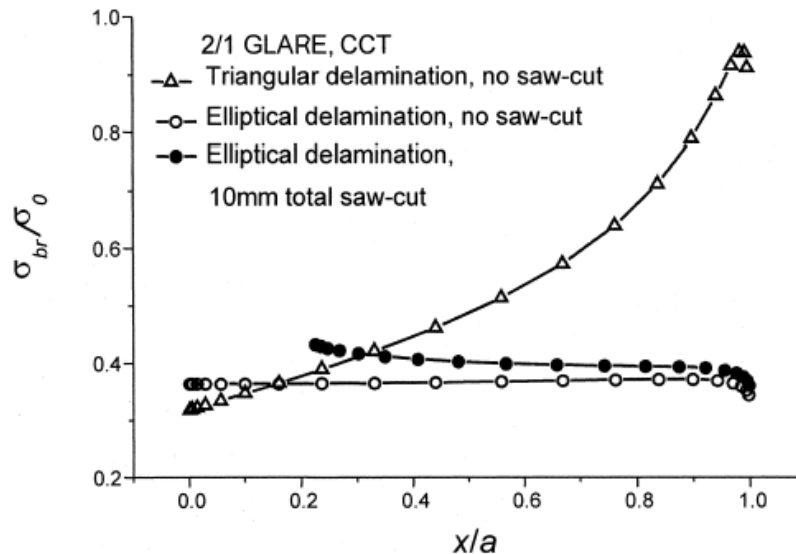


Figure 4.9 Bridging stress distributions in centre crack tension Glare specimens calculated with the method of Guo and Wu [22]

The bridging stress distribution calculated with this method for a triangular and an elliptical delamination shape is given in Figure 4.9. The authors compare in [22] their calculations with corresponding measurements, by means of calculated and observed crack opening shapes, which shows that the calculated results match quite well with the experimental observations.

It furthermore illustrated that the assumption of an elliptical delamination shape gives an almost constant bridging stress distribution, as can be seen in Figure 4.9, and a crack opening shape, close to an ellipse as well, which seems to support the derivation of Marissen for the case of an elliptical delamination shape.

Compared with the method proposed by Marissen, the extra complexity of the method proposed by Guo and Wu is the numerical calculation of the bridging stress along the crack for each crack length in the crack growth calculation. However, it adds a large flexibility to calculate bridging stresses for arbitrary delamination shapes.

Although the calculated bridging stress distributions result in crack opening shapes that match well with the measured crack opening shapes, this does not necessarily mean that any of these bridging stress distributions occur in the fatigue crack configuration in Glare. Neither does it mean, that Marissen's assumption of an elliptical delamination shape with a constant bridging stress is justified.

Since most delamination shapes in practise are closer to a triangular shape than an elliptical shape, Guo and Wu already suggested that the elliptical delamination shape with a constant bridging stress might be questionable.

Although they fail to do so, Guo and Wu could have explained with their calculated bridging stresses, that the delamination shape in practise is neither an ellipse, nor a

triangle. The constant bridging stress for the elliptical delamination shape would induce constant delamination growth along the total crack length, which gives a deviation from the elliptical shape. On the other hand, the bridging stress distribution for the triangular delamination shape would induce more delamination growth near the crack tip than at the rest of the crack length. From their analysis, the authors could have explained in a qualitative way, that the delamination should have a shape in-between an ellipse and a triangle.

4.3.6 Method of Wu

A higher-order theory developed by Wu and Cheng [23] for laminates consisting of isotropic layers under the generalized plane-stress conditions, has been extended by Wu [24] to derive expressions for the fatigue crack growth behaviour in Glare.

The higher-order theory is based on the Taylor expansions of displacements up to the second order in the direction normal to the laminate. Following from the required interfacial strain compatibility at the interfaces, interlaminar stresses can be derived from the harmonic stress potentials.

Wu extends the theory isotropic layers to Fibre Metal Laminates consisting of isotropic metal layers and orthotropic glass fibre layers, deriving a set of equations in accordance with the complex variable representation of Lekhnitskii [25] and Muskhelishvili [26]. Using the First Fundamental Problem for the isotropic and orthotropic layers Wu derives solutions for a patched isotropic panel containing an open hole and a Fibre Metal Laminate panel containing a fatigue crack.

The theory has a different nature compared to the analytical methods described before, as it describes the complete stress field in the laminate based on harmonic stress potentials together with strain compatibility requirements, instead of describing the stresses at the crack or delamination tip only.

The delamination shapes and sizes in the previous described analytical methods were assumed to enable bridging stress calculation, where the delamination shape in the theory according to Wu follows from the displacement discontinuity. Wu concluded that this displacement discontinuity, which is a region of strain incompatibility, see Figure 4.10, corresponds with delamination shapes observed in experiments, however any quantitative comparison has not been made.

The results for the stress intensity factor as function of the fatigue crack length Wu presents, see Figure 4.11, seem to differ from the stress intensity factor relation obtained from the experiments. For the case of a fatigue crack with an infinite small starter notch, similar to the case in Figure 4.11, would imply a stress intensity factor rising within a few millimetres to an approximately constant level.

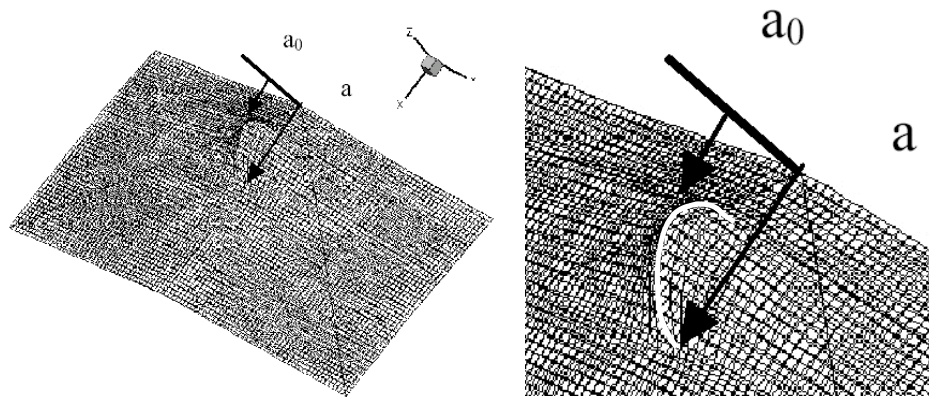


Figure 4.10 The in-plane displacement discontinuity at the interface, which Wu attributes to the delamination. [24]

The results obtained by Wu show a curve close to a square root shape as can be seen for the monolithic case (follows directly from the K-expression), but a factor smaller.

The fact that the theory provides the complete stress field instead of the stresses at the crack makes it an interesting approach. Nevertheless, since the stress intensity factors following from the theory as illustrated in Figure 4.11, are known to be incorrect, the proposed approach is not suitable for predicting the crack growth behaviour in Glare.

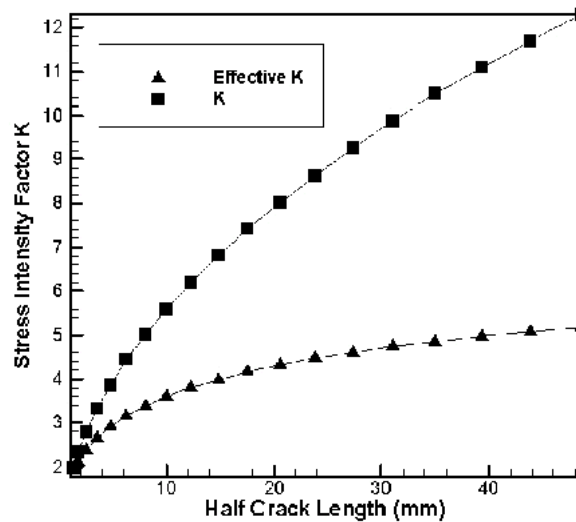


Figure 4.11 Comparison between stress intensity factors for monolithic aluminium and a Fibre Metal Laminate [24]

4.4 Finite Element and Boundary Element methods

4.4.1 Method of Yeh

Yeh [27,28] investigated the fatigue crack and delamination growth of Arall laminate using a finite element method. When considering the delamination at the interface between the aluminium and fibre aramid layer, Yeh developed an FE-model using six-node singular elements around the delamination tip, surrounded by eight-node isoparametric elements [27]. From a convergence study and comparison with experimental data he concluded that the presented analysis method was accurate and reliable. Yeh found that the energy release rate and stress intensity factor are not dependent on the delamination length and obtained relationships for the mode II energy release rate as function of the stress in the fibre layer for as cured and post stretched laminates. For the fatigue crack configuration a centre crack tension Arall specimen Yeh utilizes the Paris law for both the crack growth rate and the delamination growth rate [28]. He adopts the assumption of Marissen [10], constant energy release rate along the delamination boundary, simplifying his derivation and allowing him with some additional assumptions to develop a two-dimensional model. The model consists of four-node plane stress elements for the aluminium layer and two-node truss elements representing the stiffening aramid fibre layers, connected using special interface elements.

From the analysis, Yeh obtained the energy release rate at the crack tip in the aluminium layers and the energy release rate at the delamination tip, which can be related to crack growth and delamination growth respectively using the Paris type relations. Yeh states that the model is developed for tension-to-tension fatigue loads only, as it does not incorporate buckling induced compression.

Although Yeh concludes that the proposed models are convenient to calculate the delamination and crack growth behaviour of Arall and other Fibre Metal Laminates, some remarks can be made with respect to the presented results. The calculated delamination shapes and bridging stress distributions presented in [27] do not correspond to the observed delamination shapes in [10], and the calculated bridging stress distribution presented by Guo and Wu [22]. The peak stresses at the saw-cut tip induce in the calculations large delamination extensions at the saw-cut tip, which do not occur in practise. Furthermore, the delamination growth results seem to be dependent on the initial delamination size assumption, as large steps in delamination shapes and bridging stress are visible near the crack tip.

Finally, the approach to model the fibre layers as stiffening elements limits the applicability of the method to Fibre Metal Laminates with unidirectional fibre layers under in-axis fatigue loading, which is an unacceptable limitation for the current research.

4.4.2 Method of Burianek

To describe the fatigue crack growth behaviour of Titanium-carbon laminates, Burianek [29,30] presented a three-dimensional hierarchical global-local Finite Element model consisting of eight-node elements. Using the symmetry conditions half the length and half the thickness were modelled over the full width, as the experimentally investigated specimens consisted of edge cracks configurations.

The calculated loads and displacements in the vicinity of the crack in the global model were exported to a more refined local model, which was used to determine the stress intensity factor at the crack tip employing the virtual crack-closure technique (VCCT). Burianek modelled the delamination as a triangular shape, because he observed in the crack growth experiments on the Titanium-carbon laminates triangular instead of elliptical delamination shapes. One of his studies consisted of the effect of the triangular delamination angle and the effect of a bilinear delamination shape.

Comparison with a two-dimensional Finite Element model showed some unconservative predictions with the two-dimensional model compared to his three-dimensional model. Burianek explains the mismatch with the absence of out-of-plane stresses and strains in the two-dimensional model. Therefore, a three-dimensional model is needed to describe the behaviour accurately.

Comparison with a bridged crack model showed significant discrepancy between the three-dimensional model and the bridged crack model. However, the calculated crack opening shape for a triangular delamination shape and the correlation between crack opening displacement and delamination length obtained in his study seem to correlate quite well with the numerical results of Guo and Wu [22]. This raises questions with respect to Burianek's claim that the bridged crack solution could not be correlated to the experimental results.

To investigate whether the model could be used to describe the crack growth behaviour in Glare, Burianek's method was modified in a follow-up investigation by Shim et al. [31] and evaluated with experimental data on Glare. The experimental results consisted of Glare lay-ups up to eight aluminium layers with cross-ply glass fibre layers in-between [9]. The method predicts the difference in stress intensity factor at the crack tip in the inner aluminium layers and the surface aluminium layer, consisted with the different crack lengths observed in these layers by Takamatsu et al. [3].

However, applying the Paris law for monolithic aluminium resulted in a mismatch between calculated and measured crack growth. After fitting the Paris parameters on one of the test results, a perfect match between calculations and other measurements was obtained. Apparently, the model does not include all relevant parameters correctly, resulting in a consistent mismatch.

Parallel to the investigation of Shim et al. [31] the model was fitted to predict the crack growth in Glare 3-3/2-0.3 by Antonelli and De Rijck [32]. In this investigation

the predicted stress intensity factors were compared with the stress intensity factor that follows from applying the COD-extrapolation method [33]. Antonelli reported that the stress intensity factor from both methods match quite well for the inner aluminium layer, but differ up to 11% for the surface aluminium layer.

An explanation for the higher predicted stress intensity factors based on the COD-extrapolation, might be found in the work reported by Suiker and Fleck [34], where the mixed mode stress intensity factor at the delamination tip adjacent to the surface aluminium layer results in larger delamination lengths compared to the delamination lengths at the inner interfaces induced by the mode II stress intensity factor.

Although the delamination shapes in the Glare 3-3/2-0.3 configuration modelled by Antonelli are identical, the inner aluminium layer faces more efficient bridging and crack opening restraint compared to the surface aluminium layer.

From the investigation of Burianek [29,30] and the follow-up research by Shim [31] and Antonelli [32], it becomes clear that the Finite Element models have a great potential to describe the fatigue crack configuration in Glare and other Fibre Metal Laminates. However, from the evaluation with experimental data on Glare, it is concluded that the obtained models need further modifications to describe the crack growth mechanisms correctly, before they can be applied on Glare.

4.5 Conclusions

From the discussion of the methodologies in this chapter, it can be concluded that the phenomenological methods as described in [1-7] are not suitable for further development of fatigue crack propagation in Fibre Metal Laminates such as Glare. The complexity of the mechanisms that occur cannot be described with the simplicity of the proposed phenomenological methods.

The analytical methods described in [10,14,22,24] have the potential of further development and refinement. Guo and Wu [22] have shown that a different assumption (describing the method in terms of crack opening) increases the complexity of the equations in the method developed by Marissen [10], but can still be solved numerically.

This supports the assumption that further development of the methods of Marissen and Guo and Wu will lead to an analytical method that accurately describes the fatigue crack growth mechanisms in Glare.

Although the Finite Element models have the potential of accurate description of the fatigue crack growth behaviour in Glare, further investigation and modification of the models is needed before they can be applied to describe the crack growth behaviour in Glare accurately.

The analytical models as well as the Finite Element models need further investigation and modification. Since the analytical methods are more generic and preferred by designers, the current research will aim for the development of an analytical method. However, the development of an accurate analytical model requires not only experimental results, but also the use of dedicated Finite Element models to validate the results from the analytical model.

References

- [1] **Toi, R.**, *An Empirical Crack Growth Model for Fiber/Metal Laminates*, Proceedings of the 18th Symposium of the International Committee on Aeronautical Fatigue, Melbourne, Australia, 899-909 (1995).
- [2] **Alderliesten, R.C.**, *An empirical crack growth model for Fiber Metal Laminates*, Preliminary (Master) Thesis, Delft University of Technology, 1998.
- [3] **Takamatsu, T., Matsumura, T., Ogura, N., Shimokawa, T., Kakuta, Y.**, *Fatigue crack growth properties of a GLARE3-5/4 Fiber/metal laminate*, Engineering Fracture Mechanics **63** 253-272 (1999).
- [4] **Takamatsu, T., Matsumura, T., Ogura, N., Shimokawa, T., Kakuta, Y.**, *Fatigue crack growth of a GLARE3-5/4 Fiber/metal laminate and validity of methods for analysing results*, 20th Symposium International Committee on Aeronautical Fatigue, Bellevue Washington, USA, 841-860 (1999).
- [5] **Takamatsu, T., Shimokawa, T., Matsumura, T., Miyoshi, Y., Tanabe, Y.**, *Evaluation of fatigue crack growth behaviour of GLARE3 fiber/metal laminates using compliance method*, Engineering Fracture Mechanics **70** 2603-2616 (2003).
- [6] **Cox, B.N.**, *Life Prediction for Bridged Fatigue Cracks*, Life Prediction Methodology for Titanium Matrix Composites, ASTM STP 1253, W.S. Johnson, J.M. Larsen, B.N. Cox, Eds. ASTM, 552-572 (1996).
- [7] **Guo, Y.J., Wu, X.R.**, *A phenomenological model for predicting crack growth in Fiber-reinforced metal laminates under constant-amplitude loading*, Composites Science and Technology, **59** 1825-1831 (1999).
- [8] **Homan, J.J., Alderliesten, R.C.**, *Test data for fatigue crack propagation in unstiffened Glare*, report B2V-99-39, Delft University of Technology, 1999 (restricted)
- [9] **Alderliesten, R.C.**, *Development of an empirical fatigue crack growth prediction model for the Fibre Metal Laminate Glare*, Master Thesis, Delft University of Technology, 1999.
- [10] **Marissen, R.**, *Fatigue Crack Growth in ARALL, A hybrid Aluminium-Aramid Composite Material, crack growth mechanisms and quantitative predictions of the crack growth rate*, PhD Thesis, Delft University of Technology, 1988.
- [11] **Roebroeks, G.H.J.J.**, *Towards Glare, The development of a fatigue insensitive and damage tolerant aircraft material*, PhD Thesis, Delft University of Technology, 1991.
- [12] **Ritchie, R.O., Weikang, Yu, Bucci, R.J.**, *Fatigue crack propagation in Arall® Laminates: Measurement of the effect of crack-tip shielding from crack bridging*, Engineering Fracture Mechanics, **32** 361-377 (1989).

- [13] **Lin, C.T., Kao, P.W.**, *Effect of fiber bridging on the fatigue crack propagation in carbon fiber-reinforced aluminium laminates*, Material Science and Engineering, **A190** 65-73 (1995).
- [14] **Koning, A.U. de**, *Analysis of the fatigue crack growth behaviour of "through the thickness" cracks in fibre metal laminates*, Report NLR-CR-2000-575, National Aerospace Laboratory NLR, 2000 (restricted).
- [15] **Tada, H., Paris, P.C., Irwin, G.R.**, *The Stress Analysis of Crack Handbook*, 3rd ed., The American Society of Mechanical Engineers, 2000.
- [16] **Alderliesten, R.C.**, *Modelling Fatigue Crack Propagation in Glare, Interim Status Report*, Report TD-R-02-022, Fibre Metal Laminates Centre of Competence, January 24, 2003 (restricted).
- [17] **Bouwman, V.P., Koning, A.U. de**, *Fatigue crack growth methodology of 'through the thickness' cracks in fiber metal laminates*, Report NLR-CR-2003-032, National Aerospace Laboratory NLR, 2000 (restricted).
- [18] **Kim, J.H., Lee, S.B.**, *Calculation of stress intensity factor using weight function method for a patched crack with a debonding region*, Engineering Fracture Mechanics, **67** 303-310 (2000).
- [19] **Rose, L.R.F.**, *Crack reinforcement by distributed springs*, Journal of the Mechanics and Physics of Solids **35** 383-405 (1987).
- [20] **Cox, B.N., Rose, L.R.F.**, *A self-consistent approximation for crack bridging by elastic/perfectly plastic ligaments*, Mechanics of Materials **22** 249-263 (1996).
- [21] **Guo, Y.J., Wu, X.R.**, *A theoretical model for predicting fatigue crack growth rates in Fibre-reinforced Metal Laminates*, Fatigue & Fracture of Engineering Materials & Structures, **21** 1133-1145 (1998).
- [22] **Guo, Y.J., Wu, X.R.**, *Bridging stress distribution in center-cracked fiber reinforced metal laminates: modelling and experiment*, Engineering Fracture Mechanics, **63** 147-163 (1999).
- [23] **Wu, X.J., Cheng, S.M.**, *Trans. ASME, Journal of Applied Mechanics*, **66** 95-100 (1999).
- [24] **Wu, X.J.**, *A higher-order theory for fiber-metal laminates*, Proceedings of the 23rd International Congress on Aeronautical Sciences, Toronto, Canada, (2002).
- [25] **Lekhnitskii, S.G.**, *Theory of Elasticity of an Anisotropic Body*, Mir Publishers Moscow 1981.
- [26] **Muskhelishvili, N.I.**, *Some Basic Problems of The Mathematical Theory of Elasticity (translated by J.R.M. Radok)*, Noordhoff, Groningen, The Netherlands, 1953.

- [27] **Yeh, J.R.**, *Fracture Mechanics of delamination in Arall laminates*, Engineering Fracture mechanics, **30** 827-837 (1988).
- [28] **Yeh, J.R.**, *Fatigue crack growth in Fiber-Metal Laminates*, International Journal of Solids and Structures, **32** 2063-2075 (1995).
- [29] **Burianek, D.A.**, *Mechanics of Fatigue Damage in Titanium-Graphite Hybrid Laminates*, Ph.D. Thesis, Massachusetts Institute of Technology, 2001
- [30] **Burianek, D.A.**, *Interacting damage modes in Titanium-Graphite Hybrid Laminates*, Proceedings of the 13th International Conference on Composite Materials, Beijing, China, (2001).
- [31] **Shim, D.J., Alderliesten, R.C., Spearing, S.M., Burianek, D.A.**, *Fatigue crack growth prediction in GLARE hybrid laminates*, Composites Science and Technology **63** 1759–1767 (2003).
- [32] **Antonelli, V., Rijck, J.J.M. de**, *Initial study on crack growth modelling of FML with FE-analysis*, TNO report 020530168-VA, 2002 (restricted)
- [33] **Ewalds H.L., Wanhill, R.J.H.**, *Fracture Mechanics*, Delftse Uitgevers Maatschappij, Delft, The Netherlands, 1984
- [34] **Suiker, A.S.J., Fleck, N.A.**, *Crack tunnelling and plane-strain delamination in layered solids*, International Journal of Fracture, **125 (1)** 1-32 (2004).

Fatigue crack propagation and delamination growth in Glare

5

Experimental Programmes and Data Evaluation

Abstract – This chapter provides an overview of the experimental programmes that form a basis for the modelling work described in the this thesis. A description of the tests, specimens and measurement techniques is given as well as a first description of the evaluation of results.



5.1 Introduction

To obtain the experimental substantiation necessary for modelling the mechanisms that are qualitatively described in chapter 3, several test programmes have been carried out to investigate the mechanisms in more detail.

In section 5.2, the investigation of the delamination behaviour is described. The crack opening shape investigations in Centre Crack Tension (CCT) specimens are described in section 5.3, while the investigation of the delamination shapes in these CCT specimens is discussed in the succeeding section. The research on the crack propagation behaviour in aluminium and Glare CCT specimens is discussed respectively in section 5.5 and 5.6. The measurement techniques utilized in the various investigations presented in this chapter are described in section 5.7, while the data evaluation is discussed in the last section.

5.2 Delamination growth behaviour

5.2.1 Programme objective

The objective of the delamination growth investigation is to obtain a relation between the delamination growth rate db/dN and the energy release rate for delamination, which is representative for the delamination growth at the interfaces in a Glare CCT specimen.

5.2.2 Specimen geometry

Marissen [1] investigated the delamination behaviour of Arall on delamination specimens with the geometry as illustrated in Figure 5.1 (a,b). Similar research was performed for the current thesis to investigate the delamination behaviour in Glare. However, in addition to the geometry investigated by Marissen, a second geometry was investigated, given in Figure 5.1 (c-f), based on the work performed by Suiker and Fleck [2]. From their numerical analysis, they concluded that the delamination in the specimen used by Marissen faces a mode I as well as a mode II loading contribution, which they denoted as mixed-mode. Furthermore, they calculated that at least a 5/4 lay-up with the pre-crack in the middle layer is needed to obtain pure mode II loading.

The objective of the delamination tests is to determine the delamination behaviour as function of the energy release rate for delamination. This relation must be representative for the delamination in Glare CCT specimens, where the interfaces adjacent to the outer aluminium layers and inner aluminium layers face different loading modes. The outer aluminium layers face beside the loading mode II (shear), also a mode I loading (peel), which can be described by delamination behaviour under mixed-mode loading. The inner aluminium layers face mode II only, for which case the delamination behaviour must be determined as well.

Because the delamination behaviour within a Glare CCT specimen is averaged over all interfaces, the intention was to find a relation between the delamination growth rate and the energy release rate for delamination by interpolating between the two loading mode cases investigated with the specimen geometries in Figure 5.1.

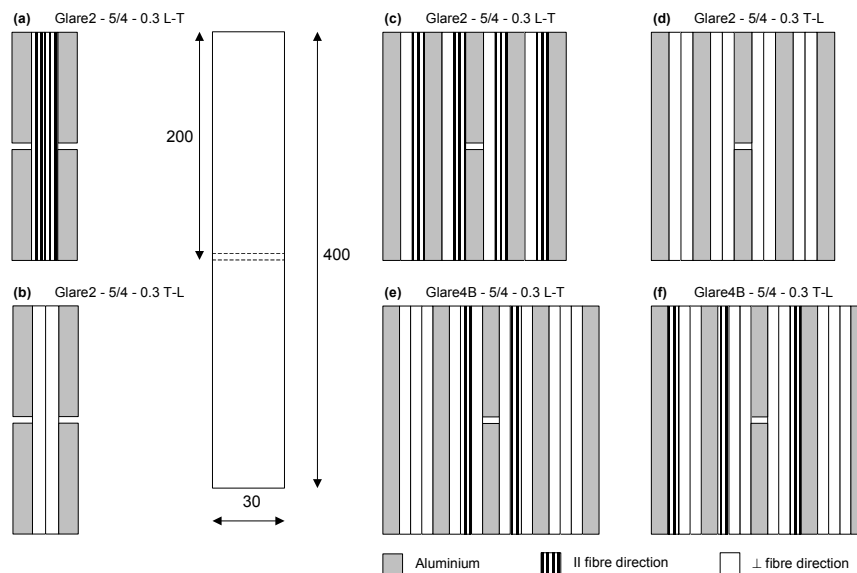


Figure 5.1 Illustration of the cross sections of the delamination specimen geometry for mixed-mode delamination (a,b) and the mode II delamination (c-f)

Therefore, the experimental program consisted of two specimen types: the (mixed-mode) Glare specimens with a 2/1 lay-up containing pre-cracks in both metal layers, see Figure 5.1 (a,b), and the (mode II) Glare specimen with a 5/4 lay-up containing a pre-crack in the centre aluminium layer, see Figure 5.1 (c-f).

The specimens were manufactured at Delft University of Technology. The artificial pre-crack was created during laminating, by positioning two aluminium sheets head-to-head. The edges of the aluminium sheets were deburred to avoid any unwanted damage to the neighbouring prepreg layers. An example image of the deburred aluminium sheet edges at the artificial crack is given in Figure 5.2. Example images of the delaminated specimen captured during the delamination tests, are presented in chapter 6.

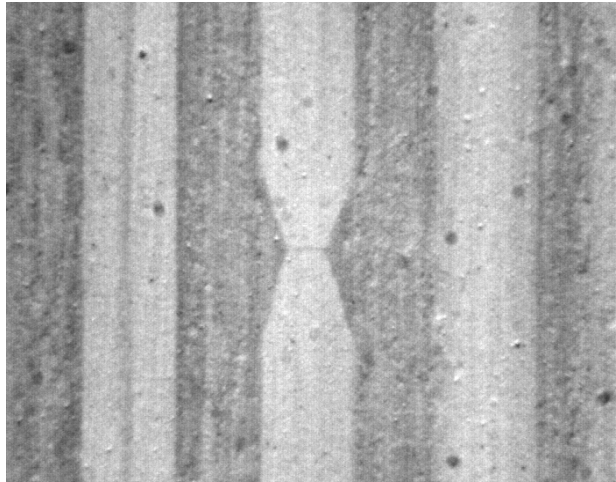


Figure 5.2 Image of the deburred aluminium layers at the artificial crack prior to performing the delamination test.

5.2.3 Test matrix and test set-up

In total 15 delamination specimens were tested to investigate the delamination behaviour; 2 mixed-mode 2/1 lay-up specimens, and 13 mode II 5/4 lay-up specimens. The test matrix is given in Table 5.1, with the specimen type referring to the specimen geometries in Figure 5.1. The specimens were tested at the 100 kN servo-hydraulic, closed loop mechanical and computer controlled testing machine at a frequency of 10 Hz.

At regular intervals, the delamination length at the interface between the aluminium and fibre layers was measured at the specimen edge with a digital camera and recorded with the number of fatigue cycles and the maximum applied stress level. With the same camera, images were captured such as for example in Figure 5.2, to enable analysis of the delamination of matrix crack trajectory in a later stage of the investigation.

Table 5.1 Test matrix of the delamination specimens

Type	Material & direction	S_{max} [MPa]	R [-]	Number of specimens
(a)	Glare2A-2/1-0.3 L-T	70,80,100,120,140,160,180	0.05	1
(a)	Glare2A-2/1-0.3 L-T	100,120,140,160,180,200,220,240	0.5	1
(b)	Glare2A-2/1-0.3 T-L	-	-	1 ¹
(c)	Glare2A-5/4-0.3 L-T	240,280,300	0.05	2
(c)	Glare2A-5/4-0.3 L-T	240,250,260,320,360,380,400,420	0.5	2
(d)	Glare2A-5/4-0.3 T-L	180	0.5	1
(d)	Glare2A-5/4-0.3 T-L	60-140	0.25	1 ²
(e)	Glare4B-5/4-0.3 L-T	100-140	0.05	1 ³
(e)	Glare4B-5/4-0.3 L-T	160-180	0.25	1 ³
(e)	Glare4B-5/4-0.3 L-T	140-190	0.5	1 ³
(f)	Glare4B-5/4-0.3 T-L	200,240,260	0.05	3

¹ Specimen failed at first load cycle

² Specimen failed before delamination growth occurred

³ Matrix crack without delamination growth

Theoretically, the delamination length does not affect the energy release rate for delamination, which means that the delamination growth rate is independent of the delamination length. This independency was validated with three delamination tests on Glare4B-5/4-0.3 T-L specimens at only one load level. Although the delamination lengths obtained until specimen failure were limited due to fast crack initiation in the aluminium layers no dependency was observed.

Therefore, two Glare2A-5/4-0.3 L-T specimens and three Glare2A-5/4-0.3 L-T specimens were tested stepwise at several subsequent load levels with the same stress ratio, to obtain several data sets of delamination growth rate versus energy release rate for delamination from one test specimen. The remaining specimens could not be tested at subsequent load levels, because insufficient delamination growth was observed before specimen failure.

5.2.4 Measurements and observations

From the recorded data sets of the delamination length versus the number of cycles, delamination growth rates were calculated using the point-to-point method [3]. During the first millimetre of delamination growth, a start-up effect was visible with initial high delamination growth rates, decreasing to a lower constant value. This effect corresponds to the numerical calculations from [2] and it can be attributed to the mixed-mode loading present at the pre-crack, due to non-uniform stress distribution through the thickness and deburred aluminium sheet edges (Figure 5.2).

Therefore, to determine the delamination growth rate at the first load level, the first millimetre of the delamination length was excluded from the analysis. The calculated delamination growth rates are presented together with the calculated energy release rates in Table 5.2. The determination of the relation between the delamination growth rates and the energy release rate is discussed in the next chapter as part of the method development.

Table 5.2 Recorded delamination growth results and calculated energy release rates

Type	Material & direction	S_{\max} [MPa]	R [-]	$G_{d,\max}$ [MPa mm]	$G_{d,\min}$ [MPa mm]	db/dN [mm/cycle]
(a)	Glare2A-2/1-0.3 L-T	70	0.05	$7.94 \cdot 10^{-2}$	$1.99 \cdot 10^{-4}$	$8.00 \cdot 10^{-6}$
		80		$1.04 \cdot 10^{-1}$	$2.59 \cdot 10^{-4}$	$1.00 \cdot 10^{-5}$
		100		$1.62 \cdot 10^{-1}$	$4.05 \cdot 10^{-4}$	$2.00 \cdot 10^{-5}$
		120		$2.33 \cdot 10^{-1}$	$5.83 \cdot 10^{-4}$	$2.84 \cdot 10^{-4}$
		140		$3.18 \cdot 10^{-1}$	$7.94 \cdot 10^{-4}$	$4.40 \cdot 10^{-4}$
		160		$4.15 \cdot 10^{-1}$	$1.04 \cdot 10^{-3}$	$9.50 \cdot 10^{-4}$
		180		$5.25 \cdot 10^{-1}$	$1.31 \cdot 10^{-3}$	$1.55 \cdot 10^{-3}$
(a)	Glare2A-2/1-0.3 L-T	100	0.5	$1.62 \cdot 10^{-1}$	$4.05 \cdot 10^{-2}$	$8.00 \cdot 10^{-6}$
		120		$2.33 \cdot 10^{-1}$	$5.83 \cdot 10^{-2}$	$1.00 \cdot 10^{-5}$
		140		$3.18 \cdot 10^{-1}$	$7.94 \cdot 10^{-2}$	$2.00 \cdot 10^{-5}$
		160		$4.15 \cdot 10^{-1}$	$1.04 \cdot 10^{-1}$	$2.84 \cdot 10^{-4}$
		180		$5.25 \cdot 10^{-1}$	$1.31 \cdot 10^{-1}$	$4.40 \cdot 10^{-4}$
		200		$6.48 \cdot 10^{-1}$	$1.62 \cdot 10^{-1}$	$9.50 \cdot 10^{-4}$
		220		$7.84 \cdot 10^{-1}$	$1.96 \cdot 10^{-1}$	$1.55 \cdot 10^{-3}$
		240		$9.33 \cdot 10^{-1}$	$2.33 \cdot 10^{-1}$	$1.55 \cdot 10^{-3}$
(c)	Glare2A-5/4-0.3 L-T	240	0.05	$9.22 \cdot 10^{-2}$	$2.30 \cdot 10^{-4}$	$5.67 \cdot 10^{-7}$
		280		$1.25 \cdot 10^{-1}$	$3.14 \cdot 10^{-4}$	$1.13 \cdot 10^{-5}$
		300		$1.44 \cdot 10^{-1}$	$3.60 \cdot 10^{-4}$	$9.67 \cdot 10^{-5}$
(c)	Glare2A-5/4-0.3 L-T	240	0.5	$9.22 \cdot 10^{-2}$	$2.30 \cdot 10^{-2}$	$1.50 \cdot 10^{-8}$
		250		$1.00 \cdot 10^{-1}$	$2.50 \cdot 10^{-2}$	$1.20 \cdot 10^{-7}$
		260		$1.08 \cdot 10^{-1}$	$2.70 \cdot 10^{-2}$	$1.70 \cdot 10^{-7}$
		320		$1.64 \cdot 10^{-1}$	$4.10 \cdot 10^{-2}$	$5.00 \cdot 10^{-7}$
		360		$2.07 \cdot 10^{-1}$	$5.18 \cdot 10^{-2}$	$8.25 \cdot 10^{-7}$
		380		$2.31 \cdot 10^{-1}$	$5.78 \cdot 10^{-2}$	$2.08 \cdot 10^{-6}$
		400		$2.56 \cdot 10^{-1}$	$6.40 \cdot 10^{-2}$	$1.93 \cdot 10^{-6}$
		420		$2.82 \cdot 10^{-1}$	$7.06 \cdot 10^{-2}$	$1.55 \cdot 10^{-5}$
(f)	Glare4B-5/4-0.3 T-L	200	0.05	$8.97 \cdot 10^{-2}$	$2.24 \cdot 10^{-4}$	$2.00 \cdot 10^{-6}$
		240		$1.29 \cdot 10^{-1}$	$3.23 \cdot 10^{-4}$	$1.50 \cdot 10^{-5}$
		260		$1.52 \cdot 10^{-1}$	$3.79 \cdot 10^{-4}$	$2.50 \cdot 10^{-5}$

5.3 Crack Opening Shape

5.3.1 Programme objective

The objective of the crack opening shape investigation is to obtain the crack opening contour of fatigue cracks in CCT specimens under maximum applied fatigue loading, which is necessary to validate the theoretical crack opening shape utilized in the prediction method.

5.3.2 Specimen geometry and test set-up

The specimens used in the crack opening shape investigations were Glare3-4/3-0.4, Glare3-6/5-0.4 and Glare3-8/7-0.4 CCT specimens that were fatigue tested as part of the crack propagation investigation discussed in section 5.5 [4]. The specimen geometry is presented in Figure 5.7, with corresponding values in Table 5.5.

5.3.3 Measurement and analysis approach

During the fatigue crack growth tests the specimens were loaded to the maximum fatigue load S_{max} to obtain the maximum crack opening. With the digital imaging system images were captured and stored from the open crack at several crack lengths. An example of such an image is presented in Figure 5.3.

Because the magnification of the camera and the resolution of the image is fixed, the dimensions of one pixel are known [5]. For the images investigated within this research, one pixel corresponds to $2.8 \times 2.8 \mu\text{m}$.

From the captured images, the crack opening was determined at a number of locations along the crack length using a criterion based on the pixel colour. The approach is illustrated in Figure 5.3. The crack itself contains black pixels, while the aluminium consists mainly of grey pixels. The edge of the crack was determined based on the colour scheme between black and grey at the location of the crack edge using engineering judgement. If the crack opening is locally larger than the size of one pixel, the edge of the crack can be determined with this criterion with an accuracy of half a pixel width, which is $1.4 \mu\text{m}$.

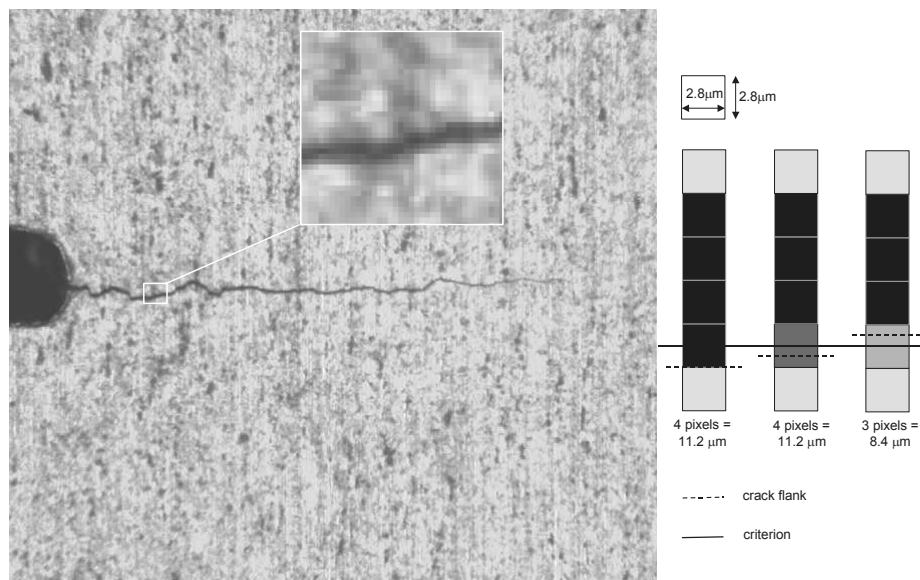


Figure 5.3 Illustration of digital crack image with the crack opening measurement criterion

With the digital camera system, an array of images could be captured for cracks larger than the width of a single image (2.1 mm). The crack opening shape of several cracks larger than 2.1 mm was investigated with this option. An example of the obtained crack opening shapes for short cracks between 0.5 and 2 mm is presented in Figure 5.4. From this figure the roughness due to the pixel size is evident. However, the results are accurate enough to be used in the development of the method, as discussed in chapter 6.

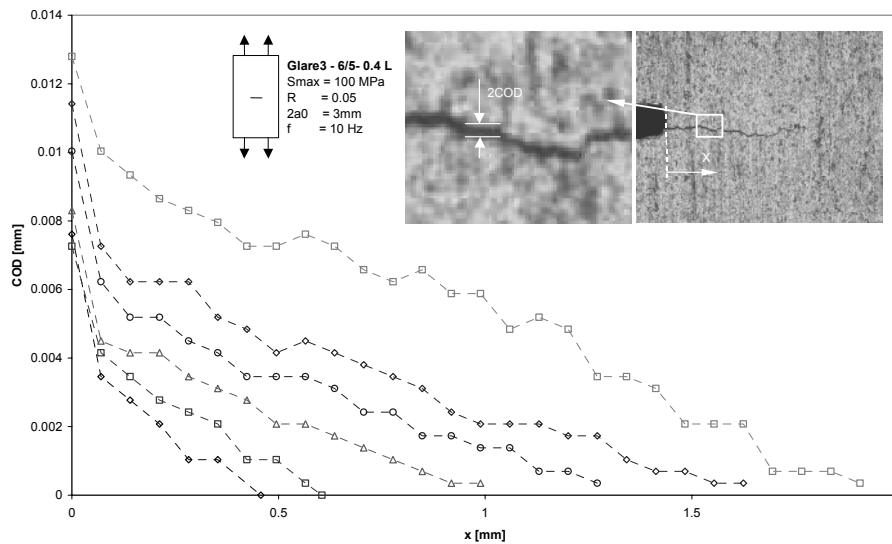


Figure 5.4 Example of the crack opening shapes for different fatigue crack lengths in a Glare3-6/5-0.4 specimen, measured from the notch tip ($x=0$) to the crack tip.

Fatigue crack growth tests on large panels containing a large starter notch, the crack opening shape was measured using the same digital camera system during the tests instead of analysing image captures after the test. However, in principle the measurement system is the same.

5.4 Delamination Shape

5.4.1 Programme objective

The objective of the delamination shape investigation is to obtain quantitative information about the delamination shapes at the interfaces at fatigue cracks in CCT specimens. This information is necessary to validate the theoretical delamination shape utilized in the method.

5.4.2 Specimen geometry

The specimens used for the delamination shape investigations were Glare CCT specimens from the fatigue crack propagation test programmes discussed in section 5.5 and which are reported in [4,6,7]. The specimen geometry is presented in Figure 5.7, with corresponding values in Table 5.5.

5.4.3 Measurement and analysis approach

The investigation of the delamination shape can be performed in several ways. Two main techniques are the non-destructive ultrasonic C-scanning of the laminate and the destructive etchings of the outer aluminium layers, revealing the subsurface interface containing the delamination contour.

The advantage of the ultrasonic C-scanning technique is the possibility to investigate the delamination areas during the fatigue crack propagation tests. The specimen can be taken from the test frame and C-scanned after which it can be inserted in the testing frame again to continue the crack propagation test.

However, the major disadvantage of C-scanning the specimens containing cracks is the superposition of the delamination areas. The delamination areas at each aluminium/fibre interface are not exactly positioned above each other and do not have identical shapes, which results in a superimposed C-scan shape which is larger than each individual shape. Notwithstanding the accuracy of the C-scan method, based on the obtained C-scan image one cannot be sure what the size and shape of the delamination at one interface is. This phenomenon is illustrated in Figure 5.5.

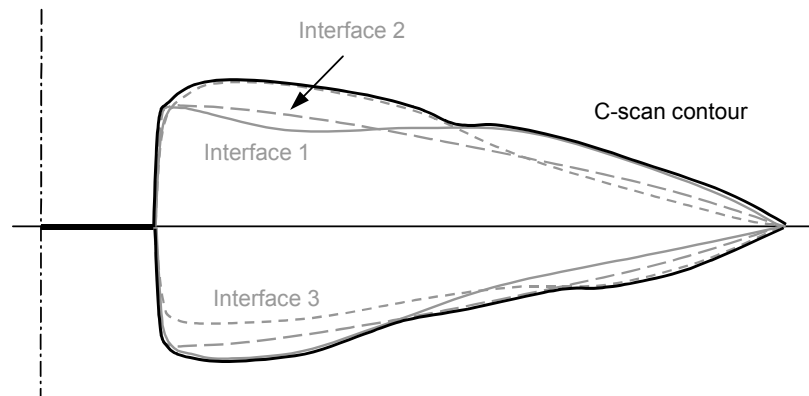


Figure 5.5 *Illustration of the relation between the delamination areas at each interface and the delamination area measured with the C-Scan.*

In order to obtain more accurate delamination shapes at the interfaces, the technique of etching the outer aluminium layers was utilized in this investigation. Once the fatigue crack propagation tests were finished, the aluminium layers were etched away and the delamination shapes were investigated. Further details on the applied etching technique are given in section 5.6.4.

A disadvantage of the etching technique for delamination investigation is the fact that the delamination size obtained can differ from the delamination size at the inner aluminium/fibre interfaces. Due to the mixed fracture mode at the interface adjacent to the outer aluminium layer [2], compared to the mode II at the inner interfaces, a difference between delamination areas can be expected.

Another disadvantage of the etching technique is, that it can only be applied after the crack propagation test is finished. The evolution of the delamination shape during the crack propagation life cannot be monitored with this technique. To overcome this problem, Quinn [8] tested two specimens containing four parallel cracks. After each 15 mm crack extension, he cut off one specimen for delamination investigation after etching, while continuing the crack propagation test with the remaining specimen. An example of the measured delamination shapes is given in Figure 5.6.

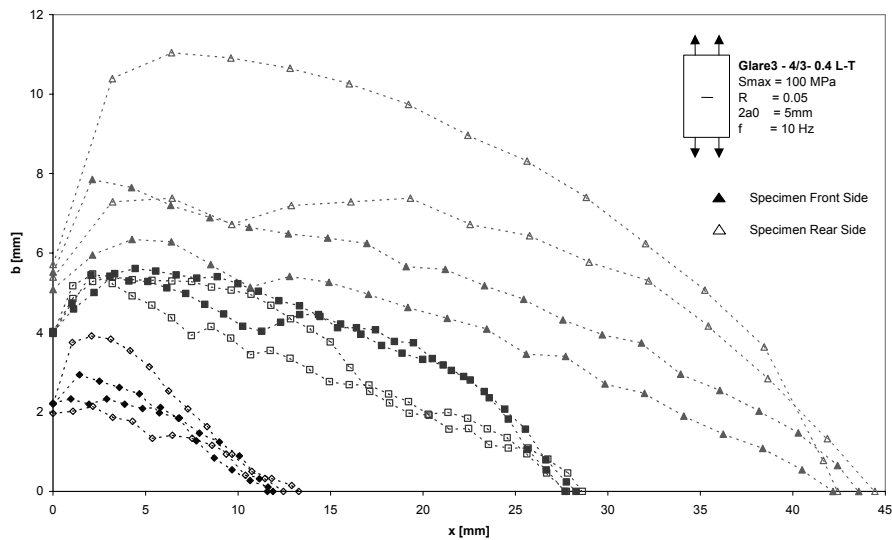


Figure 5.6 Measured delamination shapes from a crack growth test on a Glare3-4/3-0.4 CCT specimen containing four parallel cracks, data from [8]

Although the approach followed by Quinn, provided a qualitative insight in the delamination growth during crack propagation in the Glare specimens, quantitative delamination growth investigation remained impossible. The obtained delamination shapes do not belong to the same crack. As result of scatter in crack propagation and delamination growth results from the four parallel cracks, errors can be introduced in the observed delamination growth trend, which makes comparison unreliable.

5.5 Fatigue crack growth in aluminium

5.5.1 Programme objective

The objective of the fatigue crack propagation tests on monolithic aluminium is to determine the empirical Paris relation between the experimentally observed crack growth rate and the corresponding calculated stress intensity factor range [9].

5.5.2 Specimen geometry

The specimens used in the crack propagation tests were thin monolithic aluminium CCT specimens, of which the geometry is presented in Figure 5.7. The values for the parameters indicated in Figure 5.7 are listed in Table 5.3.

Table 5.3 Geometrical parameters of tested aluminium CCT configurations

W [mm]	L [mm]	2a ₀ [mm]	Number of parallel cracks	Number of specimens	Ref.
140	580	5	2	9	9

5.5.3 Test matrix and test set-up

Homan [9] fatigue tested in total 9 specimens to determine the parameters for the empirical Paris equation for aluminium 2024-T3. The specimens consisted of thin aluminium sheets instead of laminated aluminium sheets (without fibres), because the objective was to exclude any interaction effect occurring in the laminate. Buckling of the thin sheets was prevented using anti-buckling guides. The material and loading parameters applied in the tests are presented in Table 5.4. All tests have been applied at a loading frequency of 5 Hz.

Table 5.4 Material and loading parameters used in the test programme

Aluminium	Orientation	Aluminium thickness [mm]	S _{max} [MPa]	R
2024-T3	L-T, T-L	0.3, 0.4, 0.5	100	0.05

From the tests crack growth versus number of cycles data sets were obtained, which could be recalculated to crack growth rate versus stress intensity factor ranges, using the assumption that the stress intensity factor can be described with equation 3.1. Homan concluded based on comparison of the test data with other data on thicker aluminium 2024-T3 sheets, available in the literature, that the difference between the crack growth behaviour of thin and thick aluminium sheets was small. The differences between the crack growth behaviour of the three sheet thicknesses appeared to be small as well. Therefore, he plotted the data sets on double log scale and fitted one linear trend line through the data sets, which is known as the Paris equation.

$$\frac{da}{dN} = C\Delta K^n \quad (5.1)$$

The parameters for the equation were found to be $C = 2.17 \cdot 10^{-12}$ and $n = 2.94$ for ΔK in $[\text{MPa}\sqrt{\text{mm}}]$ and da/dN in $[\text{mm}/\text{cycle}]$. Using the assumption that the crack growth rate in the aluminium layers of Glare is similar to the crack growth behaviour of one thin aluminium sheet, this Paris equation provides the relation between crack growth rate and stress intensity factor range for the aluminium layers in Glare.

5.6 Fatigue crack propagation tests on Glare

5.6.1 Programme objective

The objective of the fatigue crack propagation investigations is to obtain the relation between the crack growth rate and the crack length for Glare CCT specimens under various material-, geometrical- and constant amplitude loading conditions. This data can be obtained from the measured data, which consists of crack length versus the number of cycles

5.6.2 Specimen geometry

The specimens used in the crack propagation tests were Glare CCT specimens, of which the geometry is presented in Figure 5.7. To summarize the various geometries utilized in the different test programmes, the values for the parameters indicated in Figure 5.7 are listed in Table 5.5. Except for the fatigue tests on the large crack configuration, all specimens consisted of two or more parallel cracks. The reason to apply parallel cracks is to increase the amount of test data for one configuration without increasing the number of tests specimens in the test programme.

The distance between the parallel cracks is chosen such that the stress distribution over the specimen width halfway between the cracks is uniform, as can be determined with [10]. Therefore, it is assumed that the parallel cracks do not have any influence on each other. The test data of the parallel cracks are depicted separately in the crack growth figures presented in this thesis.

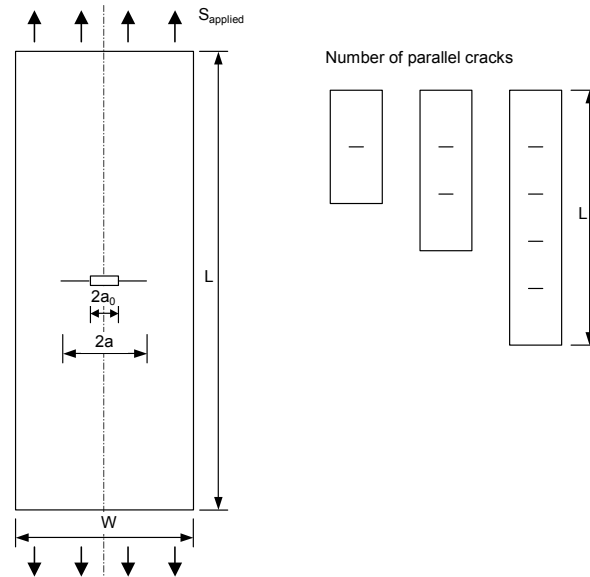


Figure 5.7 Specimen geometries for CCT specimens

Table 5.5 Geometrical parameters of tested CCT configurations

W [mm]	L [mm]	2a ₀ [mm]	Number of parallel cracks	Distance between cracks	Number of specimens	Ref.
100	700	3, 10, 20	2	300	18	4
140	580	5, 30	2	160	78	6
160	1170	5	4	160	2	8
500	750	75	1	-	4	7

5.6.3 Test matrix and test set-up

The crack propagation tests, which serve as basis for the method development presented in this thesis, belong to different research projects, each with a specific research objective. In this section, only a brief overview of the variation of material and test parameters within these test programmes is presented. A complete overview of all the test conditions in these programmes is given in Appendix D. To present all the observations and findings from these test programmes goes beyond the scope of this thesis. Therefore only the relevant parameters and findings will be given.

For crack propagation, cross-ply Glare3 and Glare4 were investigated. The material parameters are identified in Table 5.6. Within the different tests, several ranges of maximum applied load, stress ratio and frequencies were applied. The investigated ranges for the tests used in the current work are presented in Table 5.7.

With these specimens, the effect of the Glare grade, laminate lay-up and aluminium layer thickness on the crack growth behaviour were determined for different applied loading cycles. Examples of the effect of the material and geometrical parameters on the crack growth behaviour of Glare are given in Figure 5.8 to Figure 5.11.

Table 5.6 Material parameters varied in the test programmes

Grade	Lay-up	Aluminium thickness [mm]	Number of specimens
Glare3	3/2, 4/3, 5/4, 6/5, 8/7	0.3, 0.4, 0.5	48
Glare4B	3/2, 4/3, 5/4, 6/5, 8/7	0.3, 0.4, 0.5	48

Table 5.7 Test parameters varied in the test programmes

S _{max} [MPa]	R	f [Hz]
80, 100, 120, 160	0.05, 0.1, 0.5	4, 10

5.6.4 Measurement and analysis approach

Within the different programmes, crack length measurements have been performed using the visual techniques, such as the binocular microscope and the digital camera, and the Potential Drop Method, which will be further explained in the following section. All crack length have been measured by taking the average of the crack on the left side and the right side of the notch. In one of the investigations, the calculation of the stress intensity factor at the crack tip was verified using the strain gauge technique presented in [12] and discussed in section 5.7.3.

The large amount of crack growth results obtained with the experimental programmes cannot be presented here. However, with the help of some examples the most important observed effects of material- and geometrical parameters on the crack growth behaviour will be discussed. The effect of the Glare grade on the crack growth behaviour is presented in Figure 5.8. As discussed in the previous chapter, the crack growth behaviour for small cracks is dominated by the aluminium crack growth behaviour, due to the absence of efficient fibre bridging. Since the far field aluminium stress cycles of the three depicted Glare laminates are similar, the crack growth rates of the three depicted Glare laminates start initially approximately at the same level. Glare3-4/3-0.4 and Glare4B-4/3-0.4 L-T have the same amount of fibre layers oriented in loading direction, while the Glare4B-4/3-0.4 L-T has twice the amount of fibre layers perpendicular to the loading direction. As result, the crack growth behaviour does not differ significantly. The difference becomes significant for Glare4B-4/3-0.4 T-L, where the amount of fibre layers oriented in loading direction is twice the amount of Glare3-4/3-0.4 L-T. This results in more efficient fibre bridging and thus slower crack growth rates.

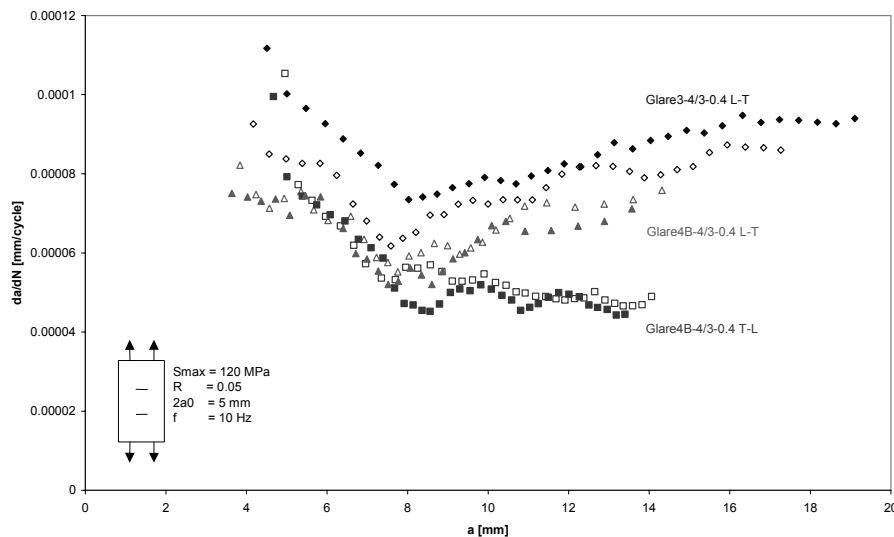


Figure 5.8 Effect of the Glare grade on the crack growth behaviour of Glare [6]

The effect of the laminate lay-up is presented in Figure 5.9, where it is visible that increasing the laminate lay-up gives a reduction in the crack growth rate. The far field aluminium stress cycles are similar for the three illustrated cases. However, this trend can be explained with load transfer at the aluminium/fibre interfaces as result of fibre bridging. The ratio of number of aluminium layers over the number of interfaces decreases with increasing laminate lay-up. This means that for increasing laminate lay-ups the load transfer per interface decreases and thus the delamination growth. As a consequence, the fibre bridging is more efficient for thicker laminates and the crack growth rates are lower.

Fatigue crack propagation and delamination growth in Glare

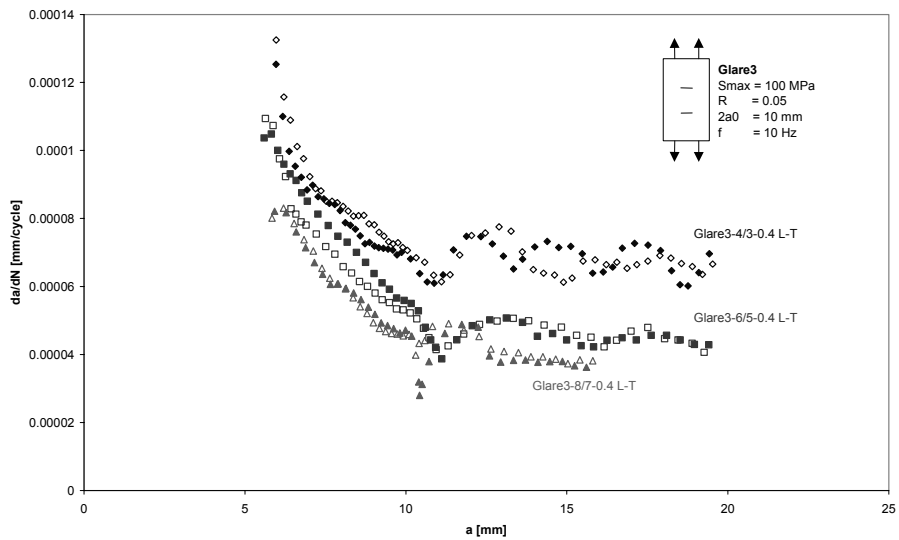


Figure 5.9 Effect of the laminate lay-up on the crack growth behaviour of Glare [4]

Similar to the discussion of the effect of the laminate lay-up, the effect of the aluminium layer can be explained, illustrated in Figure 5.10. Increasing the aluminium layer thickness for a given laminate lay-up, results in similar far field aluminium stress cycles, but increases the load transfer per aluminium/fibre interface. As result, the delamination growth increases, the bridging efficiency increases and the crack growth rate increases as well.

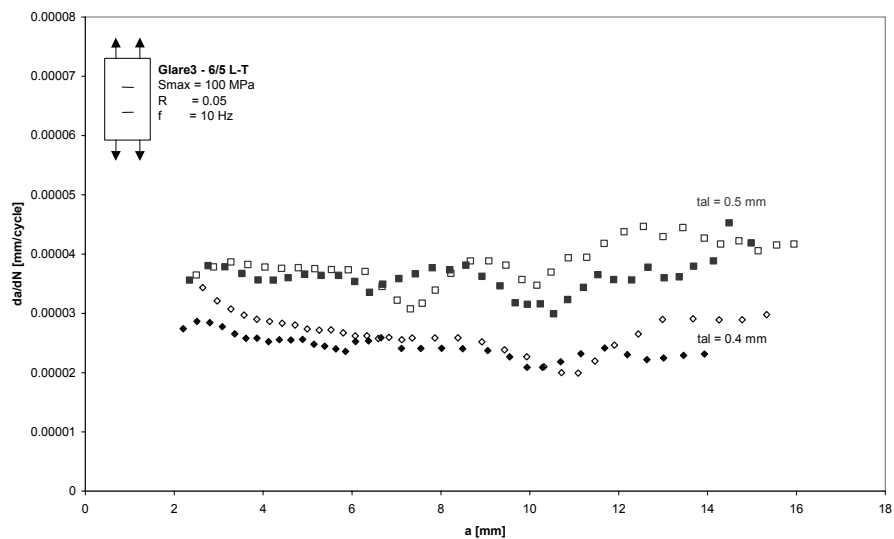


Figure 5.10 Effect of the aluminium thickness on the crack growth behaviour of Glare [4]

The effect of the starter notch length on the crack growth behaviour is illustrated in Figure 5.11. The crack growth rate for specimen with larger starter notch lengths is larger compared to the small starter notch lengths. This can be explained by the absence of bridging fibres in the starter notch. On the other hand, it can also be seen that the length until the approximately constant crack growth rate is reached increases with increasing starter notch lengths, as was reported in [4]. This means that the crack length needed for the fibres to obtain an efficient balance increases with increasing starter notch length.

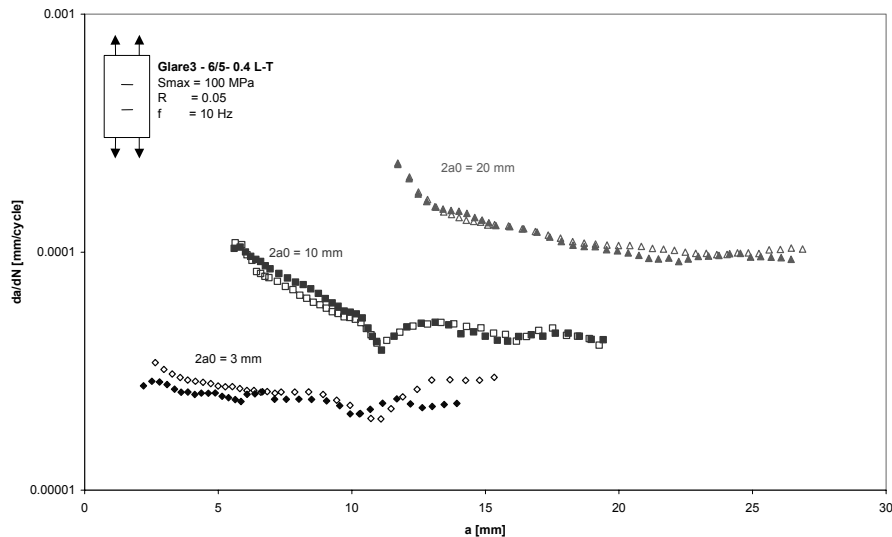


Figure 5.11 Effect of the starter notch length on the crack growth behaviour of Glare [4]

5.7 Measurement techniques

To measure the parameters in the experimental programmes discussed in the previous sections, several measurement techniques were used, of which the most significant devices will be discussed in the present section.

To measure the crack lengths during the crack propagation tests a digital imaging system and the Potential Drop Measurement Technique were used beside visual measurements with binocular microscopes. The digital imaging system was not only used for crack length measurement, but also used to investigate the crack opening shape of the fatigue cracks and the delamination growth in the delamination specimens. Both techniques will be further discussed in section 5.7.1 and 5.7.2.

To estimate the Stress intensity Factor at the crack tip at a predefined crack length application of strain gauges has been utilized, see section 5.7.3. To measure the delamination area in the CCT specimen configurations, a C-scan technique has been used, together with visual inspection after etching away the aluminium layers. Both techniques are discussed in respectively section 5.7.3 and 5.7.4.

5.7.1 Digital Imaging System

The digital imaging system consists of a CCD camera and imaging software, which was partly developed in-house at Delft University of Technology [5]. The xyz-controls of the CCD camera with a moving range of 170 mm parallel and 50 mm perpendicular to the specimen surface, are controlled by a computer, which also captures the images from the video output of the camera with the in-house developed software package Impress.

With this software package, crack length measurements can be performed during test, but also captured crack images can be stored for further measurement and investigation. An example of such a captured image is given in Figure 5.3. The captured images have the dimensions of 735 x 570 pixels where the pixels have the dimensions of 2.8 x 2.8 μm . However, the imaging software allows digital merging of image arrays, which gives the possibility of measuring larger areas than the 2.1 x 1.6 mm covered by a single image.

5.7.2 Potential Drop Method

The Potential Drop Method (PDM) is a crack measurement method based on the relation between the potential field and the cross section of a metal wire or sheet. The potential field in a CCT specimen changes with increasing crack length, causing a potential drop over the crack. This potential drop is a measure for the crack length. Once the correlation between the crack length and the potential drop over the crack has been determined for certain specimen geometry by means of calibration, the potential drop measurements can be applied without further visual crack measuring techniques. This gives the opportunity to fully automate the fatigue crack propagation tests, which is highly desirable for tests that last for a couple of days.

Another advantage of the PDM is the fact that crack length measurements can be performed in temperature chambers, where access with a binocular microscope or digital imaging systems is nearly impossible, and opening the temperature chamber for regular measurements is not an option.

The application of the PDM technique as utilised for the experimental test programmes is described in detail in [11]. The calibration curve was obtained by comparison of measurements obtained with the PDM technique and the values measured with the digital imaging system [4]. The obtained data pairs consist of PDM values and actual crack length, which can be plotted in a graph as illustrated in Figure 5.12. The calibration curve for the specimen geometries used in the crack propagation investigations was described by a second order relation for the small crack length region and a linear relation for the large crack length region. The calibration curve was determined from data sets given in Figure 5.12 at room temperature at one outer aluminium layer of the Glare specimen.

Due to the sensitivity to deviations in the applied current and measured potentials, the PDM measurements contain a certain amount of scatter. This scatter can be attributed to a large extent to the scatter in the obtained signal and the time frame over which the signal is grabbed and stored.

5 Experimental Programmes and Data Evaluation

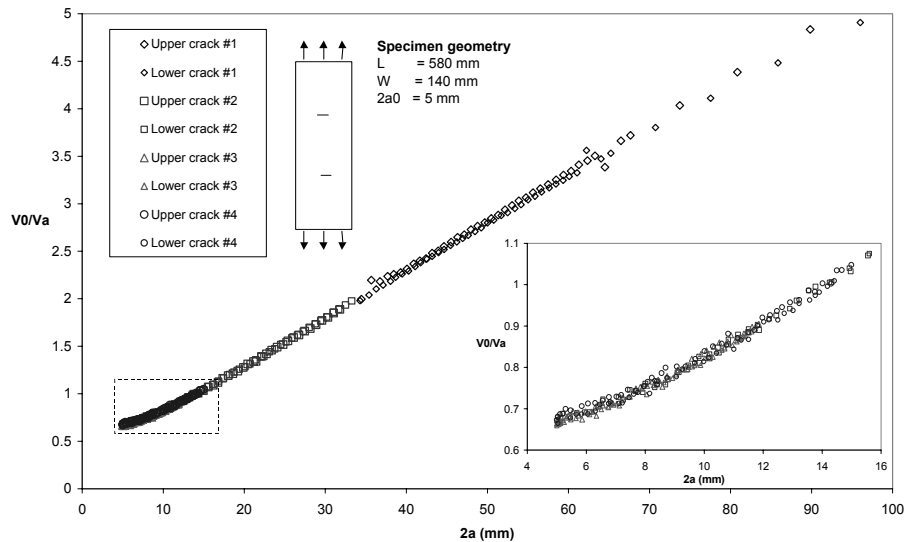


Figure 5.12 Calibration curves obtained from 4 different test specimens with equal geometry, but different loading conditions.

The PDM machine used in the Structures and Materials Laboratory averages the signal over an adjustable time range. Increasing the time range results in a decrease of signal variation, see Figure 5.13, which is preferable for scatter reduction reasons. However, increase of the time range, increases the time for each measurement. Since the measurements are performed while the testing machine is stopped at the maximum load level to open the crack, this means an increase of testing time.

Because most specimen geometries in the experimental programmes contain two or more parallel cracks, see Table 5.5, the signal must be measured over each crack. For this purpose, an automated switch was used to select the subsequent cracks during the signal readout. However, each switch induced a signal peak, after which the signal had to become stable at the correct level.

Increasing the time range over which the signal is averaged, results in an increase of time needed for the readout signal to become constant, see Figure 5.14, and thus an increase of time needed for each measurement. Therefore, an optimum is chosen, such that the scatter has an acceptable level and the interval between switch set and signal readout is about 4 seconds.

The amount of scatter in the signal readout is also related to the measurement interval, i.e. the number of fatigue cycles, as is illustrated in Figure 5.15. In this figure it can be seen clearly that signal readout every 2 kcycles results in recording negative crack growth rates over several intervals, while in spite of the scatter the trend of the data is linear increasing. Setting the measurement interval in Figure 5.15 at 4 kcycles, results in this case in positive crack growth rates over each interval.

Fatigue crack propagation and delamination growth in Glare

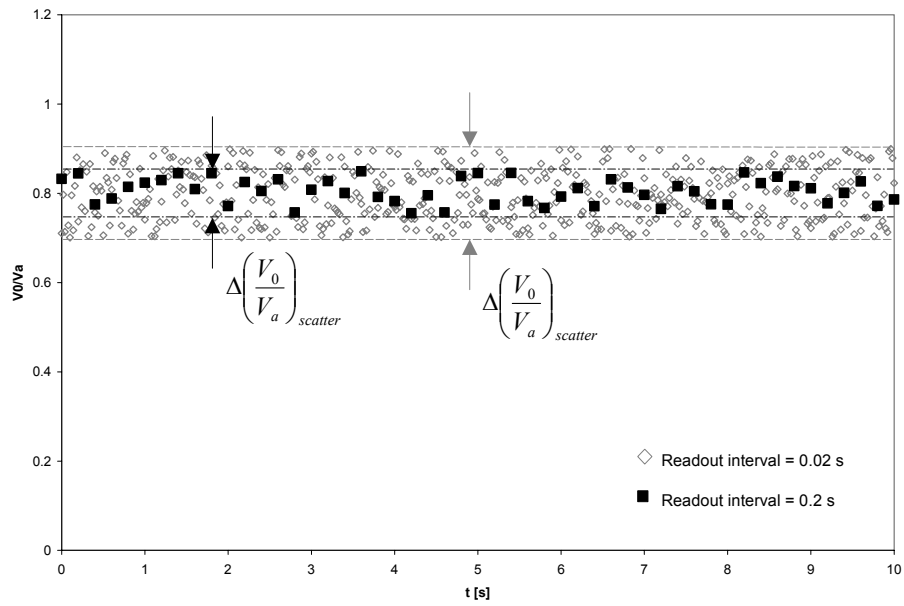


Figure 5.13 Illustration of the PDM signal scatter reduction due to an increase in the readout interval over which the readout signal is averaged.

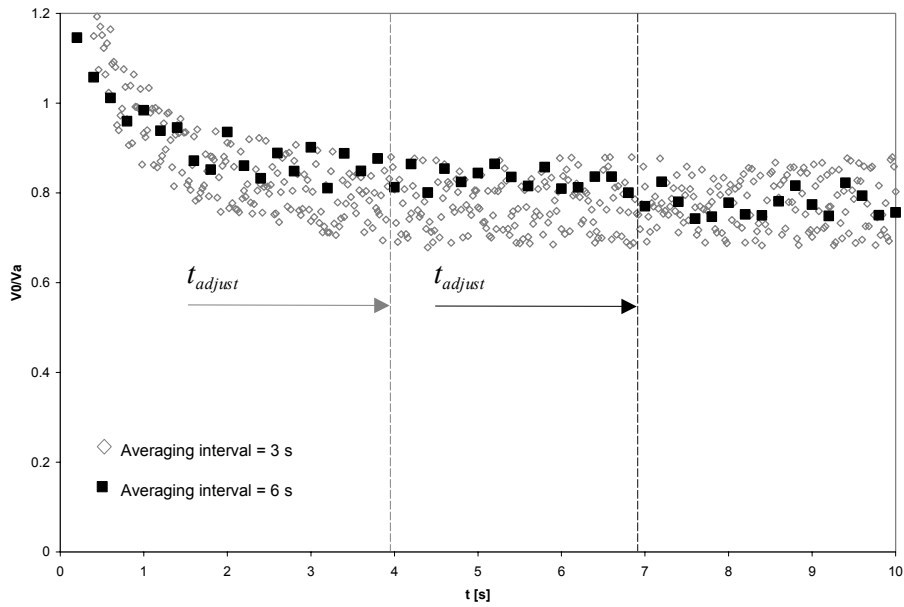


Figure 5.14 Illustration of the increase of the time needed for the signal to reach the constant level due to the increasing averaging interval.

The above discussion illustrated the sensitivity of the application of the Potential Drop method towards data scatter. The scatter can be reduced by the PDM machine by averaging the readout over a certain interval, but the scatter is also related to the combination of actual crack growth rates and measurement interval.

The higher the crack growth rate, or the steeper the slope, the smaller the measurement interval can be set. This means that equal measurement intervals for all tests, results in different amount of scatter for specimens showing different crack growth rates, which has to be adjusted later on with scatter reduction techniques [3] to obtain the same amount of scatter in all data.

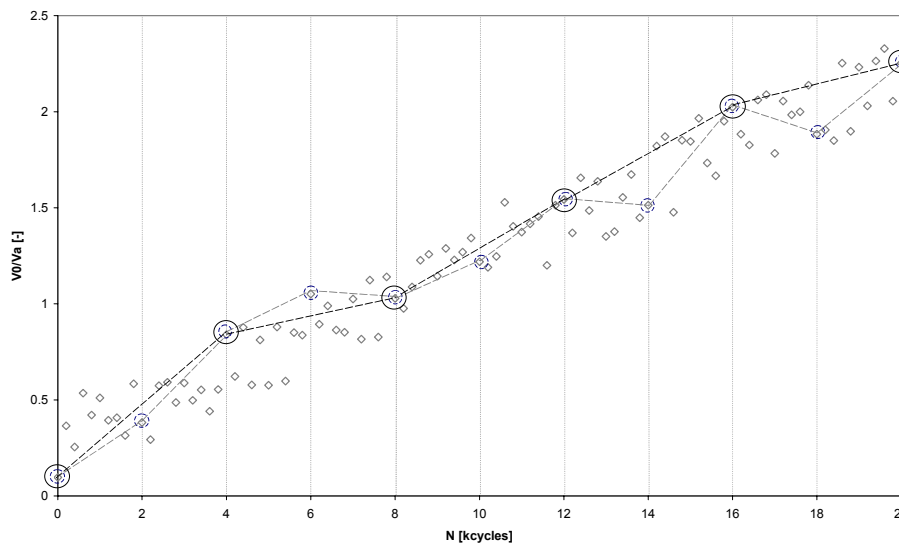


Figure 5.15 Illustration of the influence of measurement interval on the scatter in the data due to potential drop signal scatter

5.7.3 Application of strain gauges

To determine the stress intensity factor at the crack tip experimentally, strain gauges can be used [12]. The stress intensity factor can be determined using the strain measurement from the strain gauge positioned at a specific position and angle with respect to the crack tip in the aluminium layer.

The area around the crack tip can be divided into three regions, see Figure 5.16 (a). The inner boundary consists of a circle with a radius of half the sheet thickness and describes region I. The outer boundary consists of a circle with a radius of 30% of the half crack length and describes region III. Region II is the region between the two boundaries, see Figure 5.16 (a). The method presented here is only valid in region II of the aluminium layers with a Poisson's ratio of $\nu = 0.33$ [13]. If the strain gauge is positioned in region II under an angle of 60 degrees with respect to the crack tip, the stress intensity factor can be calculated with [13]

$$K_I = E \varepsilon_{x'x'} \sqrt{\frac{8}{3} \pi r} \quad (5.2)$$

where $\varepsilon_{x'x'}$ is the measured strain using the strain gage and r is the distance of the strain gage to the crack tip. The stress intensity factor determined with this method can be compared with the stress intensity factor calculated out of the crack growth data.

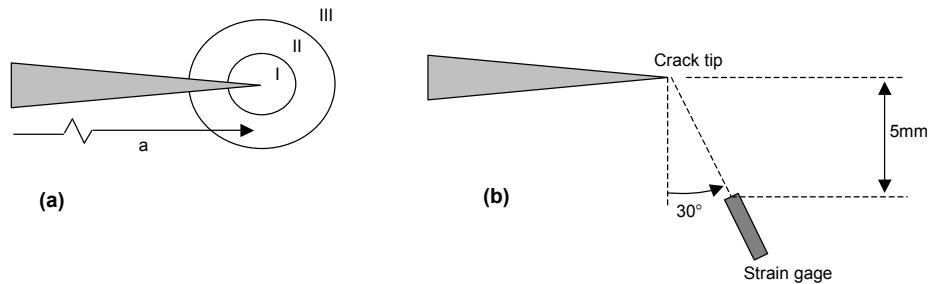


Figure 5.16 Three regions adjacent to the crack tip (a) and the position of the strain gage relative to the crack tip as used in the current test set-up (b).

Based on this theory, strain gauges were positioned as illustrated in Figure 5.16 (b) on the specimens that were fatigue tested in the experimental programme reported in [4]. The 5 mm long strain gauges, manufactured by Kyowa, were bonded on the outer surface of the aluminium layer.

Once the crack tip reached the location with respect to the strain gauge, as illustrated in Figure 5.16 (b), the strains were measured at the maximum applied load and at the unloaded situation. Since the crack path is quite irregular, the strains were measured several times with small intervals while the crack tip was close to the location. With the variation in measured strains being small, the correct value could easily be determined. The stress intensity factor obtained with the strain gauge method with the stress intensity factor calculated from the crack growth rate with the Paris equation were compared in [4] and a good correlation was reported.

5.7.4 Etching the outer aluminium layers

Etching the aluminium layers is a chemical process where the aluminium layer is removed at a controlled speed. The etching procedure discussed here has been reported by Vogelesang [14]. The etching speed depends on the concentration and the temperature of the sodium hydroxide (NaOH) bath and the amount of already dissolved aluminium. The etching depth is determined by the length of time the specimen is in the bath. The temperature of the bath is between 60 and 80°C.

In order to expose the bare aluminium to the etching bath, the primer layer was removed using sand paper. Sanding the area near the fatigue crack only reduces the etching process to a smaller area, making the process more efficient. After sanding

the surface the specimen is degreased in a P₃RST alkali bath at a temperature of 70°C for about 10 minutes, after which the specimen is etched. An example of an etched specimen is given in Figure 5.17.

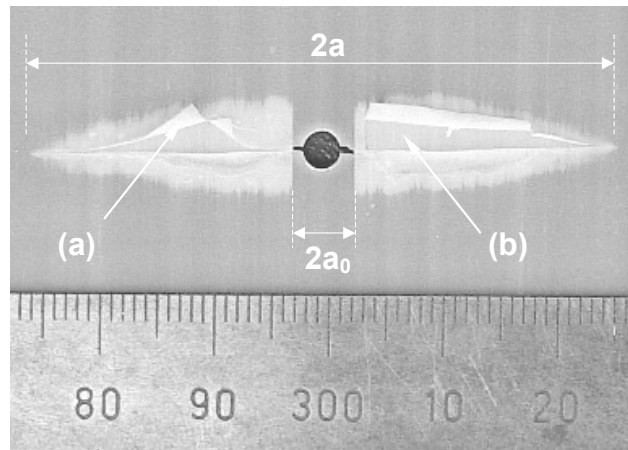


Figure 5.17 Example of a delamination area after etching the outer aluminium layer. The thin resin residue (a) and the fibre/adhesive layer (b) are visible.

5.8 Data Evaluation

Once the crack length measurements are performed and the data is available for evaluation, available techniques for scatter reduction were applied to minimise the scatter further [3]. Two methods in particular were used to calculate the crack growth rates using the crack length measurements: the Point-to-point method and the Seven Point Polynomial Incremental method, both described in [3]. The first method calculates the crack growth rate between two succeeding data points using a linear relation, corresponding to a crack length halfway the two measured crack lengths. The second method calculates the crack growth rate over a set of seven succeeding data points using a second order polynomial relation. The calculated crack growth rate follows from the polynomial relation at the crack length in the middle of the set of seven crack lengths.

The latter method has the advantage of reducing the scatter in the data as the second order polynomial relations acts to a certain extent as an average relation between the seven data points. This method is however sensitive for data points that deviate significantly from the trend in the data, as the effect of one extreme data point is visible over a range of seven successive new calculated data points. The test data was evaluated and extreme data points were eliminated using engineering judgement prior to application of the polynomial method.

References

- [1] **Marissen, R.**, *Fatigue Crack Growth in ARALL, A hybrid Aluminium-Aramid Composite Material, crack growth mechanisms and quantitative predictions of the crack growth rate*, PhD Thesis, University of Technology Delft, 1988.
- [2] **Suiker, A.S.J., Fleck, N.A.**, *Crack tunnelling and plain-strain delamination in layered solids*, International Journal of Fracture, **125** 1-32, 2004.
- [3] **ASTM E647 - 95a**, *Standard Test Method for Measurement of Fatigue Crack Growth Rates*, Annual Book of ASTM Standards, American Society for Testing and Materials, 1995.
- [4] **Alderliesten, R.C.**, *Development of an empirical fatigue crack growth prediction model for the Fibre Metal Laminate Glare*, Master Thesis, Delft University of Technology, 1999.
- [5] **Vries, T.J. de**, *Blunt and sharp notch behaviour of Glare laminates*, PhD Thesis, Delft University of Technology, 2001.
- [6] **Homan, J.J., Alderliesten, R.C.**, *Test data for Fatigue Crack Propagation in unstiffened GLARE – Through Cracks*, Report B2V-99-39, Delft University of Technology, 1999 (restricted).
- [7] **Alderliesten, R.C.**, *The influence of large saw-cuts on the fatigue crack propagation behaviour of Glare*, Report B2V-02-13, Delft University of Technology, 2002 (restricted).
- [8] **Quinn, B.G.**, *Delamination of Glare*, Masters of Engineering Thesis, Queen's University of Belfast, 2004.
- [9] **Homan, J.J.**, *Crack growth properties of thin aluminium sheets, Issue 2*, Report B2V-01-16, Delft University of Technology, 2002 (restricted).
- [10] **Tada, H., Paris, P.C., Irwin, G.R.**, *The Stress Analysis of Crack Handbook*, 3rd ed., The American Society of Mechanical Engineers, 2000
- [11] **Alderliesten, R.C., Hooijmeijer, P.A.**, *Guidelines for the application of the Potential Drop Method as a crack measurement technique in FML*, Report B2-99-30, Delft University of Technology, 1999.
- [12] **Sanford, R.J.**, *Principles of fracture mechanics*, Upper Saddle River: Prentice-Hall PTR, 2003.
- [13] **Nijssen, P.J.M.**, *Qualitative Investigation of Disbond Mechanisms under Simple-Sided Adhesively Bonded Repairs*, Master Thesis, Delft University of Technology, 1997.
- [14] **Vogelesang, L.B.**, *Handleiding voor het diepetsen*, Manual, Technische Hogeschool Delft, 1968 (dutch).

6

Crack Growth Prediction Model

Abstract – This chapter presents the crack growth model for fatigue crack propagation of through thickness cracks in Glare. Using the delamination model the relation between delamination growth and the Energy Release Rate is derived, which is implemented in the method describing the fatigue crack growth in Glare. Writing the Stress Intensity Factor at the crack tip as a function of the far field opening stress in the aluminium layer and the crack bridging stress, results in a phenomenological model describing the fatigue crack growth in Glare. The model is implemented in a numerical program and validated with a wide range of test data. Good correlation between predictions and experimental results is obtained over a wide range of conditions.



6.1 Introduction

It was explained qualitatively in the previous chapters, that the fatigue crack growth mechanism of Glare is a rather complex phenomenon. To develop an analytical method describing this phenomenon, several simplifying assumptions are necessary to describe the crack growth behaviour in straightforward relations. However, the method should remain sufficiently accurate compared to the real crack growth behaviour.

Two main assumptions for the method presented are that Linear Elastic Fracture Mechanics may be applied, and that the empirical relation between the crack growth rate da/dN and the effective stress intensity factor range ΔK_{eff} for thin monolithic aluminium sheets is also valid for the aluminium layers in Glare.

As a consequence, the crack growth in the aluminium layers in Glare is described using the effective stress intensity factor at the crack tip. This effective stress intensity factor needs to incorporate the effect of crack opening restraint, fibre bridging and delamination.

To determine the effective stress intensity factor, the superposition principle is used, which allows superimposing individual stress intensity factors. For the fatigue crack configuration in Glare it is assumed that the stress intensity factor consist of a crack

opening contribution due to far field stresses and a crack closing contribution due to the bridging stresses. The stress intensity factor at the crack tip is then written as

$$K_{tip} = K_{farfield} + K_{bridging} \quad (6.1)$$

It is important to make a distinction between the crack closing effect described in this chapter and plasticity induced crack closure. The latter describes the effect of cracks that close at stress levels above the minimum stress level, reducing the effective stress range and therefore affecting the crack growth behaviour. The crack closing effect described in this chapter is defined as the restraint on crack opening due to the bridging fibres only.

The approach presented in this chapter consists of several steps in order to derive the expression for the effective stress intensity factor. Due to the interdependency of crack opening restraint, fibre bridging and delamination, some intermediate steps with corresponding assumptions are made to determine the contribution of each mechanism to the overall crack growth behaviour.

The first step consists of the assumption that the delamination growth perpendicular to the fatigue crack in the aluminium layers, thus in loading direction, can be approximated by the delamination behaviour in a one-dimensional configuration. Ignoring any effect in the second and third dimension reduces the problem of delamination growth to a closed form expression, where the delamination growth rate is directly related to the known stress state in that particular configuration. This approach is presented in section 6.2.

The second step consists of the derivation of the bridging stresses along the crack length for a given fatigue crack geometry in Glare. This geometry includes the delamination shape and crack opening contour under the maximum applied loading. For this derivation, which is based on the description of the crack opening contour, the delamination can in principle have any continuous shape, as both the delamination shape and the bridging stresses are related to each other. The actual shape depends on the delamination growth behaviour derived in section 6.2 and the actual bridging stresses along the crack, which are derived in section 6.3.

Once the delamination growth behaviour and the bridging stresses as function of an arbitrary delamination shape are known, the actual delamination shape can be determined by iteration between the relations derived in the first two steps. The results of this third step, which is discussed in section 6.4, consist of actual delamination shapes. These actual delamination shapes are then used as input parameter for the bridging stress determination, discussed in section 6.3.

The fourth step, presented in section 6.5, consist of the derivation of the expression for the stress intensity factor due to bridging $K_{bridging}$ by integrating the effect of the derived bridging stresses over the total crack length. The stress intensity factor at the

crack tip can then be determined by subtracting the stress intensity factor due to bridging from the far field stress intensity factor according to equation (6.1).

The applied numerical approach will be discussed briefly in section 6.6 and the method will be validated with experimental results in section 6.7 based on the following three criteria:

- *Physical realistic* - The relations must describe the physical mechanisms without any fitting parameter or correction factor.
- *Accuracy* - The method should predict the crack growth behaviour sufficiently accurate compared to the test results over a sufficiently wide range of conditions
- *Robustness* - The results must be correctly dependent on the initial values for crack length and delamination shape and size

6.2 Step 1: delamination growth behaviour

The delamination growth can be approximated by the delamination growth behaviour in a one-dimensional configuration by ignoring any effect in the direction perpendicular to the principal load. The problem is reduced to a configuration where the stress state is known and where a close form solution can be derived between the known stress state and corresponding delamination growth.

The approach is illustrated in Figure 6.1 where the stress state at a certain location along the crack length in a three-dimensional fatigue crack configuration, is represented by a strip of width dx and length L . For this strip, the delamination behaviour is approximated by the two-dimensional delaminated strip of width W and length L for which the stress state is known.

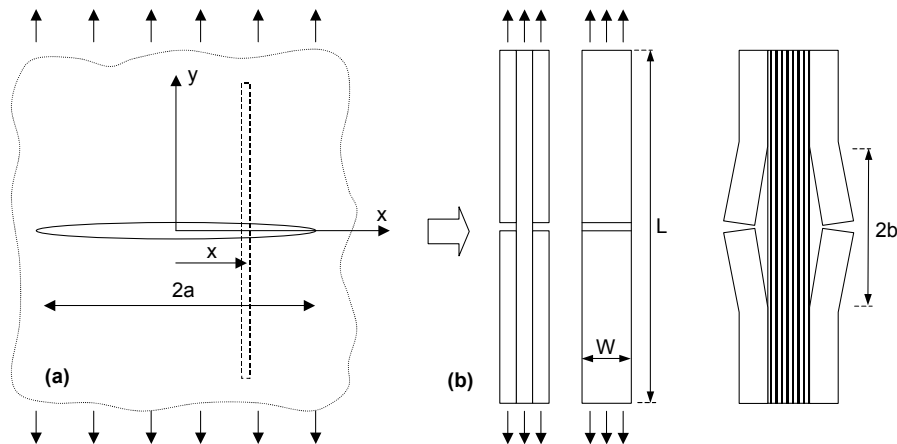


Figure 6.1 Delamination approach in a fatigue crack configuration in Glare

In the fatigue crack configuration a portion of the load is transferred through the fibre layers over the crack in the aluminium layers, and a part of the load is transferred through the net section in the aluminium layers. The second part is ignored when looking at a one-dimensional delamination configuration as illustrated in Figure 6.1 (b), where all load is transferred through the fibre layers. The stress in the fibre layers in the centre crack tension configuration is not known at this stage, because it is not known which part is transferred through the fibre layers and which part through the net section. Therefore, to correlate the one-dimensional configuration to the fatigue crack configuration, the comparison must be made on basis of crack opening. It is assumed that equal crack opening and corresponding delamination length in both configurations, yield equal fibre stress.

This assumption is only valid if the fibre stresses in the delaminated area of the centre crack tension configuration are not redistributed perpendicular to the loading direction. In view of the relatively low in-plane shear stiffness of the fibre layers (shear modulus is 5.55 GPa compared to 27.6 GPa for monolithic aluminium), it can be argued, that this redistribution is indeed negligible and that the one-dimensional modelling is acceptable.

6.2.1 Energy Release Rate and delamination growth

To predict the delamination growth, the relation between the stress intensity factor range ΔK_{II} at the delamination tip and the delamination growth rate must be determined. This relation can be described with an empirical Paris type equation, similar to the mode I crack growth rate da/dN in the aluminium layer and the corresponding stress intensity factor range ΔK_I , see Figure 6.2.

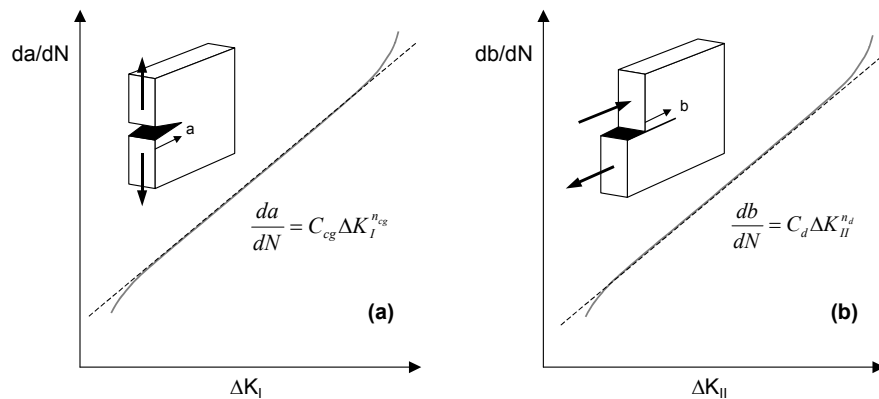


Figure 6.2 Characteristic curves for mode I crack growth (a) and mode II delamination growth (b) approximated with the Paris type equation.

However, the delamination occurs at the interface between two different materials (isotropic aluminium and orthotropic fibre layers). This means that the mode II

stress intensity factor at the delamination tip differs from the stress intensity factor at the crack tip in a homogeneous material. To avoid detailed calculation of the stress intensity factor at the delamination tip at the interface of two different materials, the delamination growth rate can also be calculated based on the energy release rate. Assuming a one-dimensional delamination configuration in Glare, the energy drop per unit length delamination extension can be directly derived from the calculated fibre stresses in the delaminated area. For that case, the Paris relation for delamination growth can be derived according to Marissen [1]

$$\frac{db}{dN} = C_d \left(\sqrt{G_{d,\max}} - k \sqrt{G_{d,\min}} \right)^{n_d} \quad (6.2)$$

where C_d and n_d are the Paris constants for a given delamination interface. The dimension of C_d depends on the value of n_d . Rewriting the Paris relation from stress intensity factor to energy release rate with equation (6.2) gives $k = 1$.

The value of $k = 1$ differs from the value $k = 0.69$ obtained by Marissen for Arall. He observed an effect of the mean stress on the delamination growth when comparing the calculated shear stresses at the interface and the measured delamination growth rates. From the correction on the calculated minimum shear stress at the interface, Marissen derived the value for k [1].

Since the Paris relation is empirical anyway, other forms for db/dN can also be used, such as the one given by Yeh [2]

$$\frac{db}{dN} = q \Delta G_d^m \quad (6.3)$$

where the effect of mean stress or stress ratio must be included in the definition of G_d . However, in the methodology proposed in this chapter, the delamination growth rate db/dN will be described by the Paris relation given in equation (6.2) for $k = 1$.

6.2.2 Delamination growth experiments

The delamination growth behaviour has been investigated for two Glare grades, both with a symmetric prepreg lay-up: Glare2B (90°/90°) and Glare4B (90°/0°/90°) [3]. The specimens are tested in L-T and T-L direction to investigate the effect of the prepreg layer direction adjacent to the cracked aluminium layer.

To investigate the effect of the loading mode, two specimen configurations were tested. The first configuration with a 5/4 lay-up, contained a crack in the inner aluminium layer, resulting in a mode II loading, while the second configuration with a 2/1 lay-up containing cracks in both aluminium layers, represented a combined mode I and mode II loading, hereafter denoted as mixed-mode.

The specimen geometry was chosen to be similar to the geometries numerically investigated by Suiker and Fleck [4], who investigated delamination growth in laminates consisting of two different elastic and isotropic materials under quasi-static loading.

Although the quasi-static loading and the dynamic fatigue loading yield significantly different characteristics, several results from their finite element modelling work applying linear elastic fracture mechanics, can be used to explain the behaviour observed during the experiments.

Suiker and Fleck [4] calculated with finite element analysis an initial mode-mixture for the mode II delamination specimens. The calculated mode-mixture follows from the calculation of the energy release rate, which depends on the delamination length for small delaminations. Starting from the artificial crack, the delamination propagates under increasing mode-mix until pure mode II is reached for delamination lengths of about three times the aluminium layer thickness. This effect is more pronounced for the tested specimens than calculated in their numerical work, because the aluminium layer edges were tapered due to sheet edge deburring, to avoid any sharp edge.

Examples of mode II delaminations propagating from the artificial crack along the interfaces are shown in Figure 6.3. Images of mixed-mode delaminations are given in Figure 6.4.

From these images, it can be seen that the delaminations propagate at the aluminium/prepreg interface when the fibres in the prepreg layer adjacent to the cracked aluminium layer are oriented in the loading direction. When the fibres are oriented perpendicular to the loading direction, the artificial crack continues as a mode I matrix crack through the prepreg layer until either an aluminium layer or a prepreg layer with fibres in loading direction is reached.

For the specimen with fibres oriented in loading direction, the delamination growth was measured. Two examples of delamination growth curves are given in Figure 6.5 and Figure 6.6. The Glare2A-5/4-0.3 specimen in Figure 6.5 was subsequently tested at five different load levels at a stress ratio of $R = 0.05$. The Glare4B-5/4-0.3 specimen in Figure 6.6 was only tested at one load level, because cracks initiated in the intact aluminium layers before the test was continued at the second load level.

6 Crack Growth Prediction Model

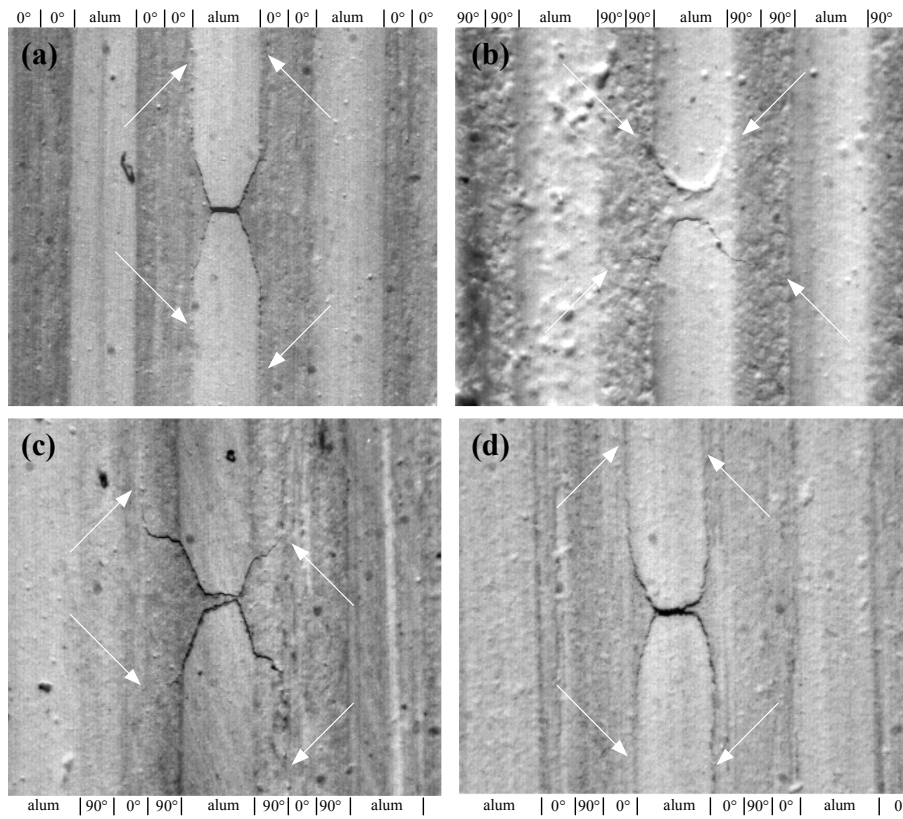


Figure 6.3 H-shape mode II delaminations in Glare2-5/4-0.3 L-T (a), Glare2-5/4-0.3 T-L (b), Glare4B-5/4-0.3 L-T (c) and Glare4B-5/4-0.3 T-L (d); arrows indicate position of delamination tips

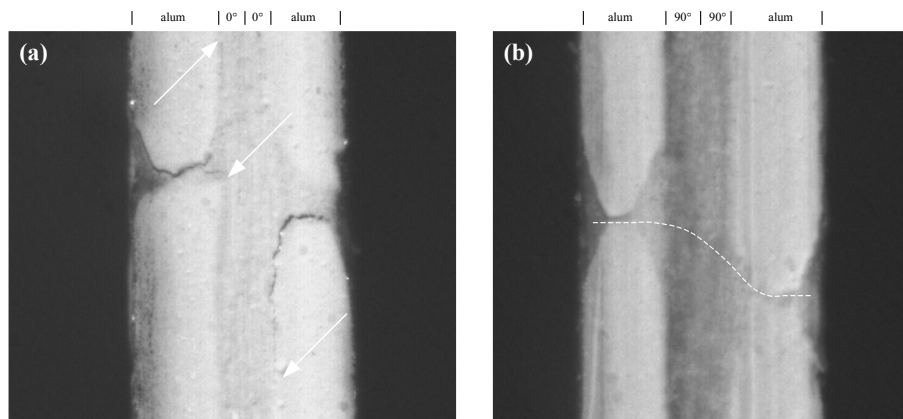


Figure 6.4 Mixed-mode delaminations in Glare2-2/1-0.3 L-T (a) and Glare2-2/1-0.3 T-L (b); arrows indicate position of delamination tips and dotted line indicates failure path during first load increment after inserting specimen.

Fatigue crack propagation and delamination growth in Glare

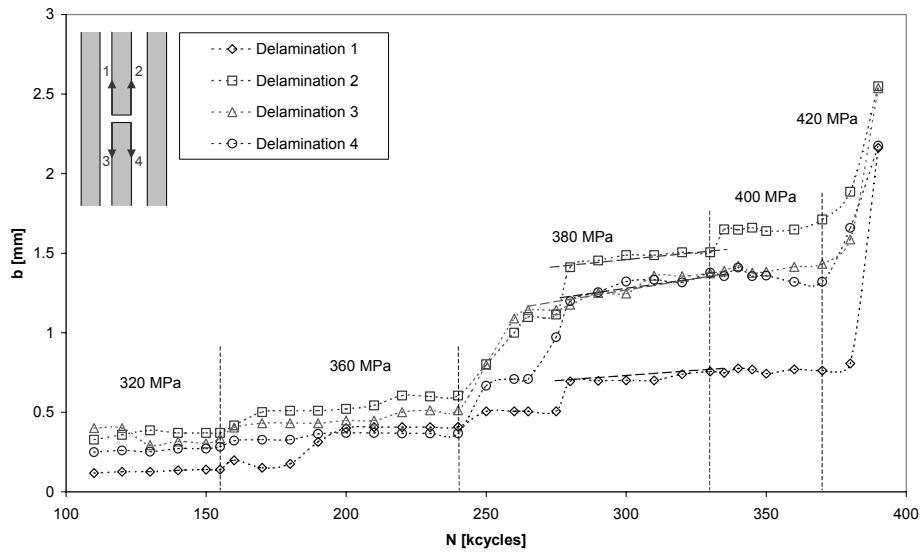


Figure 6.5 Delamination growth curve for Glare2A-5/4-0.3 tested in L-T direction at $S_{max}=320-420$ MPa and $R=0.05$

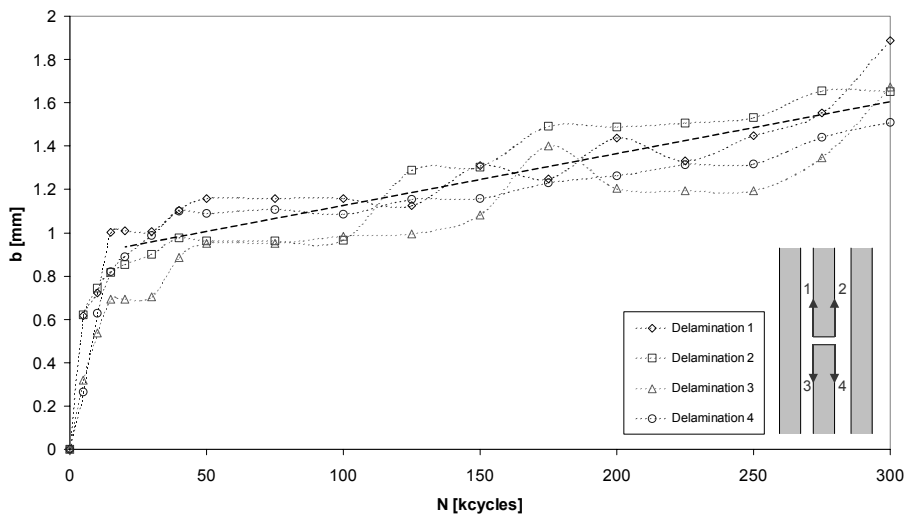


Figure 6.6 Delamination growth curve for Glare4B-5/4-0.3 tested in T-L direction at $S_{max}=200$ MPa and $R=0.05$

The effect of initial mode-mixture is observed as initial higher delamination growth rates, which decrease gradually to approximately constant rates. An example is given in Figure 6.6, where the delamination growth curve is presented for a mode II delamination specimen. Initially, the curve is quite steep, but then the delamination rate reduces and after a delamination length of about 0.9 mm is reached the curve shows an approximately constant slope.

Although the observed behaviour correlates with the numerical work performed by Suiker and Fleck, some mismatch was observed between the experimental and the numerical results, which can be attributed to parameters that were not taken into account in the numerical work.

Suiker and Fleck concluded based on their calculations, that the $5/4$ lay-up is the minimum lay-up necessary to obtain pure mode II at the interface with the pre-cracked centre layer, because the $3/2$ lay-up still contained a mode I contribution at the interface with pre-cracked centre layer.

However, very high stresses must be applied to find delamination growth under cyclic loading at the interface with the pre-cracked centre layer in a $5/4$ lay-up. As result of these high applied stresses, cracks initiate in the intact aluminium layers, before sufficient delamination extension at the interfaces is obtained.

The specimen with the $2/1$ lay-up and both aluminium layers pre-cracked contains in theory equal delamination lengths at all four interfaces. In practice, the thin specimen is very sensitive to small material and loading deviations, resulting in significant variation of the delamination lengths at each interface. This variation can be seen in Figure 6.7 and Figure 6.8, where the delamination growth curves for the two tests are given. The maximum and minimum length measured at the end of the first test was 15.9 mm and 0 mm and at the end of the second test 23.6 mm and 1.4 mm.

A part of this variation can be attributed to a significant increase in delamination growth rate of two delaminations at the fourth load level, Figure 6.7 and Figure 6.8. The out of plane displacement of the delaminated aluminium layers is not restraint and gives under cyclic loading an additional loading mode I contribution to the loading mode mix calculated for quasi-static loading [4]. This contribution is in contradiction with the assumption in section 5.2.3, that the energy release rate and the delamination growth rate are independent of the crack length.

The individual delamination rates are averaged to determine the relation between delamination rate and energy release rate, which reduces the effect of dependency on delamination length to some extent. However, it can be argued that the results from the mixed-mode delamination tests are not suitable for the current investigation, because the actual loading mode-mix for these specimens during progress of the delaminations is not exactly known. Nevertheless, the data will be included in the analysis to give a qualitative indication of the effect of loading mode mix.

As the effects discussed for the mixed loading mode were not observed during the mode II delamination tests, the results for the mode II loading can be used for the current investigation.

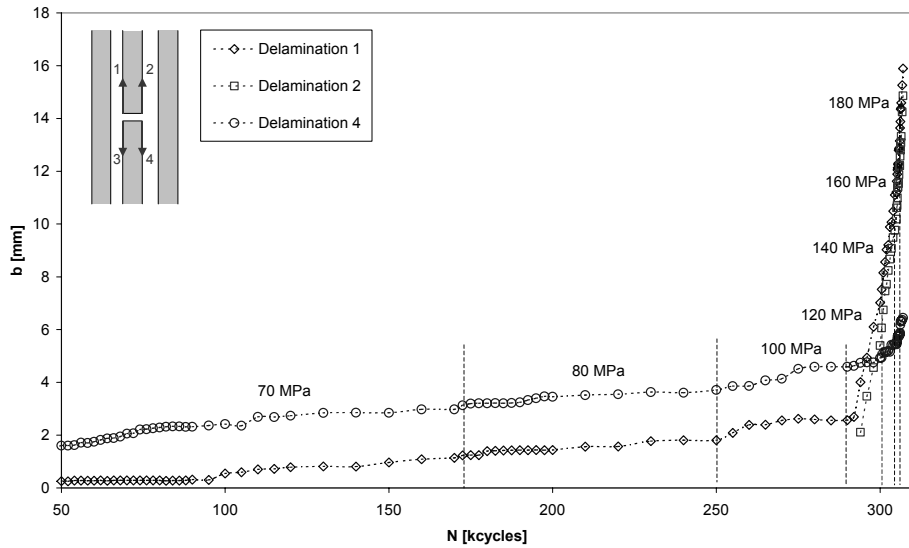


Figure 6.7 Delamination growth curve for Glare2A-2/1-0.3 tested in L-T direction at $S_{max}=70-180$ MPa and $R=0.05$

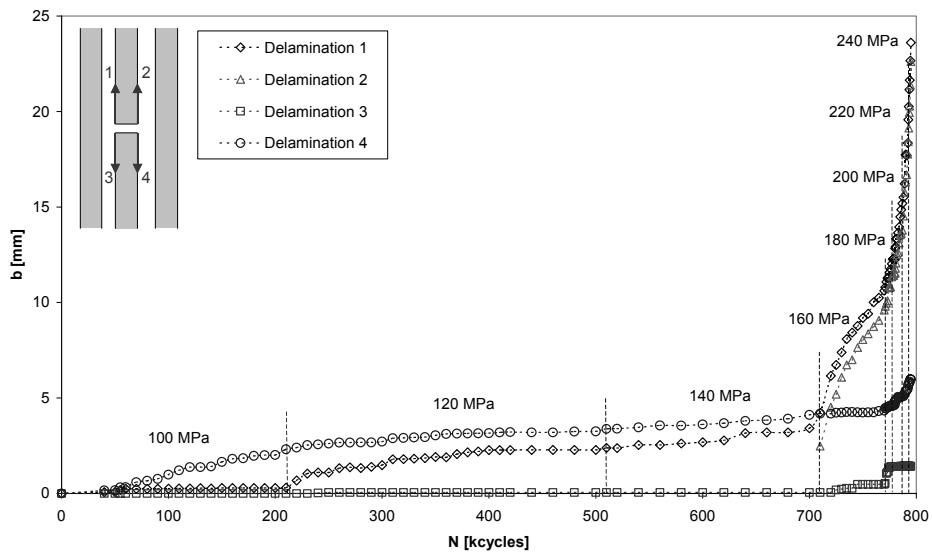


Figure 6.8 Delamination growth curve for Glare2A-2/1-0.3 tested in L-T direction at $S_{max}=100-240$ MPa and $R=0.5$

6.2.3 Delamination growth relation for Glare

The delamination growth rate db/dN was obtained by fitting a trend line through the linear part of the test data at a particular applied stress level, as illustrated in Figure 6.5 and Figure 6.6. The average values for the delamination growth rate are given in Table 5.2. For each delamination growth rate the energy release rate was calculated with the corresponding maximum stress level. By doing so, data pairs were generated that are plotted together in one graph, presented in Figure 6.9.

The data for Glare2A-2/1-0.3 at $R = 0.05$ and at $R = 0.5$ respectively were generated at successively increased load levels in each test. The same is true for Glare2A-5/4-0.3 at $R = 0.05$, while the curve for Glare2A-5/4-0.3 at $R = 0.5$ consist of data pairs generated from two different tests. The three data pairs for Glare4B-5/4-0.3 follow from three tests at different load levels.

Based on Figure 6.9, one can conclude, that equation (6.3) does not need a correction for the effect of stress ratio, because the data for the two stress ratios $R = 0.05$ and $R = 0.5$ occur in the same band, except for the 2/1 lay-up. The stress range and stress ratio are incorporated in the definition of $G_{d,max}$ and $G_{d,min}$, which means that the assumption of $k = 1$ is sufficient, reducing equation (6.3) to

$$\frac{db}{dN} = C_d \left(\sqrt{G_{d,max}} - \sqrt{G_{d,min}} \right)^{n_d} \quad (6.4)$$

Furthermore, the definition of the energy release rate incorporates the material parameters quite well, as the data for Glare2 and Glare4B as well as for the 5/4 lay-up and the 2/1 lay-up occur in the same band. Since material and loading parameters are incorporated correctly in the definition of the energy release rate, this means that the Paris relation for Glare can be defined independent of the Glare grade and stress ratio.

Several characteristics can be observed from Figure 6.9. The Paris relation for the mixed-mode loading condition (2/1 lay-up) yields equal delamination growth rates, compared to the mode II loading conditions (5/4 lay-up). As discussed in the previous section, the delamination behaviour of the mixed-mode 2/1 lay-up specimens differs essentially from the behaviour of the mode II 5/4 lay-up configuration. Nevertheless, the obtained delamination relation in Figure 6.9 is the same for the 2/1 lay-up as well as the mode II 5/4 lay-up.

For Glare, the parameters C_d and n_d can be determined for the empirical Paris relation, in equation (6.4). The values for these parameters are given in Table 6.1.

Table 6.1 Paris equation parameters for delamination growth in Glare, eq. (6.4)*

	C_d	n_d
Glare	0.05	7.5

* Values yield for db/dN in [mm/cycle] and G_d in [MPa mm]

Fatigue crack propagation and delamination growth in Glare

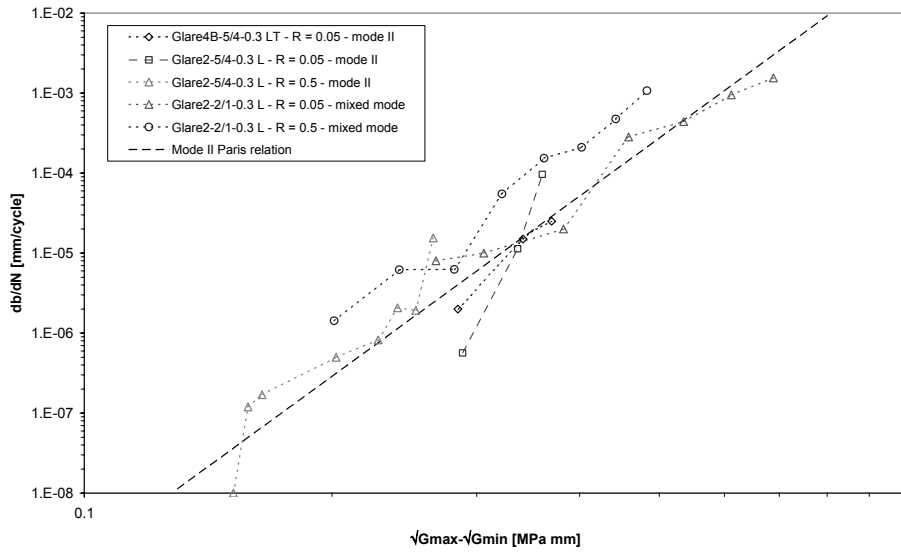


Figure 6.9 Relation between mixed-mode and the mode II Energy Release Rate and the delamination growth rate

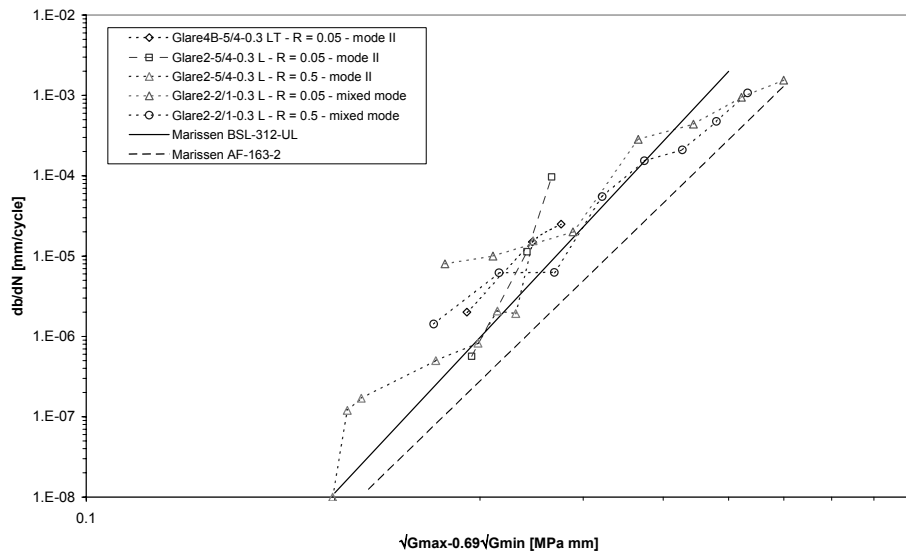


Figure 6.10 Comparison between the straight lines for BSL-213-UL and AF-163-2 determined by Marissen and the Glare results recalculated with equation (6.3) for $k = 0.69$.

The present Paris relation characterises the delamination resistance behaviour under cyclic loading of standard Glare described in Chapter 2. For each particular Fibre Metal Laminate this relation must be determined with delamination experiments. Marissen derived the Paris relations from experimental results on Arall with a 2/1 lay-up, containing Twaron fabric BSL-312-UL, and AF-163-2 prepreg. The present Paris relation for Glare is now compared with the relations derived by Marissen. The Glare results are recalculated with the Marissen relation (equation (6.3) with $k = 0.69$), see Figure 6.10. The Paris relations for the two types of Arall with a 2/1 lay-up are shown in the same figure as two straight lines. Marissen's results for Arall are close to the data obtained here for Glare. Nevertheless, both Arall laminates seem to have a higher delamination resistance than currently investigated Glare laminate.

It should be concluded here that the delamination resistance under cyclic loading of Fibre Metal Laminates depends on the characteristics properties of these laminates including the production process. The delamination resistance of each new type of Fibre Metal Laminate should be determined by relevant experiments. For this purpose, the empirical Paris relation between delamination growth rate and energy release rate is very suitable.

6.3 Step 2: bridging stress for arbitrary crack

The bridging stress is the stress that restrains the crack opening and reduces the stress intensity factor at the crack tip in the aluminium layers. The bridging stress is related to the delamination shape and the crack opening contour. It is important to use a clear definition of the bridging stress, because several definitions are used in the literature. Marissen [1] and Guo and Wu [5] define the bridging stress as the crack closing stress based on the total thickness of the laminate, where others define the bridging stress based on the aluminium layer thickness or the fibre layer thickness. If the bridging stress is defined on the total laminate thickness, the other stresses need to be defined accordingly as well, to remain consistent in the approach. Otherwise, one has to calculate the bridging stress to the real stresses in a particular layer.

To avoid any problem with stresses defined on bases of total laminate thickness, the current method utilizes the stresses as they occur in the individual layers. In the method presented in this thesis, the bridging stress is defined as the crack closing stress present in the fibre layers.

In this thesis, the approach of Guo and Wu is followed to determine the bridging stresses. This means that the bridging stress is determined by equalling the relations describing the crack opening in the aluminium layers and the relations describing the elongation and deformation of the fibre layers in the delaminated area. The relations for the crack opening in the aluminium layers are derived in section 6.3.1, while the relations for the fibre elongation and deformation are derived in section 6.3.2.

6.3.1 Crack opening due to applied and bridging stresses

The crack opening of a fatigue crack in an infinite Glare panel at any location x along the crack in Figure 6.11 can be written as

$$v(x) = v_{\infty}(x) - v_{br}(x) \quad (6.5)$$

where $v_{\infty}(x)$ denotes the crack opening as result of the far field opening stress in the aluminium layer and $v_{br}(x)$ denotes the crack closing effect due to the bridging stress. The first component in this equation can be calculated with Linear Elastic Fracture Mechanics for infinite monolithic sheets containing a crack loaded in the far field [6]

$$v_{\infty}(x) = 2 \frac{S_{al}}{E_{al}} \sqrt{a^2 - x^2} \quad (6.6)$$

where the far field stress in the aluminium layer S_{al} can be derived from the applied laminate stress using the classical laminate theory [7].

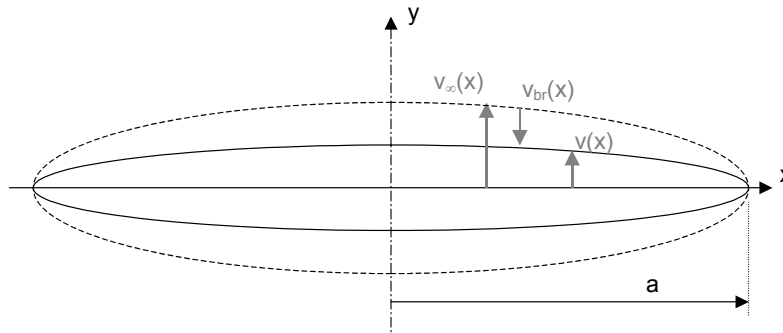


Figure 6.11 Definition of the crack opening of an arbitrary crack

The second component in equation (6.6) can be calculated with the methods for crack opening as result of point loads, described by Tada et al. [6]. Assuming that the bridging stress can be represented as a distributed number of infinite point loads, as illustrated in Appendix A, the crack opening for a given bridging stress is given by

$$v_{br}(x) = \int_0^a v(x, x_p) dx_p \quad (6.7)$$

In this equation, x_p is the coordinate where a fibre stress is applied on the crack flank. Because the fibre stresses along the crack flank are affecting the crack flank

displacement at any location x , an integration as given in equation (6.8) must be carried out. This is described in detail in Appendix A.

6.3.2 Crack opening due to elongation and deformation

The effective crack opening $v(x)$ in equation (6.6) can be attributed also to the elongation of the fibres over the delaminated length and the deformation of the prepreg layer

$$v(x) = \delta_f(x) + \delta_{pp}(x) \quad (6.8)$$

In this formulation, the deformation of the aluminium in the delaminated area is ignored, because the aluminium stress in the delamination area is equal or close to zero. For the elongation of the fibre layers in equation (6.8) one can then write

$$\delta_f(x) = \varepsilon_f(x)b(x) = \frac{S_{f,tot}(x)}{E_f}b(x) = \frac{S_f + S_{br}(x)}{E_f}b(x) \quad (6.9)$$

where $b(x)$ is the delamination length at location x .

The second component in equation (6.9) describes the contribution of the deformation of the prepreg layer. This prepreg deformation deserves some further attention, as it differs from the deformation component applied by Marissen [1], who attributed this component primarily to the deformation of the adhesive rich layer within the fibre layer and denoted it as adhesive shear deformation.

In the discussion of the method of Marissen, section 4.2.1, it was argued that the adhesive rich layer in Glare is significantly smaller than in Arall. Using the definition of Marissen, the crack opening contribution in Glare is significantly smaller as well, which seems in contradiction with experimental observations [8].

For this reason the contribution of the deformation is attributed to the total fibre layer, instead of the adhesive rich layer only. As the fibre orientation in the prepreg has an effect on the shear stiffness of the prepreg, it must be incorporated in the relations for the prepreg shear deformation. For uni-directional fibre layers, such as in Glare2, the deformation of the fibre layer can be determined for both principal directions, but for cross-ply laminates the derivation is more complicated.

A significant difference between the adhesive shear deformation according to Marissen and the prepreg deformation presented in this section is the case of zero delamination. Marissen assumed that in case of zero delamination, some crack opening occurs as result of adhesive shear deformation due to a crack in the adhesive rich layer. However, if it is assumed that the fibres are distributed uniformly over the total prepreg thickness, no crack in the adhesive exists and thus no crack opening due to prepreg shear deformation is possible. Once delamination occurs, the prepreg can deform. For small delamination lengths, the prepreg shear

deformation depends on the delamination length, but after a certain delamination length is reached, the magnitude of the prepreg shear deformation becomes independent of the delamination length. This behaviour is schematically illustrated in Figure 6.12.

The crack opening due to the prepreg shear deformation can be calculated with

$$\delta_{pp} = \gamma t_f = \tau_f \frac{t_f}{G_f} \quad (6.10)$$

where γ is the shear strain, τ_f the maximum shear stress at the delamination tip, G_f the shear stiffness of the prepreg layer and t_f the prepreg layer thickness. The shear stress along the interface near the delamination tip can be calculated with the approach presented in Appendix B.

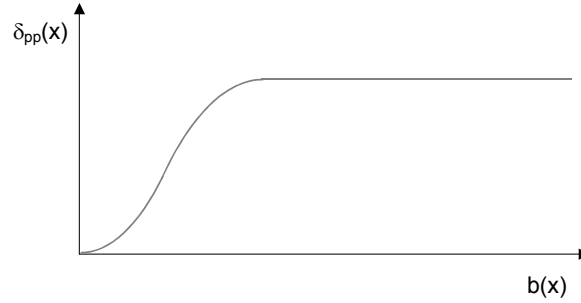


Figure 6.12 Illustration of the crack opening due to prepreg shear deformation of a uni-directional prepreg layer as function of the delamination length

For the maximum shear stress at the delamination tip at the aluminium/prepreg interface in a laminate with unidirectional prepreg layers one can write

$$\tau_{al} = -S_{al} t_{al} \sqrt{\frac{G_f}{t_f} \left(\frac{1}{F_{al}} + \frac{1}{F_f} \right)} \quad (6.11)$$

and for cross-ply prepreg layers

$$\tau_{al} = -S_{al} t_{al} \sqrt{\left(\frac{G_{f1}}{t_{f1}} + \frac{G_{f2}}{t_{f2}} \right) \left(\frac{1}{2F_{al}} + \frac{1}{F_{f1} + F_{f2}} \right)} \quad (6.12)$$

where the subscripts *al* and *f* denote the aluminium and fibre layer respectively and the numbers 1 and 2 the two individual prepreg layers in the cross-ply. The stiffness *F* is obtained by multiplication of the Young's modulus with the thickness of all layers. For example for aluminium the stiffness F_{al} is defined as

$$F_{al} = n_{al} t_{al} E_{al} \quad (6.13)$$

As mentioned before, the crack opening due to the prepreg shear deformation is zero, if the delamination is zero. A certain delamination length must be present to obtain the crack opening related to the maximum shear stress in equations (6.12) and (6.13). Using the previous approach, the dependency of the crack opening term on the delamination lengths can be determined. For uni-directional prepreg layers the correction factor is

$$C(b) = 1 - \left(\cosh \sqrt{\alpha_{UD}} b - \tanh \sqrt{\alpha_{UD}} b \sinh \sqrt{\alpha_{UD}} b \right) \quad (6.14)$$

where b is the delamination length. The stiffness parameter α is defined in Appendix B. In equation (6.15) α_{UD} must be replaced by $2\alpha_{CP}$ for a cross-ply layer. Substitution into equation (6.13) then gives the crack opening due to prepreg shear deformation for uni-directional prepreg layers

$$\delta_{pp}(x) = C_b S_{al} t_{al} \sqrt{\frac{t_f}{G_f} \left(\frac{1}{F_{al}} + \frac{1}{F_f} \right)} \quad (6.15)$$

which is very similar to the expression derived by Marissen. However, the stiffness and thickness of the total fibre layer is applied. For the cross-ply prepreg layers the equation becomes

$$\delta_{pp}(x) = C_b S_{al} t_{al} \frac{t_{fi}}{G_{fi}} \sqrt{\left(\frac{G_{f1}}{t_{f1}} + \frac{G_{f2}}{t_{f2}} \right) \left(\frac{1}{2F_{al}} + \frac{1}{F_{f1} + F_{f2}} \right)} \quad (6.16)$$

where $i = 1$ for fibres in the prepreg adjacent to the interface parallel to the loading direction and $i = 2$ for fibres perpendicular to the loading direction.

6.3.3 Derivation of the bridging stress distribution

The bridging stress distribution can now be determined by equalling equation (6.6) and (6.9)

$$v_{\infty}(x) - v_{br}(x) = \delta_f(x) + \delta_{pp}(x) \quad (6.17)$$

The solution of this equation can only be found numerically, because no closed-form solution exists due to the non-uniform bridging stress present in the integral of equation (6.8) and in the total fibre stress in equation (6.10).

For the numerical solution, the crack geometry is divided into N bar elements with equal width $w=(a-a_s)/N$, as illustrated in Figure 6.13 for a starter notch length a_s . This means that the integral of equation (6.8) is written as a summation of the individual crack opening relations for each bar element

$$v_{br}(x_i) = \sum_{j=1}^N v(x_i, x_j) \quad (6.18)$$

where x_i is located at the centre of each bar element and where the bridging stress over one bar element width is defined as $S_{br}(x) w$.

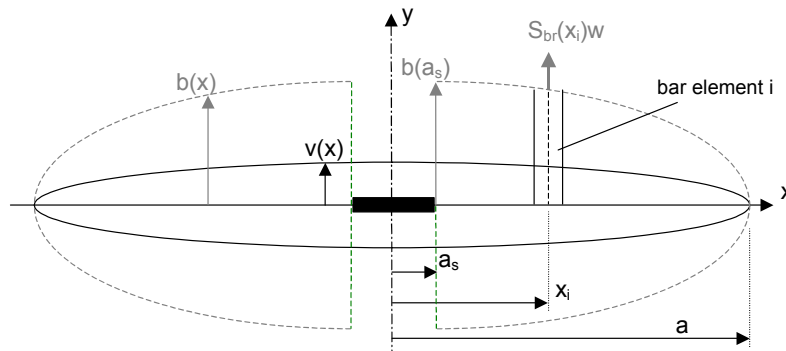


Figure 6.13 Crack geometry with total crack length divided into N bar elements

The solution for the bridging stress can be found by substitution of equation (6.7), (6.10), (6.17) and (6.19) into equation (6.18), which is written in the reduced form as

$$H S_{br} = Q \quad (6.19)$$

where

$$H = \sum_{j=1}^N \frac{v(x_i, x_j)}{S_{br}(x_j)} - \frac{b(i)}{E_f} \delta(i, j) \quad (6.20)$$

where $\delta(i,j)$ is the Kronecker delta, and

$$Q = v_{\infty}(i) - \delta_{pp}(i) - \frac{S_f}{E_f} b(i) \quad (6.21)$$

To calculate the bridging stress the matrix H must be inverted

$$S_{br} = H^{-1}Q \quad (6.22)$$

The bridging stress distributions for an arbitrary fatigue crack configuration in Glare3-6/5-0.4, calculated with the above-described method, are presented in Figure 6.14 for some typical delamination shapes, identified as being close to the observed delamination shapes (ellipse, parabola, triangle, cosine) [8]. Including the presence of a notch a_s the delamination shapes are defined as

$$\begin{aligned} b(x)_{\text{ellipse}} &= b(a_s) \sqrt{1 - \left(\frac{x - a_s}{a - a_s} \right)^2} \\ b(x)_{\text{parabola}} &= b(a_s) \sqrt{1 - \frac{x - a_s}{a - a_s}} \\ b(x)_{\text{triangle}} &= b(a_s) \left(1 - \frac{x - a_s}{a - a_s} \right) \\ b(x)_{\text{cosine}} &= b(a_s) \cos \left(\frac{\pi}{2} \frac{x - a_s}{a - a_s} \right) \end{aligned} \quad (6.23)$$

with $b(a_s)$ the delamination length at the starter notch tip, see Figure 6.13.

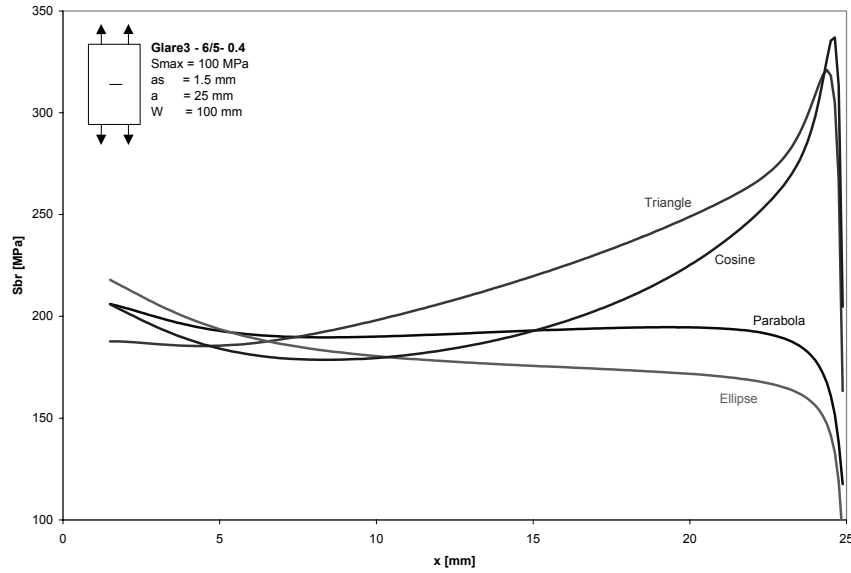


Figure 6.14 Bridging stress distributions for Glare3-6/5-0.4 in L-T direction with $W=100$ mm, $a=25$ mm, $a_s=1.5$ mm and $S_{max}=100$ MPa for the typical delamination shapes defined in equation (6.24) with $b(a_s)/(a-a_s)=0.2$

Although the geometries are not grossly different, the bridging stress levels near the crack tip are very different. As the bridging stress near the crack tip highly influences the crack growth, this would lead to rather different crack propagation rates. It is therefore necessary to consider the delamination shape and its consequences for crack propagation in more detail.

6.4 Step 3: determination of delamination shape

From the previous sections, it can be concluded that the bridging stress, crack opening contour and delamination shape are in balance. The observed delamination shapes were reported to be in-between a triangular shape and an elliptical shape. This means that a fatigue crack configuration with an initially triangular delamination shape should gradually change with the propagating crack into the experimentally observed delamination shape. On the other hand, a fatigue crack with an initially elliptical delamination shape should gradually change into the same experimentally observed delamination shape with increasing crack lengths.

The far field stress in the prepreg layers can be calculated with the classical laminate theory. For the far field stress following from the applied laminate stress, thus without the curing stress, the minimum stress correlated to the minimum applied stress, can be calculated by multiplication with the laminate stress ratio R .

However, this is not true for the bridging stress $S_{br}(x)$. Due to the presence of tensile curing stresses in the aluminium layers in absence of applied laminate stresses, some crack opening will be calculated by equation (6.8). Corresponding to this crack opening, a crack closure effect as a result of bridging will be calculated as well. This means that in case of $S_{lam} = 0$, the bridging stress has a certain positive value. The bridging stress ratio R_{br} is in that case not equal to zero, while the laminate stress ratio is.

Therefore, the maximum and minimum energy release rate must be calculated separately based on the maximum and minimum bridging stress levels respectively. Using the derivation given in [1] the maximum energy release rate is calculated as a function of the fibre stress with

$$G_{\max} = \frac{n_f t_f}{2jE_f} \left(\frac{n_{al} t_{al} E_{al}}{n_{al} t_{al} E_{al} + n_f t_f E_f} \right) (S_f + S_{br,\max}(x))^2 \quad (6.24)$$

and the minimum energy release rate

$$G_{\min} = \frac{n_f t_f}{2jE_f} \left(\frac{n_{al} t_{al} E_{al}}{n_{al} t_{al} E_{al} + n_f t_f E_f} \right) (RS_f + S_{br,\min}(x))^2 \quad (6.25)$$

where $S_{br,\max}$ and $S_{br,\min}$ denote the bridging stress at maximum and minimum applied stress respectively.

For delamination growth the empirical Paris relation for delamination in equation (6.5) is applied using the constants for mode II loading mode, given in Table 6.1. The mode II loading mode is believed to be the best representative mode for the average delamination behaviour of all aluminium-prepreg interfaces.

However, at this stage, the precise delamination shape is still unknown and can only be approximated by an arbitrary shape close to the observed delamination shapes during experiments, such as an elliptical or triangular shape [1,5]. Once the delamination growth can be determined in relation to crack growth in the aluminium layers, the precise delamination shape can be determined.

6.5 Step 4: determination of the Stress Intensity Factor

Since the bridging stress for a given configuration is known and the corresponding delamination growth can be calculated, the Stress Intensity Factor as defined in equation (6.1) can be determined. The Stress Intensity Factor as result of the far field stress present in the aluminium layers follows from the Linear Elastic Theory for monolithic metals

$$K_{farfield} = S_{al} \sqrt{\pi a} \quad (6.26)$$

which corresponds to the crack opening defined in equation (6.7). The second component in equation (6.1) is a function of the bridging stress. Since the bridging stress is defined as a stress present in the fibre/adhesive layers, see equation (6.10), the bridging stress must be recalculated to the stress for one particular aluminium layer. For a cross-ply laminate this recalculation is given as

$$S_{br,al} = S_{br} \frac{n_{f1} t_{f1} + n_{f2} t_{f2}}{n_{al} t_{al}} \quad (6.27)$$

Substitution of $P = S_{br,al} W$ in equation (A.16) in Appendix A and summation of the total crack length then gives the bridging stress intensity factor

$$K_{br} = 2 \sum_{i=1}^N \frac{S_{br,al}(x_i) w}{\sqrt{\pi a}} \frac{a}{\sqrt{a^2 - x_i^2 + b_i^2}} \left(1 + \frac{1}{2} (1 + \nu) \frac{b_i^2}{a^2 - x_i^2 + b_i^2} \right) \quad (6.28)$$

The resulting Stress Intensity Factor at the crack tip can then be determined with equation (6.1).

In order to calculate the crack growth rate with the Paris relation, an effective Stress Intensity Factor range must be determined. Following from relations derived in [9] a stress ratio correction was introduced for thin aluminium sheets in Glare

$$\Delta K_{eff} = (1 - R^{1.35}) K_{tip} \quad (6.29)$$

which was at that time determined for the application of an empirical prediction method [10]. The question is whether this correction is still accurate for the application of the current method. Because insufficient test data on thin aluminium 2024-T3 sheets with different stress ratio's is available, it is assumed for the time being to be accurate enough to calculate the stress intensity factor range with equation (6.30). Further investigation of the stress ratio effect must reveal whether this assumption is correct.

The crack growth rate can now be calculated with

$$\frac{da}{dN} = C_{cg} \Delta K_{eff}^{n_{cg}} \quad (6.30)$$

where the values of C_{cg} and n_{cg} for 2024-T3 in Glare were determined in [11] and are given in Table 6.2.

Table 6.2 Paris relation parameters for crack growth in Glare, eq. (6.31)

	C_{cg}	n_{cg}
2024-T3	$2.17 \cdot 10^{-12}$	2.94

For fatigue crack growth in finite width geometries, the method must be corrected with a finite width correction factor. In the current model the empirical Dixon-correction factor is applied [12]

$$\beta_{Dixon} = \frac{1}{\sqrt{1 - \left(\frac{2a}{W}\right)^2}} \quad (6.31)$$

This factor is applied on the stress intensity factor at the crack tip in the aluminium layer, as defined by equation (6.1) and is applied, in accordance with this correction, on the total crack opening contour as defined in equation (6.18).

6.6 Numerical calculation approach

The method as derived in the previous sections is implemented in a numerical calculation model. The structure of the computer program is shown in Figure 6.15, while the input parameter structure is presented in Figure 6.16. The approach to

implement the method in a numerical method is described in detail in Appendix C. It can be summarized as follows.

- *The matrix size is variable with crack length*
The initial matrix size in the numerical model is equal to the initial number of bar elements over which the initial crack length is divided. The bar element width is fixed, which means that crack length extension as result of calculated crack growth is incorporated as extension of the matrix size.
- *Delamination tip shape is assumed*
Starting from an initial delamination size, the delamination extension can only be calculated perpendicular to the crack growth direction. This means that between the extended delamination shape and the new crack tip, thus in the crack length extension, the delamination shape must be assumed. The current model utilises a parabolic shape.

Depending on the delamination shape near the crack tip, the delamination length can be very small and the corresponding calculated bridging stresses very large. Due to the nature of the numerical model, the calculated delamination growth is decoupled from the surrounding locations.

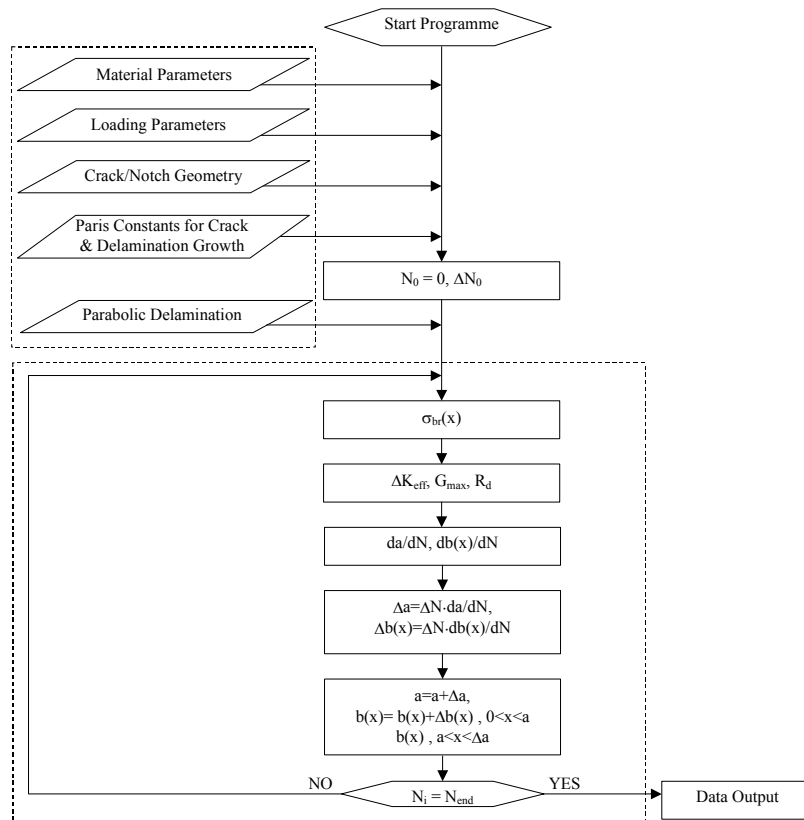


Figure 6.15 Flow diagram for the crack growth prediction method

Fatigue crack propagation and delamination growth in Glare

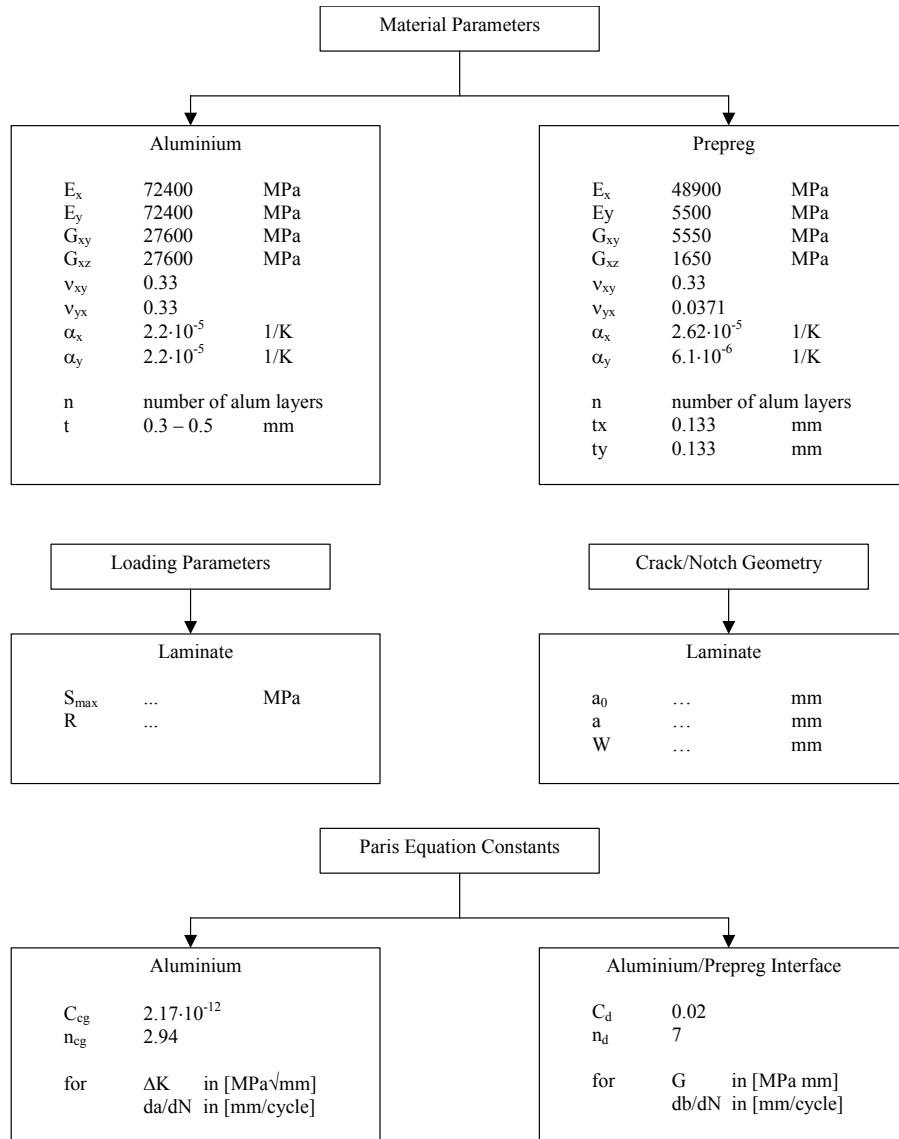


Figure 6.16 Input parameters used for the crack growth prediction method corresponding to the flow diagram in Figure 6.15

This means that as result of large bridging stresses near the crack tip and large crack length extensions, unrealistic delamination lengths can be calculated. These unrealistic delamination lengths appear as large peaks in the calculated extended delamination shape. In the subsequent calculation steps, unrealistic bridging stresses corresponding to this unrealistic delamination length is calculated.

To avoid any of such sensitivity in the numerical model, the maximum crack length extensions are limited to two bar element widths and the delamination tip assumption is calculated between a location behind to previous crack tip and the extended crack tip. A more detailed description of this approach is given in Appendix C.

6.7 Results and discussion

To evaluate and validate the developed model, three criteria were given in section 6.1. From the presented derivation in this chapter, the first of the three criteria is met as the developed method is physically sound.

The accuracy and the robustness of the method must be validated with experimental data. In section 6.7.1, the model prediction will be compared with a reference tests from which experimental data on crack growth, crack opening and delamination shape is available.

To calculate crack growth for a given geometry with the current model, an initial crack length, a number of bar elements over which this crack length is divided, and an initial delamination shape and length must be chosen. The robustness of the model means that the model should predict the crack growth behaviour regardless the initial delamination ratio and delamination shape. The balance between the crack growth and delamination growth mechanisms must therefore also be present in the model.

The robustness of the model will be discussed in section 6.7.2 with respect to the

- Initial delamination shape
- Initial delamination length

The effect of the assumption of the delamination shape near the crack tip is discussed in section 6.7.3, while the validity range of the model is presented in section 6.7.4.

6.7.1 Comparison between model and reference test

To validate the method and numerical model presented in the previous sections, a large number of cases have been calculated, which have been experimentally investigated in [13, 14]. In this section, the prediction with the presented method for one reference configuration and loading case is compared with the crack growth, crack opening and delamination shape results obtained from [13]. To determine the validity range, a comparison with crack growth results of other configurations will be presented in section 6.7.4.

The reference test consists of a Glare3-6/5-0.4 centre crack tension specimen of $W = 100$ mm width containing two parallel cracks with a starter notch length of $2a_0 = 3$ mm, see section 5.6. The maximum applied load is $S_{\max} = 100$ MPa with a stress ratio of $R = 0.05$. The predicted crack growth rates are given together with the experimentally obtained crack growth rates in Figure 6.17.

Fatigue crack propagation and delamination growth in Glare

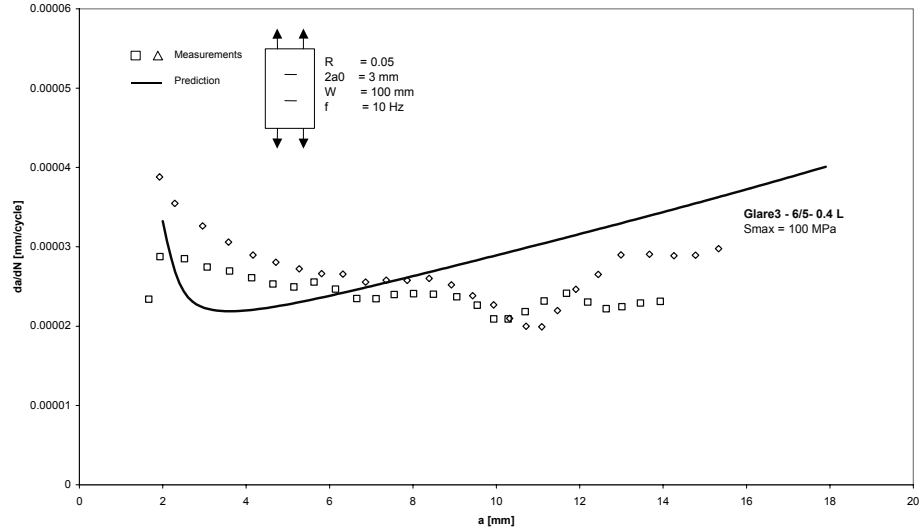


Figure 6.17 Comparison between the predicted and measured crack growth rate of Glare3-6/5-0.4 tested in L-T direction, with $W=100$ mm, $a_0=1.5$ mm and $S_{max}=100$ MPa with $R=0.05$

The overall predicted crack growth behaviour corresponds quite well with the observed crack growth behaviour. The predicted initial crack growth rate, due to inefficient fibre bridging, coincides with the measured crack growth rate. However, the initial decrease in crack growth rate and the increase at larger crack lengths seem to be exaggerated by the model. Comparison between model and other experiments must point out whether the differences visible in Figure 6.17 indicate a prediction model inaccuracy.

The bridging stress cannot be measured directly in fatigue crack growth experiments, which means that the calculated bridging stress cannot be validated directly with experimental results. In order to verify the presented method, the crack opening due to the bridging stress, given in equation (6.19), is determined with the calculated bridging stress and the corresponding delamination shape. This bridging crack opening is then subtracted from the far field crack opening according to equation (6.6).

$$v(x) = 2 \frac{S_{al}}{E_{al}} \sqrt{a^2 - x^2} - \int_0^a v(x_i, x_j) dx_j \quad (6.32)$$

The resulting crack opening contour is compared with the crack opening contour measured in the experiments. This comparison between measured and calculated crack opening contours is given in Figure 6.18. The calculated bridging stresses and delamination shapes are presented in Figure 6.19 and Figure 6.20 respectively.

6 Crack Growth Prediction Model

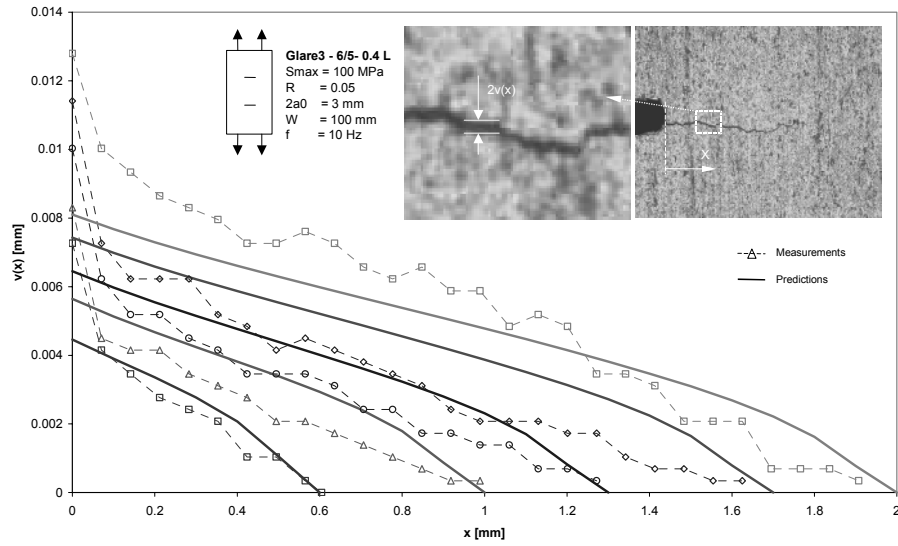


Figure 6.18 Comparison between the predicted and measured crack opening of Glare3-6/5-0.4 in L-T direction with $W=100 \text{ mm}$, $a_s=1.5 \text{ mm}$ and $S_{max}=100 \text{ MPa}$ with $R=0.05$

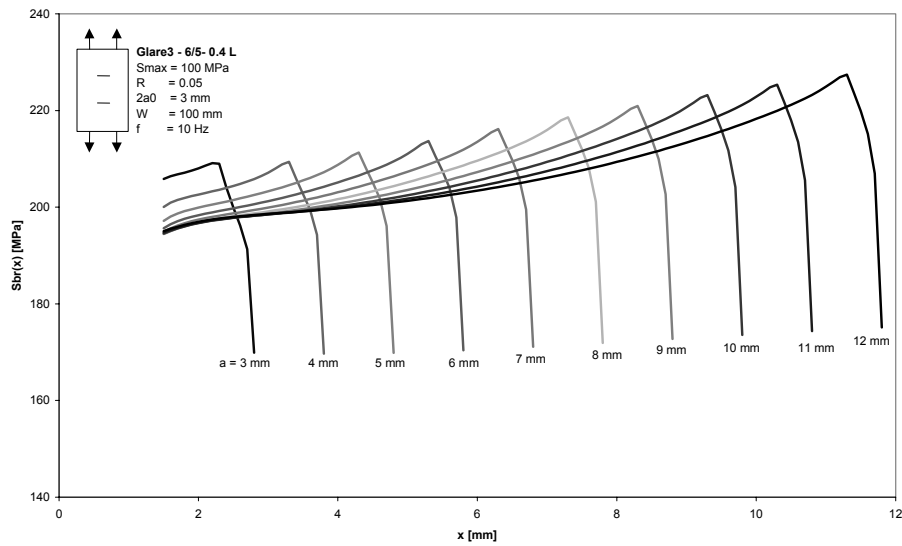


Figure 6.19 Calculated bridging stress distributions for the Glare3-6/5-0.4 in L-T direction with $W=100 \text{ mm}$, $a_s=1.5 \text{ mm}$ and $S_{max}=100 \text{ MPa}$ with $R=0.05$

Fatigue crack propagation and delamination growth in Glare

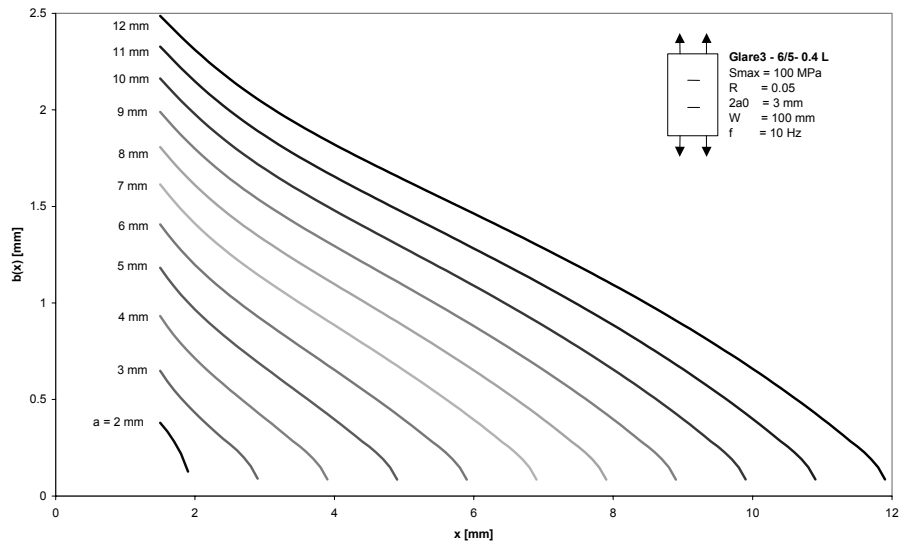


Figure 6.20 Calculated delamination growth for the Glare3-6/5-0.4 in L-T direction with $W=100$ mm, $a_s=1.5$ mm and $S_{max}=100$ MPa with $R=0.05$

An excellent correlation is observed between the predicted and measured crack opening contours. Except for a small difference between prediction and measurement locally at the starter notch tip, the crack opening contour is quite well predicted by the model. As mentioned before, this gives a positive indication with respect to the accuracy of the calculated bridging stress distribution by the model.

From the bridging stress distribution, several characteristics can be seen. The overall shape of the bridging stress distribution does not change with the propagating crack. The bridging stress peak near the crack tip increases with the crack growth, while the bridging stress near the starter notch decreases. Similar to the predicted bridging stress distribution, the predicted delamination shapes do not change with progressing crack lengths, which indicates a balanced crack propagation and delamination growth mechanism.

Finally, the observed delamination shape after etching away the outer aluminium layers is compared with the predicted delamination shape for Glare3-6/5-0.4 in Figure 6.21. The delamination size is over predicted by the model, but the delamination shape corresponds quite well with the measured delamination shape, especially near the crack tip.

From the comparison between the predicted and measured crack growth rates, the crack opening contours and the delamination shape and size a good correlation is obtained.

6 Crack Growth Prediction Model

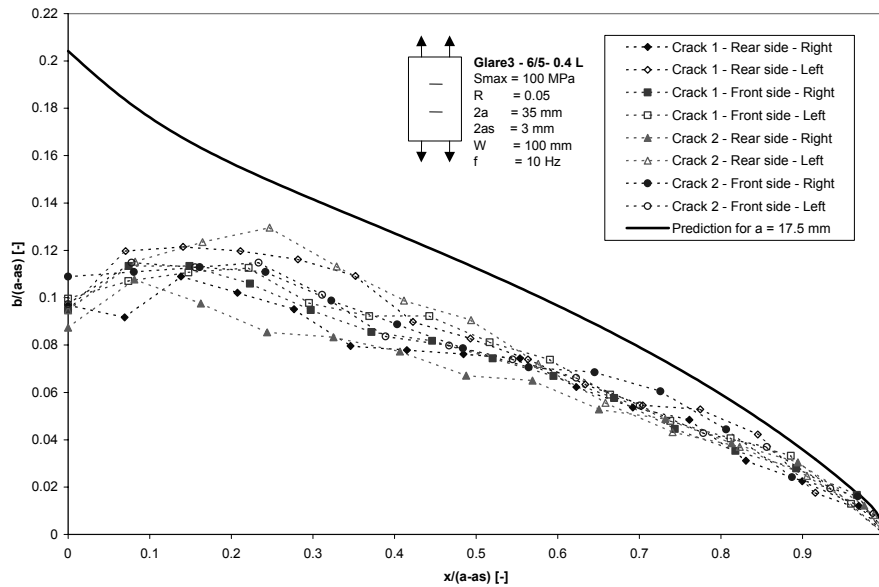


Figure 6.21 Comparison between calculated delamination shape and measured delamination shape for the Glare3-6/5-0.4 in L-T direction with $W=100 \text{ mm}$, $a=17.5 \text{ mm}$, $a_s=1.5 \text{ mm}$ and $S_{max}=100 \text{ MPa}$ with $R=0.05$

6.7.2 Model robustness

It was mentioned in section 6.4, that the delamination shape observed during the experiments were reported to be in-between a triangular and an elliptical delamination shape. This behaviour can be explained with the calculated bridging stress distributions given in Figure 6.14. The bridging stress distribution corresponding to a triangular delamination shape will change the delamination shape towards an elliptical shape, while the bridging stress corresponding to an elliptical shape forces the delamination shape towards a triangular shape.

The question to be answered in the current section is whether the model is physically correct and robust, which means that in spite of the initial chosen delamination shape, the delamination will always propagate towards the same shape.

For the case of Glare3-6/5-0.4 used for comparison with test data in section 6.7.1, the crack propagation and delamination growth is calculated with the numerical model for the four initial delamination shapes given in equation (6.24). The results are compared with each other in Figure 6.22.

For the cases in Figure 6.22 the four initial delamination shapes propagate towards the same delamination shape within five calculation steps, corresponding to a total crack extension of 0.5 mm. After these five calculation steps the calculated delamination and crack growth are identical for all four initial delamination shapes.

Fatigue crack propagation and delamination growth in Glare

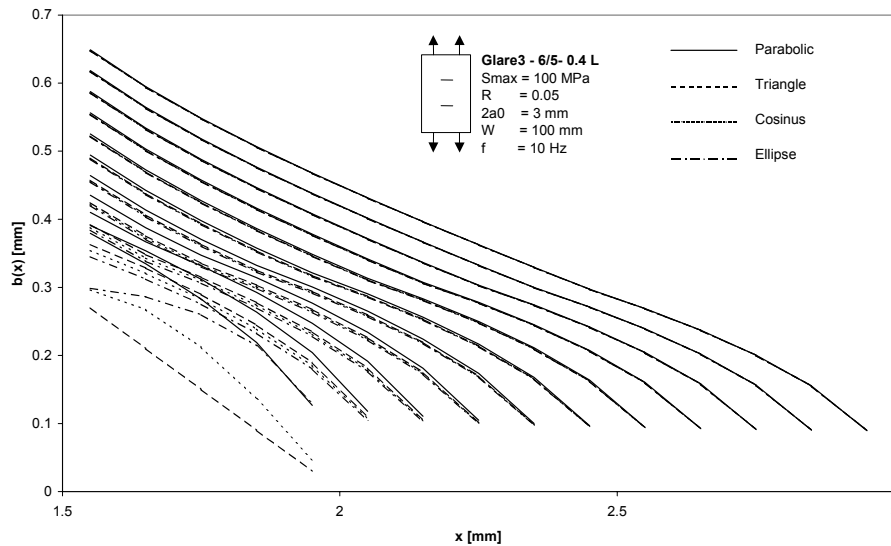


Figure 6.22 Calculated delamination growth for the Glare3-6/5-0.4 in L-T direction with $W=100$ mm, $a_s=1.5$ mm and $S_{max}=100$ MPa with $R=0.05$ starting from 4 initial delamination shapes

The comparison in Figure 6.22 is based on a crack extension increment of 0.1 mm, which is equal to a single bar element for each calculation step. Changing the calculated crack extension per calculation step, or changing the crack length represented by one bar element in the model, will also affect the crack length needed to level out the effect of the initial delamination shape. The time needed for all four delamination shapes to propagate towards the same shape, must therefore be related to the calculation steps in the model, rather than the total crack length extension.

Besides the initial delamination shape, the initial delamination size also determines the calculated crack growth behaviour. As the effect of an initial delamination size is determined by the initial crack length, the current discussion focuses on the ratio between the initial delamination length at the starter notch tip and the crack length, hereafter denoted as the delamination ratio.

The progress of this delamination ratio is presented in Figure 6.23 for several initial delamination ratios. This figure shows that within a certain range of initial delamination ratios, the delamination ratio will propagate asymptotically towards the same curve. However, if the initial delamination length is taken too small or too large the calculated crack growth and delamination growth will not progress towards the same behaviour.

Figure 6.23 shows that the model is more sensitive to initial values of the delamination ratio that are too small than to values that are too large. This sensitivity is related to the bridging stress calculated for the initial delamination size. If the initial delamination size is taken too small, the corresponding calculated bridging stresses are extremely large, resulting in an extremely large delamination extension

in the subsequent calculation step. This large overshoot in delamination growth starting from a small initial delamination length determines the crack growth behaviour afterwards significantly. This overshoot in the delamination growth does not occur when the initial delamination size is taken too large.

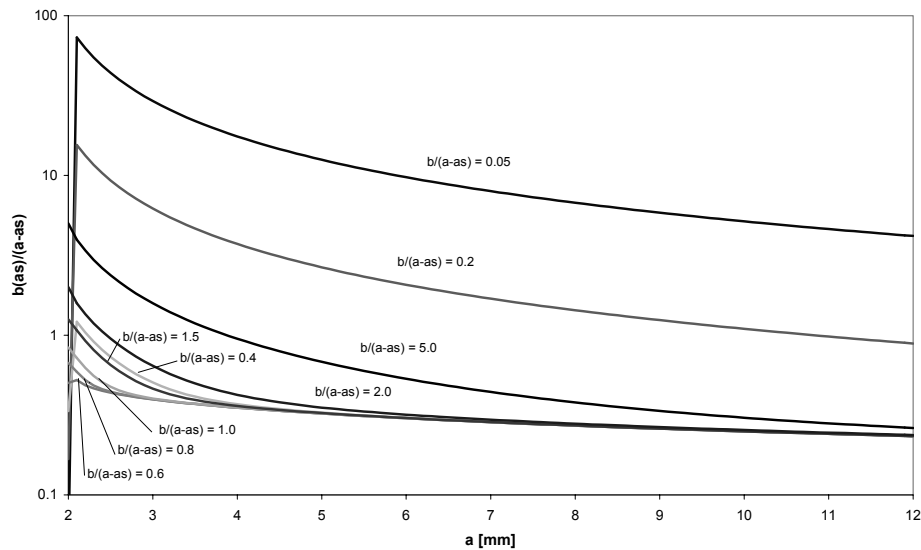


Figure 6.23 Progress of the delamination over crack length ratio as function of the crack length for different values of the initial delamination ratio

With respect to the initial delamination ratio, it can be concluded that the model satisfies the robustness criterion if the initial value is chosen within a range of 0.5 and 2.

Although the model has proven to be robust with respect to the ratio of initial delamination size over initial crack length, the accuracy of the model for small crack length increases when the initial values are taken close to the actual values. For this reason, the initial value must be taken close to 0.6 for cracks starting from small starter notch lengths and close to 1.5 for cracks starting from a large initial starter notch length, as will be discussed later in this chapter, when comparing the model with other crack growth experiments.

6.7.3 Delamination shape near the crack tip

The crack growth model consists of calculation of the crack growth rate in crack length direction and the delamination growth rate perpendicular to the crack direction. The delamination shape can therefore only be calculated over the crack length, where the bridging stresses can be determined. In the crack length extension (distance between two subsequent crack tip locations) the delamination shape cannot be calculated, but has to be assumed.

Appendix C explains how the delamination shape assumption near the crack tip is utilised in the model. To avoid excessive delamination propagation near the crack tip as result of model sensitivity to potential high peak stresses, the delamination shape assumption is extended to a small crack length behind the crack tip. Thus, the assumed shape excludes potential peaks in the calculated delamination contour.

In the current model, the delamination shape assumption near the crack tip consists of a parabolic shape. However, other shapes could be applied as well. To investigate the effect of the delamination shape assumption crack growth calculations are performed based on the four characteristic delamination shapes described in equation (6.24).

Starting from an initial parabolic delamination shape, the crack growth behaviour for the four identical cases with different delamination shapes near the crack tip are compared in Figure 6.24. The corresponding bridging stress distributions and delamination shapes are given in Figure 6.25.

The crack growth rates are different, but the slopes of the curves in Figure 6.24 are almost identical, which means that the overall crack growth behaviour of the four delamination tip approximations is the same. Only the crack growth rates predicted with the parabolic and cosine delamination approximation are close to the test data. However, the initial higher crack growth rate, is only predicted well with the parabolic delamination approximation near the crack tip, which means that the parabolic delamination tip approximation gives the most accurate results.

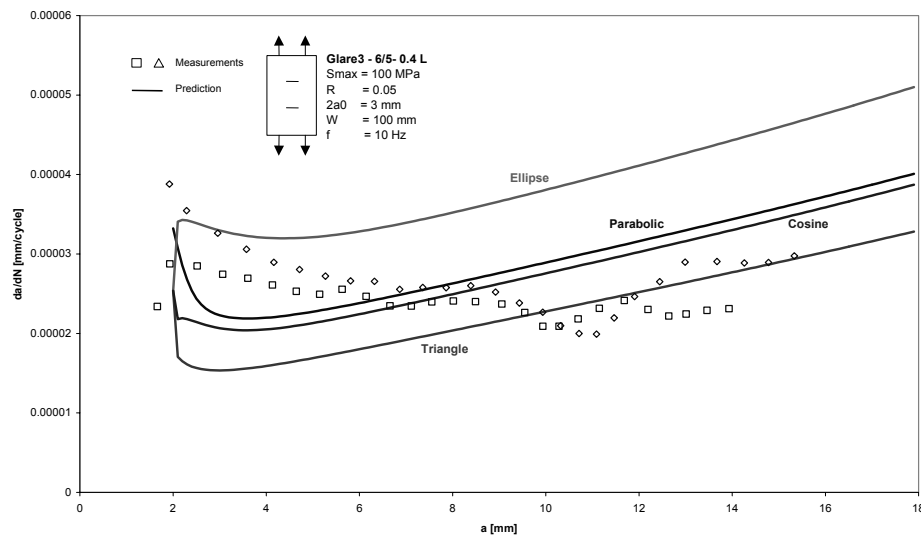


Figure 6.24 Comparison between the four delamination tip approximations and the test data presented in Figure 6.17

The difference in crack growth rates can be explained with the bridging stress distributions in Figure 6.25 and the relation for the bridging stress intensity factor, equation (6.29).

The bridging stress near the crack tip gives a greater contribution in the definition of the bridging stress intensity factor in proportion to the bridging stress further away from the crack tip. This means that lower and higher values of the bridging stress near the crack tip, give lower and higher values of the bridging stress intensity factor respectively. The extreme peak values of the bridging stress in Figure 6.25 for the triangular delamination shape near the crack tip give a significant increase in the bridging stress intensity factor and thus a lower crack growth rate, while the lower values for the elliptical delamination shape result in a lower bridging stress intensity factor and thus a higher crack growth rate.

The triangular and cosine shape both contain a sharp delamination tip at the crack tip, while the parabolic and elliptical delamination shape contain a blunt delamination tip at the crack tip, as result of the asymptotic behaviour of the elliptical and parabolic relations. Due to the sharp delamination tip, the bridging stress near the crack tip contains a peak value, which is clearly visible for the triangular delamination shape, and less clear, but also present for the cosine shape. As result of the blunt delamination tip, peak values are not present in the bridging stress distributions of the parabolic and elliptical delamination shapes.

The cosine shape near the crack tip results in a dip in the bridging stress distribution adjacent to the peak value at the crack tip, which can be attributed to the dent in the delamination contour at the intersection between the calculated delamination shape and the assumed cosine shape near the crack tip. Determining the transition between the two shapes tangentially would prevent the dent to occur in the delamination contour. However, that would make the calculation in the current model too complicated. From Figure 6.24 it can be concluded that the small peak in bridging stress distribution compensates the adjacent dip in the relation for the bridging stress intensity factor.

Although the horizontal asymptote at the intersection is also present for the elliptical delamination shape, the corresponding bridging stress distribution does not show the dip and peak. The bridging stress decreases significantly due to the elliptical shape at the crack tip.

From the comparison it becomes clear, that the elliptical and cosine shape contain a physically incorrect bump in the delamination contour due to the horizontal asymptote of both relations, which gives a dip and peak in the bridging stress distribution for the cosine shape. The elliptical shape results in a bridging stress intensity factor which is too small. The triangular delamination shape contains a high peak in the bridging stress distribution, giving too high values for the bridging stress intensity factor.

In general it can be concluded, that of the four delamination shape approximations presented in Figure 6.24 and Figure 6.25, the parabolic shape is the best assumption.

Fatigue crack propagation and delamination growth in Glare

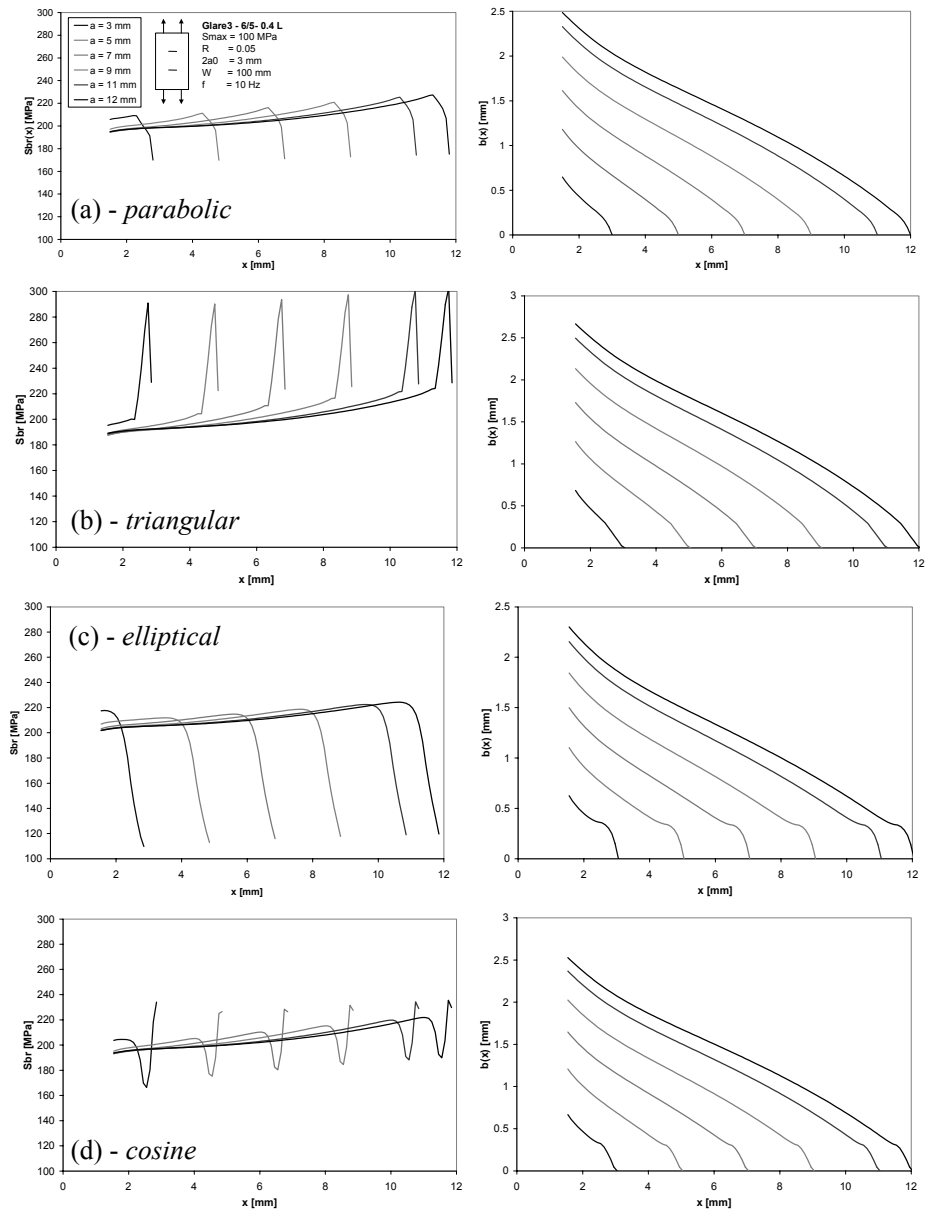


Figure 6.25 Comparison between the bridging stress distributions and the delamination shapes calculated for the parabolic (a), triangular (b), elliptical (c) and cosine (d) delamination tip approximation.

6.7.4 Validity range of the model

An important constraint of a prediction model is the validity range; the range in which the validity of the method is proven with experimental results. Because of the large amount of parameters in the present method, the range must be properly defined with respect to the material-, the geometry- and the loading parameters.

To validate the method, the predicted crack growth behaviour is compared with experimental observations. Most of the experimental observations consist of crack length versus number of cycles data sets, which can be calculated into crack growth rate versus crack length data. The figures containing the comparisons between these data and the predicted crack growth behaviour are presented in Appendix D.

The material parameters can be divided into the Glare type, the laminate lay-up and the thickness of the aluminium layers. Two Glare types have been used for validation, Glare3 and Glare4B, both containing cross-ply prepreg layers. Although validation of the model with uni-directional Glare2 is desirable, all fatigue tests on flat CCT specimens were performed on cross-ply laminates only, because of the focus on the application of Glare as fuselage skin material.

The laminate lay-up varied between 3/2 and 8/7, while the aluminium layer thickness was varied between 0.3 and 0.5 mm. These ranges define the common range of laminates currently applied in the structural applications of aircrafts fuselages [15].

The geometrical parameters can be divided into the specimen width, the crack length and the starter notch length. The specimen width is only of interest for relatively large crack lengths with respect to the application of finite width correction factors. For small crack length over specimen width ratios the model predictions are not influenced by the width. Nevertheless, the specimen width range varied between 100 and 500 mm. The total starter notch lengths varied between 3 mm and 75 mm.

The loading parameters can be divided into the maximum applied stress level and the stress ratio. The maximum applied stress levels applied in most of the experiments were in the range of 80 to 120 MPa, which is the stress level range of interest for aircraft fuselage skin applications [15]. The stress ratio R varied between 0.05 and 0.5.

Because of the exceptional starter notch length and large crack length reached at the end of the tests of the four fatigue tests executed on large 750 mm long and 500 wide panels with a total starter notch length of 75 mm, the data from these tests can be used to define an upper limit of the validation range. Besides the crack growth rate versus the crack length, also the crack opening contours were recorded during these tests and the delamination shapes were measured after completion of the tests.

Comparison between the crack growth rate versus crack length is given in Figure 6.26, while the predicted crack opening contours are compared with the measured contours in Figure 6.27 and Figure 6.28. The delamination shape measured after completion of the fatigue tests is compared with the predicted delamination shapes in Figure 6.29 and Figure 6.30. These figures show that the predicted crack growth behaviour and crack opening contours correlate very well with the experiments. Since the method is derived from the crack opening relations, these results give good confidence in the model.

However, the predicted delamination sizes are smaller than observed after the experiments. The method seems to overpredict the delamination size for small crack lengths starting from small starter notches, see Figure 6.21, and to underpredict the delamination shapes of large cracks starting from large starter notches. This trend is similar to the trend in Figure 6.29, where the difference between prediction and measurements increases for increasing crack lengths. The difference can be explained with the Paris relation for delamination utilised in the method. As discussed in section 6.4, the mode II Paris relation, derived in section 6.2.3, is applied in the model for the centre crack tension configuration. However, the delamination at the interfaces adjacent to the outer aluminium layers also face a mode I contribution, which gives higher delamination growth rates as observed during the delamination growth experiments.

The model is based on an average behaviour of all interfaces and excludes any through the thickness variation. This could mean that the mode II Paris relation is too conservative resulting in smaller delamination growth rates. Applying a Paris Relation that includes a small mode I contribution (averaged over all the aluminium-prepreg interfaces) together with a different delamination shape assumption could give a better correlation with the observe delamination shapes.

For the current method, this approach is not followed because the Paris relation to be applied does not directly follow from experiments. In spite of the differences with the measured delamination shapes, it is believed that the predicted delamination growth is sufficiently accurate to describe the crack growth behaviour in Glare under relevant service conditions.

With respect to the initial objective of the experiments with the large starter notches, no fibre failure was observed near the starter notch tip during the fatigue tests. With the current model, an explanation can be found for the absence of fibre failure even for the extremely large crack lengths. The bridging stress distribution for these cases are given in Figure 6.31. From these figures, it can be seen that the bridging stress at the starter notch is the highest at the beginning of the fatigue tests. This means that the total fibre stress at that locations decreases with increasing crack lengths. If fibre failure does not occur at the beginning of the test at that location, it will not occur during the whole fatigue tests. Looking at the location where the bridging stress is the highest, fibre failure would rather occur near the crack tip. However, during none of the fatigue tests performed on Glare any fibre failure was observed.

6 Crack Growth Prediction Model

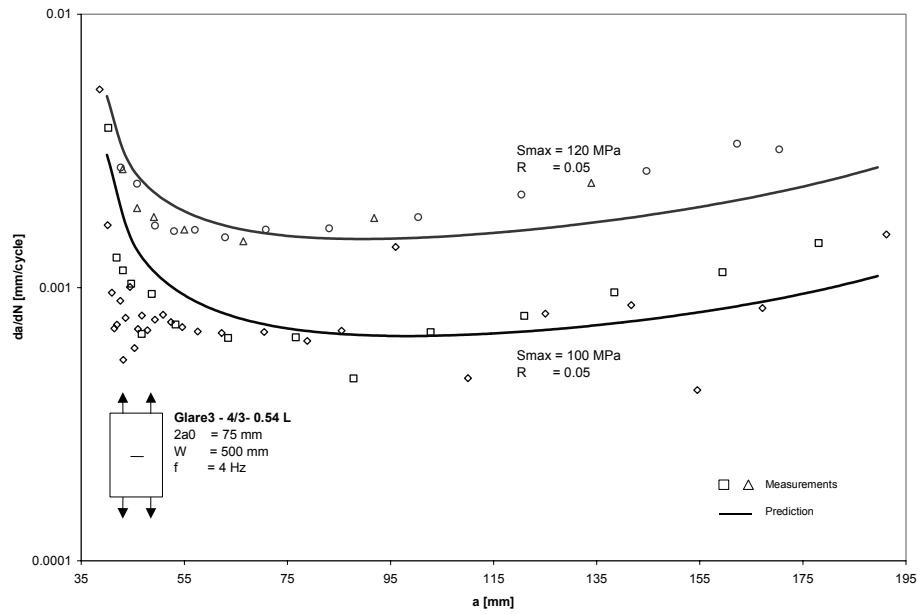


Figure 6.26 Comparison between the predicted and measured crack propagation of Glare3-4/3-0.5 in L-T direction with $W=500$ mm, $a_s=37.5$ mm and $S_{max}=100$ and 120 MPa with $R=0.05$

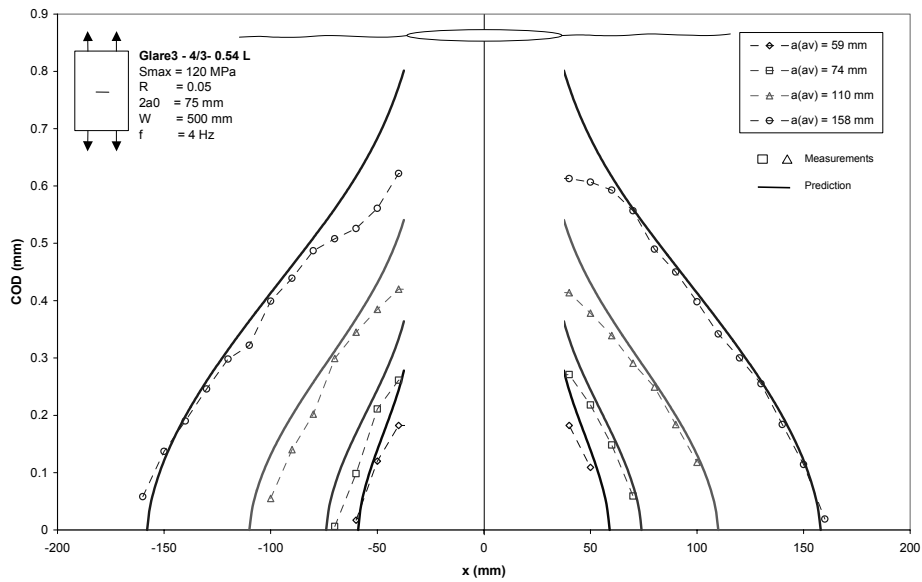


Figure 6.27 Comparison between the predicted and measured crack opening displacement of Glare3-4/3-0.5 in L-T direction with $W=500$ mm, $a_s=37.5$ mm and $S_{max}=120$ MPa with $R=0.05$

Fatigue crack propagation and delamination growth in Glare

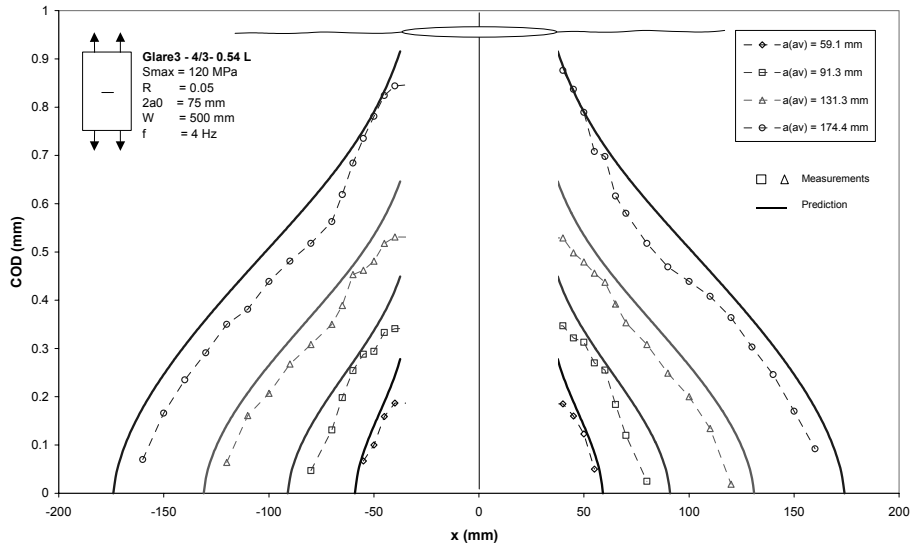


Figure 6.28 Comparison between the predicted and measured crack opening displacement of Glare3-4/3-0.5 in L-T direction with $W=500$ mm, $a_s=37.5$ mm and $S_{max}=120$ MPa with $R=0.05$

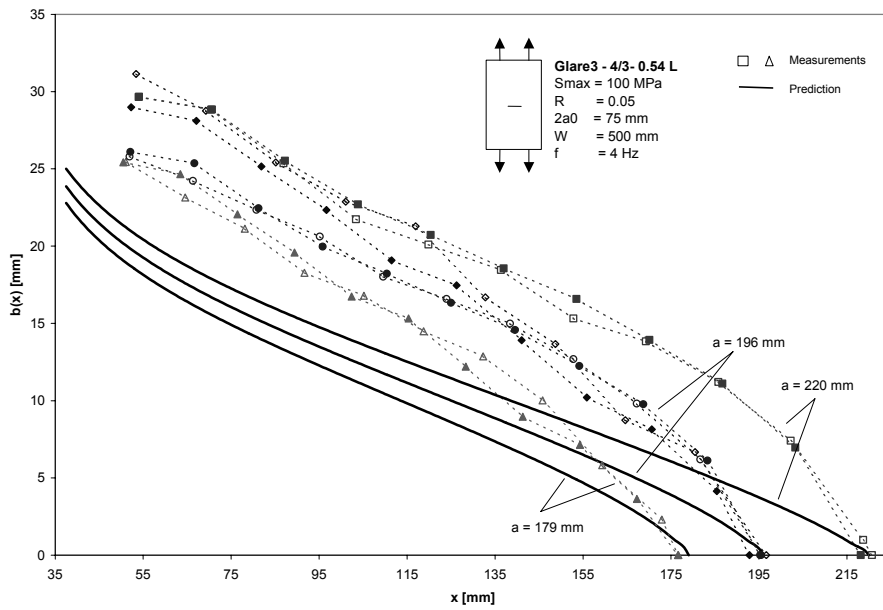


Figure 6.29 Comparison between predicted and measured delamination shapes of Glare3-4/3-0.5 in L-T direction with $W=500$ mm, $a_s=37.5$ mm and $S_{max}=100$ MPa with $R=0.05$

6 Crack Growth Prediction Model

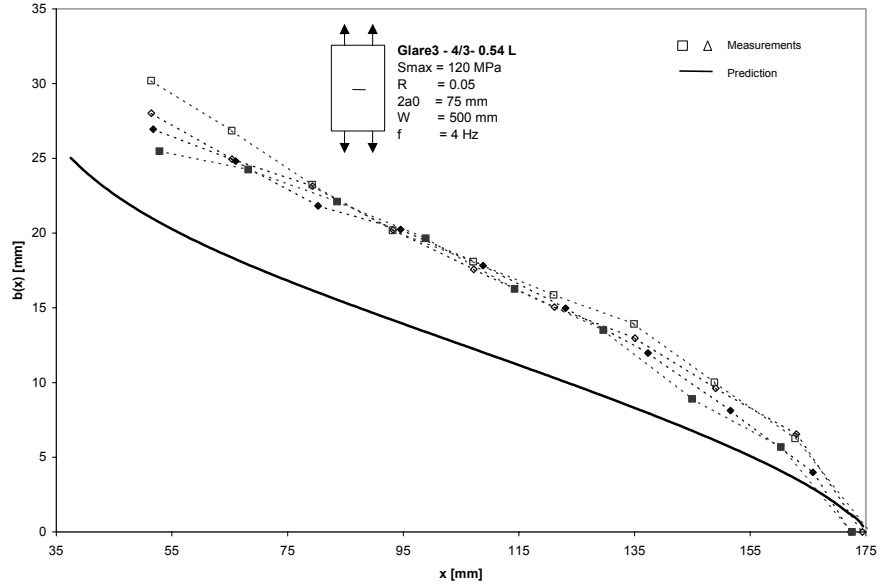


Figure 6.30 Comparison between predicted and measured delamination shapes of Glare3-4/3-0.5 in L-T direction with $W=500$ mm, $a_s=37.5$ mm and $S_{max}=120$ MPa with $R=0.05$

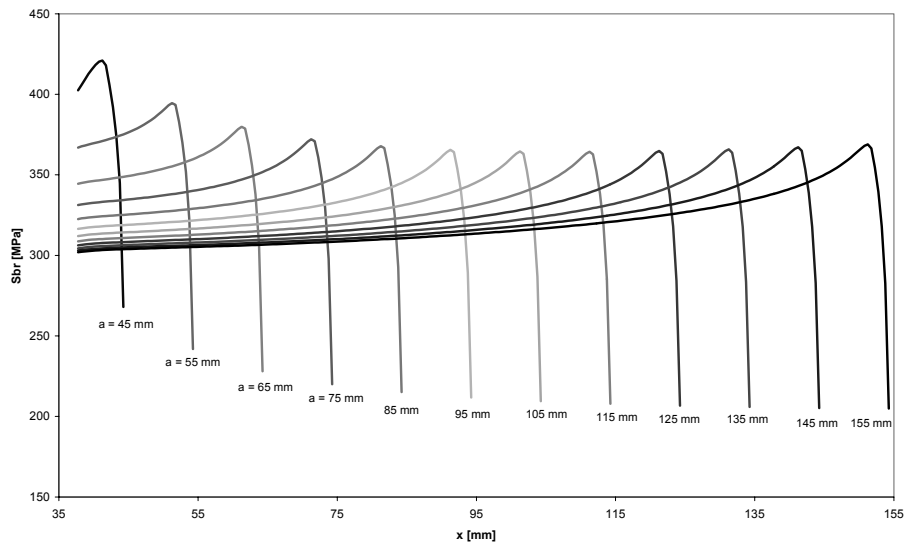


Figure 6.31 Bridging stress distributions of Glare3-4/3-0.5 in L-T direction with $W=500$ mm, $a_s=37.5$ mm and $S_{max}=100$ MPa with $R=0.05$

6.8 Summary

An analytical crack growth prediction model for Glare is derived based on the crack opening relations for monolithic aluminium and the elongation and deformation relations for the prepreg. The method is implemented in a numerical calculation program that can be represented by the program flow given in Figure 6.15. The input parameters for the model are given in Figure 6.16.

The model, based on the parabolic delamination shape extension, is substantiated with a wide range of experimental data, partly presented in Appendix C. The validity range of the model is related to the tested range of parameters, which is summarised in Table 6.3.

Table 6.3 *Tested ranges of parameters for the validity range of the model*

	<i>Minimum</i>	<i>Maximum</i>
Glare types	Glare3 and Glare4B (L-T and T-L)	
Lay-up	3/2	8/7
Aluminium thickness	0.3 mm	0.5 mm
Max. applied load	80 MPa	120 MPa
Stress ratio	0.05	0.5
Starter notch length	3 mm	75 mm
Crack Lengths	1 mm	220 mm
Specimen widths	100 mm	500 mm

References

- [1] **Marissen, R.**, *Fatigue Crack Growth in ARALL, A hybrid Aluminium-Aramid Composite Material, crack growth mechanisms and quantitative predictions of the crack growth rate*, PhD Thesis, Delft University of Technology, 1988.
- [2] **Yeh, J.R.**, *Fatigue crack growth in Fiber-Metal Laminates*, Int. J. Solids Structures, **32**, No. 14, 2063-2075, 1995
- [3] **Alderliesten, R.C.**, *Energy Release Rate approach for delamination in a fatigue crack configuration in Glare*, Submitted to Engineering Fracture Mechanics, 2005
- [4] **Suiker, A.S.J., Fleck, N.A.**, *Crack tunnelling and plane-strain delamination in layered solids*, International Journal of Fracture, **125**: 1-32, 2004.
- [5] **Guo, Y.J., Wu, X.R.**, *Bridging stress distribution in center-cracked fiber reinforced metal laminates: modelling and experiment*, Eng. Fract. Mech., 1999
- [6] **Tada, H., Paris, P.C., Irwin, G.R.**, *The Stress Analysis of Crack Handbook*, 3rd ed., The American Society of Mechanical Engineers, 2000

- [7] **Homan, J.J.**, *Fatigue Initiation in Fibre Metal Laminates*, International Journal of Fatigue, (Under review).
- [8] **Alderliesten, R.C.**, *Modelling Fatigue Crack Propagation in Glare, Interim Status Report*, Report TD-R-02-022, Fibre Metal Laminates Centre of Competence, 2003
- [9] **Alderliesten, R.C., Woerden, H.J.M.**, *Load History Effects during Fatigue Crack Propagation in Glare*, Proceedings of the 22nd symposium of the International Committee on Aeronautical Fatigue, Vol.1, Emas Publishing, 2004
- [10] **Koning, A.U. de**, *Analysis of the fatigue crack growth behaviour of “through the thickness” cracks in fibre metal laminates*, Report NLR-CR-2000-575, National Aerospace Laboratory NLR, 2000
- [11] **Homan, J.J.**, *Crack growth properties of thin aluminium sheets*, Report B2V-01-16, Delft University of Technology, Faculty of Aerospace Engineering, 2001 (restricted).
- [12] **Ewalds, H.L., Wanhill, R.J.H.**, *Fracture Mechanics*, Delftse Uitgevers Maatschappij, Delft, The Netherlands, 1984
- [13] **Alderliesten, R.C.**, *Development of an empirical fatigue crack growth prediction method for the Fibre Metal Laminate Glare*, Masters Thesis, Faculty of Aerospace Engineering, Delft University of Technology, 1999.
- [14] **Homan, J.J., Alderliesten, R.C.**, *Test data for Fatigue Crack Propagation in unstiffened GLARE – Through Cracks*, Report B2V-99-39, Faculty of Aerospace Engineering, Delft University of Technology, 1999 (restricted).
- [15] **Vlot, A, Gunnink, J.W.**, *Fibre Metal Laminates, an introduction*, Kluwer Academic Publishers, Dordrecht, The Netherlands, 2001.

Fatigue crack propagation and delamination growth in Glare

Conclusions and future prospects



7.1 Conclusions

The investigation of the present thesis is concerned with the fatigue crack growth behaviour of the aluminium layers in Glare with the corresponding delamination growth behaviour of the aluminium/fibre interfaces under constant amplitude fatigue loading. The fatigue crack geometry considered is the through crack configuration with cracks in all aluminium layers having the same length equal to the visible crack length in the outer aluminium layers.

An analytical calculation method has been developed to describe the mechanism of crack propagation and delamination growth. This model has been implemented in a numerical programme, which has been verified with the results of an extensive test program.

The assumptions, on which the model is based, are:

- The mechanisms can be described with the concepts of Linear Elastic Fracture Mechanics.
- Crack growth in the aluminium layers occurs under plane stress conditions.
- The crack growth rate can be related to the stress intensity factor with an empirical Paris equation.
- Plane strain conditions are applicable to the delamination growth at the interfaces.
- The delamination growth can be related to the energy release rate with an empirical Paris equation.
- The stress intensity factor at the crack tip can be determined by superposing of the stress intensity factor for the far field opening stress and the stress intensity for the crack closing bridging stress.
- Crack closure does not occur.

From the current investigation, several conclusions can be drawn with respect to the crack growth behaviour of Glare and the crack growth prediction model. The conclusions are summarised below.

Crack growth behaviour in Glare

The fatigue crack growth mechanism in Glare is characterised by the crack propagation in the aluminium layers of Glare and the delamination at the interfaces between the aluminium and prepreg layers. The balance between these two mechanisms is directly related to the crack growth resistance of the aluminium and the delamination resistance of the prepreg at the interface.

For cracks propagating from a starter notch, the crack growth rates starts initially at a higher level, due to the absence of fibre bridging, and subsequently decreases to an approximately constant level at which the fibre bridging is fully efficient. A gradual increase of the crack growth rate in a later stage is attributed to the finite width effect.

The delamination shape observed in the fatigue tests was neither elliptical, nor triangular, as assumed in previous investigations. The actual delamination shape was observed to be between these typical shapes, which can be explained by the bridging stress distribution along the crack.

Fibre failure was not observed during fatigue crack propagation tests, even not for very large crack lengths, initiated by a 75 mm starter notch.

Crack growth prediction model

The analytical crack growth prediction model developed leads to the following conclusions:

The bridging stress distribution along the total crack length can be determined when the delamination shape and the crack opening contour are known. This bridging stress has the highest value near the crack tip. From the calculated bridging stresses, it can be concluded that fibre failure during crack propagation does not occur at the starter notch tip, because the bridging stress at that location decreases with the progressing crack.

The analytical model is physically sound as the equations are derived from exact stress intensity solutions following a well-defined approach. The prediction model is accurate and validated with a wide range of experimental data, including crack growth results and increasing delamination areas. Finally, the model is robust, because it is insensitive to the initial crack and delamination geometry.

7.3 Future prospects

The current crack growth prediction model has the potential to be extended to other material-, geometrical and loading conditions. Investigations extending the crack growth prediction model are going on. Several fields of interest into which the model will be extended are mentioned below.

Material conditions

The material input parameters of the individual constituents are associated with the empirical Paris relation for crack growth in the aluminium layer and an empirical Paris relation for delamination growth. The current model can be extended and validated for Arall. The empirical Paris relation for crack growth in aluminium 7075-T6 is available in the literature, while Marissen obtained the delamination relation for Arall. The model can be adapted with available input data to predict crack growth in Arall. The model can be validated with the crack growth results on CCT specimens provided by Marissen.

Geometrical conditions

The current model covers CCT specimens with through cracks loaded in the fibre direction or perpendicular to the fibres. The model can be extended for the following geometrical conditions:

- Edge crack configuration – The model will be similar, but the relations for the stress intensity factor and the crack opening shape obtained for CCT specimen configurations must be replaced by edge crack relations
- Surface and part through cracks – The model will be similar to the current model, however, the intact aluminium layers will add to the bridging. The bridging stress needs to be defined based on the intact aluminium and fibre layers
- Off-axis loading – The crack propagation and delamination growth under off-axis angles with respect to the fibre directions can be determined as input for the model, after which the model can be validated with the available experimental data.

Loading conditions

The current prediction model uses a correction factor for the stress ratio, which has been determined for a previous empirical model, because not enough experimental data was available to determine the correction for the current analytical method. Research on the effect of the stress ratio on the crack growth behaviour is going on.

The model is validated for a range of positive stress ratios, thus tension-to-tension fatigue only. To make the model generally applicable for all aircraft loading conditions, further research is necessary to cover negative stress ratios as well.

Environmental conditions

The environmental temperature is known to have an effect on the crack growth behaviour of Glare. The model can be extended to the operational temperature range of an aircraft by including the crack propagation and delamination growth behaviour at low and elevated temperatures. Experimental data on crack propagation in CCT specimens at low and elevated temperatures for validation of the model is already available. Research on determination of the empirical relation for delamination at elevated temperatures has been started.

A

Crack Opening Shape

Abstract – This appendix presents the derivation of the crack opening shape as function of the bridging stress distribution along the crack acting on the delamination contour, following the analogy with the other point load cases presented in the Stress Analysis of Cracks Handbook.



A.1 Introduction

Expressions for the crack opening shape under plane stress conditions for a crack in an infinite metal sheet loaded by point loads are derived in the Stress Analysis of Cracks handbook by Tada et al. [1]. In order to obtain a crack opening shape relation for the bridging stresses acting on the delamination contour in a fatigue crack configuration in Glare several relations are presented here.

The solution for symmetric point loads from [1] which should be used to describe the crack opening is defined in terms of complex parameters. To avoid complex relations Marissen [2] derived expressions for K_I based on real variables only. However, such expressions do not exist in the literature for the crack opening shape. The approach followed here, is to derive relations based on real variables only, analogue to the other point load cases presented in [1]. With these relations the crack opening as result of bridging stresses can then be determined.

A.2 Crack Opening Shapes due to point loads

The crack opening shape under plane stress conditions for a centre crack in an infinite metal sheet loaded by point loads acting on the crack flanks in the centre of the crack, see Figure A.1, is given by

$$v(x) = \frac{2P}{\pi E} \cosh^{-1} \frac{a}{x} \quad (A.1)$$

and the corresponding Stress Intensity Factor

$$K_I = \frac{P}{\sqrt{\pi a}} \quad (A.2)$$

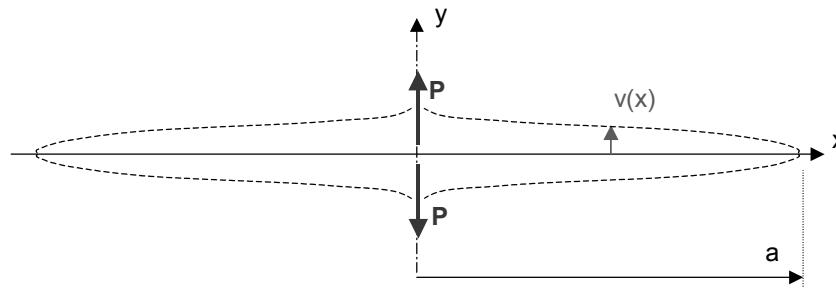


Figure A.1 Crack opening due to point-forces acting on the crack flanks.

The crack opening shape under plane stress conditions for a centre crack in an infinite metal sheet loaded by point-loads acting on a distance b from the crack flanks in the centre of the crack, see Figure A.2, is given by

$$v(x) = \frac{2P}{\pi E} \left(\tanh^{-1} \sqrt{\frac{a^2 - x^2}{a^2 + b^2}} + \frac{1}{2}(1 + \nu) \frac{b^2}{x^2 + b^2} \sqrt{\frac{a^2 - x^2}{a^2 + b^2}} \right) \quad (A.3)$$

and the corresponding Stress Intensity factor

$$K_I = \frac{P}{\sqrt{\pi a}} \frac{a}{\sqrt{a^2 + b^2}} \left(1 + \frac{1}{2}(1 + \nu) \frac{b^2}{a^2 + b^2} \right) \quad (A.4)$$

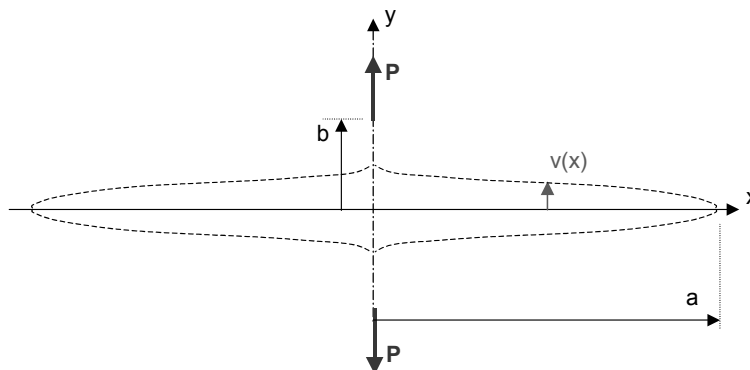


Figure A.2 Crack opening due to point-forces acting at distance b from the crack flanks.

A Crack Opening Shape

The crack opening shape under plane stress conditions for a centre crack in an infinite metal sheet loaded by symmetric point-loads acting on the crack flanks and at a distance x_p from the centre of the crack, see Figure A.3, is given by

$$v(x) = \frac{4P}{\pi E} \tanh^{-1} \sqrt{\frac{a^2 - x_p^2}{a^2 - x^2}} \quad (A.5)$$

for $|x| < x_p$, and

$$v(x) = \frac{4P}{\pi E} \tanh^{-1} \sqrt{\frac{a^2 - x^2}{a^2 - x_p^2}} \quad (A.6)$$

for $|x| > x_p$, and the corresponding Stress Intensity factor

$$K_I = \frac{P}{\sqrt{\pi a}} \frac{a}{\sqrt{a^2 - x_p^2}} \quad (A.7)$$

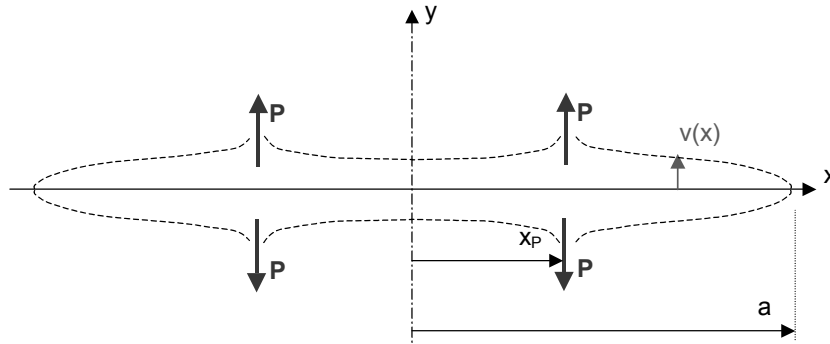


Figure A.3 Crack opening due to point-forces acting on the crack flanks.

The case of two point-loads acting on the crack flanks at the centre of the centre crack, see Figure A.1, is a simplification of the more general solution, illustrated in Figure A.2, by substituting $b=0$ in the corresponding expressions, or a simplification of the more general solution illustrated in Figure A.3, by substituting $x_p=0$ in the corresponding expressions.

A general expression for the crack opening shape under plane stress conditions for a centre crack in an infinite metal sheet loaded by symmetric point-loads acting on a distance b from the crack flanks and at a distance x_p from the centre of the crack, see Figure A.4, is not given in [1] as function of real parameters. However, a general expression can be deduced from the solutions described above. The two cases illustrated with Figure A.2 and Figure A.3 are simplifications of the general case in

Figure A.4, by substituting $x_p=0$ and $b=0$ respectively. This means that the equations for the crack opening shape and the stress intensity factor K_I should show some similarity to the equations previously presented for those configurations. They are limit cases for $b \rightarrow 0$ and $x_p \rightarrow 0$ respectively, which are presented in the following equations (A.8) to (A.13)

$$v(x) \xrightarrow{b \rightarrow 0} \frac{4P}{\pi E} \tanh^{-1} \sqrt{\frac{a^2 - x_p^2}{a^2 - x^2}} \quad (A.8)$$

for $|x| < x_p$, and

$$v(x) \xrightarrow{x_p \rightarrow 0} \frac{2P}{\pi E} \left(\tanh^{-1} \sqrt{\frac{a^2 - x^2}{a^2 + b^2}} + \frac{1}{2} (1 + \nu) \frac{b^2}{x^2 + b^2} \sqrt{\frac{a^2 - x^2}{a^2 + b^2}} \right) \quad (A.9)$$

and

$$v(x) \xrightarrow{b \rightarrow 0} \frac{4P}{\pi E} \tanh^{-1} \sqrt{\frac{a^2 - x^2}{a^2 - x_p^2}} \quad (A.10)$$

for $|x| > x_p$, and

$$v(x) \xrightarrow{x_p \rightarrow 0} \frac{2P}{\pi E} \left(\tanh^{-1} \sqrt{\frac{a^2 - x^2}{a^2 + b^2}} + \frac{1}{2} (1 + \nu) \frac{b^2}{x^2 + b^2} \sqrt{\frac{a^2 - x^2}{a^2 + b^2}} \right) \quad (A.11)$$

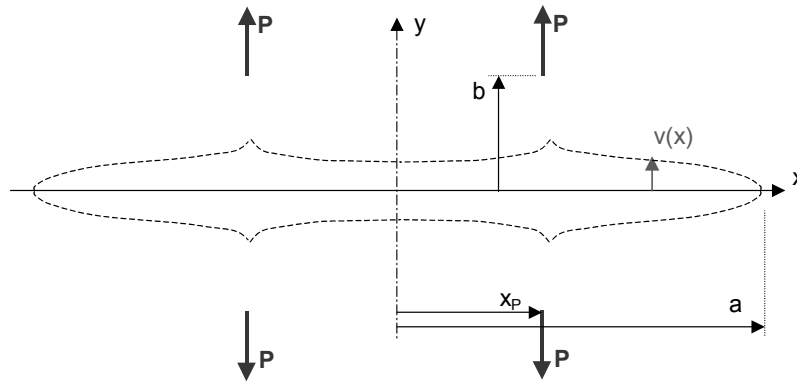


Figure A.4 Crack opening due to point-forces acting at distance b from the crack flanks.

One can write for the Stress Intensity Factor in a similar way

$$K_I \xrightarrow{b \rightarrow 0} \frac{2P}{\sqrt{\pi a}} \frac{a}{\sqrt{a^2 - x_p^2}} \quad (A.12)$$

and

$$K_I \xrightarrow{x_p \rightarrow 0} \frac{P}{\sqrt{\pi a}} \frac{a}{\sqrt{a^2 + b^2}} \left(1 + \frac{1}{2}(1 + \nu) \frac{b^2}{a^2 + b^2} \right) \quad (A.13)$$

It is noteworthy that the equations for $v(x)$ for the loading case in Figure A.4 are not reported in the literature, although an exact solution for K_I is available [1]. Using the work presented in [3] solutions could be derived by rewriting point-forces away from the crack to stress distributions at the crack flank. Since equations for $v(x)$ are needed for the present application to describe crack bridging stresses acting on a delamination contour away from the crack flanks, the following equations are proposed here

$$v(x) = \frac{4P}{\pi E} \left(\tanh^{-1} \sqrt{\frac{a^2 - x_p^2}{a^2 - x^2 + b^2}} + \frac{\frac{1}{2}(1 + \nu)b^2}{x_p^2 - x^2 + b^2} \sqrt{\frac{a^2 - x_p^2}{a^2 - x^2 + b^2}} \right) \quad (A.14)$$

for $|x| < x_p$, and

$$v(x) = \frac{4P}{\pi E} \left(\tanh^{-1} \sqrt{\frac{a^2 - x^2}{a^2 - x_p^2 + b^2}} + \frac{\frac{1}{2}(1 + \nu)b^2}{x^2 - x_p^2 + b^2} \sqrt{\frac{a^2 - x^2}{a^2 - x_p^2 + b^2}} \right) \quad (A.15)$$

for $|x| > x_p$. The corresponding Stress Intensity Factor

$$K_I = \frac{2P}{\sqrt{\pi a}} \frac{a}{\sqrt{a^2 - x_p^2 + b^2}} \left(1 + \frac{1}{2}(1 + \nu) \frac{b^2}{a^2 - x_p^2 + b^2} \right) \quad (A.16)$$

There is no proof that these equations are exact, but it is believed on heuristic arguments that the similarity with equations (A.8) to (A.13) justifies the applications for the present purpose. The equation for the K_I -value differs mathematically from the exact solution. However, a numerical comparison with the exact solution indicated that for the major part of the x_p -range ($0 \leq x_p \leq a$) the differences are negligible. Only for x_p -values very close to the crack tip ($x_p \rightarrow a$) with $b > 0$, numerical differences are substantial, but that is of little interest for the present application, because the delamination length decreases to zero at the crack tip.

A.3 Crack Opening Shapes due to bridging stress

The crack opening due to a bridging stress $S_{br}(x)$ acting at the delamination boundary described by $b(x)$, see Figure A.5, can now be derived from equation (A.14) and (A.15), assuming that point-load P is represented by the bridging load $S_{br}(x)dx$. Thus

$$v(x) = \int_0^a v(x, x_p) dx_p \quad (A.17)$$

with for $|x| < x_p$

$$v(x, x_p) = \frac{4S_{br}(x_p)dx_p}{\pi E} \left(\tanh^{-1} \sqrt{\frac{a^2 - x_p^2}{a^2 - x^2 + b(x)^2}} + [\dots] \right) \quad (A.18)$$

where

$$[\dots] = \frac{\frac{1}{2}(1+\nu)b(x)^2}{x_p^2 - x^2 + b(x)^2} \sqrt{\frac{a^2 - x_p^2}{a^2 - x^2 + b(x)^2}} \quad (A.19)$$

and for $|x| > x_p$

$$v(x, x_p) = \frac{4S_{br}(x_p)dx_p}{\pi E} \left(\tanh^{-1} \sqrt{\frac{a^2 - x^2}{a^2 - x_p^2 + b(x)^2}} + [\dots] \right) \quad (A.20)$$

where

$$[\dots] = \frac{\frac{1}{2}(1+\nu)b(x)^2}{x^2 - x_p^2 + b(x)^2} \sqrt{\frac{a^2 - x^2}{a^2 - x_p^2 + b(x)^2}} \quad (A.21)$$

and where $b(x_i)$ is an arbitrary delamination shape.

A Crack Opening Shape

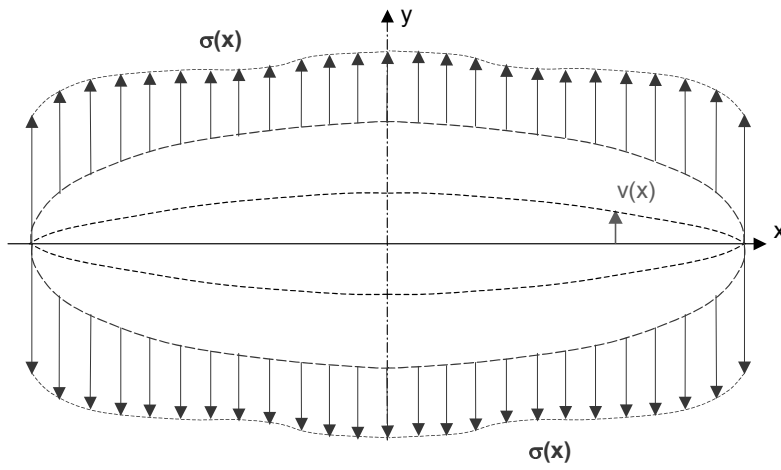


Figure A.5 Crack opening $v(x)$ as result of the distributed stress $\sigma(x)$ acting on an arbitrary delamination shape

References

- [1] Tada, H., Paris, P.C., Irwin, G.R., *The Stress Analysis of Crack Handbook*, 3rd ed., The American Society of Mechanical Engineers, 2000.
- [2] Marissen, R., *Fatigue Crack Growth in ARALL, A hybrid Aluminium-Aramid Composite Material, crack growth mechanisms and quantitative predictions of the crack growth rate*, PhD Thesis, Delft University of Technology, 1988.
- [3] Timoshenko, S.P., *Theory of Elasticity*, Auckland, McGraw-Hill, 1970.

Fatigue crack propagation and delamination growth in Glare

B

Prepreg shear deformation

Abstract — The crack opening in equation (6.9) in chapter 6 contains a component related to the prepreg shear deformations. This appendix presents the derivation of this prepreg shear deformation induced by the cyclic shear stresses at the metal/fibre interface. In the first two sections, the derivation is given for uni-directional fibre layers and for cross-ply fibre layers respectively. In the third and fourth section, the effect of the delamination length on the prepreg shear deformation for both cases is derived.



B.1 Prepreg shear deformation of uni-directional fibre layers

The approach presented in this section is similar to the adhesive shear deformation derivation of Verbruggen [1] and Marissen [2], who used an element breakdown in thickness direction, where the aluminium and fibre elements carried the tensile loading only and the adhesive element the shear loading. However, for the current investigation, the adhesive layer is assumed to be absent and the deformation is attributed to the shear deformation of the fibre layer, as illustrated in Figure B.1.

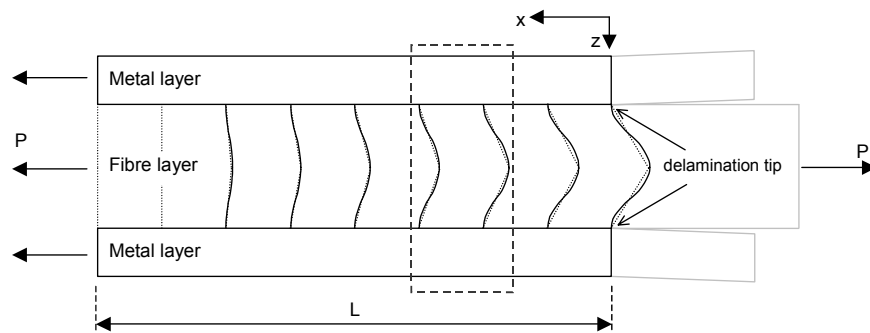


Figure B.1 *Deformation of the uni-directional prepreg under tensile loading in the fibres and shear loading at the metal/fibre interface.*

The approach is based on the assumption that the calculated deformation is independent of the y-direction (out-of-plane in Figure B.1). The loads P , P_{al} and P_f are assumed to be constant and independent of the z-direction. The non-linear deformation through the prepreg thickness is represented as a linear deformation. This means that the aluminium elements carry tensile loading only and the fibre layers carry both tensile loading and shear loading, inducing an elongation and a shear deformation of the prepreg layer.

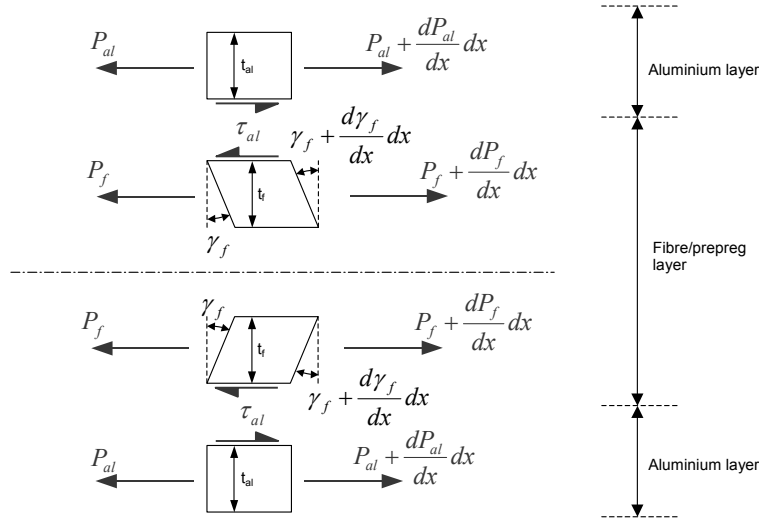


Figure B.2 Breakdown of the elements in thickness direction of the deformed uni-directional prepreg illustrated in Figure B.1

Equilibrium in the aluminium and fibre elements yields

$$\frac{dP_{al}}{dx} = -\frac{dP_f}{dx} = -\tau_{al} \quad (B.1)$$

while equilibrium over the total thickness implies

$$2P_{al} + 2P_f = P \quad (B.2)$$

For the shear deformation it follows

$$\frac{d\gamma_f}{dx} t_f = \varepsilon_f - \varepsilon_{al} \quad (B.3)$$

and with the Hooke's law

B Prepreg shear deformation

$$\varepsilon_f = \frac{P_f}{t_f E_f} \quad ; \quad \varepsilon_{al} = \frac{P_{al}}{t_{al} E_{al}} \quad ; \quad \gamma_f = \frac{\tau_{al}}{G_f} \quad (B.4)$$

Combining these equations gives the following differential equation

$$\frac{d^2 P_{al}}{dx^2} = -\frac{d^2 P_f}{dx^2} = \alpha P_{al} - \beta P_f \quad (B.5)$$

with

$$\alpha = \frac{G_f}{t_f t_{al} E_{al}} \quad ; \quad \beta = \frac{G_f}{t_f^2 E_f} \quad (B.6)$$

Using the three equations, this can be written in two single differential equations

$$\begin{aligned} \frac{d^2 P_{al}}{dx^2} &= (\alpha + \beta) P_{al} - \frac{\beta}{2} P \\ \frac{d^2 P_f}{dx^2} &= (\alpha + \beta) P_f - \frac{\alpha}{2} P \end{aligned} \quad (B.7)$$

for which the general solution is given by

$$\begin{aligned} P_{al} &= A \sinh \sqrt{\alpha + \beta} x + B \cosh \sqrt{\alpha + \beta} x + \frac{\beta P}{2(\alpha + \beta)} \\ P_f &= C \sinh \sqrt{\alpha + \beta} x + D \cosh \sqrt{\alpha + \beta} x + \frac{\alpha P}{2(\alpha + \beta)} \end{aligned} \quad (B.8)$$

With the boundary conditions $P_{al} = 0$ and $P_f = P$ at $x = 0$ (Figure B.1) it follows that

$$B = -\frac{\beta P}{2(\alpha + \beta)} \quad ; \quad D = \frac{\beta P}{2(\alpha + \beta)} \quad (B.9)$$

The boundary condition at $x=L$ (Figure B.1) is given as

$$P_{al} = \frac{F_{al}}{F} P \quad ; \quad P_f = \frac{F_f}{F} P \quad (B.10)$$

which means that $P_{al} + P_f = P$. Substitution yields

$$A = \frac{F_{al}}{F} \frac{\cosh \sqrt{\alpha + \beta} L}{\sinh \sqrt{\alpha + \beta} L} P \quad ; \quad C = -\frac{F_{al}}{F} \frac{\cosh \sqrt{\alpha + \beta} L}{\sinh \sqrt{\alpha + \beta} L} P \quad (B.11)$$

Thus equation (B.8) can be written as

$$P_{al} = \left[\frac{F_{al}}{F} \cosh \sqrt{\alpha + \beta} L \frac{\sinh \sqrt{\alpha + \beta} x}{\sinh \sqrt{\alpha + \beta} L} - \frac{F_{al}}{F} \cosh \sqrt{\alpha + \beta} x + \frac{F_{al}}{F} \right] P$$

$$P_f = \left[-\frac{F_{al}}{F} \cosh \sqrt{\alpha + \beta} L \frac{\sinh \sqrt{\alpha + \beta} x}{\sinh \sqrt{\alpha + \beta} L} + \frac{F_{al}}{F} \cosh \sqrt{\alpha + \beta} x + \frac{F_f}{F} \right] P \quad (B.12)$$

These equations satisfy the expression in equation (B.1) and (B.2). The corresponding shear stress is then

$$\tau_{al} = -\left[\frac{F_{al}}{F} \cosh \sqrt{\alpha + \beta} L \frac{\cosh \sqrt{\alpha + \beta} x}{\sinh \sqrt{\alpha + \beta} L} - \frac{F_{al}}{F} \sinh \sqrt{\alpha + \beta} x \right] \sqrt{\alpha + \beta} P \quad (B.13)$$

For values of $L \gg 1$ this equation can be simplified to

$$\tau_{al} = -\left[\cosh \sqrt{\alpha + \beta} x - \sinh \sqrt{\alpha + \beta} x \right] \frac{F_{al}}{F} \sqrt{\alpha + \beta} P \quad (B.14)$$

With the relations

$$\cosh x = \frac{e^x + e^{-x}}{2} \quad ; \quad \sinh x = \frac{e^x - e^{-x}}{2} \quad (B.15)$$

equation (B.14) can be written as

$$\tau_{al} = -S_{al} t_{al} \sqrt{\frac{G_f}{t_f} \left(\frac{1}{F_{al}} + \frac{1}{F_f} \right)} e^{-x \sqrt{\frac{G_f}{t_f} \left(\frac{1}{F_{al}} + \frac{1}{F_f} \right)}} \quad (B.16)$$

which is similar to the expression derived by Marissen for the shear stress with adhesive shear deformation. An illustration of the shear stress at the interface in equation (B.16) in comparison with the tensile stresses in the aluminium and fibre layer is presented in Figure B.3.

B Prepreg shear deformation

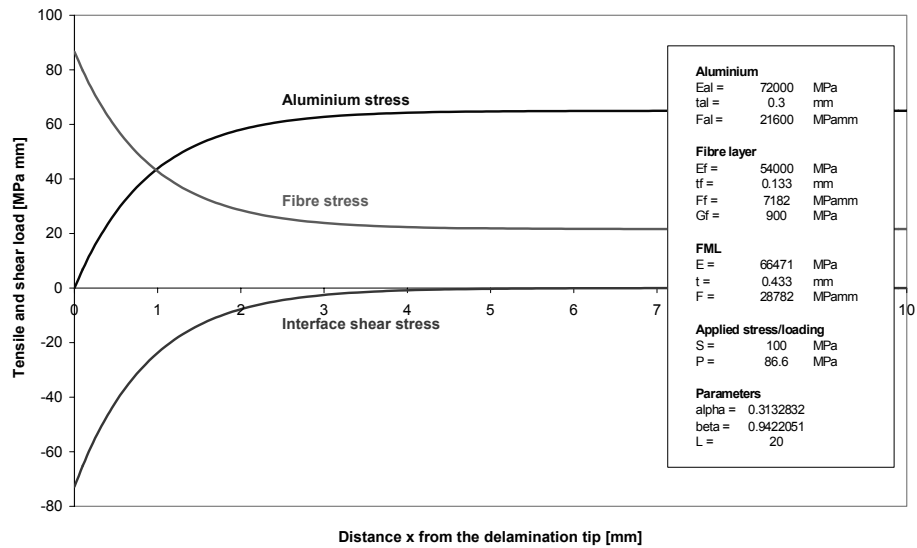


Figure B.3 Illustration of the tensile and shear stresses as function of the distance to the delamination tip, see Figure B.1.

B.2 Prepreg shear deformation of cross-ply fibre layers

In order to model the shear deformation of the cross-ply prepreg layer with the approach as presented for the uni-directional prepreg layer derived in the previous section, some assumptions have to be made. The two elements representing the prepreg layer will have different Young's moduli and shear stiffness properties, which are related to the directions parallel and perpendicular to the fibre orientation.

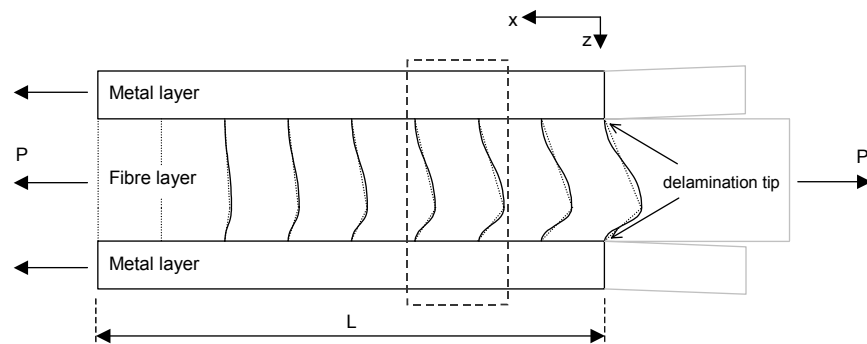


Figure B.4 Deformation of the cross-ply prepreg under tensile loading in the fibres and shear loading at the metal/fibre interface.

To match the boundary condition that the shear stress between both elements is zero and that the displacement of both elements are identical at the interface connecting the two layers, different element thicknesses have to be assumed. These element thicknesses are not related to the physical stiffnesses of both layers in the prepreg, but only to the ratio of Young's moduli and shear stiffnesses.

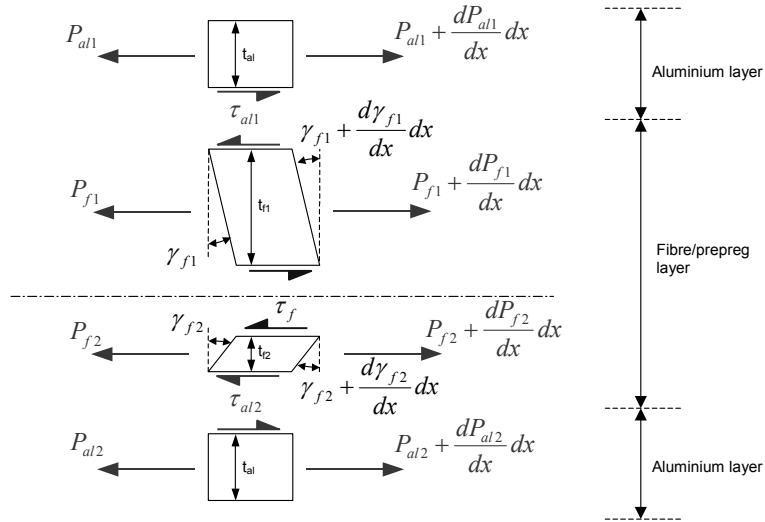


Figure B.5 Breakdown of the elements in thickness direction of the deformed cross-ply prepreg illustrated in Figure B.4

The total prepreg thickness is equal to the thickness depicted in Figure B.2

$$t_{f1} + t_{f2} = 2t_f \quad (B.17)$$

From the geometry in Figure B.5 it follows that the strain at the connection of both fibre layers is the same

$$\varepsilon_{f1} = \frac{P_{f1}}{t_{f1}E_{f1}} = \frac{P_{f2}}{t_{f2}E_{f2}} = \varepsilon_{f2} \quad (B.18)$$

and that the deflection is the same as well

$$\gamma_{f1}t_{f1} = \frac{\tau_{f1}}{G_{f1}}t_{f1} = -\frac{\tau_{f2}}{G_{f2}}t_{f2} = -\gamma_{f2}t_{f2} \quad (B.19)$$

Equilibrium in the aluminium element yields

$$\frac{dP_{al}}{dx} = -\tau_{al} \quad (B.20)$$

and equilibrium in the fibre element

$$\frac{dP_{f1}}{dx} = \tau_{al} - \tau_f \quad ; \quad \frac{dP_{f2}}{dx} = \tau_{al} + \tau_f \quad (B.21)$$

while equilibrium over the total thickness implies

$$2P_{al} + P_{f1} + P_{f2} = P \quad (B.22)$$

For the shear deformation it follows

$$\frac{d\gamma_{f1}}{dx} t_{f1} = \varepsilon_{al} - \varepsilon_f \quad ; \quad \frac{d\gamma_{f2}}{dx} t_{f2} = \varepsilon_f - \varepsilon_{al} \quad (B.23)$$

and with the Hooke's law

$$\varepsilon_{al} = \frac{P_{al}}{t_{al} E_{al}} \quad ; \quad \gamma_{f1} = \frac{\tau_{al} + \tau_f}{G_{f1}} \quad ; \quad \gamma_{f2} = -\frac{\tau_{al} - \tau_f}{G_{f2}} \quad (B.24)$$

Substitution of equations (B.24) into equations (B.23) yields

$$\frac{d\gamma_{f1}}{dx} t_{f1} = \frac{t_{f1}}{G_{f1}} \left(\frac{d\tau_{al}}{dx} + \frac{d\tau_f}{dx} \right) \quad ; \quad \frac{d\gamma_{f2}}{dx} t_{f2} = -\frac{t_{f2}}{G_{f2}} \left(\frac{d\tau_{al}}{dx} - \frac{d\tau_f}{dx} \right) \quad (B.25)$$

From equation (B.20) and (B.21) one can derive

$$\begin{aligned} \frac{d\tau_{al}}{dx} &= -\frac{d^2 P_{al}}{dx^2} \\ \frac{d\tau_f}{dx} &= -\frac{d^2 P_{al}}{dx^2} - \frac{d^2 P_{f1}}{dx^2} = \frac{d^2 P_{al}}{dx^2} + \frac{d^2 P_{f2}}{dx^2} \end{aligned} \quad (B.26)$$

Combining these equations gives the following differential equations

$$\begin{aligned}
 2 \frac{d^2 P_{al}}{dx^2} + \frac{d^2 P_{f1}}{dx^2} &= -\frac{G_{f1}}{t_{f1}} \left(\frac{P_{al}}{t_{al} E_{al}} - \frac{P_{f1}}{t_{f1} E_{f1}} \right) \\
 \frac{d^2 P_{f1}}{dx^2} &= \frac{G_{f2}}{t_{f2}} \left(\frac{P_{al}}{t_{al} E_{al}} - \frac{P_{f1}}{t_{f1} E_{f1}} \right)
 \end{aligned} \tag{B.27}$$

Combining equation (B.18) with equation (B.22) gives

$$2P_{al} + P_{f1} \left(1 + \frac{t_{f2} E_{f2}}{t_{f1} E_{f1}} \right) = 2P_{al} + \eta P_{f1} = P \tag{B.28}$$

which can be substituted into equation (B.27)

$$\begin{aligned}
 \frac{d^2 P_{al}}{dx^2} &= -\left(\alpha_1 + \alpha_2 + \frac{2}{\eta} \beta_1 + \frac{2}{\eta} \beta_2 \right) P_{al} + \frac{1}{\eta} (\beta_1 + \beta_2) P \\
 \frac{d^2 P_{f1}}{dx^2} &= \alpha_2 P - (\alpha_2 \eta + 2\beta_2) P_{f1}
 \end{aligned} \tag{B.29}$$

with

$$\begin{aligned}
 \alpha_1 &= \frac{G_{f1}}{2t_{f1} t_{al} E_{al}} & ; & \quad \alpha_2 = \frac{G_{f2}}{2t_{f2} t_{al} E_{al}} \\
 \beta_1 &= \frac{G_{f1}}{2t_{f1}^2 E_{f1}} & ; & \quad \beta_2 = \frac{G_{f2}}{2t_{f2} t_{f1} E_{f1}}
 \end{aligned} \tag{B.30}$$

The general solution is given by

$$\begin{aligned}
 P_{al} &= A \sinh \sqrt{Q_1} x + B \cosh \sqrt{Q_1} x + \frac{(\beta_1 + \beta_2)}{\eta Q_1} P \\
 P_{f1} &= C \sinh \sqrt{Q_2} x + D \cosh \sqrt{Q_2} x + \frac{\alpha_2}{Q_2} P
 \end{aligned} \tag{B.31}$$

with

$$\begin{aligned}
 Q_1 &= \alpha_1 + \alpha_2 + \frac{2}{\eta} \beta_1 + \frac{2}{\eta} \beta_2 \\
 Q_2 &= \alpha_2 \eta + 2\beta_2
 \end{aligned} \tag{B.32}$$

with the boundary conditions $P_{a1} = 0$ and $P_{f1} = P/\eta$ at $x = 0$ (Figure B.4) it follows that

$$B = -\frac{(\beta_1 + \beta_2)}{\eta Q_1} P \quad ; \quad D = \left(\frac{1}{\eta} - \frac{\alpha_2}{Q_2} \right) P \quad (B.33)$$

The boundary condition at $x=L$ (Figure B.4) is given as

$$P_{a1} = \frac{F_{a1}}{F} P \quad ; \quad P_{f1} = \frac{F_{f1}}{F} P \quad (B.34)$$

Substitution yields

$$A = \frac{\frac{F_{a1}}{F} - \frac{\beta_1 + \beta_2}{\eta Q_1} + \frac{\beta_1 + \beta_2}{\eta Q_1} \cosh \sqrt{Q_1} L}{\sinh \sqrt{Q_1} L} P$$

$$C = \frac{\frac{F_{f1}}{F} - \frac{\alpha_2}{Q_2} - \left(\frac{1}{\eta} - \frac{\alpha_2}{Q_2} \right) \cosh \sqrt{Q_2} L}{\sinh \sqrt{Q_2} L} P \quad (B.35)$$

Thus equation (B.31) can be written as

$$P_{a1} = \left[\left(\frac{\eta Q_1}{\beta_1 + \beta_2} \frac{F_{a1}}{F} - 1 + \cosh \sqrt{Q_1} L \right) \frac{\sinh \sqrt{Q_1} x}{\sinh \sqrt{Q_1} L} - \cosh \sqrt{Q_1} x + 1 \right] \frac{(\beta_1 + \beta_2)}{\eta Q_1} P \quad (B.36)$$

and

$$P_{f1} = \left[\left(\frac{F_{f1}}{F} - \frac{\alpha_2}{Q_2} - \left(\frac{1}{\eta} - \frac{\alpha_2}{Q_2} \right) \cosh \sqrt{Q_2} L \right) \frac{\sinh \sqrt{Q_2} x}{\sinh \sqrt{Q_2} L} + \left(\frac{1}{\eta} - \frac{\alpha_2}{Q_2} \right) \cosh \sqrt{Q_2} x + \frac{\alpha_2}{Q_2} \right] P \quad (B.37)$$

These equations satisfy the expression in equation (B.1) and (B.2). From equation (B.18) P_{f2} can be derived. The corresponding shear stress at the interface is thus

$$\tau_{a1} = - \left[\left(\frac{\eta Q_1}{\beta_1 + \beta_2} \frac{F_{a1}}{F} - 1 + \cosh \sqrt{Q_1} L \right) \frac{\cosh \sqrt{Q_1} x}{\sinh \sqrt{Q_1} L} - \sinh \sqrt{Q_1} x \right] \frac{(\beta_1 + \beta_2)}{\eta \sqrt{Q_1}} P \quad (B.38)$$

Substitution of equations (B.28), (B.30) and (B.32) into equation (B.38) and using the relations given in (B.15) results in

$$\tau_{al} = -S_{al} t_{al} \sqrt{\left(\frac{G_{f1}}{t_{f1}} + \frac{G_{f2}}{t_{f2}}\right) \left(\frac{1}{2F_{al}} + \frac{1}{F_{f1} + F_{f2}}\right)} e^{-x \sqrt{\left(\frac{G_{f1}}{t_{f1}} + \frac{G_{f2}}{t_{f2}}\right) \left(\frac{1}{2F_{al}} + \frac{1}{F_{f1} + F_{f2}}\right)}} \quad (B.39)$$

In the above-presented derivation, the thicknesses t_{f1} and t_{f2} are presented as input parameters. However, since they have no physical meaning, they should follow from the derivation itself. Combining equations (B.17) and (B.19) both thicknesses can be obtained using an iterative approach. The calculated thicknesses are given with the corresponding Young's moduli and shear moduli in Table B.1.

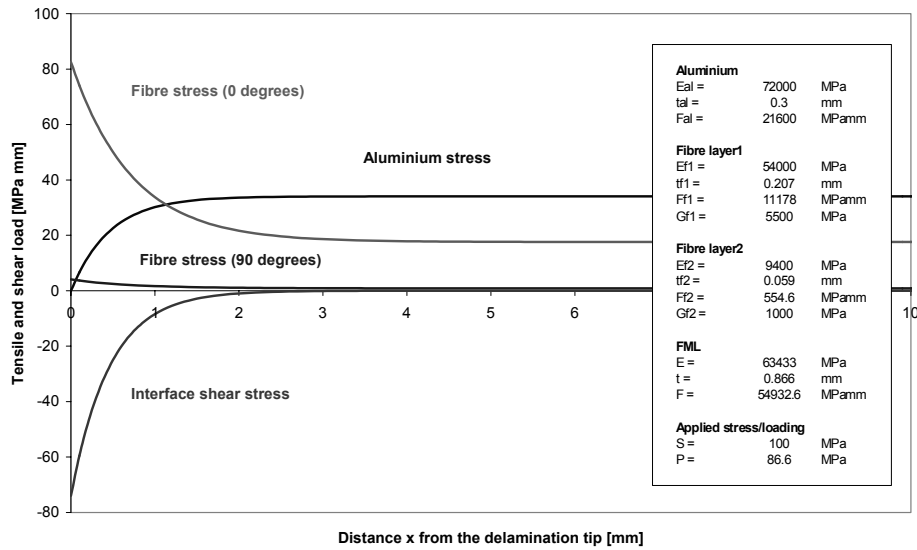


Figure B.6 Illustration of the tensile and shear stresses as function of the distance to the delamination tip, see Figure B.4.

Table B.1 Shear modulus values for S2-Glass/FM94 prepreg

	E [MPa]	G [MPa]	t [mm]
0° Fibres	54000	5500	0.207
90° Fibres	9400	1000	0.059

B.3 Prepreg shear deformation of uni-directional fibre layers for small delamination lengths

The prepreg shear deformation is the result of the cyclic shear stresses at the metal-fibre interface ahead of the delamination tip. The maximum deformation is determined at the delamination tip. However, this shear deformation in thickness direction build-up ahead of the delamination tip can only occur if it is compensated in thickness direction in the delaminated area. The relation between the maximum shear deformation and the delamination length for uni-directional fibre layers is determined in this section.

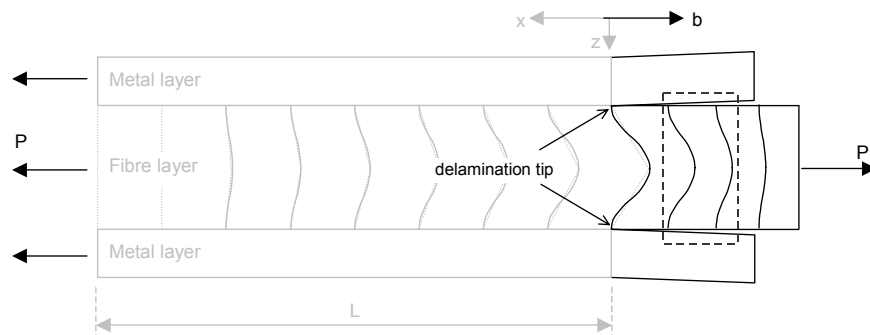


Figure B.7 Deformation of the uni-directional prepreg under tensile loading in the fibres and shear loading at the metal/fibre interface in the delaminated area.

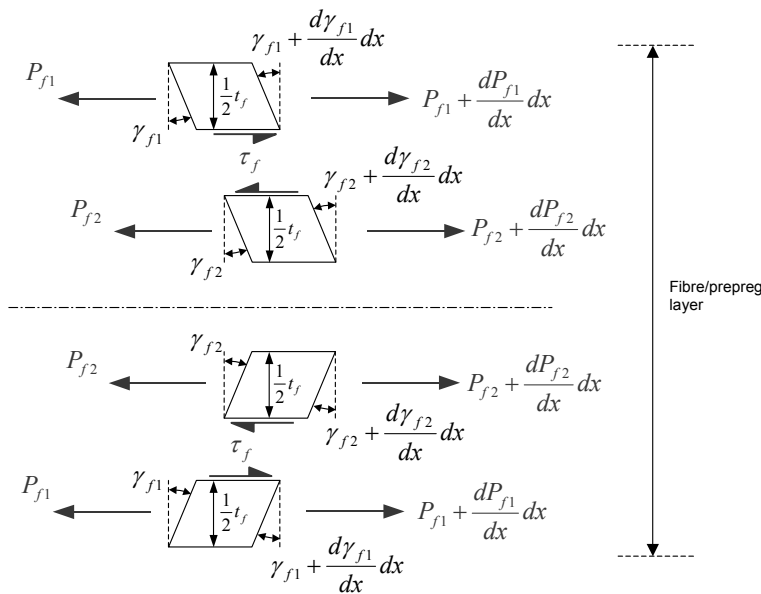


Figure B.8 Breakdown of elements in thickness direction of the deformed uni-directional prepreg in the delaminated area

The total prepreg thickness is equal to the thickness of two uni-directional prepreg layers. For the geometry depicted in Figure B.8 it follows

$$t_{f1} + t_{f2} = 2t_f \quad (B.40)$$

Equilibrium in element 1 and 2 yields

$$\frac{dP_{f1}}{dx} = -\tau_f = -\frac{dP_{f2}}{dx} \quad (B.41)$$

Equilibrium over the total thickness yields

$$P_{f1} + P_{f2} = P_f \quad (B.42)$$

For the shear deformation it follows

$$\frac{d\gamma_{f1}}{dx} t_{f1} = \varepsilon_2 - \varepsilon_1 \quad ; \quad \frac{d\gamma_{f2}}{dx} t_{f2} = \varepsilon_3 - \varepsilon_2 \quad (B.43)$$

where ε_1 is the strain at the prepreg edge, ε_2 is the strain at the interface of element 1 and 2 and ε_3 is the strain at centre of the prepreg layer. If the strain of each element is assumed to be the average of the strains at both sides, it follows from the Hooke's law

$$\frac{2P_{f1}}{t_f E_f} = \varepsilon_1 + \varepsilon_2 \quad ; \quad \frac{2P_{f2}}{t_f E_f} = \varepsilon_2 + \varepsilon_3 \quad ; \quad \gamma_{f1} = \gamma_{f2} = \frac{\tau_f}{G_f} \quad (B.44)$$

Combining equations (B.43) and (B.44) gives

$$\frac{2}{t_f E_f} (P_{f1} - P_{f2}) = \varepsilon_1 - \varepsilon_3 = -\frac{d\gamma_{f1}}{dx} t_{f1} - \frac{d\gamma_{f2}}{dx} t_{f2} = -2 \frac{d\tau_f}{dx} \frac{t_f}{G_f} \quad (B.45)$$

which results with equation (B.41) in the following set of differential equations

$$\begin{aligned} \frac{d^2 P_{f1}}{dx^2} &= 2\alpha P_{f1} - \alpha P_f \\ \frac{d^2 P_{f2}}{dx^2} &= 2\alpha P_{f2} - \alpha P_f \end{aligned} \quad (B.46)$$

where

$$\alpha_{UD} = \frac{G_f}{t_f^2 E_f} \quad (B.47)$$

which has the general solution

$$\begin{aligned} P_{f1} &= A \sinh \sqrt{2\alpha_{UD}} x + B \cosh \sqrt{2\alpha_{UD}} x + \frac{P_f}{2} \\ P_{f2} &= C \sinh \sqrt{2\alpha_{UD}} x + D \cosh \sqrt{2\alpha_{UD}} x + \frac{P_f}{2} \end{aligned} \quad (B.48)$$

At the distance of the delamination length b away from the delamination tip both P_{f1} and P_{f2} are identical. With equation (B.42) one gets

$$\begin{aligned} B &= -A \tanh \sqrt{2\alpha_{UD}} b \\ D &= -C \tanh \sqrt{2\alpha_{UD}} b \end{aligned} \quad (B.49)$$

Since relation (B.42) yields for any value of x , it follows that $A = -C$. The general solution thus becomes

$$\begin{aligned} P_{f1} &= A \sinh \sqrt{2\alpha_{UD}} x - A \tanh \sqrt{2\alpha_{UD}} b \cosh \sqrt{2\alpha_{UD}} x + \frac{P_f}{2} \\ P_{f2} &= -A \sinh \sqrt{2\alpha_{UD}} x + A \tanh \sqrt{2\alpha_{UD}} b \cosh \sqrt{2\alpha_{UD}} x + \frac{P_f}{2} \end{aligned} \quad (B.50)$$

with the corresponding shear stress between element 1 and 2

$$\tau_f = -A \sqrt{2\alpha_{UD}} \left(\cosh \sqrt{2\alpha_{UD}} x - \tanh \sqrt{2\alpha_{UD}} b \sinh \sqrt{2\alpha_{UD}} x \right) \quad (B.51)$$

The shear stress should be equal to zero at the delamination length away from the delamination tip, as both P_{f1} and P_{f2} are equal at that location as well. This means that the minimum value of the delamination length can be determined using

$$\left(\cosh \sqrt{2\alpha_{UD}} b - \tanh \sqrt{2\alpha_{UD}} b \sinh \sqrt{2\alpha_{UD}} b \right) = 0 \quad (B.52)$$

which is graphically illustrated for the case of unidirectional fibres discussed in section A.1 in Figure B.9. Due to the lower shear modulus, the minimum delamination length to match criterion (B.52) is much lower for the fibres perpendicular to the loading direction.

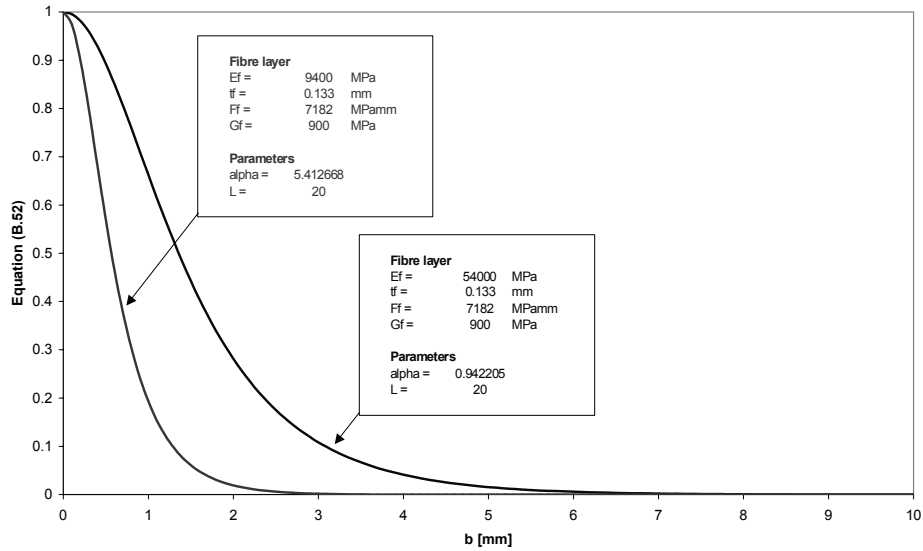


Figure B.9 Equation (B.52) as function of the delamination length b for prepreg with fibres in loading direction and prepreg with fibres perpendicular to the loading direction

As the COD is proportional to the shear stress, this means that the expression for the COD should contain a correction factor defined as

$$C(b) = 1 - \left(\cosh \sqrt{\alpha_{UD}} b - \tanh \sqrt{\alpha_{UD}} b \sinh \sqrt{\alpha_{UD}} b \right) \quad (B.53)$$

B.4 Prepreg shear deformation of cross-ply fibre layers for small delamination lengths

The relation between the maximum shear deformation and the delamination length for cross-ply fibre layers is determined in this section. The total prepreg thickness is equal to the thickness of two uni-directional prepreg layers. For the geometry depicted in Figure B.11 it follows

$$t_{f1} + t_{f2} = 2t_f \quad (B.54)$$

Equilibrium in element 1 and 2 yields

$$\frac{dP_{f1}}{dx} = -\tau_f = -\frac{dP_{f2}}{dx} \quad (B.55)$$

B Prepreg shear deformation

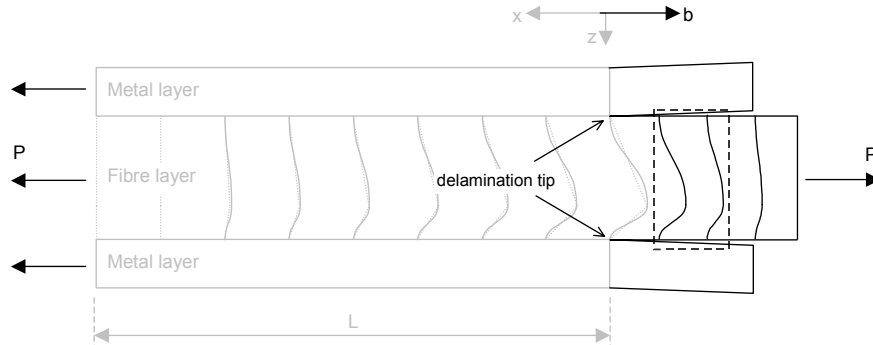


Figure B.10 Deformation of the cross-ply prepreg under tensile loading in the fibres and shear loading at the metal/fibre interface.

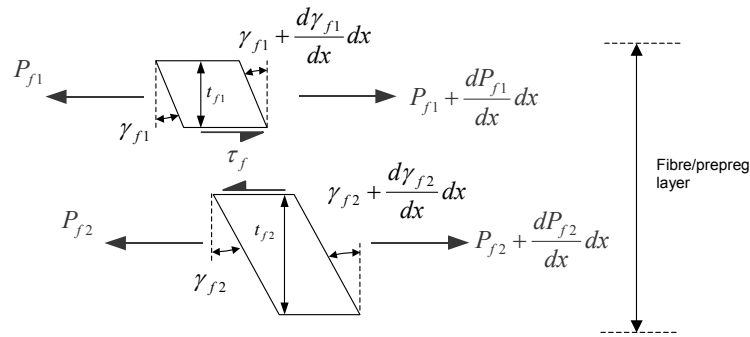


Figure B.11 Breakdown of elements in thickness direction of the deformed cross-ply prepreg in the delaminated area

Equilibrium over the total thickness implies

$$P_{f1} + P_{f2} = P_f \quad (B.56)$$

For the shear deformation it follows

$$\frac{d\gamma_{f1}}{dx} t_{f1} = \varepsilon_2 - \varepsilon_1 \quad ; \quad \frac{d\gamma_{f2}}{dx} t_{f2} = \varepsilon_3 - \varepsilon_2 \quad (B.57)$$

where ε_1 is the strain at the prepreg edge, ε_2 is the strain at the interface of element 1 and 2 and ε_3 is the strain at centre of the prepreg layer. If the strain of each element is assumed to be the average of the strains at both sides, it follows from the Hooke's law

$$\frac{2P_{f1}}{t_{f1}E_{f1}} = \varepsilon_1 + \varepsilon_2 \quad ; \quad \frac{2P_{f2}}{t_{f2}E_{f2}} = \varepsilon_2 + \varepsilon_3 \quad (B.58)$$

and

$$\gamma_{f1} = \frac{\tau_f}{G_{f1}} \quad ; \quad \gamma_{f2} = \frac{\tau_f}{G_{f2}} \quad (B.59)$$

Combining equations (B.57) and (B.58) gives

$$\frac{2P_{f1}}{t_{f1}E_{f1}} - \frac{2P_{f2}}{t_{f2}E_{f2}} = \varepsilon_1 - \varepsilon_3 = -\frac{d\gamma_{f1}}{dx}t_{f1} - \frac{d\gamma_{f2}}{dx}t_{f2} \quad (B.60)$$

which results with equation (B.55) in the following set of differential equations

$$\begin{aligned} \frac{d^2P_{f1}}{dx^2} &= 2\alpha P_{f1} - \beta_1 P_f \\ \frac{d^2P_{f2}}{dx^2} &= 2\alpha P_{f2} - \beta_2 P_f \end{aligned} \quad (B.61)$$

where

$$\alpha_{CP} = \frac{\frac{1}{t_{f1}E_{f1}} + \frac{1}{t_{f2}E_{f2}}}{\frac{t_{f1}}{G_{f1}} + \frac{t_{f2}}{G_{f2}}} \quad (B.62)$$

and

$$\beta_1 = \frac{\frac{1}{t_{f2}E_{f2}}}{\frac{t_{f1}}{G_{f1}} + \frac{t_{f2}}{G_{f2}}} \quad ; \quad \beta_2 = \frac{\frac{1}{t_{f1}E_{f1}}}{\frac{t_{f1}}{G_{f1}} + \frac{t_{f2}}{G_{f2}}} \quad (B.63)$$

which has the general solution

B Prepreg shear deformation

$$\begin{aligned}
 P_{f1} &= A \sinh \sqrt{2\alpha_{CP}} x + B \cosh \sqrt{2\alpha_{CP}} x + \frac{\beta_1}{2\alpha_{CP}} P_f \\
 P_{f2} &= C \sinh \sqrt{2\alpha_{CP}} x + D \cosh \sqrt{2\alpha_{CP}} x + \frac{\beta_2}{2\alpha_{CP}} P_f
 \end{aligned}
 \tag{B.64}$$

At the distance of the delamination length b away from the delamination tip both P_{f1} and P_{f2} are defined with

$$P_{f1} = \frac{F_{f1}}{F} P_f \quad ; \quad P_{f2} = \frac{F_{f2}}{F} P_f
 \tag{B.65}$$

With equation (B.56) one gets

$$\begin{aligned}
 B &= -A \tanh \sqrt{2\alpha_{CP}} b \\
 D &= -C \tanh \sqrt{2\alpha_{CP}} b
 \end{aligned}
 \tag{B.66}$$

Since relation (B.56) yields for any value of x , it follows that $A = -C$. The general solution thus becomes

$$\begin{aligned}
 P_{f1} &= A \sinh \sqrt{2\alpha_{CP}} x - A \tanh \sqrt{2\alpha_{CP}} b \cosh \sqrt{2\alpha_{CP}} x + \frac{F_{f1}}{F} P_f \\
 P_{f2} &= -A \sinh \sqrt{2\alpha_{CP}} x + A \tanh \sqrt{2\alpha_{CP}} b \cosh \sqrt{2\alpha_{CP}} x + \frac{F_{f2}}{F} P_f
 \end{aligned}
 \tag{B.67}$$

with the corresponding shear stress between element 1 and 2

$$\tau_f = -A\sqrt{\alpha} \left(\cosh \sqrt{2\alpha_{CP}} x - \tanh \sqrt{2\alpha_{CP}} b \sinh \sqrt{2\alpha_{CP}} x \right)
 \tag{B.68}$$

The shear stress should be equal to zero at the delamination length away from the delamination tip, as both P_{f1} and P_{f2} are equal at that location as well. This means that the minimum value of the delamination length can be determined using

$$\left(\cosh \sqrt{2\alpha_{CP}} b - \tanh \sqrt{2\alpha_{CP}} b \sinh \sqrt{2\alpha_{CP}} b \right) = 0
 \tag{B.69}$$

which is graphically illustrated for the case of unidirectional fibres discussed in section A.1 in Figure B.9. Due to the lower shear modulus, the minimum delamination length to match criterion (B.69) is much lower for the fibres perpendicular to the loading direction.

Fatigue crack propagation and delamination growth in Glare

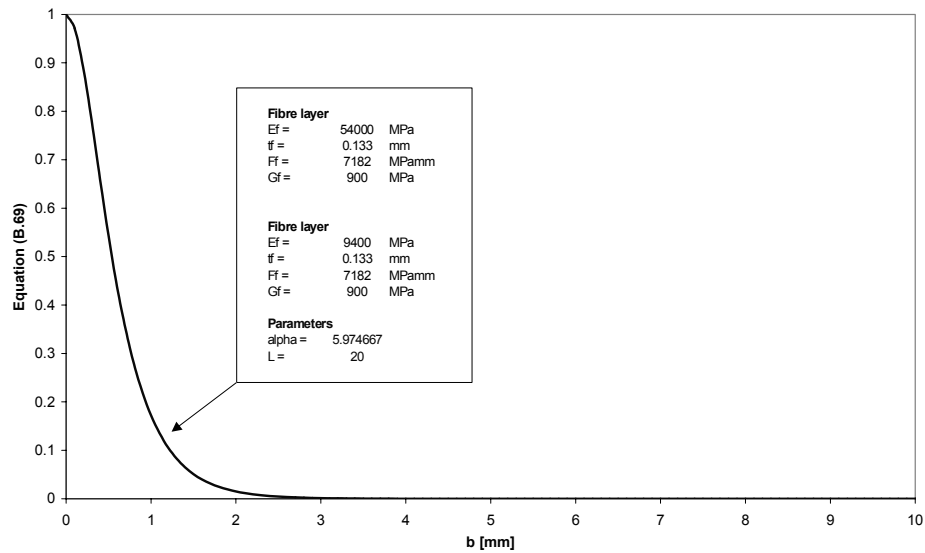


Figure B.12 Equation (B.69) as function of the delamination length b for prepreg with fibres in loading direction and prepreg with fibres perpendicular to the loading direction

As the COD is proportional to the shear stress, this means that the expression for the COD should contain a correction factor defined as

$$C(b) = 1 - \left(\cosh \sqrt{2\alpha_{CP}} b - \tanh \sqrt{2\alpha_{CP}} b \sinh \sqrt{2\alpha_{CP}} b \right) \quad (B.70)$$

References

- [1] **Verbruggen, M.L.C.E.**, *Aramid Reinforced Aluminium Laminates: ARALL, Adhesion Problems and Environmental Effects*, Vol. A, Report LR-503, Faculty of Aerospace Engineering, Delft University of Technology, 1986
- [2] **Marissen, R.**, *Fatigue Crack Growth in ARALL, A hybrid Aluminium-Aramid Composite Material, crack growth mechanisms and quantitative predictions of the crack growth rate*, PhD Thesis, Delft University of Technology, 1988.

C

Numerical delamination growth calculation

Abstract – The numerical approach to calculate the delamination extension in the calculation method is discussed in this appendix. The sensitivity with respect to the followed numerical procedure and the method to make the method more robust are presented here.



C.1 Introduction

The method presented in this thesis is based on the calculation of the bridging stress over the fatigue crack length in Glare. The delamination extension, which occurs as result of this bridging stress after a given number of load cycles, can then be calculated with a Paris law as function of the Energy Release Rate [1].

Due to the necessary inverse operation on the integral over the bridging stress, the solution can only be calculated numerically by dividing the total crack length in N bar elements.

This numerical approach however, has some limitations with respect to the calculation of the problem. For instance, the minimum crack extension that can be calculated must be equal to or greater then the width of a single bar element, otherwise the numerical representation of the fatigue crack will remain the same, which is equal to zero crack extension.

Each calculated crack extension implies an increase of the calculated matrices in the next calculation loop. The large amount of calculation loops until a large crack length is reached therefore imply very large matrices towards the end of the calculation.

This makes calculations very time consuming and thus requires to represent the fatigue crack by a number of bar elements as small as possible.

C.2 Matrix size considerations

There are in fact two ways to calculate the crack extension and corresponding delamination extension

- Increasing matrix sizes with increasing crack length
- Constant matrix size

The advantage of increasing the matrix size with increasing crack length is, that each element i in the matrix represent a specific location x_i along the crack length, which does not vary during the crack growth calculation. The disadvantage, however, is the increasing calculation time necessary to calculate the increasing matrix sizes.

The advantage of the constant matrix size is the limited calculation time, which is determined by the initial matrix size, thus the number of bar elements. The disadvantage is that for each calculation loop, the elements i in the matrix represent another location x_i along the crack length. This means that after each calculated crack extension the calculated delamination shape for given locations, must be recalculated to the new locations corresponding to the matrices for the next calculation loop. As the calculated delamination shape in one loop is only calculated for the specific locations x_i corresponding to the bar elements i , this means that an interpolation technique must be utilized to determine the shape for the locations in the next calculation loop.

To avoid any loss of accuracy during application of such interpolation approximations, the current method utilizes the increasing matrix size method, instead of the constant matrix size.

However, it should be noted that the physical prediction method itself should be independent of the followed numerical approach.

C.3 Delamination extension calculation

For a given crack and delamination geometry in Glare, the corresponding bridging stress can be calculated with the presented method. Using the Paris law for delamination (equation 6.5), the delamination extension can be calculated for a given number of cycles. Because the crack in the aluminium layers propagates perpendicular to the delamination direction, an assumption with respect to the delamination shape in the crack extension must be made.

The assumption consists of an interpolation function between the calculated extended delamination at the old crack tip and zero delamination at the new crack tip. The interpolation relation can be simply linear, but can also be a parabolic or another polynomial function. In the followed approach, the relation is taken identical to the assumed initial delamination shape.

The approach of delamination tip determination after each crack extension is illustrated in Figure C.1.

C Numerical delamination growth calculation

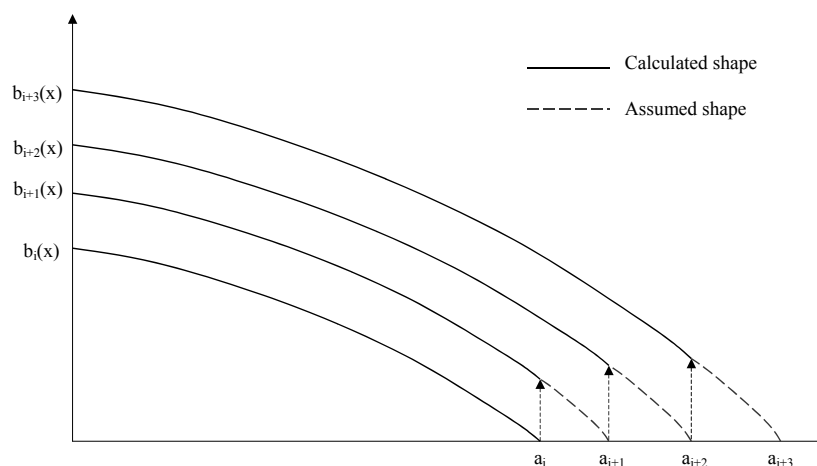


Figure C.1 Delamination tip assumption after each crack extension

The delamination shape growth is determined with a Paris law for each location x_i along the crack length corresponding to the i -th bar element.

Marissen stated that the bridging stress should be constant along the crack length [2] with the argumentation of the self-balancing behaviour between delamination growth and bridging stress. Although this self-balancing behaviour explains why the delamination propagates in a controlled manner, it cannot be used as argument for the constant bridging stress.

In reality, there is interaction between the delamination behaviour at location x_i (i -th bar element) and the surrounding area. If the delamination will extend significantly at this location, it means that the neighbourhood will keep up with this growth.

However, in the numerical approach the behaviour at location x_i is not related to the locations x_{i-1} and x_{i+1} , which are the adjacent bar elements. For moderate extensions, this is a justified approach, however, large localised delamination extensions are not limited by the surrounding area, which is the case in reality.

This means that in the numerical approach an artificial coupling should be introduced between location x_i and its neighbourhood, or extreme delamination extensions should be suppressed. Since a coupling between the locations is rather complex to incorporate in the numerical method, the solution is sought in the suppression of extreme localised delamination extensions using a delamination shape approximation. The approach applied in the method is discussed in the next section.

Fatigue crack propagation and delamination growth in Glare

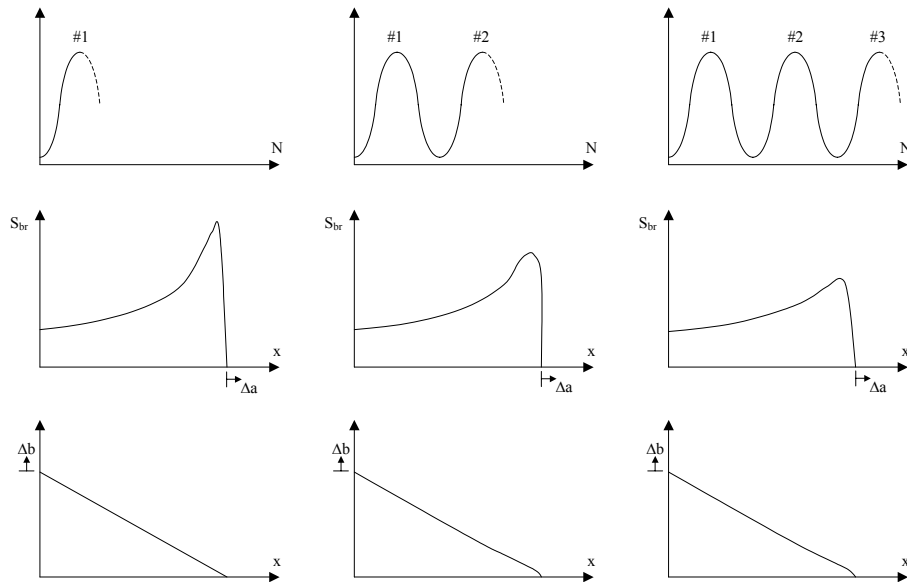


Figure C.2 Crack and delamination extension occurring during constant amplitude tests in Glare; the effect of a peak stress is damped in the following load cycles.

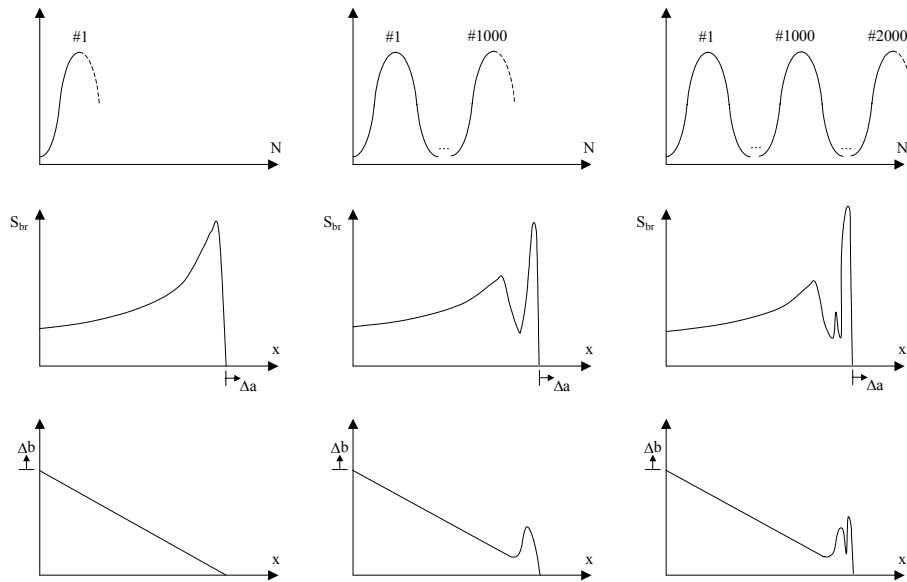


Figure C.3 Crack and delamination extension calculated for constant amplitude fatigue in Glare; the effect of a peak stress is superimposed in the following number of load cycles.

C.4 Delamination Tip Approximation

During the numerical evaluations, it was found that the extreme localised delamination extensions only occur very close to the crack tip, due to localised peak stresses as results of small delamination lengths. The suppression method chosen for the current method is to extent the parabolic delamination shape in the extended crack length towards a point behind the crack tip. This point is selected such that the parabolic delamination shape approximation covers the length near the crack tip that is vulnerable to extreme delamination extensions.

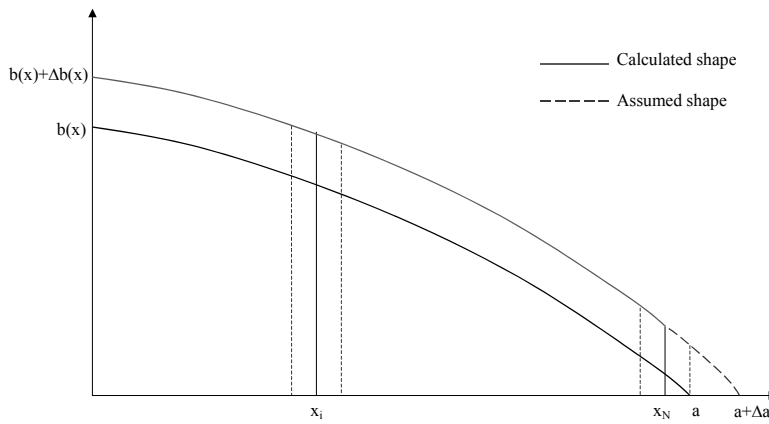


Figure C.4 Determination of the extended delamination shape, with the delamination tip assumption based on the calculated $b(x_N)$ for a crack divided into N bar elements

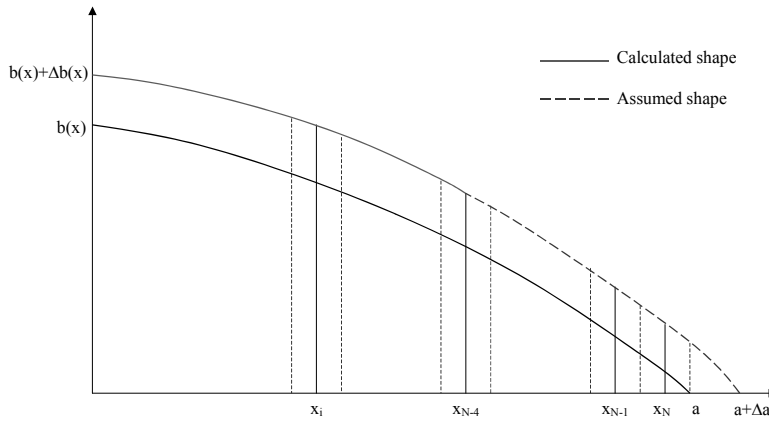


Figure C.5 Determination of the extended delamination shape, with the parabolic delamination tip assumption based on the calculated $b(x_{N-4})$ for a crack divided into N bar elements

In the numerical model the location behind the crack tip is taken at the fourth bar element behind the crack tip, corresponding to location x_{i-4} . This means that the calculated delamination shape extensions for the four locations adjacent to the crack tip are replaced by the delamination shape approximation. This approach is visualised in Figure C.4 and Figure C.5. Instead of defining the delamination shape in the extended crack length based on the calculated delamination shape at the crack tip, as illustrated in Figure C.4, the delamination length four bar elements behind the crack tip is taken as basis for the delamination tip assumption, see Figure C.5.

References

- [1] **Alderliesten, R.C.**, *Energy Release Rate approach for delamination in a fatigue crack configuration in Glare*, Submitted to Engineering Fracture Mechanics, 2004
- [2] **Marissen, R.**, *Fatigue Crack Growth in ARALL, A hybrid Aluminium-Aramid Composite Material, crack growth mechanisms and quantitative predictions of the crack growth rate*, PhD Thesis, Delft University of Technology, 1988.

D

Model validation

Abstract – This appendix presents a selection of the crack growth rates versus the crack length graphs, in which the predictions from the model are compared with the measurements from experiments.



D.1 Introduction

The crack growth prediction model developed in chapter 6 is validated with a large amount of test data from experimental test programmes [1-4]. The predicted crack growth behaviour is compared with the experimental crack growth behaviour. Because presenting of all the validation graphs goes beyond this thesis, a selection has been made, which is presented in this appendix.

A few figures presenting the validation of the method with respect to crack growth, crack opening contour and the delamination shape, have already been given in chapter 6. The figures presented in this appendix consist of crack growth rate plotted versus the crack length.

An overview of the total amount of fatigue tests that have been used to validate the method is given in Table D.1 to Table D.4. In these tables a reference is added to the figures in this thesis

The validation figures presented in Figure D.1 to Figure D.10 have been selected to give a complete overview of all the material-, geometrical- and loading parameters experimentally investigated. The effect of these parameters, which have been discussed in chapter 5, is accurately predicted by the developer crack growth model. Note that these figures form a good representation of the good correlation found between the model and all the experimental data.

Fatigue crack propagation and delamination growth in Glare

Table D.1 Survey of test conditions investigated in [1]

Glare type	Loading direction	Dimensions (mm)		Fatigue load		Results in figure:	
		W	2 a _s	S _{max} (MPa)	R		
3-3/2-0.3	L-T	140	5	100	0.05	D.3	
3-4/3-0.4			5	120			D.3
				100	0.05	0.5	D.1
			120	0.05	0.5	5.8, D.1	
			120	0.05	0.5	D.1	
3-4/3-0.5			5	100	0.05	0.5	D.2
					0.05	0.5	D.2
			120	0.05	0.5	D.2	
				0.05	0.5	D.2	
3-4/3-0.5			5	100	0.05	0.5	D.4
					0.05	0.5	D.4
			120	0.05	0.5		
	0.05	0.5					
3-6/5-0.4	5	100	0.05	0.5	D.5		
120			0.05	0.5	D.5		
3-8/7-0.4	5	100	0.05	0.5	D.6		
120			0.05	0.5	D.6		
3-8/7-0.5	5	100	0.05	0.5			
120			0.05	0.5			
4B-3/2-0.3	5	100	0.05	0.5			
120			0.05	0.5			
4B-3/2-0.3	T-L	5	100	0.05			
4B-4/3-0.4	L-T	5	100	0.05	0.5		
				0.05	0.5	5.8	
			120	0.05	0.5		
				0.05	0.5		
30	100	0.05	0.5				
		0.05	0.5				
120	100	0.05	0.5				
		0.05	0.5				

D Model validation

Glare type	Loading direction	Dimensions (mm)		Fatigue load		Results in figure:
		W	2 a _s	S _{max} (MPa)	R	
4B-4/3-0.4	T-L	140	5	100	0.05	5.8
				120	0.05	
			30	100	0.05	
				120	0.05	
4B-4/3-0.5	L-T		5	100	0.05	D.7
				120	0.05	D.7
			30	100	0.05	D.8
				120	0.05	D.8
4B-4/3-0.5	T-L		5	100	0.05	D.9
				120	0.05	D.9
			30	100	0.05	D.10
				120	0.05	D.10
4B-6/5-0.4	T-L		5	100	0.05	
120						
4B-8/7-0.4			5	100	0.05	
				120		
4B-8/7-0.4	T-L		5	100	0.05	
4B-8/7-0.5	L-T		5	100	0.05	
				120		

Fatigue crack propagation and delamination growth in Glare

Table D.2 Survey of test conditions investigated in [2]

Glare type	Loading direction	Dimensions (mm)		Fatigue load		Results in figure:
		W	2 a _s	S _{max} (MPa)	R	
3-4/3-0.4	L-T	100	3	80 100 120	0.05	5.9
			10 20	100	0.05	
3-4/3-0.5	L-T	100	3	80 100 120	0.05	5.11 5.10, 6.13, 6.14, 6.17
3-6/5-0.4			10 20	100	0.05	5.9, 5.11 5.11
3-6/5-0.5	L-T	100	3	80 100 120	0.05	5.10
3-8/7-0.4			10 20	100	0.05	5.9
3-8/7-0.5	L-T	100	3	80 100 120	0.05	5.9
			10 20	100	0.05	

Table D.3 Survey of test conditions investigated in [3]

Glare type	Loading direction	Dimensions (mm)		Fatigue load		Results in figure:
		W	2 a _s	S _{max} (MPa)	R	
3-4/3-0.5	L-T	500	75	100 120	0.05	6.25, 6.28 6.25-6.27, 6.29

Table D.4 Survey of test conditions investigated in [4]

Glare type	Loading direction	Dimensions (mm)		Fatigue load		Results in figure:
		W	2 a _s	S _{max} (MPa)	R	
3-4/3-0.4	L-T	160	5	100	0.05	5.6
4B-4/3-0.4	T-L		5			

D Model validation

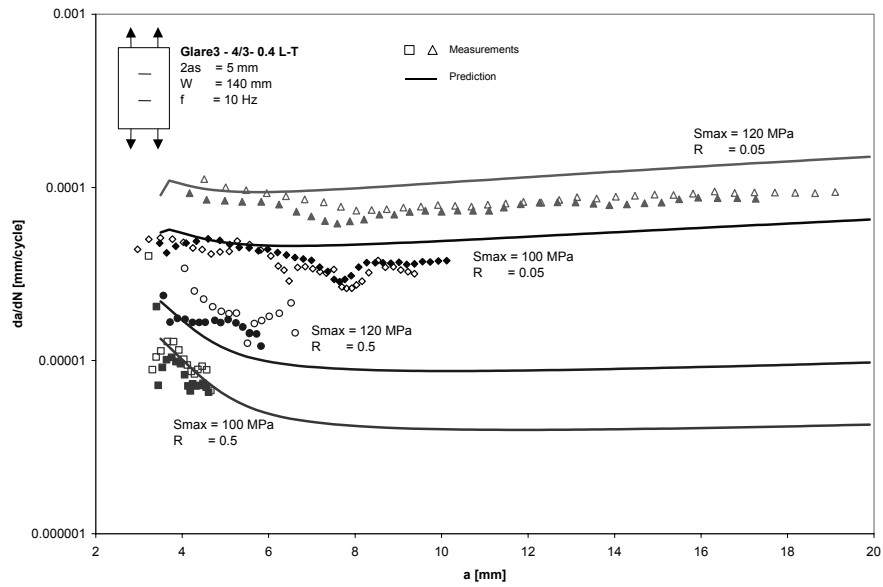


Figure D.1 Comparison between the predicted and measured crack growth rate of Glare3-4/3-0.4 in L-T direction with $W=140$ mm, $a_s=2.5$ mm for four different loading cases

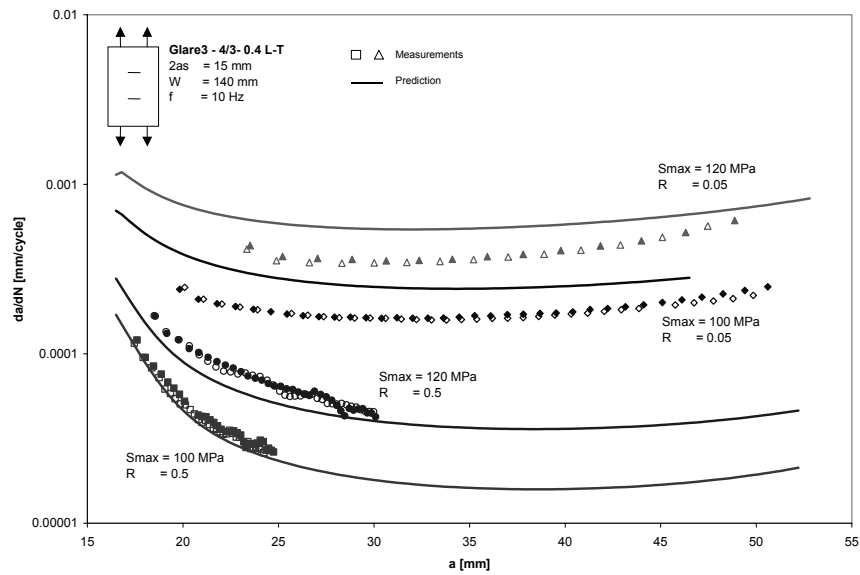


Figure D.2 Comparison between the predicted and measured crack growth rate of Glare3-4/3-0.4 in L-T direction with $W=140$ mm, $a_s=15$ mm for four different loading cases

Fatigue crack propagation and delamination growth in Glare

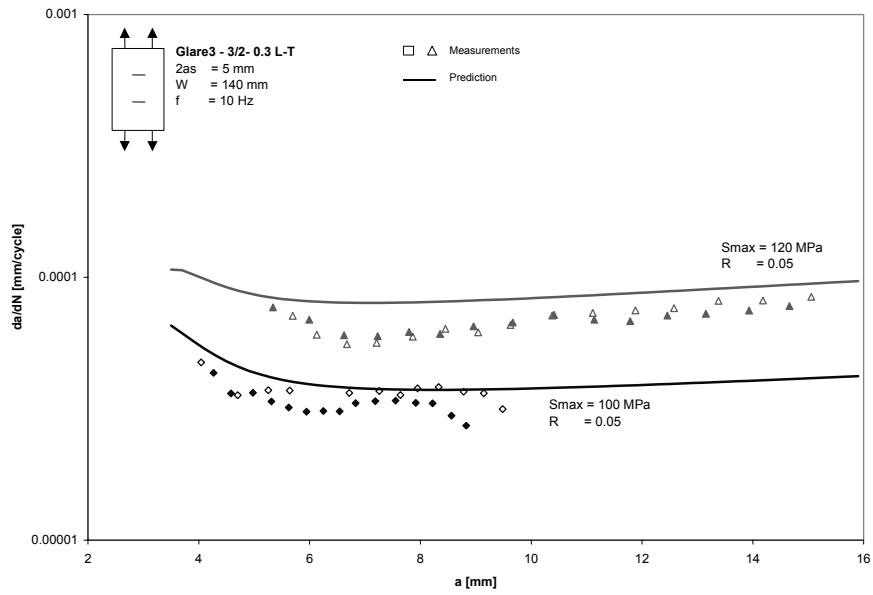


Figure D.3 Comparison between the predicted and measured crack growth rate of Glare3-3/2-0.3 in L-T direction with $W=140$ mm, $a_s=2.5$ mm for two different loading cases

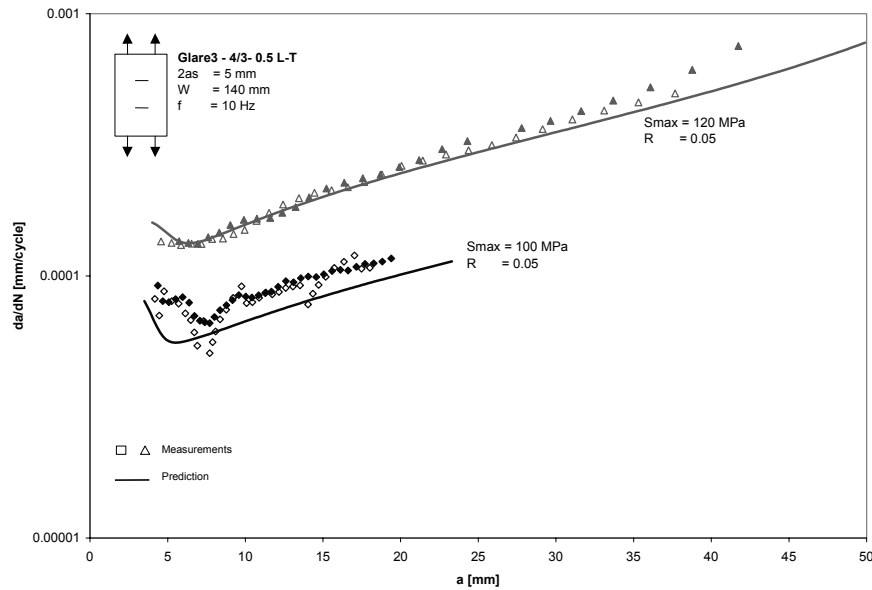


Figure D.4 Comparison between the predicted and measured crack growth rate of Glare3-4/3-0.5 in L-T direction with $W=140$ mm, $a_s=2.5$ mm for two different loading cases

D Model validation

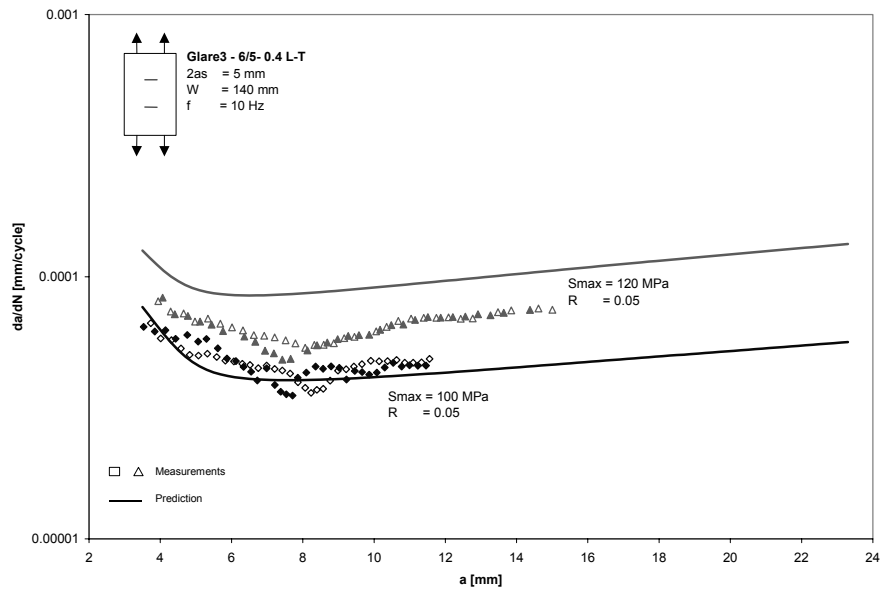


Figure D.5 Comparison between the predicted and measured crack growth rate of Glare3-6/5-0.4 in L-T direction with $W=140$ mm, $a_s=2.5$ mm for two different loading cases

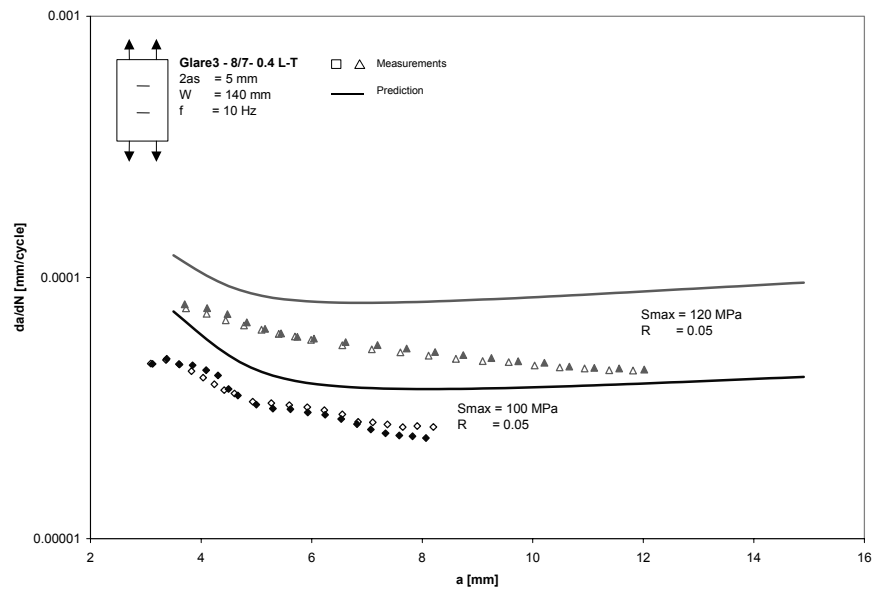


Figure D.6 Comparison between the predicted and measured crack growth rate of Glare3-8/7-0.4 in L-T direction with $W=140$ mm, $a_s=2.5$ mm for two different loading cases

Fatigue crack propagation and delamination growth in Glare

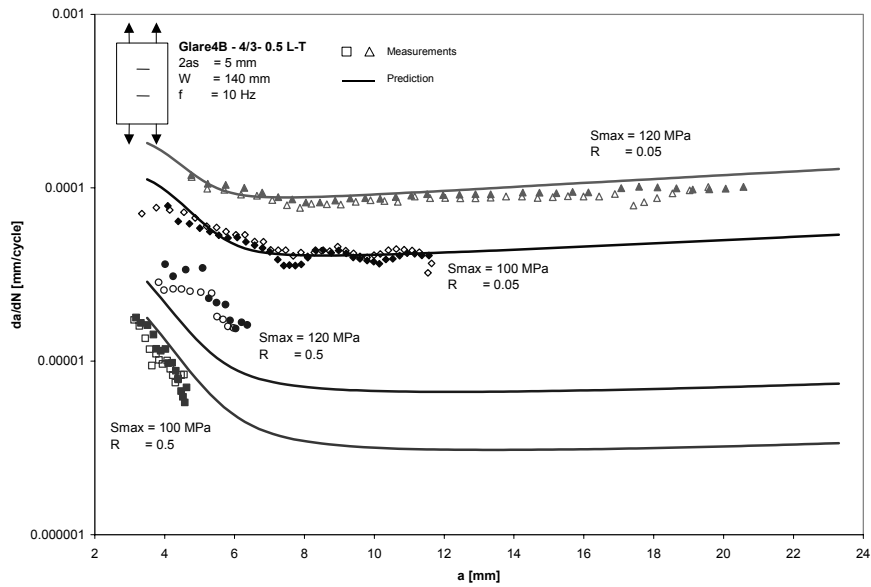


Figure D.7 Comparison between the predicted and measured crack growth rate of Glare4B-4/3-0.5 in L-T direction with $W=140$ mm, $a_s=2.5$ mm for four different loading cases

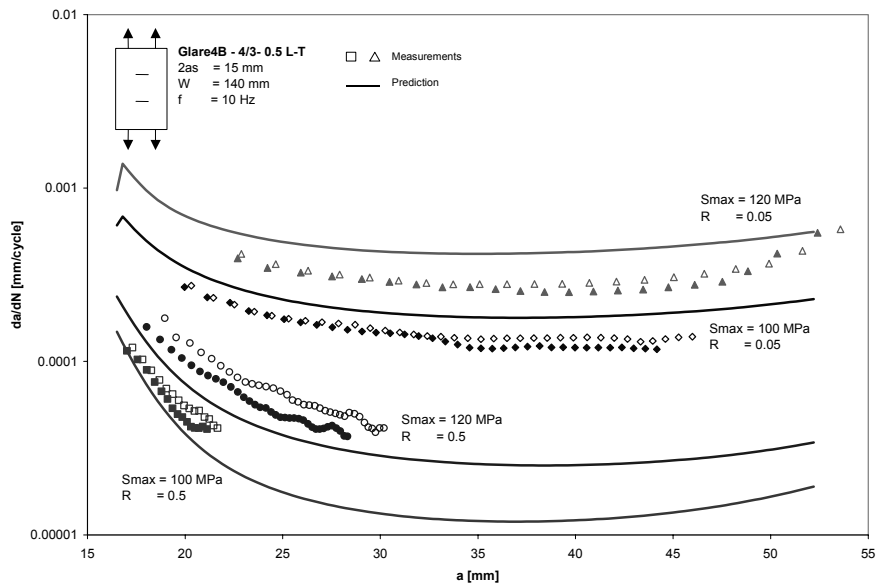


Figure D.8 Comparison between the predicted and measured crack growth rate of Glare4B-4/3-0.5 in L-T direction with $W=140$ mm, $a_s=15$ mm for four different loading cases

D Model validation

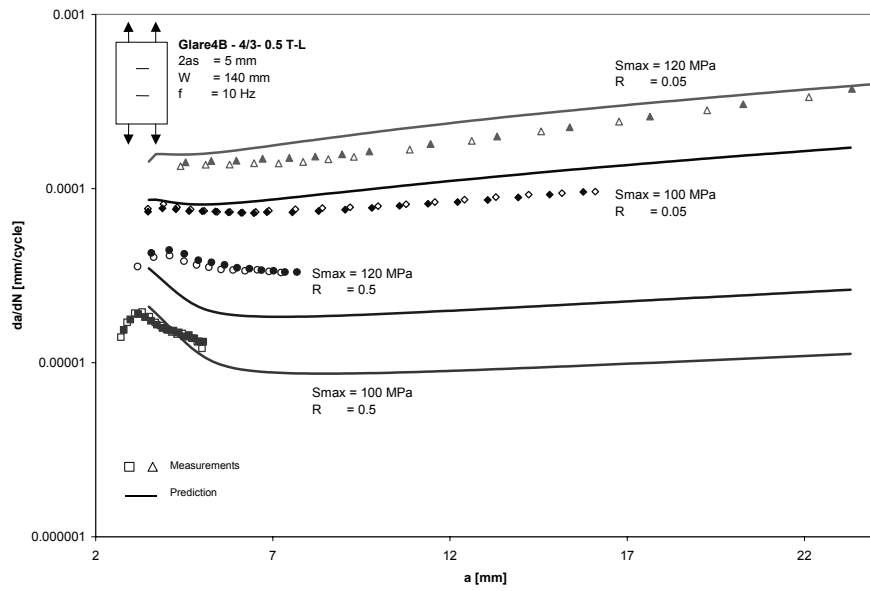


Figure D.9 Comparison between the predicted and measured crack growth rate of Glare4B-4/3-0.5 in T-L direction with $W=140$ mm, $a_s=2.5$ mm for four different loading cases

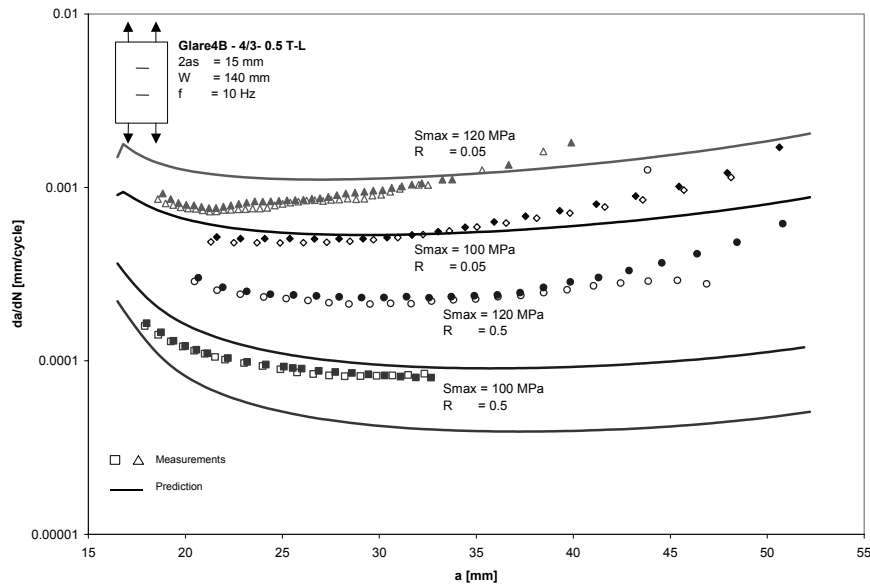


Figure D.10 Comparison between the predicted and measured crack growth rate of Glare4B-4/3-0.5 in T-L direction with $W=140$ mm, $a_s=15$ mm for four different loading cases

References

- [1] **Homan, J.J., Alderliesten, R.C.**, *Test data for Fatigue Crack Propagation in unstiffened GLARE – Through Cracks*, Report B2V-99-39, Delft University of Technology, 1999 (restricted).
- [2] **Alderliesten, R.C.**, *Development of an empirical fatigue crack growth prediction model for the Fibre Metal Laminate Glare*, Master Thesis, Delft University of Technology, 1999.
- [3] **Alderliesten, R.C.**, *The influence of large saw-cuts on the fatigue crack propagation behaviour of Glare*, Report B2V-02-13, Delft University of Technology, 2002 (restricted).
- [4] **Quinn, B.G.**, *Delamination of Glare*, Masters of Engineering Thesis, Queen's University of Belfast, 2004.

Samenvatting

“Vermoeiingsscheurgroei en delaminatiegroei in Glare”

René Alderliesten

Dit proefschrift presenteert het onderzoek naar het scheurgroei- en delaminatiegedrag van het Vezel-Metaal Laminaat Glare onder vermoeiingsbelastingen. Dit fenomeen is bestudeerd voor cyclische belastingen met een constante amplitude, die van belang zijn voor vermoeiingsbelasting van drukcabines van vliegtuigen. Zoals in het eerste hoofdstuk is gedefinieerd, is het doel van het onderzoek tweeledig: Ten eerste, het verkrijgen van een duidelijk begrip en een gedetailleerde karakterisering van de bezwijkmechanismen in Glare als gevolg van vermoeiingsbelastingen, en ten tweede, het verkrijgen van een nauwkeurig voorspellingsmodel voor de vermoeiingsscheurgroei in Glare, rekening houdend met de scheuroverbrugging van de vezels en de groei van delaminaties.

Het belangrijkste concept in dit proefschrift is, dat the spanningsintensiteit aan de scheurtip in the metaallagen van een Vezel-Metaal Laminaat de factor is die de scheuruitbreiding onder cyclische belasting bepaald. Dit betekent dat the spanningsintensiteitsfactor beschreven kan worden met Lineair Elastische Breuk-Mechanica, met inbegrip van de bijdrage van de vezellagen en de bij het scheurgroei horende delaminatiegedrag.

Dit onderzoek bedekt de theoretisch analyse van het scheurgroei fenomeen en een compleet aanvullend experimenteel programma om het nieuwe voorspellingsmodel te onderbouwen en te valideren. Het onderzoek is beperkt tot scheuren door de dikte van het laminaat met dezelfde scheurlengte lengte in alle metaallagen.

In het tweede hoofdstuk zijn de verschillende varianten en opbouw van Glare gedefinieerd, tezamen met een beschrijving van het productieproces en de procedures voor de kwaliteitscontrole. Een kwalitatieve beschrijving van het vermoeiingsscheurgroei fenomeen in Glare is gepresenteerd in hoofdstuk 3. De geïntroduceerde aspecten zijn de vermoeiingsscheurgroei in de aluminium lagen, bepaald door de spanningsintensiteit aan de scheurtip, en de delaminatie van de aluminium en vezellagen over de gehele vermoeiingsscheurlengte. De scheuropening wordt gelimiteerd door de overbruggende vezellagen, terwijl de spanning in deze vezellagen de delaminatiegroei bepalen. Hoofdstuk 4 bediscussieert de empirische en analytische scheurgroei voorspellingsmodellen gepresenteerd in de literatuur met hun tekortkomingen.

Het experimentele programma wordt gepresenteerd in hoofdstuk 5. De programma bedekt het gebied van delaminatiegedrag aan de aluminium/vezel interface, het vermoeiingsscheurgroei gedrag van het monolithische aluminium, de scheuropeningcontouren en de bijbehorende delaminatievormen van vermoeiingsscheuren in Glare, tezamen met de scheurgroei curves. The meettechnieken die gebruikt worden in dit experimentele programma worden in detail besproken in dit hoofdstuk.

Het meest belangrijke hoofdstuk van dit proefschrift is hoofdstuk 6, waarin een nieuw scheurgroei-voorspellingsmodel afgeleid wordt in vier opeenvolgende stappen. Het model beschrijft de scheurgroei van vermoeiingsscheuren in de aluminium lagen en de bijbehorende delaminatiegroei op de interface tussen de aluminium en vezellagen over de gehele scheurlengte.

In dit voorspellingsmodel is de spanningsintensiteitsfactor aan de scheurtip een functie van de scheuropening spanningen in het vrije veld en de scheursluitende spanningen als gevolg van de overbruggende vezellagen. De overbruggende spanningen langs de hele scheurlengte wordt berekend op basis van de scheuropening vergelijkingen voor de individuele mechanismen. De overbruggende spanningen worden vervolgens gebruikt om de delaminatieuitbreiding uit te rekenen, gebruik makend van een relatie tussen de delaminatiegroeisnelheid en de snelheid waarmee de energie vrijkomt.

Het voorspellingsmodel is geïmplementeerd in een numeriek programma en het is gevalideerd met een grote hoeveelheid experimentele data. Een goede correlatie is verkregen tussen de voorspelde en de gemeten scheurgroeisnelheden, scheuropeningcontouren en delaminatievormen.

Hoofdstuk 7 vat de conclusies van dit onderzoek samen. Geconcludeerd kan worden dat het voorgestelde voorspellingsmodel het mechanisme van scheurgroei en delaminatiegroei in Glare volledig beschrijft en karakteriseert. Het verkregen en gevalideerde model is nauwkeurig en heeft de potentie om uitgebreid te worden naar andere materiaal-, geometrische- en test parameters.

Curriculum Vitae

The author was born on the 4th of November 1973 in Maassluis, The Netherlands. After finishing his education at the Gereformeerde Scholengemeenschap Rotterdam, he started his study Aerospace Engineering at Delft University of Technology in 1992. During spring 1998 he performed his practical work within the Materials Laboratory at the headquarters of the National Transportation Safety Board (NTSB) in Washington D.C., USA, under supervision of J.F. Wildey II.

The author performed his Masters Thesis work within the chair of Aerospace Materials under the supervision of dr.ir. A. Vlot and prof.ir. L.B. Vogelesang on the subject of “Development of an empirical fatigue crack growth prediction model for the Fibre Metal Laminate Glare”.

After his graduation, he worked as a researcher for the chair of Aerospace Materials on fatigue and damage tolerance topics within the Glare Research Programme. Between 2001 and 2004, he was seconded to the Fibre Metal Laminate Centre of Competence (FMLC) as stress engineer. During the summer of 2004, he returned to the chair of Aerospace Materials as a full-time researcher.

The author started his PhD Thesis work in the chair of Aerospace Materials in 2001, initially under the supervision of dr.ir. A. Vlot, who passed away prematurely during spring 2002. Under the supervision of prof.dr.ir. M.J.L. van Tooren, prof.dr.ir. S van der Zwaag and prof.dr.ir. J. Schijve he finished his thesis work in 2005 on the topic of “Fatigue crack propagation and delamination growth in Glare”.

Publications

Alderliesten, R.C., Vlot, A., Fatigue crack growth modelling in Glare, USAF Aircraft Structural Integrity Program Conference, San Antonio TX USA, 2000

Alderliesten, R.C., Fatigue, In: Vlot, A., Gunnink, J.W. (Ed.), Fibre Metal Laminates: an Introduction, Kluwer Academic Publishers, Dordrecht, 155-171, 2001.

Alderliesten, R.C., Vlot, A., Fatigue crack growth mechanisms in GLARE, In: Griffiths, G.R., McCarthy, R.F.J. (Ed.), Making the Difference with innovative materials and processes, SAMPE, 41-52, 2001.

Alderliesten, R.C., Fatigue crack growth modelling in GLARE, In: Yao Zhang, (Ed.), Beijing, China: ICCM, 1-10, 2001.

Vlot, A., **Alderliesten, R.C.**, Kanter, J.L.C.G. de, Hooijmeijer, P.A., Ypma, M.S., Sinke, J., From Laboratory Material Development to Industrial application for Fibre Metal Laminates, Society of Manufacturing Engineers, (EM01-357), 1-12, 2001.

Vlot, A., **Alderliesten, R.C.**, Hooijmeijer, P.A., Kanter, J.L.C.G. de, Sinke, J., Ypma, M.S., Fibre metal laminates: a state of the art, International journal of materials & product technology, 17(1/2), 79-98, 2002.

Shim, D.J., **Alderliesten, R.C.**, Spearing, S.M., Burianek, D.A., Fatigue crack growth prediction in GLARE hybrid laminates, In -- (Ed.), Global Composites Advancement - Bridging Academia and Industry, Dearborn, USA: SEM, 1-12, 2003.

Alderliesten, R.C., Hagenbeek, M., Homan, J.J., Hooijmeijer, P.A., Vries, T.J. de, Vermeeren, C.A.J.R., Fatigue and damage tolerance of GLARE, Applied composite materials, 10(4-5), 223-242, 2003.

Shim, D.J., **Alderliesten, R.C.**, Spearing, S.M., Burianek, D.A., Fatigue crack growth prediction in GLARE hybrid laminates, Composites science and technology, 63, 1759-1767, 2003.

Alderliesten, R.C., Fatigue crack growth prediction of surface cracks in GLARE, In: Schmitt, G. E. (Ed.), Materials and Processing: Enabling Flight, Our Legacy and our future, SAMPE, Covina, USA, 1-12, 2003.

Alderliesten, R.C., Woerden, H.J.M., Load history effects during fatigue crack propagation in Glare, In: Guillaume M. (Ed.), Fatigue of Aeronautical Structures as an Engineering Challenge, Volume I, Lucerne Switzerland, 509-530, 2003

Alderliesten, R.C., Homan, J.J., Fatigue crack growth behaviour of surface cracks in GLARE, In: Varvani-Farahani, V., Brebbia, C. A. (Ed.), Fatigue Damage of Materials: Experiment and Analysis, Southampton: WIT press, 213-222, 2003.

To be published

Alderliesten, R.C., **Zwaag S. van der, Schijve, J.**, Energy Release Rate Approach for Delamination in a Fatigue Crack Configuration in Glare, to be submitted to Engineering Fracture Mechanics.

Alderliesten, R.C., **Homan, J.J.**, Fatigue & Damage Tolerance Issues of GLARE in Aircraft Structures, International Journal of Fatigue (special edition), submitted 2004.

Alderliesten, R.C., A new analytical model for fatigue crack propagation in Glare, ICAF, Hamburg Germany, 2005

Acknowledgements

The research presented in this thesis would not have been performed without the support of many people. Without pretending to be complete, I would like to mention and thank several of them.

Two questions have been of great importance to me throughout this research: “When will you write down what you know about fatigue in Glare?”, which initiated this research, and the question many times repeated “Have you developed the Alderliesten-model yet?”, to which the answer remained for quite some time: “Not yet”. Now, at the end of this work I can answer, “I did”, although it is too late for Ad Vlot who asked both questions. Nevertheless, I am grateful for his contribution in the initial phase of this research and I intend to honour him with this work.

I am also very grateful to my promotors prof. Van Tooren and prof. Van der Zwaag for taking over the work from Ad Vlot after his decease. Together with prof. Schijve, they managed to keep me motivated in order to get the work done. I thank them for their efforts to monitor the technical contents as well as the process of writing of this thesis.

Special thanks to my FMLC-colleagues with whom I have been working for quite some time on several Glare projects: Jan Willem Gunnink, Geert Roebroeks, Rob Leonard, Erik Kroon and Peter Hooijmeijer. The discussions on the various technical topics, in most cases not even related to this work, have been appreciated.

I like to thank all the colleagues within the chair of Aerospace Materials, who have contributed to the either my motivation or to the research itself. Especially, Johannes Homan I want to thank for all the discussions we had on the topics related to fatigue and damage tolerance in Glare. I hope that our cooperation may continue.

Special thanks to Thomas Beumler and Fred Pelllenkoff from Airbus for the cooperation on the Glare fatigue and damage tolerance topics and Arij de Koning for showing interest and for keeping me sharp with his ideas.

I also like to thank my family and friends for enduring my numerous excuses and for keeping faith in the outcome of my work, despite my doubts. And last, but certainly not the least, I like to thank Leonie for her endless support and for her patience with me in the months before our wedding when I was focussing on my thesis work.